SEISMIC BEHAVIOR ASSESSMENT OF LOW-RISE REINFORCED
CONCRETE STRUCTURAL WALLS USING QUASI-STATIC REVERSED
CYCLIC LOADING PROTOCOL

A THESIS SUBMITTED TO
THE GRADUATE SCHOOL OF NATURAL AND APPLIED SCIENCES
OF
MIDDLE EAST TECHNICAL UNIVERSITY

BY

POURANG EZZATFAR

IN PARTIAL FULFILLMENT OF THE REQUIREMENTS
FOR
THE DEGREE OF DOCTORATE OF PHILOSOPHY
IN
CIVIL ENGINEERING

JUNE 2016

Approval of the thesis:

SEISMIC BEHAVIOR ASSESSMENT OF LOW-RISE REINFORCED
CONCRETE STRUCTURAL WALLS USING QUASI-STATIC REVERSED
CYCLIC LOADING PROTOCOL

Submitted by **POURANG EZZATFAR** in partial fulfillment of the requirements
for the degree of **Doctorate of Philosophy in Civil Engineering Department,
Middle East Technical University** by,

Prof. Dr. Gülbin Dural Ünver
Director, Graduate School of **Natural and Applied Sciences**

Prof. Dr. İsmail Özgür Yaman
Head of Department, **Civil Engineering**

Prof. Dr. Erdem Canbay
Supervisor, **Civil Engineering Dept., METU**

Prof. Dr. Güney Özcebe
Co-Supervisor, **Civil Engineering Dept., TEDU**

Examining Committee Members:

Prof. Dr. Barış Binici
Civil Engineering Dept., METU

Prof. Dr. Erdem Canbay
Civil Engineering Dept., METU

Prof. Dr. M. Altuğ Erbirik
Civil Engineering Dept., METU

Prof. Dr. Sinan Altın
Civil Engineering Dept., Gazi University

Asst. Prof. Dr. Halit Cenan Mertol
Civil Engineering Dept., Atılım University

Date: 30.06.2016

I hereby declare that all information in this document has been obtained and presented in accordance with academic rules and ethical conduct. I also declare that, as required by these rules and conduct, I have fully cited and referenced all material and results that are not original to this work.

Name, Last Name   : Pourang Ezzatfar

Signature   :

ABSTRACT

SEISMIC BEHAVIOR ASSESSMENT OF LOW-RISE REINFORCED CONCRETE STRUCTURAL WALLS USING QUASI-STATIC REVERSED CYCLIC LOADING PROTOCOL

Ezzatfar, Pourang

PhD, Department of Civil Engineering

Supervisor: Prof. Dr. Erdem Canbay

Co-Supervisor: Prof. Dr. Güney Özcebe

June 2016, 194 Pages

The reinforced concrete shear walls of low- to mid-rise residential buildings, having height to length ratio ranging from 1 to 3, are more of a concern in research studies in recent years. Since the failure mode of these walls depends on the interaction between shear and flexural action, predicting the failure mode of this type of shear walls is not straight forward. While seismic behavior of high-rise walls (i.e. aspect ratio greater than about 3) is almost known and theoretical assumptions matches well with experimental findings, experimental and theoretical studies are still demanding to better understand the seismic behavior, failure modes, lateral load bearing and deformation capacities of low- to mid-rise RC shear walls.

Most of the available experimental studies within the relevant literature were done on isolated cantilever RC walls in laboratories. However, simulating the effect of earthquake loads on large scale RC shear walls surrounded by frame elements is very rare. In order to investigate the seismic performance of the RC shear walls in

conjunction with other structural elements as a system in low- to mid-rise buildings, two ½ scaled three-story three-bay RC test frames with RC shear wall in middle bay were tested. One of the specimens was designed to Turkish earthquake code (TEC-2007) and Turkish reinforced concrete practice code (TS500-2000) and the other was designed according to TEC-1975 and TS500-1981. Modeling parameters and acceptance criteria for nonlinear analysis given by ASCE/SEI41-13 and TEC-2007 for the investigated RC shear wall specimens were assessed.

Keywords: reinforced concrete shear walls, large scale experimental testing, seismic behavior, performance evaluation

ÖZ

AZ KATLI, PERDE DUVARLI BETONARME YAPILARDA STATİK BENZERİ TERSİNİR ÇEVRİM YÜKLEMESİ ALTINDA SİSMİK DAVRANIŞ İNCELEMESİ

Ezzatfar, Pourang

Doktora, İnşaat Mühendisliği Bölümü

Tez Yöneticisi: Prof. Dr. Erdem Canbay

Ortak Tez Yöneticisi: Prof. Dr. Güney Özcebe

Az ve orta yükseklikli betonarme yapılarda kullanılan perde duvarlar (yükseklik-uzunluk oranı 1 ile 3 arasında olan) günümüzdeki araştırmalarda daha yoğun şekilde yer almaktadır. Bu yükseklik aralığındaki binalarda kesme ve eğilme etkileşimi göçme davranışını belirlediği için, bu yapıların göçme davranışının önceden tahmin edilmesi karmaşık ve güçtür. Yüksek (yükseklik-uzunluk oranı 3'den büyük olan) perdelerin sismik davranışı büyük ölçüde bilinmektedir ve bunların sismik davranışına ilişkin teorik varsayımlar deneysel çalışmaların sonuçlarıyla uyumludur. Ancak az ve orta yükseklikli betonarme perde duvarların sismik davranışı, göçme modu, yatay yük taşıma ve deformasyon kapasitesinin tespiti için teorik ve deneysel çalışmalara ihtiyaç duyulmaktadır.

Perde duvarlar ile ilgili literatürde bulunan deneysel çalışmaların çoğu çerçevelerden bağımsız betonarme perde duvarlar üzerinedir. Çerçeve ile bağıntılı büyük ölçekli perde duvarların deprem yükünün etkisini temsil eden deneysel çalışmalar çok azdır. Çerçeve elemanlarla bağlantılı perde duvarların sismik

davranışının incelenmesi için, ½ ölçekli 3 katlı 3 açıklıklı orta açıklığında perde duvar bulunan 2 adet betonarme çerçeve ile deney yapılmıştır. Seçilen deney elemanlardan ilki TDY-2007 ve TS500-2000 yönetmelikleri doğrultusunda tasarlanmışken, diğer deney elemanı TDY-1975 ve TS500-1981 baz alınarak tasarlanmış. Seçilen deney betonarme perde duvarlar için ASCE/SEI41-13 ve TDY-2007 tarafından öne sürülen ve doğrusal olmayan analizlerde kullanılan modelleme parametreler ve kabul kriterler değerlendirilmiştir.

Anahtar kelimeler: betonarme perde duvarlar, büyük ölçekli deneysel yöntemler, sismik davranış, performans değerlendirme

To my beloved family

ACKNOWLEDGEMENTS

It is a pleasure to acknowledge my supervisors, Prof. Dr. Güney Özcebe and Prof. Dr. Erdem Canbay, for their invaluable guidance, endless support, and encouragement during my PhD studies. I have benefited from their wisdom and their experience. I also wish to sincerely thank Prof. Dr. Barış Binici for his inspiration, constructive criticism, and suggestions. It was a great pleasure and honor to work with you all.

Special thanks are also extended to Prof. Dr. Sinan Altın, Prof. Dr Murat Altuğ Erberik and Assoc. Prof. Dr. Halit Cenan Mertol for taking the time to review this dissertation and serving on the examining committee.

I would like to give a special thanks to my good friend, PhD Candidate Salim Azak for his tremendous help with the experiments in laboratory and for his moral support and constant encouragement. Special thanks are also due to my dear friend Dr. Yasemin Didem Aktaş for her precious friendship and all the help given to me over my PhD study. My deepest gratitude goes to my father Houshang, my mother Mahrokh and my sister Ronak for their incredible patience, constant support, and trust; this dissertation was simply impossible without you.

Finally, I reserve the greatest thanks for my wife Maryam Daneshvar, who is my best friend, my partner in all things, and the owner of my heart. Thank you for trusting me.

TABLE OF CONTENTS

LIST OF TABLES

LIST OF FIGURES

xxi

LIST OF EQUATIONS

CHAPTER 1

INTRODUCTION

1.1. General

Reinforced concrete shear walls are stiff structural elements which can provide considerable lateral stiffness and lateral load carrying capacity for structures against earthquake and wind loads. Sufficient seismic performance of buildings with RC shear walls were observed in past earthquakes compared to buildings without RC shear walls (i.e. California, 1971; Mexico, 1985; Chile, 1985; Armenia, 1988; Chile, 2010; New Zealand, 2011; etc.). Very few numbers of buildings with RC walls were reported as collapsed and generally RC walls have exhibited a satisfactory performance during earthquakes (Wallace 2012). Seismic design codes introduce flexural failure as the most preferred failure mode in RC shear walls. However, in low- to mid-rise buildings or generally in RC shear walls with low aspect ratios, shear failure or shear failure preceded by initial flexural yielding may happen. Since these types of failure are brittle, and rate of strength and stiffness deterioration is rapid in post-peak deformation cycles, special considerations must be made at the design stage. As stiff structures may face with large deformation ductility demands beyond the elastic region, in special and important structures it is vital to estimate available deformation capacity to predict design force demand (Whyte and Stojadinovic, 2013). In order to eliminate the shear failure in RC walls, the first step is to investigate seismic behavior of low-rise shear walls and to identify the underlying causes of this type of failure.

1

1.2. Motivation

Although many experimental works have been conducted on low-rise RC shear walls in previous years, the results are very scattered and more experimental and analytical studies are still required. Most of the experimental studies were conducted on isolated cantilevered RC shear walls and there are only a few numbers of large scale experimental studies on RC walls with adjacent frame structures. Seismic behavior and performance evaluation of low-rise RC shear walls in conjunction with surrounding frames through large scale experiments is needed. Considering interaction between surrounding frame and RC wall in tests specimens of this study provides more realistic lateral load flow through structural elements.

1.3. Research objectives and scopes

The current PhD thesis is as part of a large research project conducted in METU Structural Mechanics Laboratory. Within the scope of this research project, thirteen large scale reinforced concrete specimens with different characteristics were tested by pseudo-dynamic and quasi-static static reversed cyclic testing methods. Two tests out of the whole thirteen tests are described in the context of this thesis. This current research project contributes to the TÜBİTAK Project: "Evaluation and Advancement of the Seismic Assessment and Strengthening Methods in the Turkish Seismic Code through Experimental and Analytical Research", Project No: 108G034. The outcomes of the research project including the present thesis are intended to strengthen the Turkish Seismic Code provisions.

The objectives aimed to achieve in the current thesis are as follows:

- Investigating damage and failure characteristics of RC frames having RC shear walls through conducting two quasi-static reversed cyclic tests on two different RC frames including RC shear walls.

- Determination of the seismic performance, strength and lateral deformation capacity of tested specimens which represented low- to mid-rise buildings having RC shear walls as a lateral load bearing system and were designed according to Turkish Seismic Codes.

- Examining RC wall modeling parameters and member deformation performance limits proposed by TEC-2007 and ASCE/SEI41-13 which are practiced in performance evaluation of RC buildings using nonlinear analysis.

1.4. Thesis outline

The thesis is organized into five chapters. Chapter 2 includes a brief literature review on the most prominent experimental works completed on RC shear walls in the past. RC wall failure modes which were observed in the past earthquakes and/or laboratory tests are discussed. Seismic code provision of TEC-1975, TEC-2007 and ACI318-14 regarding RC wall design are summarized in this chapter, as well.

Chapter 3 introduces the experimental work done in the context of this thesis in detail. Test method, test setup, material properties used in the construction of test specimens and geometrical properties of two RC specimens are provided in this chapter. Experimental test results including measured forces and deformations (story displacement and member end rotations), sequence of observed damages and failures during applied loads are reported. The results indicating overall response of both specimens are compared and some parameters such as energy

absorption capacity, shear strength and displacement ductility, stiffness and strength degradation and damping ratio are discussed through comparing the test results of two experimentally studied cases.

Chapter 4 covers finite element (FEM) analysis of tested specimens. Analytical models of tested frames were constructed in SeismoStructs v7.0 software package. Structural elements comprising beams, columns and walls were modeled with beam-column line elements which were discretized to fibers in cross section. It was aimed to find approximate location of inflection point of walls bending moment diagram through pushover analysis. The shear force developed in shear walls was obtained by subtracting the base shear of exterior columns from total lateral force applied on frames. Then, extracting moment-rotation relationship of RC walls of frames would be possible. This chapter is also devoted to assess modeling parameters and numerical acceptance criteria given by TEC-2007 and ASCE/SEI41-13. Owing to the grid of LVDTs installed on the walls, contribution of shear and flexural deformations in total lateral deformation of walls are separately investigated.

Finally, thesis outcomes including summary of seismic performance of tested frames which were designed according to two different generations of Turkish earthquake code (TEC-1975 and TEC-2007) and discussion on the effect of wall detailing requirements presented by TEC-1975 and TEC-2007 on wall behavior are provided in Chapter 5.

CHAPTER 2

LITERATURE REVIEW

2.1. General

Within the scope of this chapter, three different test setup configurations exercised in wall panel tests in literature are explained in detail. Additionally, two informative parameters (aspect ratio and shear span ratio), which are used in wall classification based on behavior mode are described.

Following section of this chapter presents a brief description about characteristics of low-rise RC wall specimens tested by some researchers practicing different experimental programs. Looking in the literature, there exist some prominent experimental studies on RC shear walls under cyclic loading such as studies conducted by Kokusho (1952); Alexander, Heidebrecht and Tso (1973); Hirosawa (1975); Barda, Hanson and Corley (1977); Hernandez (1980); Paulay, Priestley and Synge (1982); Oesterle, Shiu and Corley (1984); Maier and Thurlimann (1985); Pilakoutas and Elnashai (1995); Salonikios, Kappos, Tegos and Penelis (1999); Shirai, Matsumori and Kabeyasawa (2007); Kuang and Ho (2008); Dazio, Beyer and Bachmann (2009); Fintel (1995). It was aimed to select and summarize outcomes of prominent experimental works in which aspect ratio and/or shear span ratio of investigated walls and/or their failure modes are close to the shear walls of this study. Moreover, the literature survey of Gulec and Wittaker (2009) on experimental studies of low-rise RC shear walls is considered as one of the most comprehensive reviews within the relevant literature. Within the literature, there are only a few numbers of studies on RC walls with adjacent frame

structures. Most of the experimental researches have been done on isolated RC shear walls.

The next section of this chapter covers the failure modes of RC shear (structural) walls; observed in real earthquakes and/or in laboratory tests. Furthermore, the underlying reasons of each failure mode and the parameters triggering or accelerating the failure are thoroughly explained.

Finally, the last section is devoted to seismic detailing provisions of TEC-2007, TEC-1975 and ACI318-14 codes regarding seismic design of reinforced concrete shear walls in seismic zones.

2.2. Aspect ratio and shear span ratio

The experimental studies of many researchers and the post-earthquake investigations on RC walls reveal that in most cases a correlation can be established between the geometrical configuration and behavior of RC walls during earthquakes. Some researchers and design codes (e.g. ACI 318-14) use a parameter named as "aspect ratio" to categorize the RC shear walls based on their seismic behavior. Aspect ratio is simply defined as the ratio of height to length of walls, h_w/l_w . While h_w stands for total height of the wall, l_w is the total length of the wall in the wall plane. Despite the practicality and simplicity of this geometrical parameter, another geometrical parameter called boundary conditions of RC wall affects the behavior of the RC wall especially in laboratory experiments. Within the relevant literature, the boundary conditions of tested isolated shear walls in experimental works cover racking condition, cantilever condition, and fixed-fixed conditions that are used by different researches considering their laboratory equipment and real problem conditions that are aimed to be to simulated. Figure 2.1 illustrates different boundary conditions used in wall test setups. Racking test which is similar in loading to diagonal

compression test, consists of applying lateral load at the top corner of the test specimen while the opposite bottom corner is constrained to avoid any horizontal movement. One frame responsible for controlling the vertical movement of the test specimen restricts the overturning movement that develops due to overturning at the same corner as lateral load is applied. In cantilever type of boundary condition, lateral load is applied at the top of the specimen. The wall is constructed on a rigid foundation which is ideally fixed to ground without any movement (fixed base). In general, lateral load is applied on a RC beam constructed on the top of test wall. As a result, the inflection point (or the point that the lateral load is applied) is located slightly higher than the wall height. Therefore, the moment arm is slightly higher than the wall height (vertical distance between the lateral load location and foundation). In fixed-fixed condition which requires more costly test setup, the rotation of the both upper and lower parts of the wall is restricted (e.g. set up used in Bekő and Roško, 2013). The inflection point is approximately located at the mid-height of the wall. (Dillon, 2015)
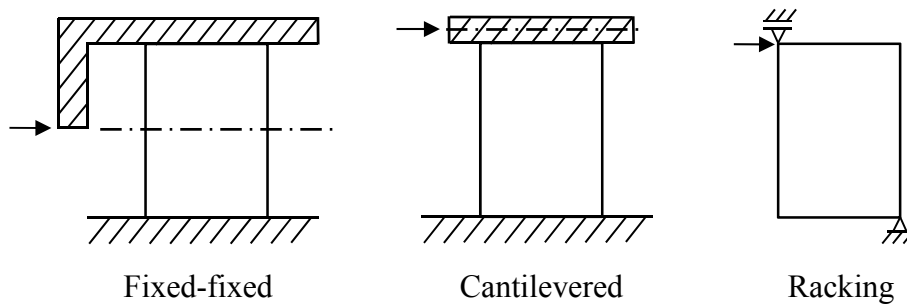
Figure 2.1 Different boundary conditions used in wall test setups

Two different failure modes may be observed for walls having same aspect ratio but different test set up and boundary conditions. Looking to the literature of experimental wall studies, it is noticed that since different researches practice different test setups with different boundary conditions, comparison of test

specimens, even the ones having same aspect ratio leads to irrelevant correlations. In order to overcome this deficiency, some researchers used another parameter called "shear span ratio" that inherently covers both boundary condition and geometry and serves as a better representative parameter. The shear span ratio is defined as the ratio of the height between the points of maximum and zero moment and the shear length of the wall and is represented by a/D or $M_u/V_u l_w$, identical within the literature. Shear span ratio can also be represented by h_e/l_w where h_e is the effective wall height between the points of maximum and zero moment and equals to M_u/V_u (Dillon, 2015).

$$\frac{a}{D} \equiv \frac{M_u}{V_u l_w} \equiv \frac{h_e}{l_w} \tag{2.1}$$

where

> a= vertical distance from the inflection point to point of maximum moment,
> M_u = the ultimate moment at a point along the height of the wall panel,
> V_u = the ultimate shear at the same height on wall panel,
> $D = l_w$ = the shear length of the wall panel,
> h_e = the effective wall height (M_u/V_u).

Generally, the values of shear span ratio and aspect ratio of one RC wall are not equal. Though, in single-story buildings (cantilever shear walls), where lateral forces are assumed to be applied at the top of the walls, aspect and shear span ratios possess same values. In multi-story walls, lateral loads are assumed to be distributed in the height of the building (e.g. triangular distribution). Therefore, the moment arm or effective wall height will be different than total height of the wall and can be approximately assumed as $\frac{2}{3} h_w$. Accordingly, the shear span ratio will be equal to almost $\frac{2}{3}$ of the aspect ratio (Kappos and Penelis, 2010).

8

2.3. Previous Experimental works in literature

Kokusho (1952) performed cyclic and monotonic tests on 35 barbell shaped RC walls. Aspect ratio (h_w/l_w) of tested specimens was approximately between 0.3 and 0.9 (shear span ratio ranging from about 0.5 to 0.86). Wall aspect ratio, horizontal and vertical web reinforcement and vertical edge reinforcement ratio were the test variables. No axial force representing gravity loads was applied on the walls. Reportedly, all of the specimens failed in shear (from Hirosawa, 1975). Alexander et al. (1973) investigated behavior of five rectangular RC walls under cyclic load tests. The aspect ratios of tested walls having a scale factor of ½ varied from 0.5 to 1.5. The cantilever isolated shear wall models represented a complete wall or an inter-floor part of a multi-story wall. The aspect ratio and vertical load level were investigated as the test variables. Improved energy dissipation and ductility were reported, due to the presence of single vertical bars in wall edges and starter bars extending from wall foundation into the wall panel. Within this study, it is stated that starter bars improved cracking pattern lifting up the initial cracks from the base level.

Hirosawa (1975) completed monotonic and cyclic tests on 49 rectangular and barbell shaped RC shear walls. The test variables of this study were aspect ratio ranging from about 1 to 2.3 (shear span ratio ranging from about 1.05 to 2), axial force, horizontal and reinforcement ratio. Both flexural and shear failure modes were observed in these tests.

Barda et al. (1977) presented an equation to estimate shear strength of low-rise RC shear walls based on a cyclic test program performed by Barda (1972) on eight low-rise RC shear wall specimens including boundary columns. The test variables were web horizontal and vertical reinforcement, flange vertical reinforcement and wall aspect ratio. The governed failure mode was shear failure (preemptive web crushing and preemptive sliding shear) for the tested walls with

9

h_w/l_w of 0.5 to 1 and scale factor of $\frac{1}{3}$. No axial force was applied on test walls. The research by Barda (1972) was one of the earliest experimental works on low-rise RC shear walls which the outcomes composed the bases of the first editions of ACI code.

Hernandez (1980) accomplished cyclic tests on 23 RC wall specimens. Studied test variables were aspect ratio, horizontal and vertical reinforcement ratio, concrete compressive strength, axial load, and boundary conditions. Shear span ratio of tested walls was ranged between 0.5 and 2.0. He also proposed an equation to estimate shear resistance of walls (Gulec and Wittaker, 2009).

Paulay et al. (1982) investigated the failure modes of low-rise RC shear walls through quasi-static revered cyclic tests on four ½ scale wall specimens. All the test walls had shear span ratio of 0.57 and two of them had diagonal reinforcement. The sequence of damages which resulted in a particular failure mode of studied squat wall specimens was explained in detail in their study. Additionally, ductile flexural and flexure-sliding shear behavior modes were reported. It was concluded that diagonal reinforcement can effectively control sliding shear by reducing the base slip and consequently improve the hysteretic behavior reducing the pinching associated with sliding in hysteresis diagram.

Oesterle et al. (1984) completed relatively large experimental test constituting cyclic loading tests on twenty 1/3 scale rectangular, barbell and flanged shaped RC wall specimens having aspect ratio of 2.4. The test variables were horizontal and vertical reinforcement content, axial load, confined boundary elements, load history and concrete strength in their experiments. It is concluded that the behavior of the wall is governed by the shear stress level and stressed the positive effect of confined boundary in performance of RC walls including strength and deformation capacity enhancement.

Maier and Thurlimann (1985) conducted cyclic and monotonic tests on ten flanged and rectangular shaped RC shear walls with aspect ratio of about 1.0 (shear span ratio of 1.12). All specimens had a scale factor of $\frac{1}{3}$. The test variables were reinforcement content of walls and axial force. Flexure-diagonal tension and flexure-diagonal compression were the observed failure modes of tested low-rise walls. The collected data by the authors throughout the experiments is still used to validate analytical methods and finite element modeling of shear walls in some commercial codes like DIANA.

Pilakoutas and Elnashai (1995) completed cyclic tests on six RC shear walls with the aspect ratio of 2.0. The rotation of the walls at the top was obstructed by a special test setup which forces wall to deform in double curvature, reducing shear span ratio to 1.0. Tested walls were isolated walls with scale factor of 1:2.5. All the test observations were reported. The test variables were flexural reinforcement in boundary element ratio, confinement and shear reinforcement content.

Salonikios et al.(1999) attempted to evaluate the validity of Eurocode 8 and ACI 318 design codes through an experimental study on eleven low-rise cantilever shear walls comprising five RC shear wall with 1.1 aspect ratio (shear span ratio) and six of 1.6. Different layouts of reinforcement (conventional and bi-diagonal) were examined in the test specimens. It is deduced that diagonal reinforcement, particularly when intersected each other within the plastic hinge length, can efficiently participate in lateral load resistance and control of sliding shear. Within the scope of this study, other test variables were axial load level, quality of construction joint, web and edge reinforcement ratio. It is mentioned that flexure dominant behavior can be developed even in well-designed low-rise shear walls and the subsequent sliding shear at higher lateral displacement demands can be eliminated or effectively controlled by bidiagonal reinforcement.

Shirai et al. (2007) reported a shake table test on wall-frame 3D full-scale six-story RC structure which was designed and detailed according to Building Standard Low of Japan (1975). Aspect ratio of RC wall was about 2.89 and moment-to-shear ratio (shear span ratio) of the tested wall calculated as about 2.1, considering inverted triangular lateral load pattern which was used in design stage. Flexure-shear cracks followed by sliding shear failure after flexural yielding in the shear wall at first story level were observed under consecutively applied scaled versions of Kobe earthquake. It is mentioned that the calculated shear strength of RC wall within the structure is 1.3 times larger than wall flexural strength. Thus, according to the new code it is assumed as a wall with flexural behavior mode.

Kuang and Ho (2008) examined experimentally seismic behavior and ductility of eight large-scale low-rise RC shear walls applying cyclic loading. In this study, all of the wall specimens were detailed without considering seismic design requirements. However, it is pointed out that how minor modification in detailing has considerably enhanced ductility of low-rise walls. The test walls were large-scale rectangular RC walls having the aspect ratios between 1.0 and 1.5 (shear span ratio between 1.13 and 1.63). Variable parameters of this research were aspect ratio, vertical reinforcement distribution, boundary region confinement, and horizontal reinforcement configuration.

Dazio et al. (2009) tested cyclic behavior of six large scale RC walls with and without confined boundary elements. The tested walls with scale factor of ½ represented lower stories of a six story reference building. The investigated parameters of this research were vertical reinforcement content and layout, as well as different reinforcement ductility properties. Very detailed descriptions of observed dames during loading reversals were provided. Although the shear span ratio of the Dazio et al. (2009) specimens, which was about 2.3, is larger than the

12

shear span ratio of specimens tested in the context of the present thesis, the aspect ratios of both studies are close to each other (h_w/l_w=2.3).

Massone and Wallace (2004) investigated the interaction between flexure and shear response of slender walls. They assessed the contribution of flexure and shear deformations to total inelastic lateral displacement. Massone and Wallace (2004) reviewed quasi-static test results conducted on six ¼-scale wall specimens including three walls with rectangular cross section and three walls with T-shaped cross section and one barbell-shaped wall. The aspect ratio of tested wall walls was 3 and the variables of test program were cross section shape and boundary confinement detailing. The shear walls were designed using capacity approach to eliminate shear failure. The axial load of 0.10 $A_g f_c'$ was applied on specimens and kept constant during the tests. A grid of deformation measurement tools was utilized to obtain panel deformations. It is concluded that inelasticity in shear and flexure behavior may approximately start at the same level of lateral displacement while nominal shear strength are twice the lateral load corresponding to flexural yielding.

Similarly, Beyer et al. (2011) concluded that shear response of the walls may be highly nonlinear for walls with flexural dominant behavior. Investigating experimental results of 34 slender RC wall tests conducted by different researchers, they stated that linear shear response assumption in the analysis of RC walls with flexural behavior is not valid in all cases and shear deformation may not be constant after flexural yielding and my increase with increasing total lateral displacements.

2.4. Failure modes of RC shear wall

Reported damage observations from past earthquakes and experimental studies on reinforced concrete shear walls reveals that most probable failure modes of shear walls can be one or combination of the following failures as diagonal tension failure, diagonal compression failure, sliding shear failure, boundary column or overall out-of-plane buckling of shear wall, longitudinal reinforcement buckling or rupture, and rupture of horizontal reinforcement. These failure types can be put into three major groups as; flexural, shear, and mixed flexure-shear failure, based on the developed state of stress that results in that specific type of failure.

2.4.1. Flexural failure

Most of the reinforced concrete design codes aim to introduce and develop design and detailing criteria to design RC shear walls exhibiting flexural behavior and flexural failure (if it take place) in larger levels of lateral displacement during earthquakes. There are two underlying reasons behind it. Firstly, flexural failure is a ductile failure mode. The second reason is the response of the walls with flexural behavior against lateral forces can be predicted pretty accurately (Gulec and Whittaker, 2009). Ductile flexural and boundary compression failure or both may occur in flexural failure mode. Minor inclined shear cracks with limited width may be observed, however they do not significantly affect the behavior (Gulec and Whittaker, 2009; FEMA306, 1998).

2.4.1.1. Ductile flexural failure

Signs of ductile flexural failure mode can be listed as wide flexural cracks along with the fractured or extremely yielded longitudinal reinforcements in the plastic hinge zone near the wall toe and concrete spalling or vertical cracking at the outer edge of the wall in compression part near the base. Figure 2.2 presents typical

damage pattern of a wall with flexural failure. This type of failure occurs in well-designed walls with sufficient horizontal reinforcement and without heavy flexural reinforcement (FEMA306, 1998).
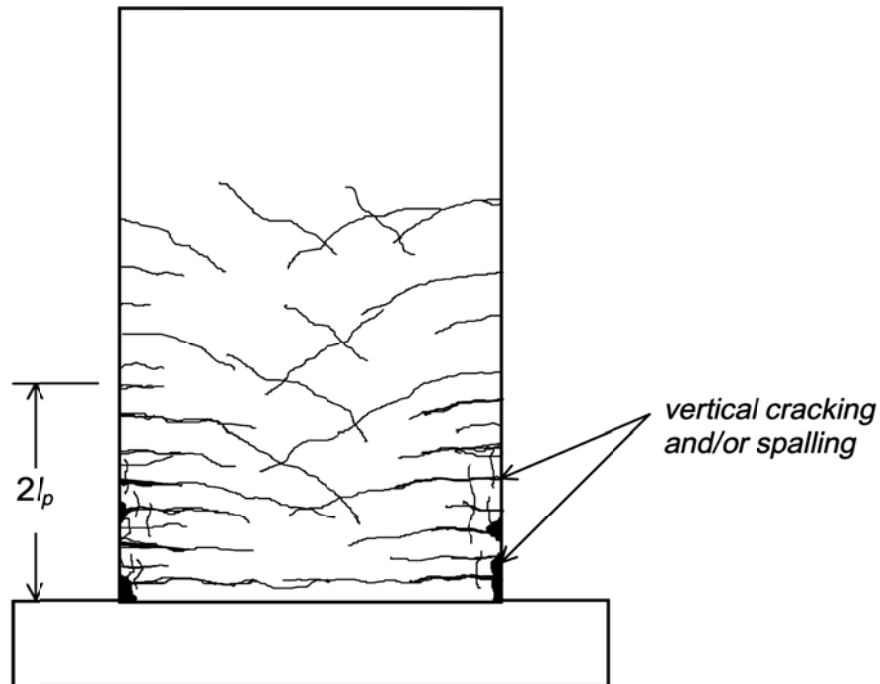
Figure 2.2 Typical damage patterns of RC walls in ductile flexural failure
(FEMA 306, 1998)

2.4.1.2. Boundary compression failure

Characteristics of boundary compression failure are concrete spalling or vertical cracking in outer region of the wall compression zone in plastic hinge zone, buckling of longitudinal reinforcement and/or core concrete crushing in boundary zone near the toe region of the wall, Figure 2.3. This type of failure is observed in RC wall with sufficient horizontal reinforcement, however, suffering from inadequate well confined boundary region (FEMA 306, 1998).

a)

$2l_p$

buckled reinforcement and/or
heavily damaged concrete
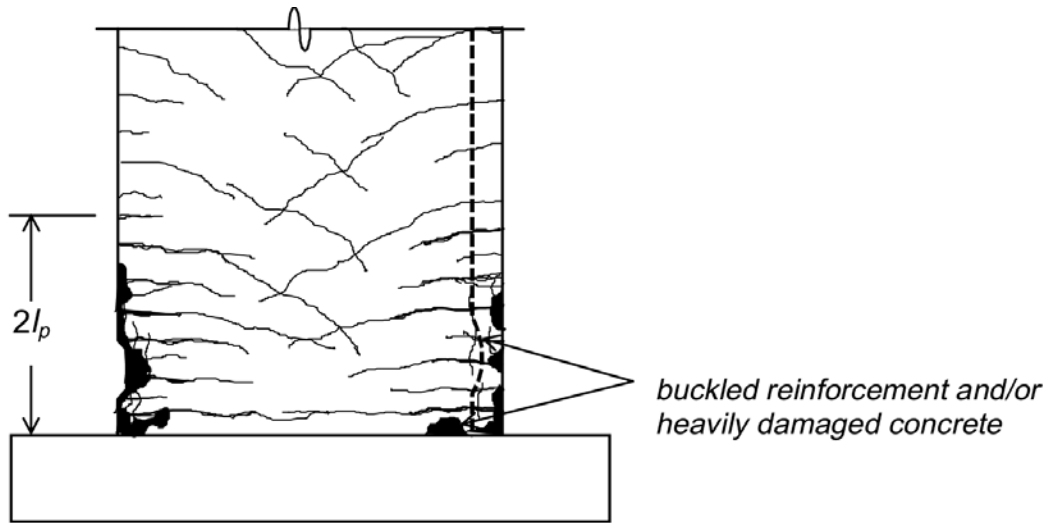
b)
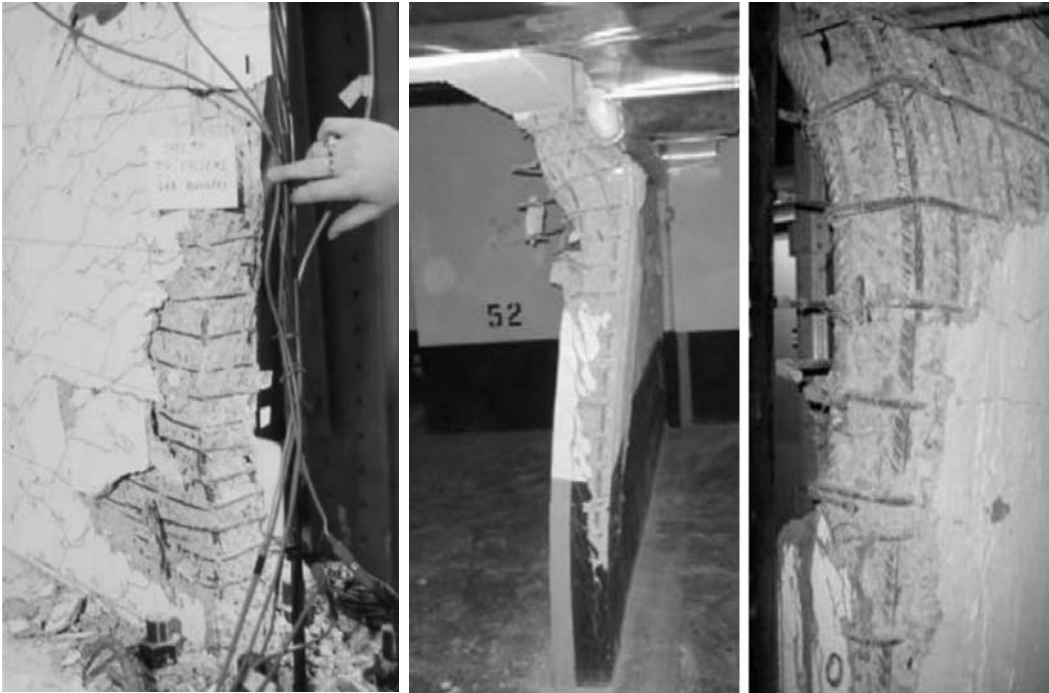
Figure 2.3 a) Demonstrative scheme of boundary compression failure (FEMA306,
1999) b) Examples of overall wall lateral instability and web boundary buckling
(Wallace, 2012)

In addition, in very thin and slender rectangular walls overall buckling may happen. Figure 2.3a and 2.3b show damage pattern for boundary compression failure and an example of overall buckling, respectively.

2.4.2. Shear failure

Shear failure is a brittle failure mode. Diagonal tension, diagonal compression and sliding shear failure are the three failure patterns associated with shear.

2.4.2.1. Diagonal tension failure

This type of failure occurs after opening corner to corner diagonal crack due to lack of sufficient horizontal reinforcement which resist against principal tensile stresses. In this type of failure, yielding of horizontal reinforcement is followed by continuously growing diagonal corner to corner or 45° cracks (Whyte and Stojadinovic, 2013). Figure 2.4 shows an example of diagonal tension failure.
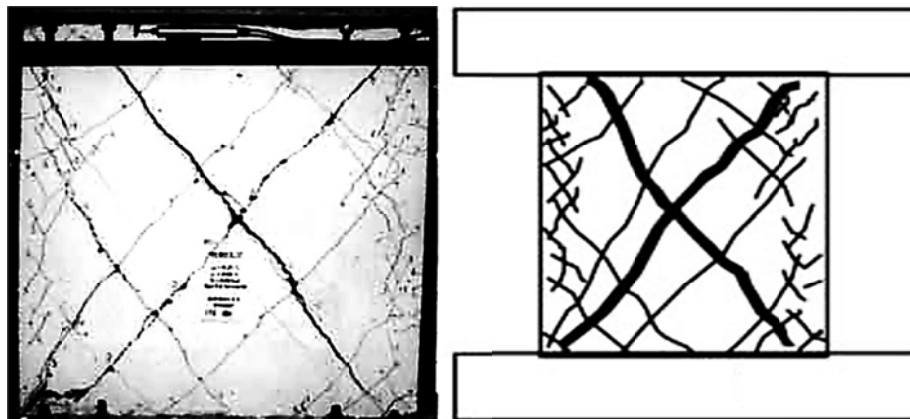
Figure 2.4 An RC wall failed in diagonal tension (Hidalgo et al., 2002)

2.4.2.2. Diagonal compression

Diagonal compression failure involves crushing of web concrete in RC walls with large flexural capacities and adequate horizontal reinforcement (Paulay et al., 1982). When diagonal tension is prevented because of sufficient amount of horizontal reinforcement, strength of compression struts is deteriorated due to opening and closing of inclined cracks in load reversals, which results in crushing of the struts, Figure 2.5. Large amount of longitudinal reinforcement in boundary elements especially in barbell or flange shaped boundary regions of RC walls increases flexural induced shear forces. In addition to the horizontal reinforcements, axial forces increase the shear strength through controlling the crack width. However, high axial forces in developed compression struts result in concrete crushing in diagonal compression failure. Some considerations in design stage must be made to eliminate diagonal compression failure which is more brittle than diagonal tension failure (Gulec and Whittaker, 2009). However, this type of failure is observed in laboratory tests and has not been detected in real buildings. It is because foundations of typical buildings do not have enough overturning capacity to resist the high forces associated with preemptive diagonal compression failures (FEMA 307, 1998)
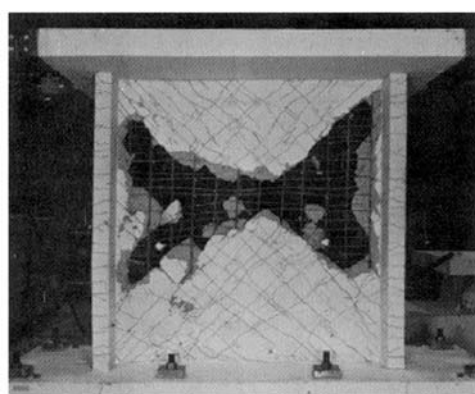
Test specimen at conclusion of loading
$\Delta = 3.0$ in $\Delta/h_w = 0.040$ $\lambda_Q = 0.2$
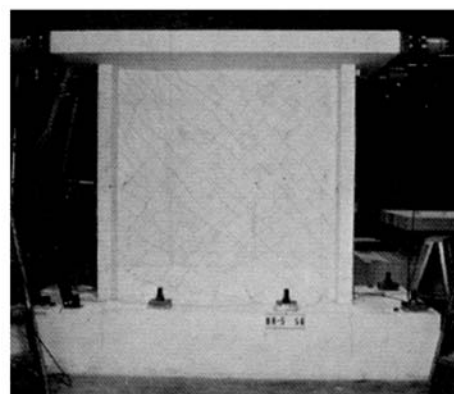
Test specimen at ultimate load
$\Delta = 0.2$ in $\Delta/h_w = 0.005$ $\lambda_Q = 1.0$

Figure 2.5 Diagonal compression failure (FEMA 307, 1998 from Barda, 1972)

2.4.2.3. Preemptive sliding shear

Another type of failure that is associated with shear is sliding shear failure which is similar to diagonal compression failure and preempts flexural yielding. This type of failure is initiated with concrete crushing in heavily reinforced very squat walls. Inclined cracks form in each direction and intersect each other in loading reversals resulting in strength deterioration of web concrete between these cracks. As the RC wall is heavily reinforced the inclined cracks are evenly distributed and un-concentrated. Crushing of the concrete struts over the length of the wall and in a narrow band forms a horizontal sliding plane near the base of wall web (Gulec and Whittaker, 2009). Sliding shear failure may happen at poor construction joints as well (FEMA306, 1998). As it is shown in Figure 2.6, crushing the web concrete provide a potential sliding surface.
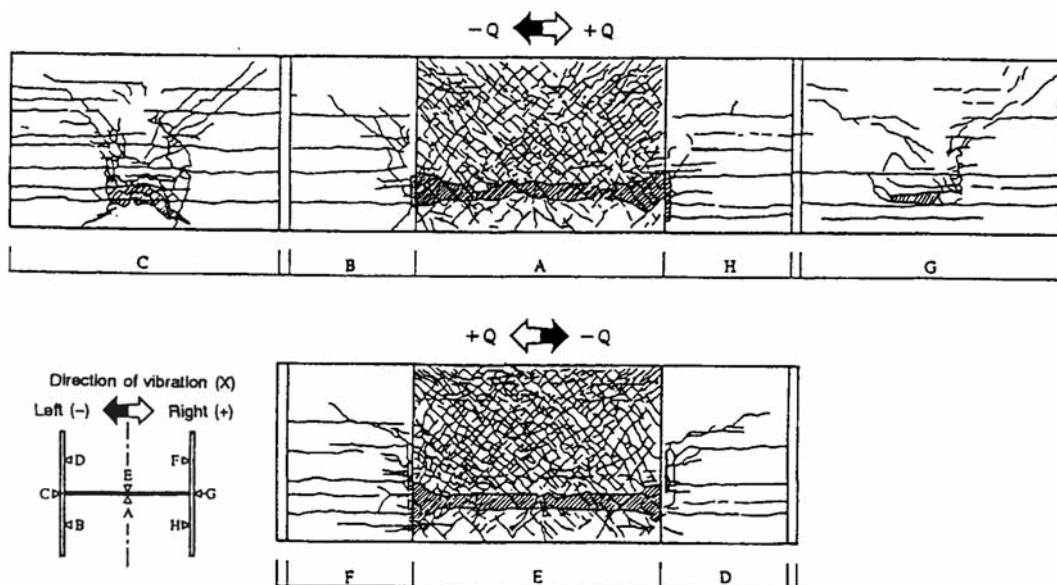
Figure 2.6 Preemptive sliding shear (OECD, 1996)

19

2.4.3. Mixed flexure-shear failure

Flexure-shear failure is a type of failure which is initiated by flexural yielding, like flexural cracking and yielding of longitudinal bars in boundary regions of walls, and followed by shear failure as displacement increases. In flexure-shear mode, after initiation of flexural yielding, the shear strength of RC wall decreases during greater displacement cycles. When the shear strength of wall reduces to an amount lower than the shear strength associated with formerly developed flexural yielding, one of the shear type failures occur despite the fact that the shear strength was equal or larger than shear before flexural yielding (Gulec and Whittaker, 2009).

2.4.3.1. Flexural-diagonal tension

Flexure-diagonal tension failure may occur in RC walls with low to moderate horizontal reinforcement and heavy flexural reinforcement (FEMA 306, 1998). A main observable damage characteristic of flexural-diagonal tension failure is concentration of damage in a wide diagonal crack. This failure mode is very similar to preemptive diagonal tension failure in nature but occurs after flexural yielding. Figure 2.7 depicts typical flexural-diagonal tension damage pattern.
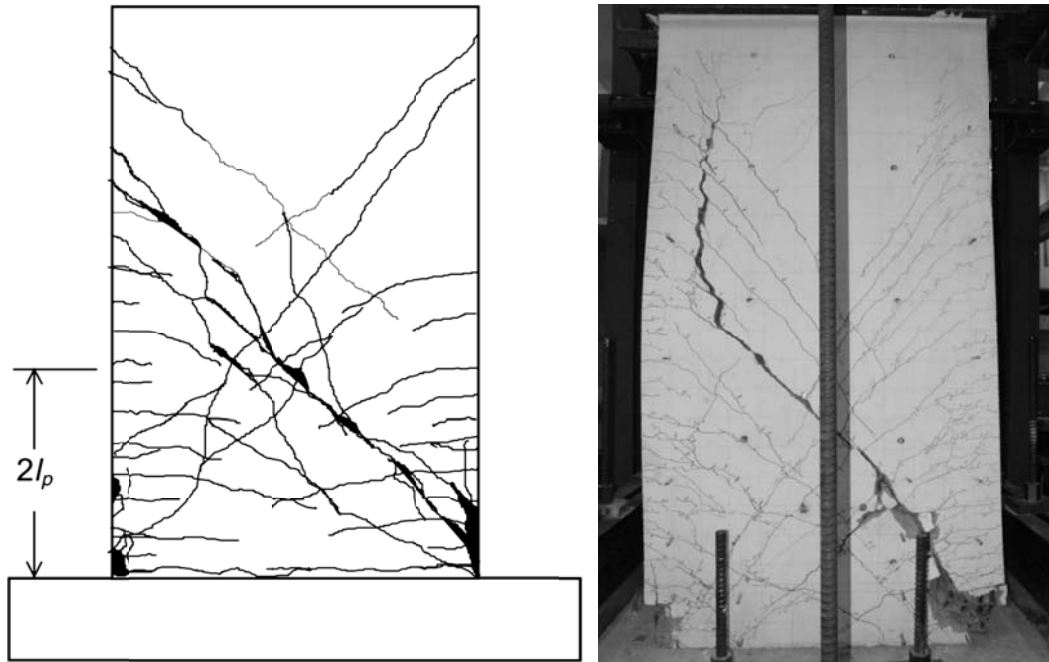
Figure 2.7 Flexural-diagonal tension failure; a) typical appearance (FEMA 306, 1998), b) wall with $h_w/l_w = M_u/V_u l_w = 2$ tested by Tran and Wallace (2012)

2.4.3.2. Flexural-diagonal compression

Flexure-diagonal compression failure is very similar to preemptive diagonal compression failure, Figure 2.8. However, unlike preemptive diagonal compression failure, flexure-diagonal compression failure occurs after flexural yielding (shear wall reaches its flexural capacity first). This type of failure is more common in low-rise walls, walls subjected to high axial loads, L-shaped or T-shaped walls with flanges or walls with heavy boundary elements. Extensive concrete spalling and voids in web concrete are signs of failure at extreme stages (FEMA 306, 1998).

a)

$2l_p$
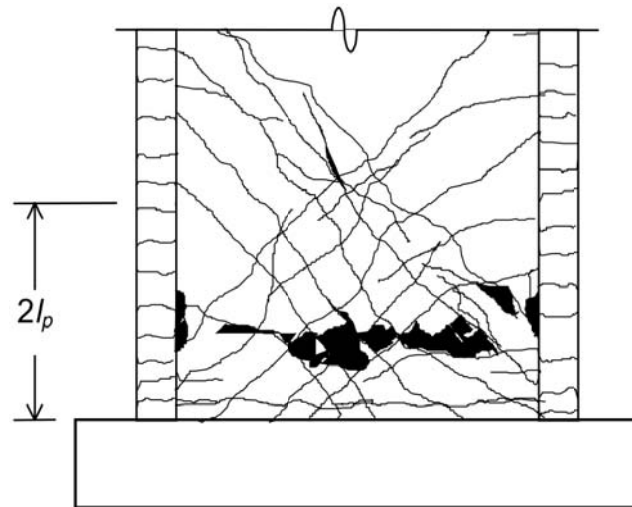
b)
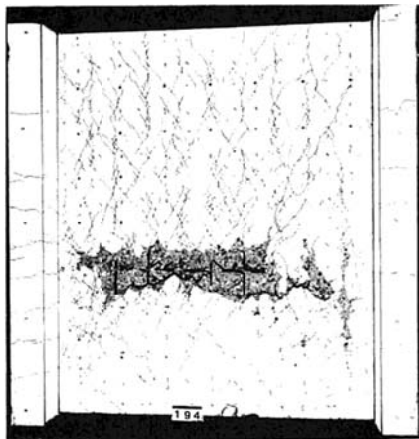
c)
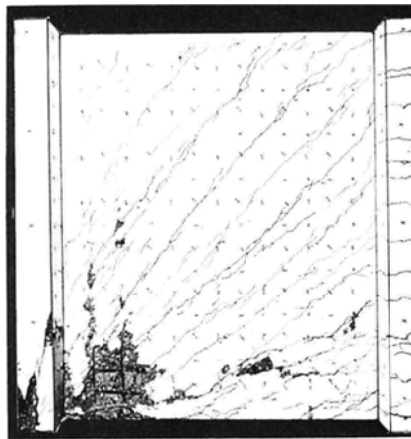
Figure 2.8 Flexural-diagonal Compression failure; a) representative damage pattern (FEMA 306, 1998) b, c) two specimens tested by Maier and Thurlimann (1985)

2.4.3.3. Flexural-sliding shear

Sliding shear failure is typically observed in deep members such as low-rise shear walls and deep beams. In cases where diagonal tension and compression failures are prevented through placement of large amount of horizontal reinforcements and reduction of shear stresses in the wall web, respectively, sliding shear failure may be observed along the critical sections, typically near the support. Basically, concrete could be extensively damaged due to opening and closing horizontal flexural cracks during loading reversals. When two major horizontal cracks, which were formed in opposite directions, meet each other a continuous cracking surface is formed. On the sliding surface shear friction and aggregate interlock decreases. As a consequence, shear load bearing capacity of member is reduced to shear strength developed by dowel action, see Figure 2.9 and Figure 2.10. Increasing the amount of horizontal reinforcement cannot prevent this type of failure (Paulay, 1972; Tegos, Psarras, Kalkinis, Papadopoulos and Legbelos, 2012). This type of failure is brittle and causes significant reduction in stiffness which results in pinching in hysteresis behavior and reduction in energy dissipation consequently (Greifenhagen and Lestuzzi, 2005; Salonikios et al., 1999). RC shear walls with low longitudinal web reinforcement content, no or lightly reinforced boundary columns and low axial forces are more prone to fail in this mode (Gulec & Wittaker, 2009).
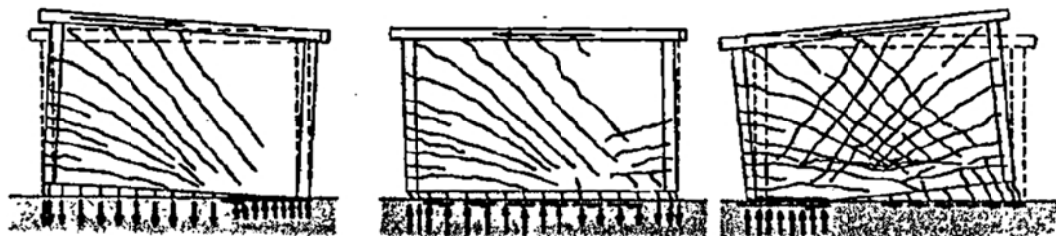
Figure 2.9 Sliding shear mechanism (Paulay and Priestley, 1992)
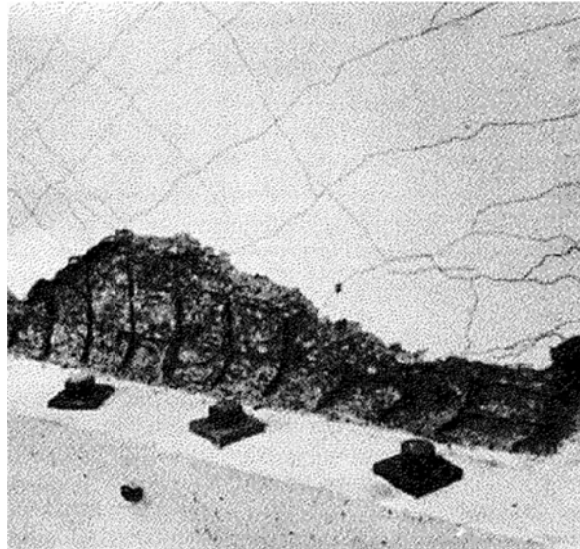
Figure 2.10 An example of flexure-sliding shear failure (Gulec and Wittaker, 2009 from Synge, 1980)

Different parameters such as concrete and reinforcing steel material properties, geometrical configuration of walls like cross section dimensions and aspect ratio, dynamic properties of wall, reinforcement detailing, and existence of confined boundary zones can trigger one or a number of mentioned failure modes. Among these parameters, wall aspect ratio is the key parameter that likely failure mode of wall can accordingly be predicted by statistical calculations.

Based on the field investigations on damaged and/or failed RC walls in past extensive earthquakes and seismically tested RC walls in laboratories, it is generally agreed that dominant failure mode of squat shear walls ($h_w/l_w < 1.5$) is pure shear failure. The failure mode changes to pure flexure failure for high-raise shear walls with larger value of aspect ratio, $h_w/l_w > 3$ (ASCE/SEI 41-13, 2014). For low- to mid-rise walls ($1.5 < h_w/l_w < 3$) interaction between shear and flexure determines failure mode. For instance, flexural damage or failure can trigger or be followed by failure in shear (Ozcebe and Saatcioglu, 1989). Flexural-sliding shear

failure is one of the clear examples of this type. Since parameters like horizontal and vertical reinforcement content, wall geometry, axial force, loading type, and higher mode effects may affect the behavior of RC wall, especially in squat walls, there may be some exceptions in the above classification (Gulec and Whittaker, 2009). It is known that yielding in flexure reduces shear capacity of a RC member. Therefore, after a member yields in flexure, shear failure may happen if shear capacity of that member is slightly larger than flexural capacity. According to JSCE seismic design code, shear failure may occur in RC members that their shear capacity is not larger than twice of flexural capacity (Maekawa et al., 2003).

2.5. Seismic code provisions regarding wall section dimensioning and reinforcement detailing

2.5.1. Turkish earthquake code (TEC-2007)

According to Turkish earthquake code (TEC-2007) shear wall is considered as vertical load bearing elements with length to thickness ratio of at least seven. This code classifies reinforced concrete walls into two categories as walls with normal ductility level and walls with high ductility level. However, except provision about design moment and shear forces and provisions about coupled walls and walls with openings all other detailing requirements are the same for normal and high ductility walls.

In the cases that Eq (2.2) and Eq (2.3) are simultaneously satisfied, wall web thickness (b_w) must not be smaller than $\max\left(\frac{h_{st}}{20}; 150 \, mm\right)$. Otherwise, wall web thickness must not be smaller than $\max\left(\frac{h_{st}}{20}; 200 \, mm\right)$.

$$\sum A_g / \sum A_p \geq 0.002 \qquad (2.2)$$

$$V_t / \sum A_g \leq 0.5 f_{ctd} \qquad (2.3)$$

Where $\sum A_g$ stands for total cross section area of RC shear walls parallel to the considered direction of earthquake at each story level. $\sum A_p$ is the sum of plan area of all stories. f_{ctd} represents concrete design tensile strength and V_t is the total base shear. h_{st} is the highest story height of the building.

For walls having $H_w/l_w > 2.0$ boundary confined regions must be provided. H_w and l_w is wall height and wall length, respectively. For walls within this range of aspect ratio except for the cases that Eq (2.2) and Eq (2.3) are simultaneously satisfied, thickness of wall boundary region must not be smaller than $\max(\frac{h_{st}}{15}; 200\ mm)$. RC wall minimum detailing requirements of TEC-2007 are schematically illustrated in Figure 2.11.

Critical wall height starting from foundation or the level corresponding to more than 20% reduction in wall length and over which plastic hinge is expected to be formed must satisfy Eq (2.4).

$$\max(l_w; H_w/6) \leq H_{cr} \leq 2l_w \qquad (2.4)$$

Minimum total area of transvers and longitudinal reinforcement in wall web cannot be less than 0.0025 times the gross section area of wall web (area between exterior boundary regions). If $H_w/l_w \leq 2.0$, whole gross section of the wall including boundary regions shall be considered as wall web. Transvers and longitudinal reinforcement spacing in wall web must not be larger than 250 mm. In the cases that Eq (2.2) and Eq (2.3) are simultaneously satisfied, minimum total area of transvers and longitudinal reinforcement in wall web can be reduced to 0.0015 times the gross section area of wall web. However, transvers and longitudinal reinforcement spacing in wall web must not be larger than 300 mm in this case.

Wall end region

End region vertical reinforcement $\geqslant 0.001\, b_w \ell_w$ min $4\phi14$

$\leqslant 250$ mm $\leqslant 250$ mm

min $\phi8$

$s \leqslant 200$ mm
$s \leqslant b_w$

End region vertical reinforcement $\geqslant 0.002\, b_w \ell_w$ min $4\phi14$

Critical wall height H_{cr}

50 mm $\leqslant s \leqslant 100$ mm
$s \leqslant b_w/2$

Wall end region

$\ell_w \geqslant 7\, b_w$

Wall end region   Wall web   Wall end region

b_w

$a \leqslant 25\phi_{etr}$ a ℓ_u ℓ_u

Kesit a-a

$\left.\begin{array}{l}\ell_u \geqslant 2\, b_w \\ \ell_u \geqslant 0.2\ell_w\end{array}\right\}$ Along the wall critical height $\left\{\begin{array}{l}\geqslant 10\ pieces\,/\,m^2 \\ cross\text{-}tie\end{array}\right.$

$\left.\begin{array}{l}\ell_u \geqslant b_w \\ \ell_u \geqslant 0.1\ell_w\end{array}\right\}$ Outside the wall critical height $\left\{\begin{array}{l}\geqslant 4\ pieces\,/\,m^2 \\ cross\text{-}tie\end{array}\right.$

Wall end region   Wall web   Wall end region

b_w

Area $\geqslant b_w \ell_u$

$\ell_w \geqslant 7\, b_w$

Horizontal web reinforcement $\geqslant (\ell_u + \ell_b)$ $\geqslant (\ell_u + \ell_b)$

Figure 2.11 Section dimensioning and reinforcement detailing requirements

27

Longitudinal reinforcement ratio in each boundary regions must not be less than 0.001 above the critical height. However this amount is increased to 0.002 over the critical height. Figure 2.11 shows detailing requirements for boundary region. Minimum confinement reinforcement of boundary regions over the critical height is calculated using the Eq (2.5).

$$A_{sh} \geq \frac{2}{3}\left[0.075sb_k\left(\frac{f_{ck}}{f_{ywk}}\right)\right]$$
(2.5)

Where s is horizontal reinforcement spacing. b_k is core dimension which is separately considered for both directions. f_{ck} and f_{ywk} are concrete characteristic compressive strength and reinforcement characteristic yield strength.

According to a provision of TEC-2007, layers of reinforcement in both faces of RC wall web (interior part of wall section between exterior boundary regions) must be connected by 10 special cross-ties per 1 m^2 up to critical height and 4 special cross-ties per 1 m^2 above the critical height.

2.5.2. Turkish earthquake code (TEC-1975)

Vertical load bearing RC elements with length to thickness ratio of at least five is denoted as shear walls based on TEC-1975. In this code, minimum thickness of reinforced concrete shear walls is specified not less than $\frac{1}{20}$ of wall width, nor less than 150 mm. This minimum thickness shall be used for the first 10 m of wall height. In the cases that more detailed analysis is available for thickness calculations and the minimum thickness shall be increased in the lower stories by 20 mm per each additional 6 m height.

Shear walls minimum reinforcement ratio shall not be less than 0.0020 of total vertical reinforcement cross section area over gross cross sectional area of the shear wall in vertical direction. Additionally, Minimum horizontal reinforcement ratio shall not be less than 0.0025 of total horizontal reinforcement cross section area over gross cross sectional area of the shear wall in horizontal direction. The reinforcement spacing shall not be more than 1.5 times the wall thickness, nor more than 300 mm.

There is no explicit provision regarding confined boundary regions in TEC-1975. However, it is stated in a provision that at either end of shear walls, within a distance of 0.1 times the larger plan dimension, the vertical reinforcement spacing shall be halved.

However, in the cases that tensile stresses are present on the wall cross section; the vertical reinforcement ratio provided at the ends of walls shall not less than 0.005 for St I, 0.004 for St II and 0.005 for St III.

2.5.3. ACI318-14

Similar to TEC-2007, ACI318-14 classifies cast-in-place reinforced concrete shear walls into special and ordinary shear walls. However, this code provides seismic provisions only for special RC shear walls in chapter 18. Ordinary RC shear walls complying with chapter 11 need not satisfy any detailing provisions in chapter 18.

According to ACI 318-14 for load bearing walls, axial force limit is defined as $P_u \leq \phi P_{n,max}$ where P_u is the factored design load, $P_{n,max}$ is the maximum nominal axial compressive strength and ϕ is the strength reduction factor. $P_{n,max}$ is calculated by $P_{n,max} = 0.8P_0$ for nonprestressed elements with ties. In this

relation P_0 is nominal axial strength at zero eccentricity and is calculated by $P_0 = 0.85f_c'(A_g - A_{st}) + f_y A_{st}$ where A_g and A_{st} is the gross section area of the wall section and longitudinal reinforcement area, respectively. Axial strength reduction factor, ϕ, is 0.65 and 0.9 for compression-controlled and tension-controlled members, respectively. For transition-zone section, ϕ linearly changes from 0.65 to 0.9.

For special structural walls, the distributed longitudinal and transverse web reinforcement ratios, ρ_l and ρ_t, for structural walls shall not be less than 0.0025, except that if $V_u \leq 0.083 A_{cv} \lambda \sqrt{f_c'}$, these ratios can be reduced to 0.0015 for ρ_l and 0.0025 for ρ_t. A_{cv} refers to the shear plane area which is equal to web thickness multiplied by wall length. λ is one for normal weight concrete. Longitudinal and horizontal reinforcement spacing shall not exceed (450 mm). According to ACI318-14 walls shall have distributed shear reinforcement in two orthogonal directions in the plane of the wall and if $h_w/l_w \leq 2.0$ longitudinal reinforcement ratio ρ_l shall be at least equal to transverse web reinforcement ratio ρ_t. In the cases that $V_u > 0.17 A_{cv} \lambda \sqrt{f_c'}$ or $h_w/l_w \geq 2.0$ at least two curtains of reinforcement at both faces of wall shall be used. h_w and l_w are total height and length of the wall, respectively. Transvers reinforcements which are considered in nominal shear capacity shall be continues and distributed across the shear plane.

For shear wall with flanged sections, effective flange width shall be considered from the face of the wall to a distance equal to the lesser of one-half the distance to an adjacent wall web and 25 percent of the total wall height.

Specially confined boundary elements are needed in the case of high compressive stresses and strains in wall edges. According to ACI318-14 there are two approaches, stress based and strain based, to determine whether special boundary regions in wall edge are needed or not.

Considering strain based approach, walls with $h_w/l_w \geq 2.0$ shall have confined boundary regions in compression zones where $c \geq \dfrac{l_w}{600\left(\frac{1.5\delta_u}{h_w}\right)}$. Parameter c corresponds to the largest neutral axis depth calculated for the factored axial force and nominal moment strength consistent with the direction of the design displacement δ_u. Ratio δ_u/h_w shall not be taken less than 0.005. Reinforcement detailing requirements of boundary elements when strain based approached is utilized are schematically illustrated in Figure 2.12.
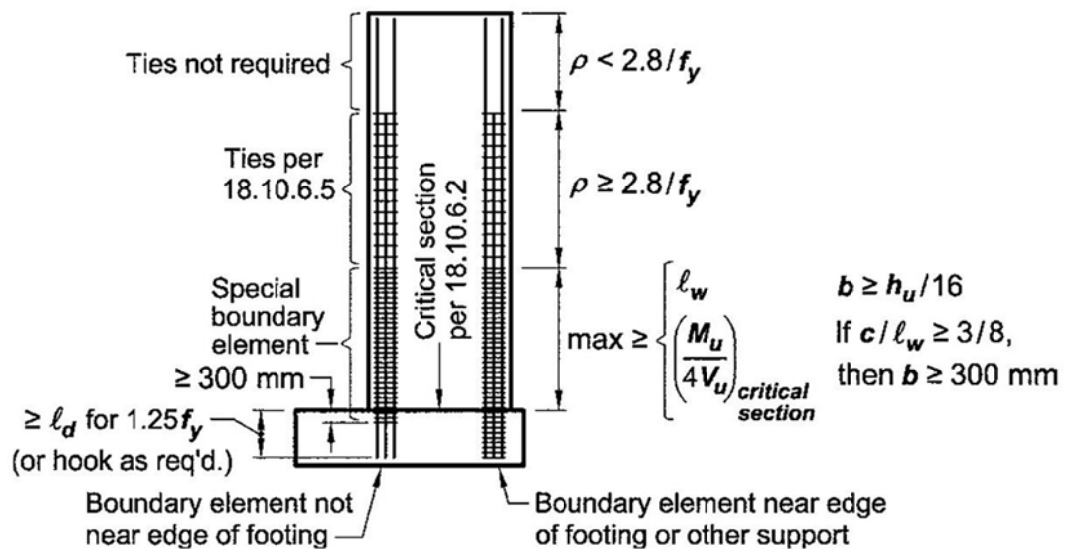
Figure 2.12 Boundary element requirements-strain based approach (ACI318-14)

According to stress base method, special boundary element is needed where the maximum compressive stress in extreme fiber of wall section exceeds $0.2f_c'$ under factored loads. Special boundary element can be discontinued at a point over the wall height where compressive stress is less than $0.15f_c'$. Figure 2.13 schematically illustrates reinforcement detailing requirements of boundary elements when stress based approached is utilized.
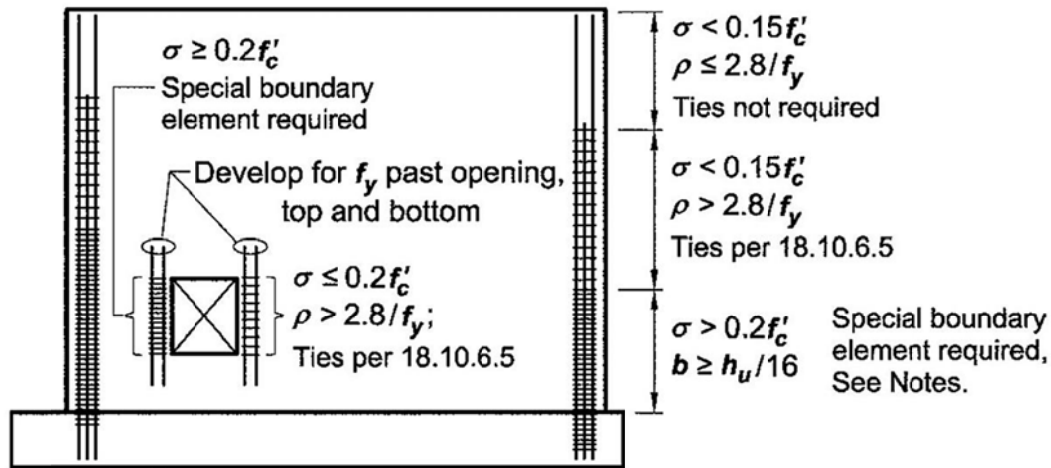
Figure 2.13 Boundary element requirements-stress based approach (ACI318-14)

In flanged sections, up to effective flange width shall be considered as part of boundary element and shall extend at least 300 mm into the web.

The amount of transverse reinforcement, A_{sh}, for rectilinear hoops is calculated according to Eq (2.6) and Eq (2.7).

$$A_{sh} \geq sb_c \left[0.3 \left(\frac{A_g}{A_{ch}} - 1 \right) \frac{f'_c}{f_{yt}} \right] \qquad (2.6)$$

$$A_{sh} \geq sb_c \left[0.09 \frac{f'_c}{f_{yt}} \right] \qquad (2.7)$$

Where A_{ch} is the core cross-sectional area of boundary element measured to the outside edges of transverse reinforcement. A_{sh} stands for total cross-sectional area of transverse reinforcement, including crossties, within spacing s and perpendicular to dimension b_c, which is cross-sectional dimension of boundary element core measured to the outside edges of the transverse reinforcement. A_g is the gross area of boundary element. Some other detailing requirements such as

32

horizontal reinforcement spacing and dimensions of boundary element are provided in Figure 2.14.

Even if special boundary elements are not required, ties or transvers reinforcements are needed in order to prevent buckling of longitudinal reinforcements in wall boundaries which may happen in load reversals. If the longitudinal reinforcement ratio at the wall boundary $\rho > 2.8/f_y$, the horizontal distance, h_x, between longitudinal bars laterally supported by the corner of a crosstie or hoop leg shall not exceed 350 over the length l_{be} which is grater of $c - 0.1l_w$ and $c/2$. Within a distance equal to the greater of l_w and $M_u/4V_u$ above and below critical sections vertical spacing of transvers reinforcements shall not exceed the lesser of 150 mm and $6d_b$ of smallest longitudinal bar. Outside this range of wall height this amount must not exceed the lesser of 200 mm and $8d_b$.

If special boundary element is not required, except where $V_u < 0.083A_{cv}\lambda\sqrt{f_c'}$ horizontal reinforcement shall have a standard hook engaging the edge vertical reinforcement or the edge vertical reinforcement shall be enclosed in U-stirrups having the same size and spacing as, and spliced to, the horizontal reinforcement.

$$\ell_{be} \geq \begin{cases} \dfrac{c}{2} \\ c - 0.1\ell_w \end{cases}$$

$$h_x \leq \begin{cases} 350\ mm. \\ \dfrac{2}{3}b \end{cases}$$
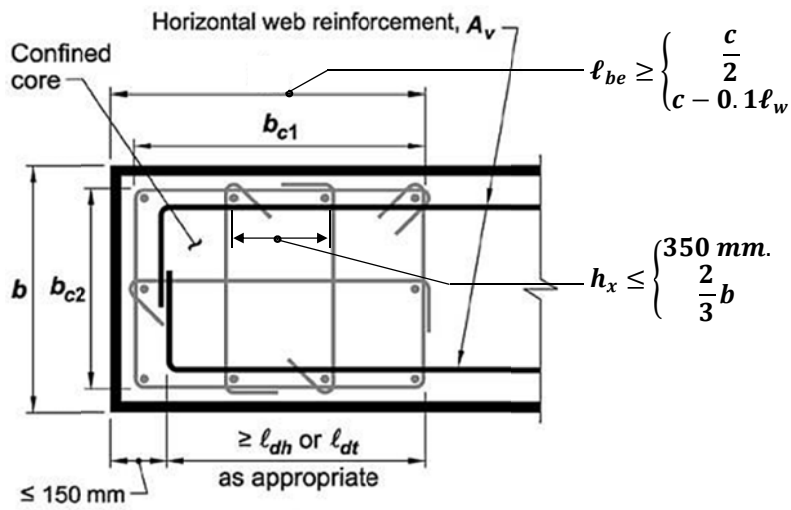
$$S_{sh} \leq \begin{cases} \dfrac{1}{3}\ of\ min(\ell_{be}, b) \\ 6d_b\ (smallest\ longitudinal\ bar) \\ 100\ mm \leq s_o = 100 + \left(\dfrac{350 - h_x}{3}\right) \leq 150\ mm \end{cases}$$

ℓ_{dh} = Development length in tension of deformed bar with a standard hook, measured from outside end of hook

ℓ_{dt} = Development length in tension of headed deformed bar, measured from the bearing face of the head
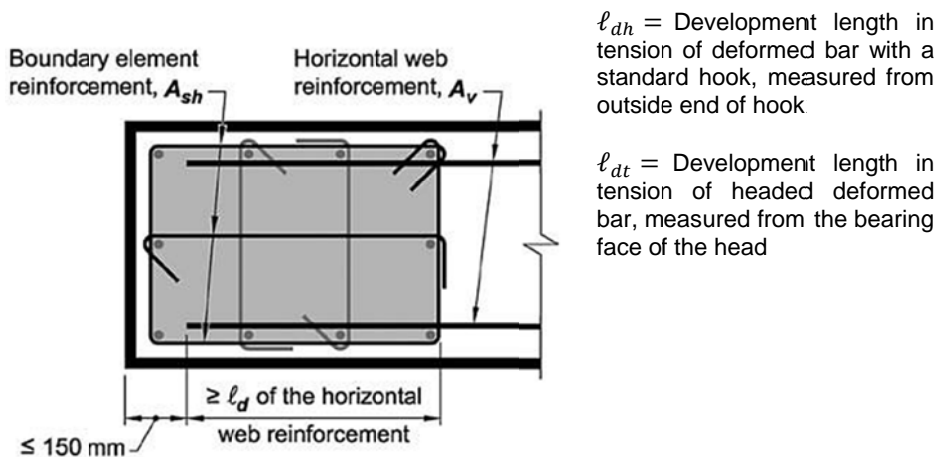
If $\ell_{be} \geq 150mm + \ell_d$ and $\dfrac{A_{sh} \times f_{ysh}}{s_{sh}} \geq \dfrac{A_v \times f_{yv}}{s_v}$

Figure 2.14 Wall boundary detailing requirements (ACI318-14)

CHAPTER 3

QUASI-STATIC REVERSED CYCLIC TESTS ON RC SHAER WALL SPECIMENS

3.1. General

In the context of this thesis, the seismic performance of two code compliant reinforced concrete (RC) frames were investigated by reversed cyclic quasi-static loading schemes. This chapter presents the details of experimental setup and instrumentation, employed loading protocol, specimen geometry, reinforcement detailing and material properties used in the construction of specimens. In addition, the observed behavior of the specimens during the tests is discussed in following parts of this chapter.

The seismic behavior of the selected test frames, in terms of actual deformation and lateral load strength obtained through implementation of reversed cyclic quasi-static loading tests, is also examined in this chapter. Furthermore, shear capacities are calculated according to the code equations and compared with test results in order to predict failure modes.

All the test frames were ½-scaled, three-story and three-bay RC frames which were constructed for this study in the Middle East Technical University Structural Mechanics Laboratory. These frames represent one of internal frames of three-story prototype buildings designed and constructed based on two different generations of Turkish Earthquake Code namely TEC-2007 and TEC-1975. The first specimen, named here after in this thesis as RC-SW1, was a RC frame with

RC shear wall in the middle bay. RC-SW1 specimen was designed and constructed based on TEC-2007. Some rigid criteria such as low spaced stirrups and large longitudinal and transvers reinforcement ratio for detailing of boundary regions in RC shear walls are given by TEC-2007, which drives designers to abandon using shear walls as lateral load-carrying system. In order to investigate the effect of confinement requirements of boundary regions of RC shear walls, it was aimed to compare one more detailed and one lightly detailed boundary regions. Therefore, another RC frame with RC shear wall in the middle bay, designed based on TEC-1975, was constructed and tested. The latter specimen was tagged as RC-SW2 throughout the thesis. It is noteworthy to mention that TEC-1975 specifies minor requirements without confinement reinforcements for boundary regions of shear walls.

3.2. Test frames, experimental setup and instrumentation

The test specimens are three-story, three-bay RC frames. These frames represent the interior bays of three-story prototype buildings which were scaled to ½ based on similitude law (Figure 3.1).
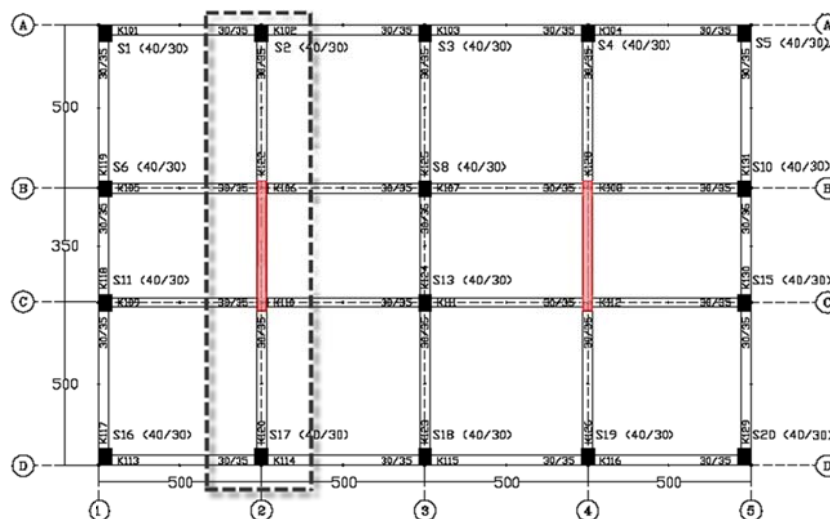
Figure 3.1 Plan view of prototype building

36

Global dimensions of the test frames were 4,500 mm in height and 6,950 mm in length in the direction of loading. The first story's height is 1,438 mm. This amount is 1,500 mm for second and third stories. Total length of the RC shear wall which covers the entire middle bay is 1945 mm. Free span length of beams adjacent to RC wall was 2302.5 mm for exterior bays. The general view of the RC-SW1 and RC-SW2 specimens are presented in Figure 3.2 and Figure 3.7, respectively. The 175 mm × 150 mm T-shaped section was selected for beams including 500-mm wide, 60-mm thick slab (Figure 3.3 and Figure 3.8). The slab part of beams was provided to consider the slab effect and to provide support for the steel blocks which represent the gravity loads. Slab didn't continue through RC shear wall. Columns were proportioned as rectangular shaped section with dimensions of 200 mm in length and 150 mm in width (Figure 3.4 and Figure 3.9).

The amount of reinforcement and tie spacing used were in compliance with the Turkish Earthquake Code (2007) provisions for specimens RC-SW1 and Turkish Earthquake Code (1975) provisions for RC-SW2 specimen. Eight mm and 10-mm deformed (ribbed) bars were used as longitudinal reinforcement in beams and columns. Four mm plain (smooth) bars were used as transverse reinforcement in the beams and the columns. Slab reinforcements are 4-mm plain bars as well (Figure 3.3 and Figure 3.8). Detailing of the interior RC shear walls in RC-SW1 and RC-SW2 are illustrated in Figure 3.5 and Figure 3.10, respectively.

Top and bottom longitudinal reinforcements of exterior beams were anchored in the shear wall in the length of about 500 mm (Figure 3.3). Since the thickness of the shear wall was less than beams width, top and bottom rebar of beam section were bended inside with the slope of $\frac{1}{6}$ to be anchored in the core part of wall section, Figure 3.3.

Figure 3.2 Overall view of the specimen RC-SW1

* All dimension units are in mm
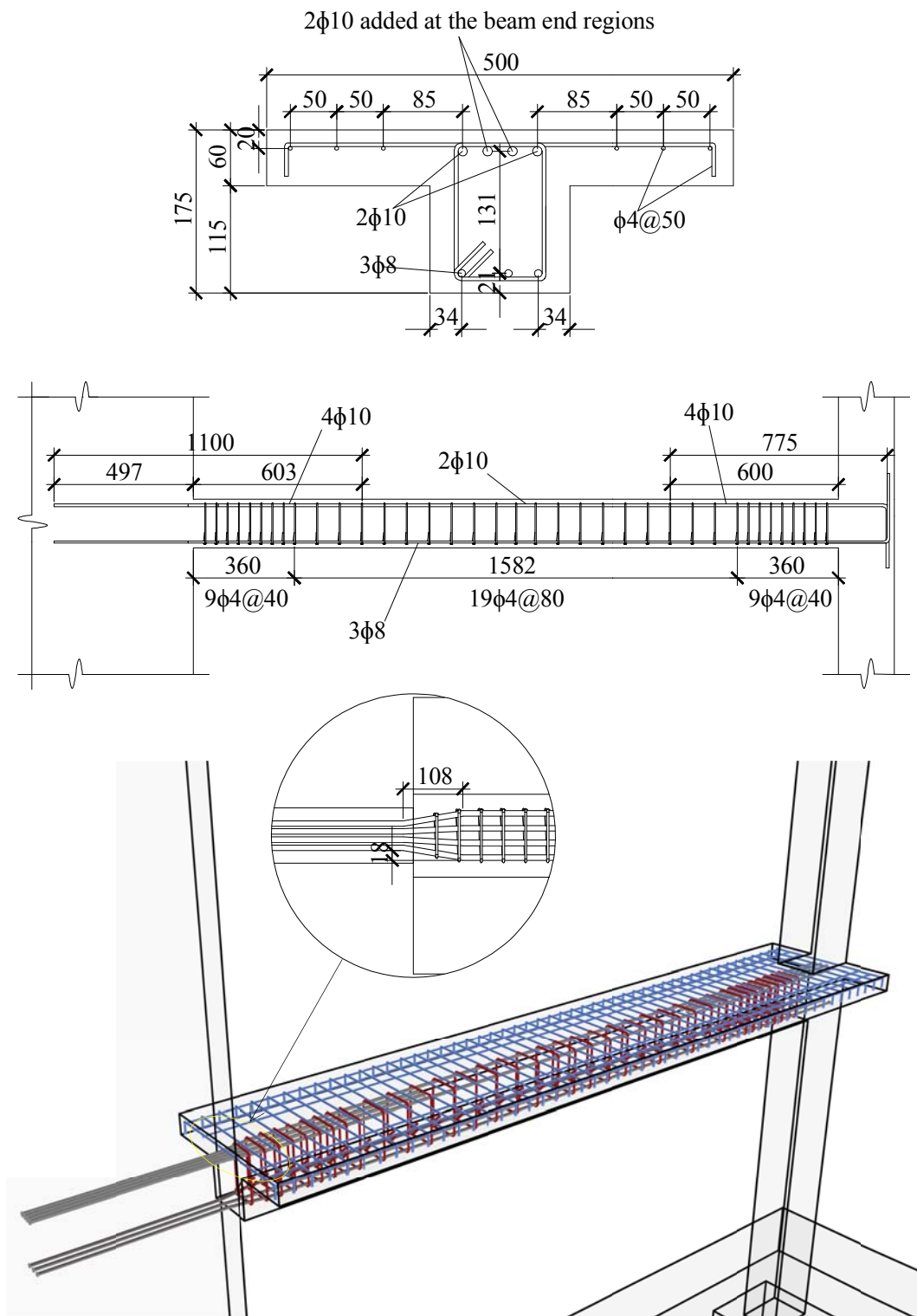
Figure 3.3 Beam section in RC-SW1
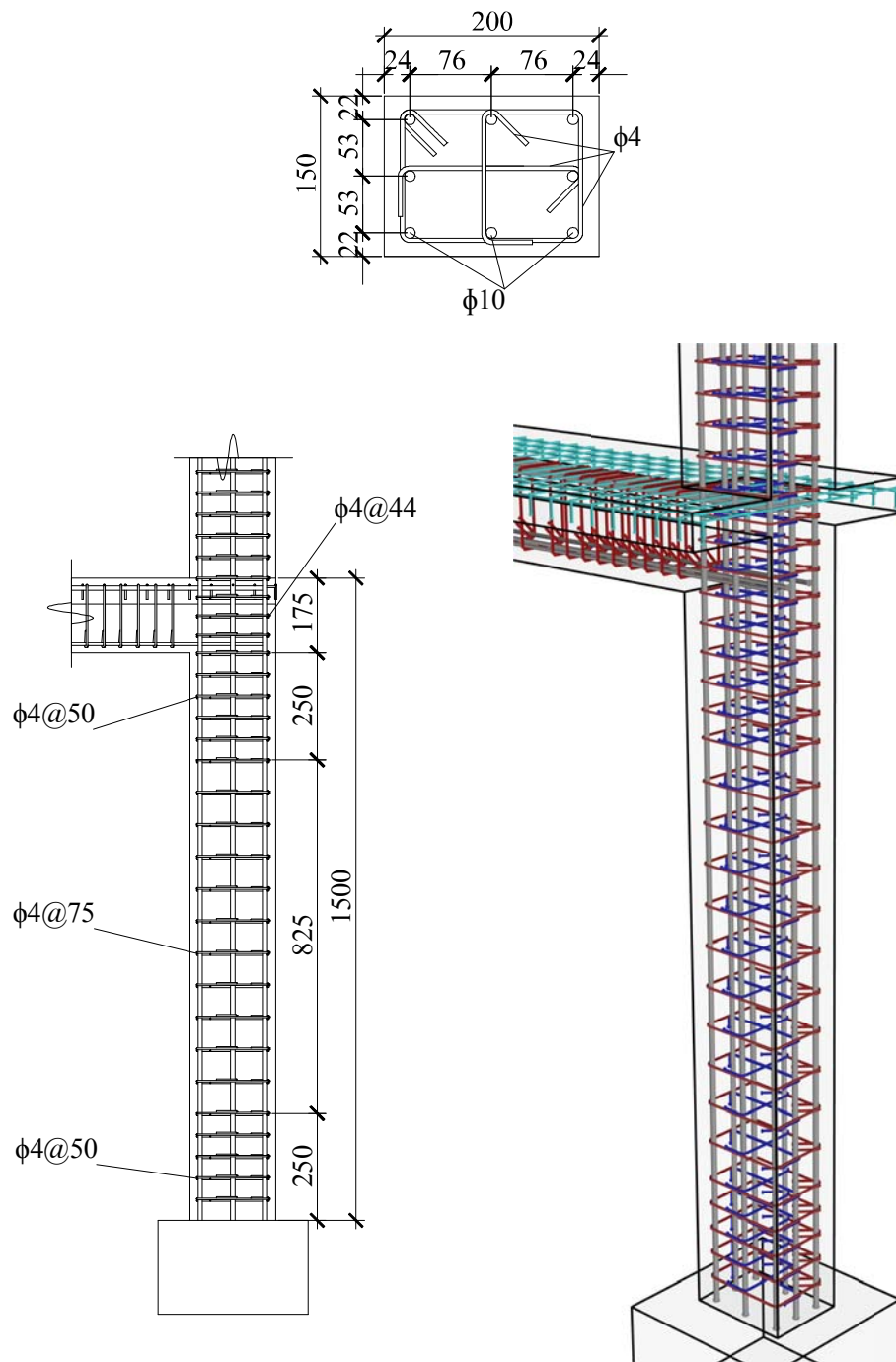
Figure 3.4 Column section in RC-SW1
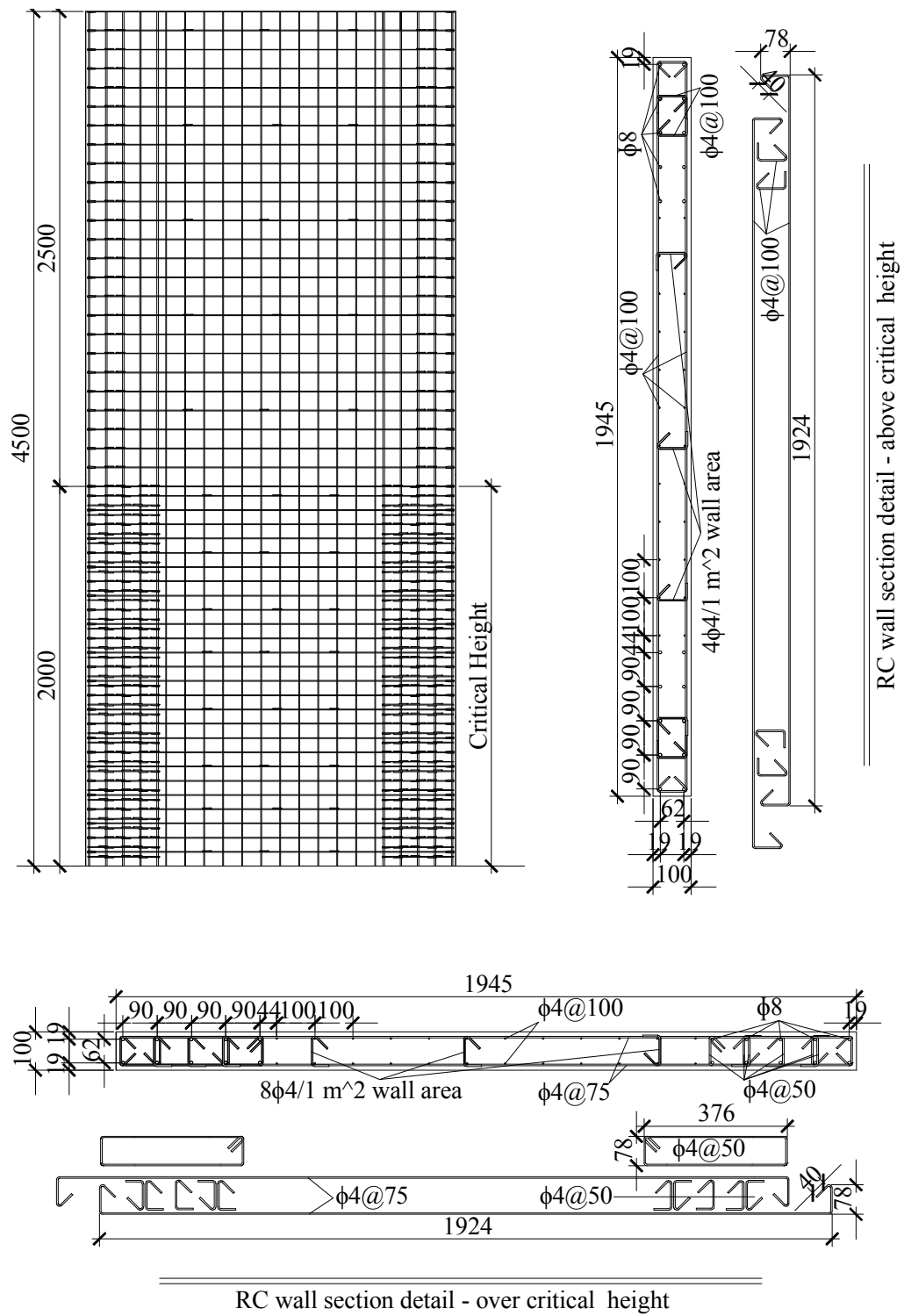
Figure 3.5 Characteristics of RC shear wall in RC-SW1

41

All longitudinal reinforcements of exterior columns were welded to the base plates connected to the force transducers which were attached to the foundations. Some of the shear wall longitudinal bars that intersected the base plates fixed to the foundation surface were directly welded to them. To provide load transfer between shear wall and existing foundation, total 8 dowels constituting four 12-mm and four 10-mm ribbed bars were used as anchorage dowels along the center line in the direction of shear wall width. Figure 3.6 shows anchorage detail of shear wall for RC-SW1. In order to place anchorage dowels, two holes with depth of 180 mm (15ϕ) were drilled located inside of each boundary regions of shear wall. Four equally spaced (300 mm) holes with a depth of 150 mm (15ϕ) were drilled out inside the shear wall as well. Afterwards, the surface of the foundation was scratched to secure better adhesion between formerly casted and newly placed concrete (Figure 3.13). Later, the surfaces of the foundation and anchorage holes were cleaned up. Anchorage holes were filled up with epoxy and 12- and 10-mm dowels were inserted in holes in boundary and middle regions, respectively. Total cross section area of dowels in boundary region and middle region exceeded the total cross section area of longitudinal reinforcements in boundary region and middle region, respectively. As indicated in Figure 3.6, 360 mm of 12-mm and 300 mm of 10-mm anchorage dowels were left above the foundation. Since the foundation and anchorage dowels remained undamaged during cyclic tests on RC-SW1, they were reused for foundation and anchorage of shear wall in specimen RC-SW2.
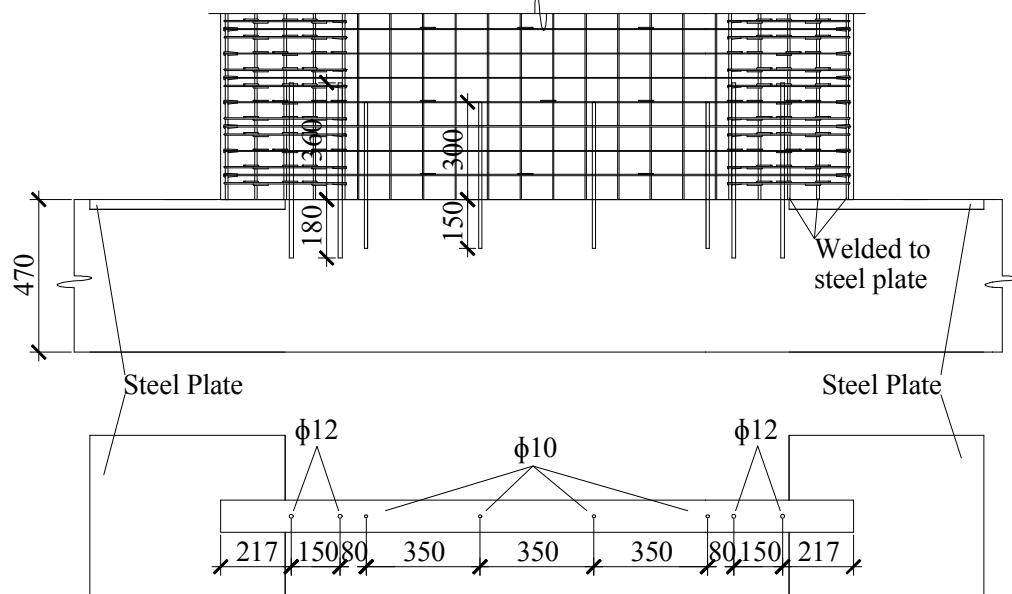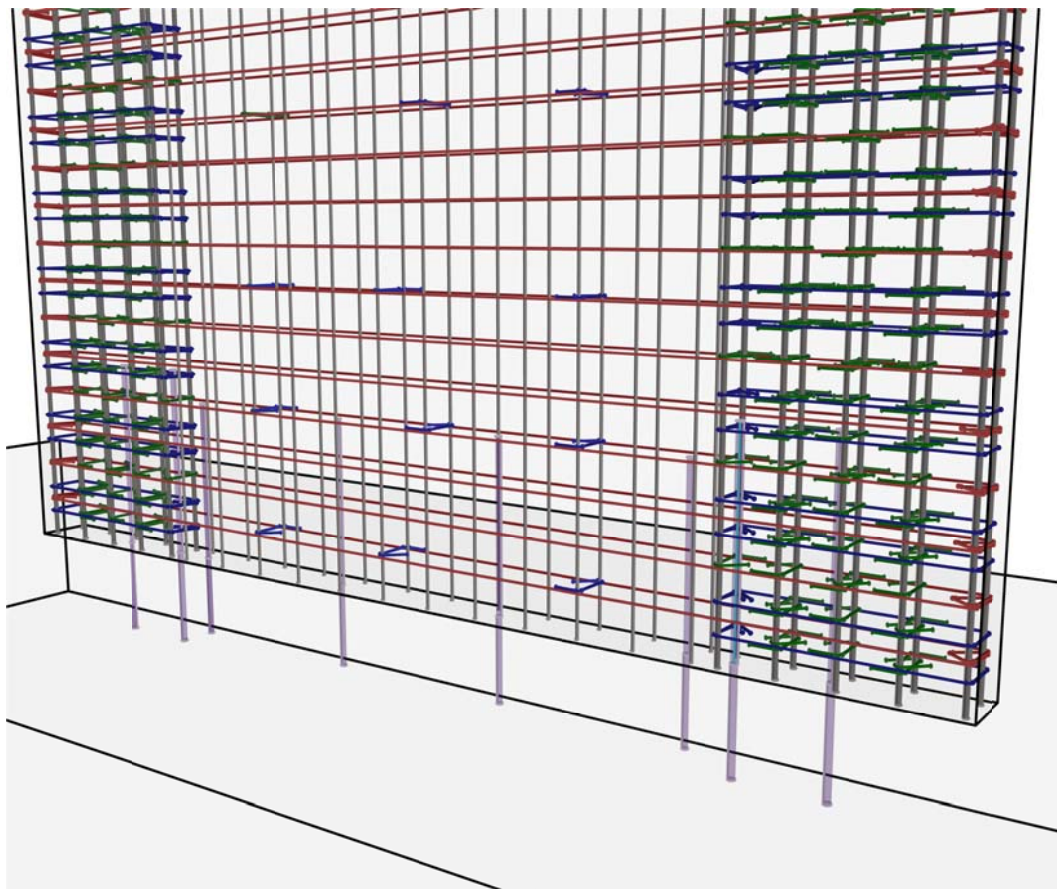
Figure 3.6 3D view of lower part of RC-SW1wall detailing and anchorage details

Figure 3.7 Overall view of the specimen RC-SW2

44

2ϕ10 added at the beam end regions
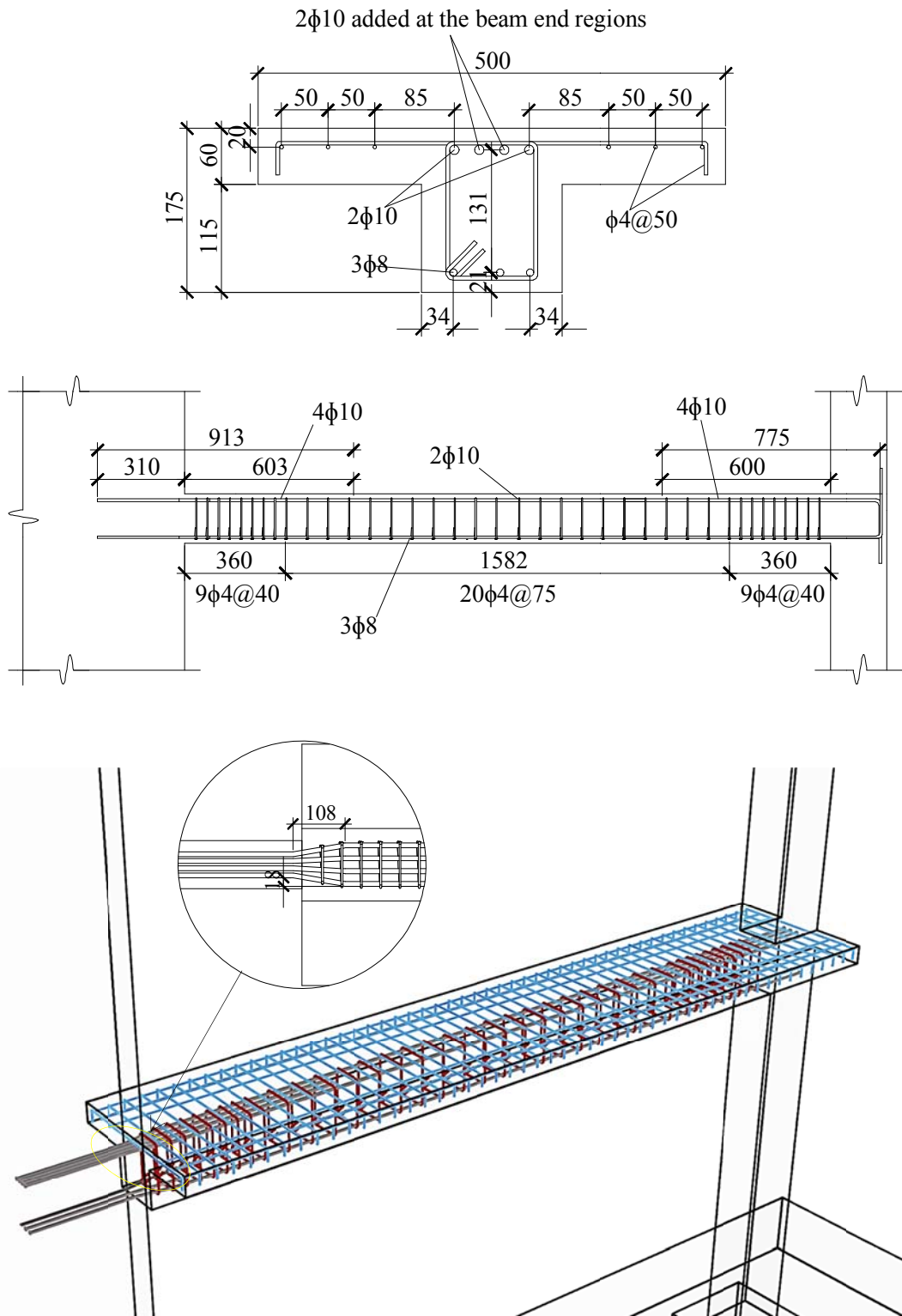
Figure 3.8 Beam section in RC-SW2

45
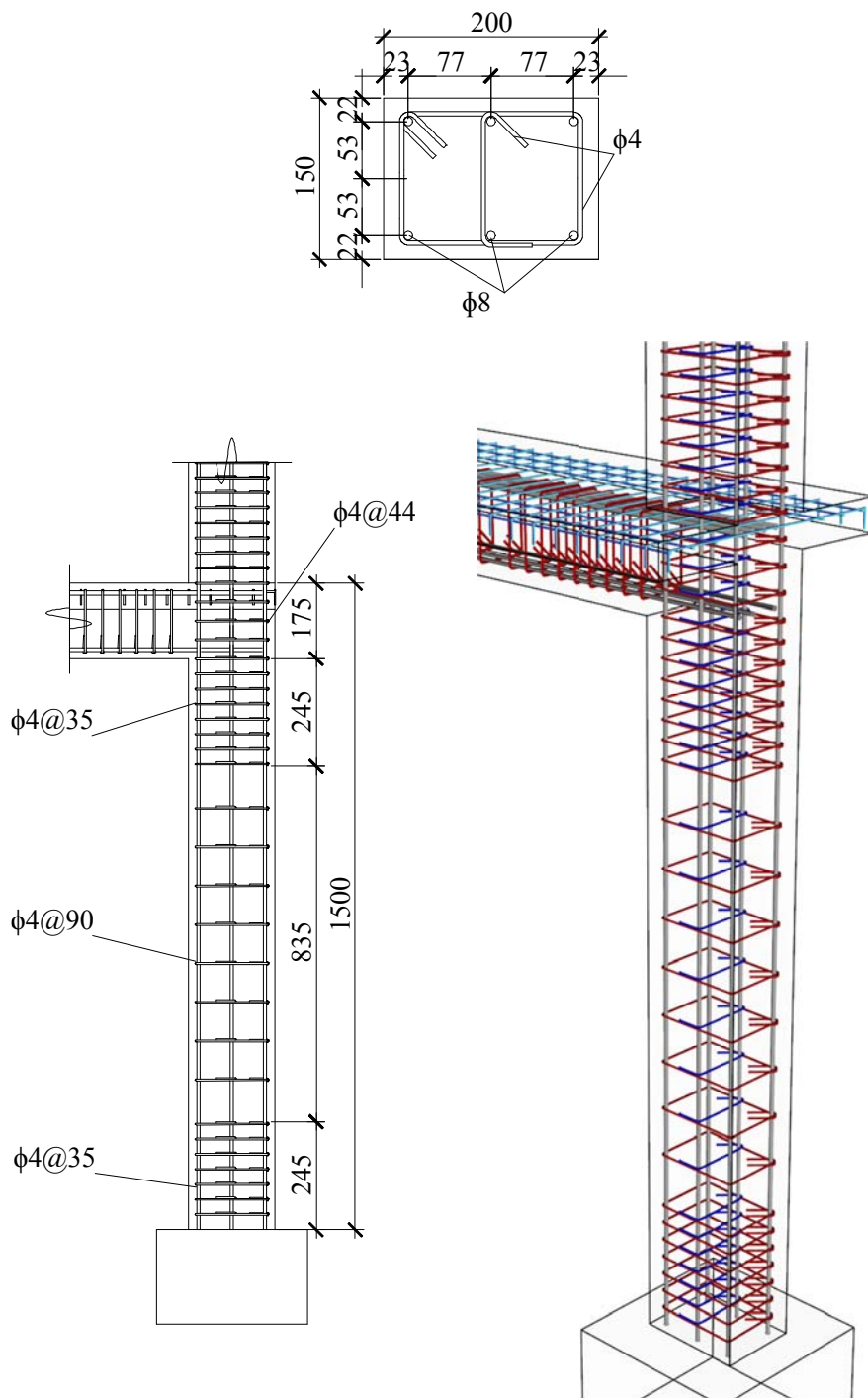
Figure 3.9 Column section in RC-SW2

4500

1945

50 50 50 61 00 100   φ4@100   4φ4@50 17

100 17 17 99

5φ4/1 m^2 wall area   φ4@100

φ4@100

1924   40 78

RC wall section detail
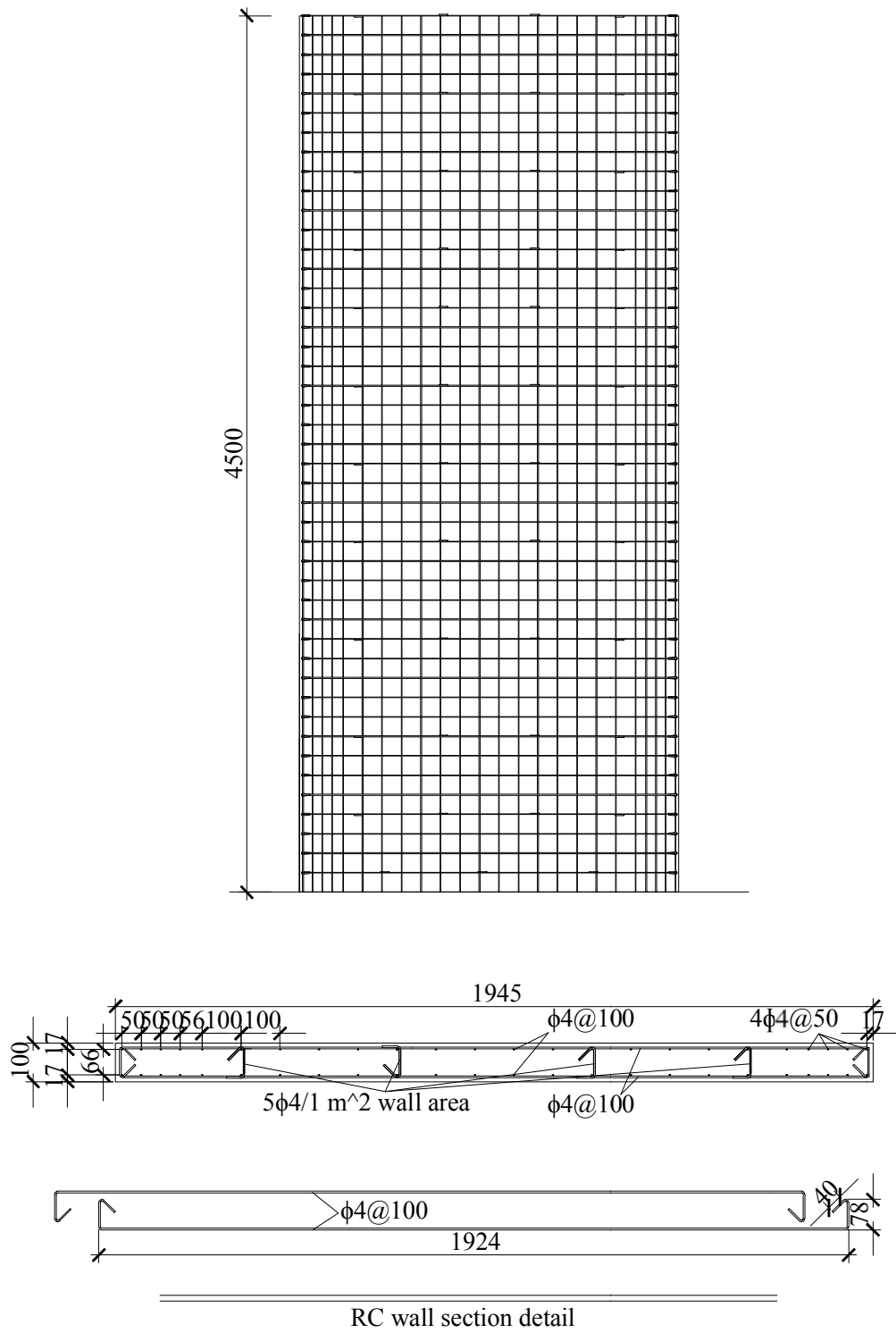
Figure 3.10 Characteristics of RC shear wall in RC-SW2
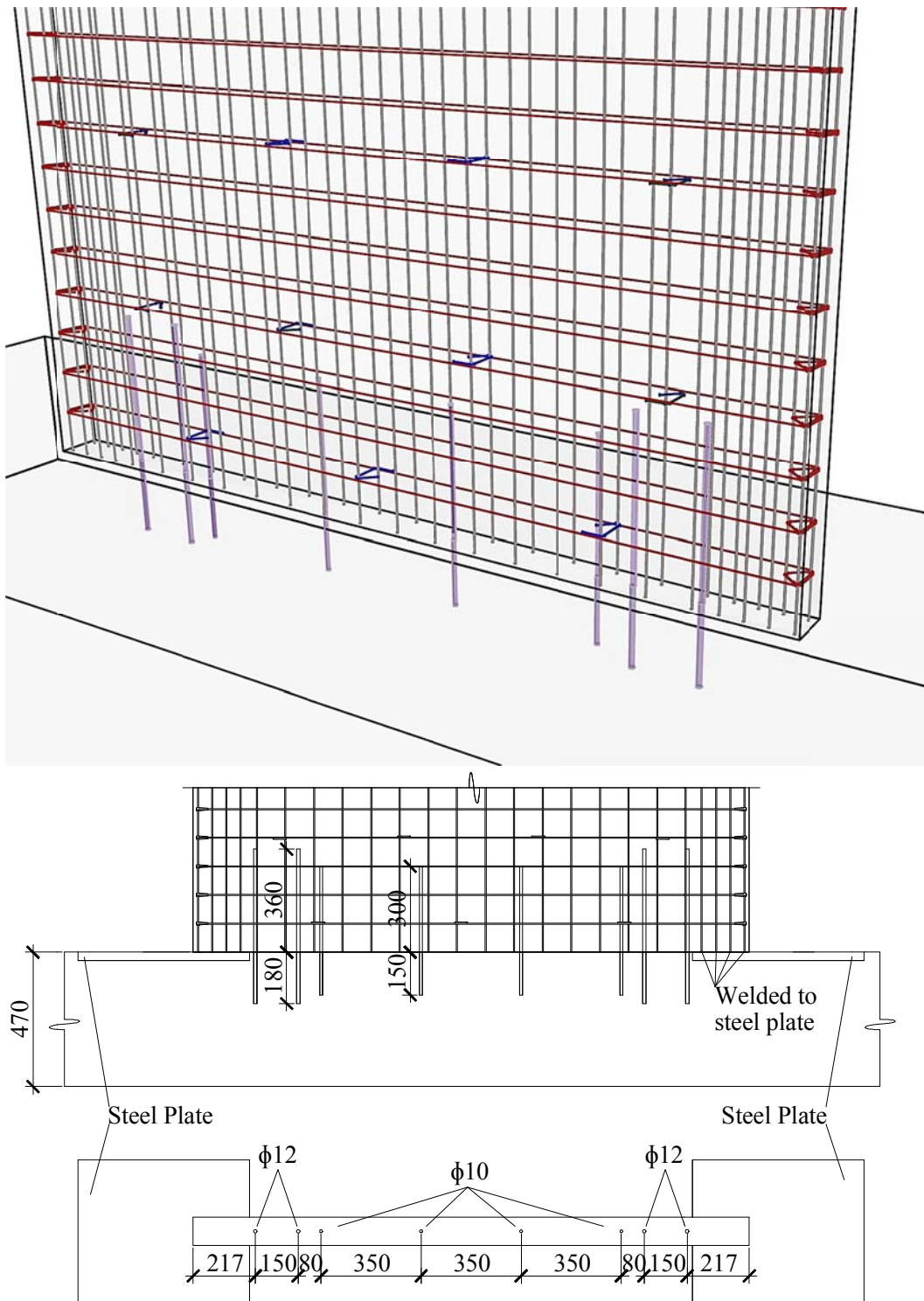
Figure 3.11 3D view of lower part of RC-SW2 wall detailing and anchorage details

Reactions (bending moment, axial force and shear force) at the base of external columns were measured using two special force transducers developed by Canbay et al. (2004). These transducers were manufactured, calibrated, and placed between base of the external columns and the foundation block. Longitudinal reinforcements of external columns were welded to base plates that were connected to transducers (Figure 3.13). Transducers were fixed to the foundation block by using bolts (Figure 3.14).

During the tests, global and local behavior of the test frame were monitored through taking measurements including story displacements and forces, end rotations of beams and columns of first and second stories, and shear deformation of RC wall. Figure 3.12 shows the layout of instrumentation installed on the test frame. The story displacements were recorded by 2 Linear Variable Differential Transformer (LVDT) and one High Accuracy Linear Encoder (HEIDENHAIN length gauges) attached to one of the frame outer faces at the center of area of T-beam at each story level. Three load cells were located between the actuator and test frame at story levels. Beams' and columns' end rotations were calculated using the recorded elongations and contractions of the outer edges of these members by means of LVTDs over the predefined plastic hinge length of about 200 mm for columns and 110 mm for beams. These average rotations were obtained from the average curvatures and average strains. The average curvature profile of the RC wall over the height of the RC wall was computed using the LVDT measured wall edge elongations and contractions at the same height at both edges considering Euler–Bernoulli bending theory assumption which is plane section remain plane role. Shear deformations of the RC wall were determined using diagonal measurements on wall panel.

The arrangement of the LVDT chains on RC wall made it possible to derive the contribution of the shear and flexural deformations separately to the total displacement of the wall. Flexural displacements of the wall panel were obtained

49

Figure 3.12 Layout of instrumentation

50

by double-integrating the wall average curvature profile (Dazio, Beyer, & Bachmann, 2009).

Figure 3.2 illustrates schematic view of loading system. The lateral loads were applied to the specimen with three servo-controlled hydraulic actuators. They were mounted on the laboratory reaction wall at each story level (Figure 3.2 and Figure 3.7). The actuators directly push the test frame at each story level and pull it with rods tied to the stiffened thick plates attached to the outer sides of the frame. Load cells, having capacity of 500 kN, were located between actuators and test frame to measure story forces. Gravity loads were simulated using steel blocks located on the slabs (Figure 3.2 and Figure 3.7) during the construction stage. The total weight of steel blocks on exterior spans in first, second and third stories are 90.6, 90.6 and 86.8 kN, respectively.

Some sample pictures of reinforcement placement and casting stage, steel molds, welding detail of columns longitudinal reinforcements and surrounding framework were also presented in Figure 3.13 and Figure 3.15. Some of longitudinal reinforcements of internal RC shear wall which crossed the base plate left on the surface of the foundation block during casting the foundation were directly welded to it.

6φ8 were welded to base plate

←Weld

Figure 3.13 Construction stages of RC-SW1

Figure 3.14 Test setup and instrumentation

8ϕ4 were welded to base plate

Weld

Figure 3.15 Construction stages of RC-SW2

3.3. Material Properties

The mechanical properties of materials used in the construction of the specimens such as average tensile yield strength (f_y) and tensile strength of reinforcements (f_u) and average concrete compressive strength (f_c) were tabulated in Table 3.1 and Table 3.2. The concrete compressive strength was the average compressive strength of 150 mm diameter and 300 mm high cylindrical concrete samples taken during the fabrication of the frames and tested on frame test date. No tensile test was done.

Table 3.1 Mechanical properties of steel reinforcements

Property	Reinforcement type		
	ϕ4 (Smooth)	ϕ8 (Ribbed)	ϕ10 (Ribbed)
Nominal diameter, d, mm	4	8	10
Equivalent diameter, d_{eq}, mm	4.02	8.40	9.86
Yield strength f_y, MPa	272.5	434.9	451.4
Yield strain, ε_y	0.001389	0.002177	0.002287
Ultimate strength, f_u, MPa	396.9	571.4	718.6
Ultimate strain, ε_u	0.138205	0.155668	0.121
Rupture strain, ε_r	0.26	0.286	0.24

Note. *Tensile strength of reinforcements was obtained based on equivalent diameter of bars instead of nominal diameter.

Table 3.2 Concrete compressive strength, MPa

Specimen	1st story	2st story	3st story
RC-SW1	29.9	28.4	29.75
RC-SW2	36.4	32.7	32.5
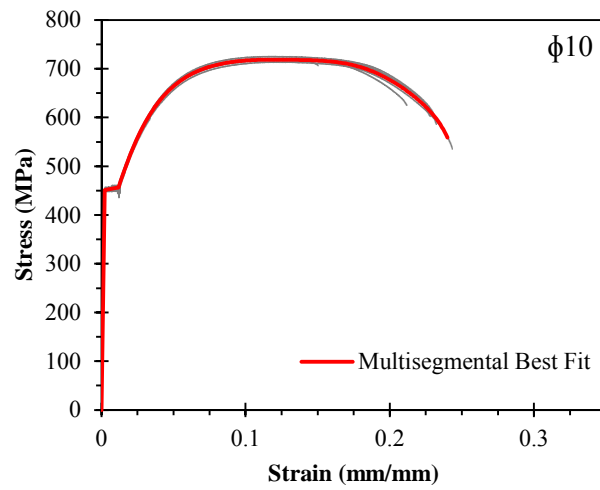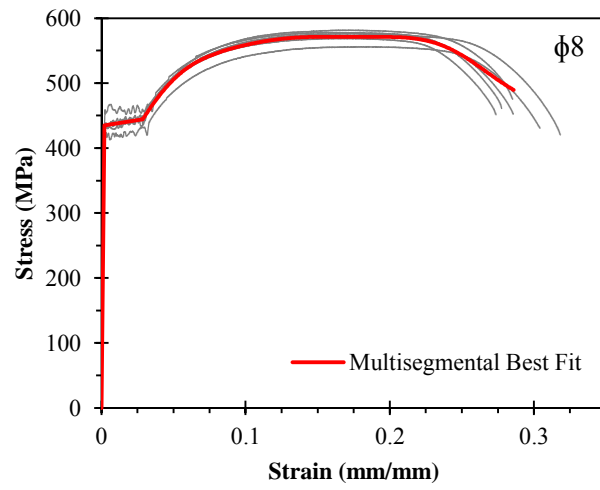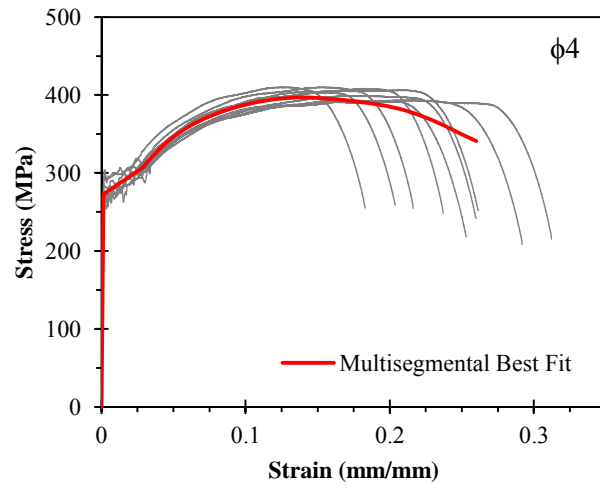
Figure 3.16 Average stress-strain relationship of steel reinforcements

3.4. Test results

3.4.1. Observed damages, sequence of events in frames and measured responses

3.4.1.1. Specimen RC-SW1

This part presents test results for specimen RC-SW1 which was designed to study the seismic performance of RC frames with RC shear walls. Additionally, it was aimed to criticize the minimum requirements of boundary regions such as minimum longitudinal reinforcement ratio; minimum stirrup ratio and spacing in that region given by TEC-2007.

This specimen was tested under lateral loads using quasi-static reversed cyclic loading protocol. A lateral load profile in accordance with first vibrating mode shape with increasing top displacement was applied to the frame. During the experiment top displacement was adjusted to reversed cycles with increasing magnitudes of amplitude by utilizing displacement control algorithm. Figure 3.17 shows the history of applied displacement at third story level. Due to technical problems in servo controlled actuators, the lateral loading system was stopped and unloaded two times at different loading cycles during the experiment. Each time the loading restarted from the point corresponding to frame residual force at uncompleted cycle and displacement history was applied from the beginning of the uncompleted cycle. Since in each abruption there were some residual force and displacement in structure and loading protocol was not adjusted to those residuals, there was some asymmetry in loading cycles.

By employing load control algorithm, actuator forces at the first and second stories were fixed to 20 and 58 (compatible with first vibrating mode) percent of applied third story force, respectively. Doing this, actually, reversed cyclic push

over loading was carried out on the specimen. This loading scheme enabled commenting on system ductility, shear force bearing capacity and damage-displacement correlations.
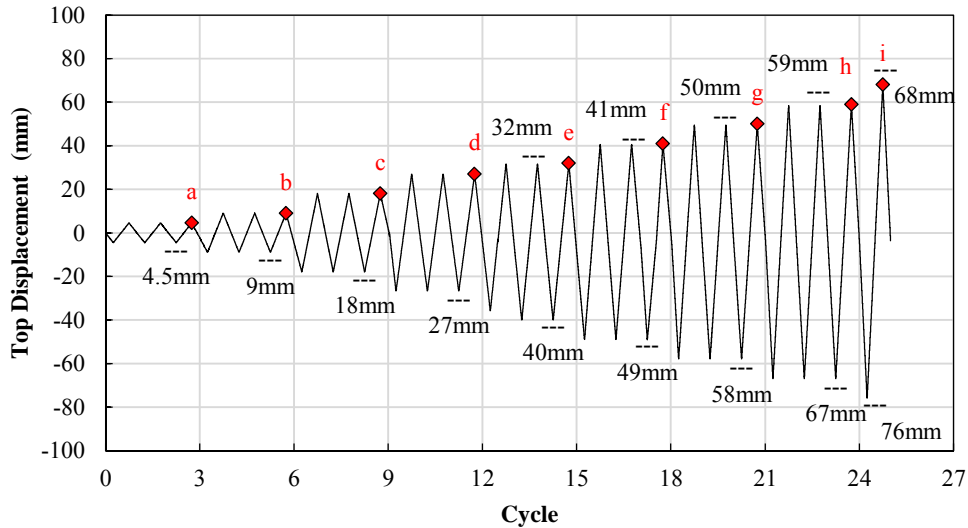
Figure 3.17 Loading cycles with increasing amplitudes of displacement applied on RC-SW1

Force and displacement histories which were recorded at each story level during the test are provided separately in Figure A.22 in Appendix A.

Hysteretic load-displacement behavior of each story are presented in Figure 3.18 and Figure 3.19. Figure 3.18 shows story shear versus inter-story drift diagram of each stories for RC-SW1. Inter-story drift ratio histories are also provided in the same figure. Overall response of frame is illustrated in Figure 3.19 demonstrating base shear-top displacement/overall drift ratio relationship.

The observed damage states at the end of cycles with same amplitude are displayed in Figure 3.20. The points corresponding to reported damage are marked as points a, b, c, d, e, f, g, h and i in Figure 3.17.
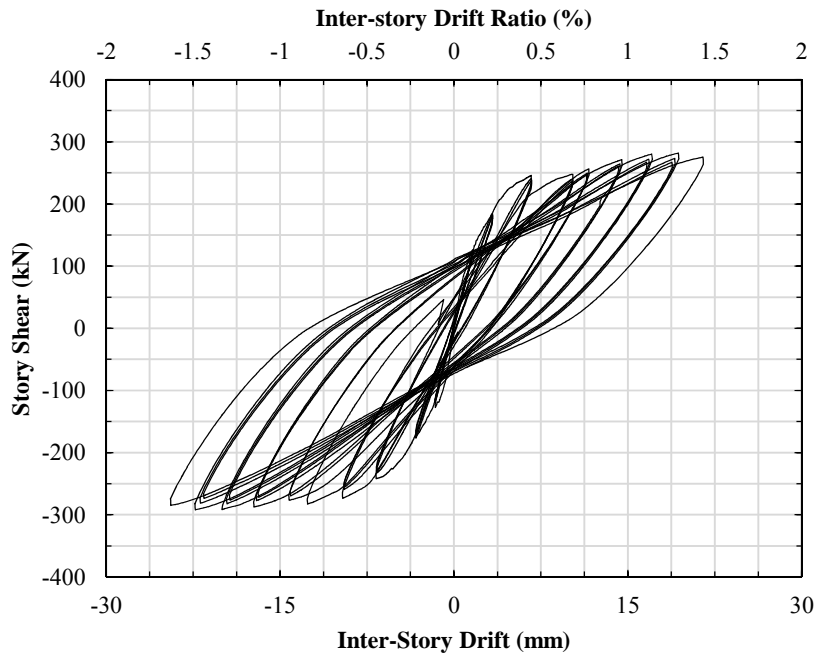
58

a)

b)

Figure 3.18 Story shear versus Inter-story displacement response of RW-SW1; a) first story, b) second story 3), third story

c)
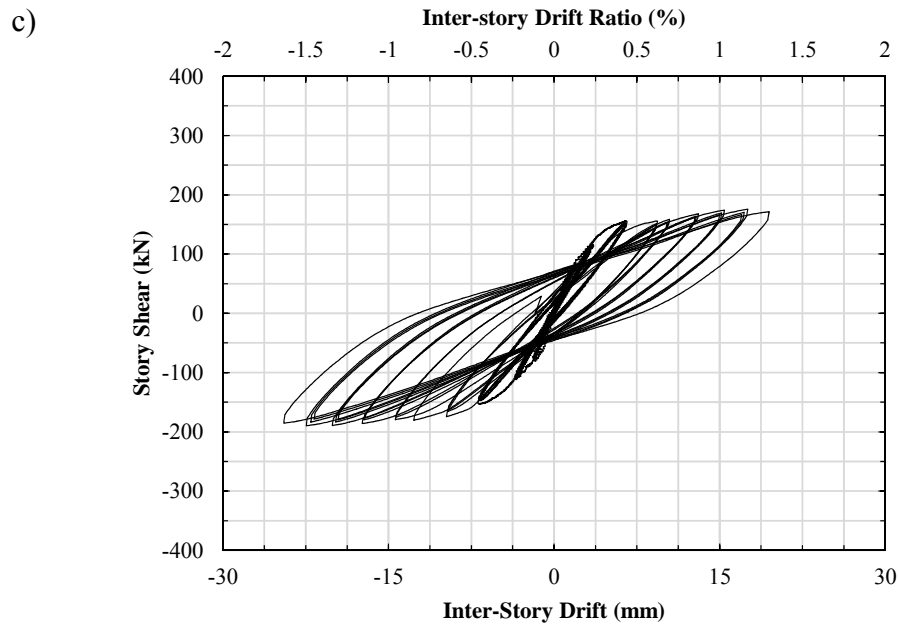
Figure 3.18 Story shear versus Inter-story displacement response of RW-SW1; a) first story, b) second story 3), third story (cont'd)

First cracks in shear wall were observed at 0.07% of first story drift ratio corresponding to overall drift ratio of 0.1% and total base shear of 142.5 kN. These cracks were a few horizontal hair line flexural cracks formed at the wall edge over the height of the wall.

At point "a" where first story drift ratio and overall drift ratio are 0.075% and 0.1% respectively, two opposite horizontal flexural cracks extended from both edges into almost half of the wall depth (

Figure 3.20). The height of the wall at which these two cracks formed was approximately 400 mm above the base of the wall. It is worth noting that anchorage dowels were cut at 360 mm and 300 mm from the base at boundary columns and wall web, respectively. Moving forward to the next peak, first diagonal crack took place at first story drift ratio of 0.1% and overall drift ratio of 0.14%. At this instance, total base shear was measured as 160.5 kN. This diagonal crack started from upper right region of
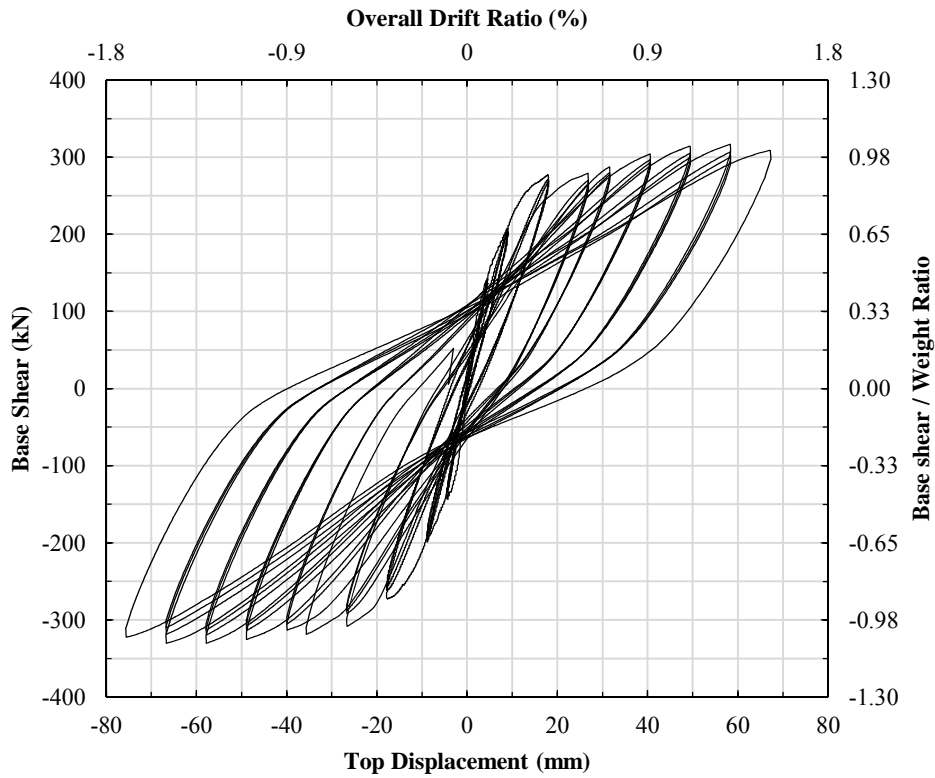
Figure 3.19 Base shear versus top displacement hysteretic response of RC-SW1

the wall at the first story level and continued downward and interconnected at the middle of wall depth with horizontal flexural crack formed in previous cycles above the anchorage dowels. During the cycles of point "b", two diagonal cracks and a flexural crack were reported as the major crack state at each direction of lateral loading. Cycle stiffness was degraded by 27% associated with formation of these cracks. First story drift ratio of 0.15% and 0.16% in negative and positive directions respectively, overall drift ratio of 0.2% and maximum of 192 kN and 204 kN of total base shear in pull and push directions were recorded at peak points of the cycles represented by point "b" (Figure 3.20).

Similar to the top-right to bottom-left diagonal crack formed in previous cycles, during the next cycle with 180 mm of top displacement, previously formed top-

left to bottom-right diagonal crack interconnects with flexural crack extended from opposite direction.

By increasing the number and amplitude of displacement cycles, flexural cracks at wall boundary regions were distributed over the height of the wall at first and second stories. Moreover, two major opposite diagonal shear cracks and two opposite flexural cracks which were formed just above the anchorage dowels got wider by increasing levels of drift ratio (points "c", "d", "e" and "f"). After extensive flexural yielding and expansion in major shear cracks RC-SW1 reached its total lateral load bearing capacity which was 316.4 kN at overall drift ratio of 1.3% in positive direction (about 1.5% of first story drift ratio) and 330.3 kN at overall drift ratio of 1.5% in negative direction (about 1.5% of first story drift ratio). Sliding shear mechanism initiated at the first peak of cycles corresponding to this level of drift ratio. Observed damage during the last cycle of point "g" was cover spall and concrete crushing in compression zone in wall edge, buckling of longitudinal bars in wall exterior edge, and buckling of some web longitudinal bars, evenly distributed flexural cracks in tension zone of the wall, wide major shear cracks and formation of sliding surface in the wall above the anchorage dowels (Figure 3.20).

By increasing drift ratio, shear capacity was reduced slightly due to accumulated damage in RC wall. Lateral load bearing capacity of the frame reduced by 2.5% and was 308.9 kN in positive direction at overall drift ratio of 1.5% (about 1.8% of first story drift ratio) and reduced by 2.5% and was 322.5 kN in negative direction at 1.7% of overall drift ratio corresponding to 1.8% of first story drift ratio in that direction. States of damage in frame elements at point "i" were flexural cracking in exterior columns, moderate damage in joints due to shear cracking, cover spall and hinging in beam ends at beam to wall intersections, extensive damage on RC wall due to the flexural-sliding shear mechanism.

a (4.5 mm)

b (9 mm)

c (18 mm)

St1 - Exterior Joint - Left
b (9 mm)

c (18 mm)

c (18 mm)
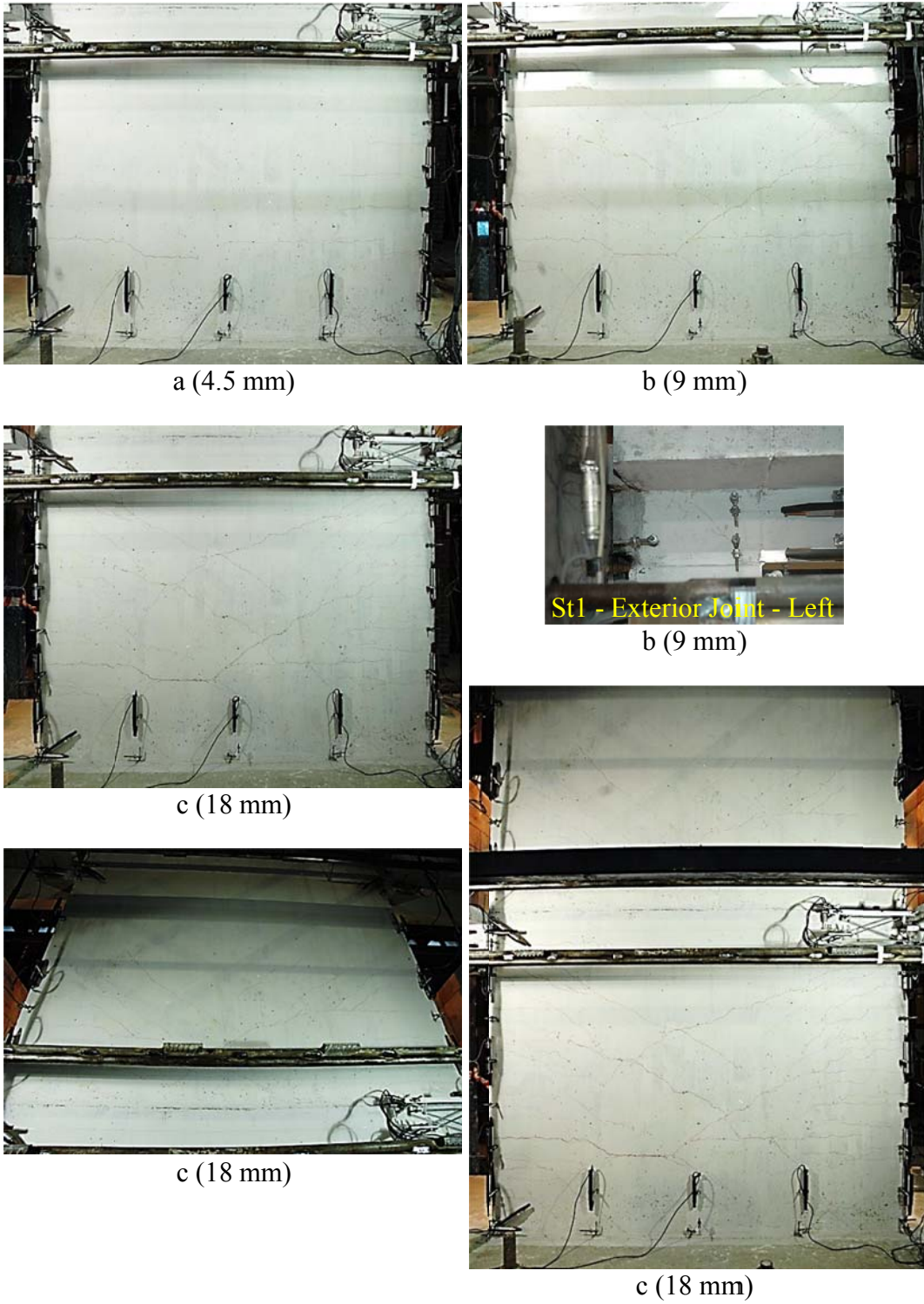
Figure 3.20 Damage states in RC-SW1 associated with the points marked in Figure 3.17
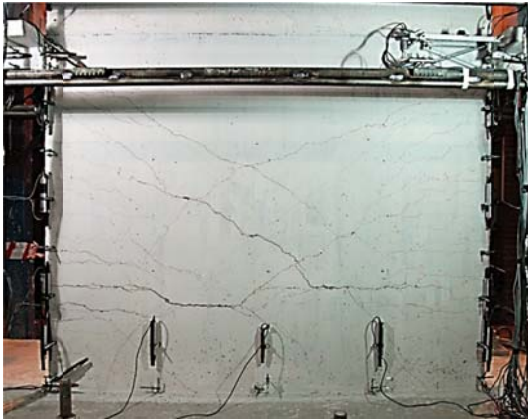
d (27 mm)

d (27 mm)

e (36 mm)

f (45 mm)

St1 - Exterior Joint - Left

St1 - Exterior Joint - Right
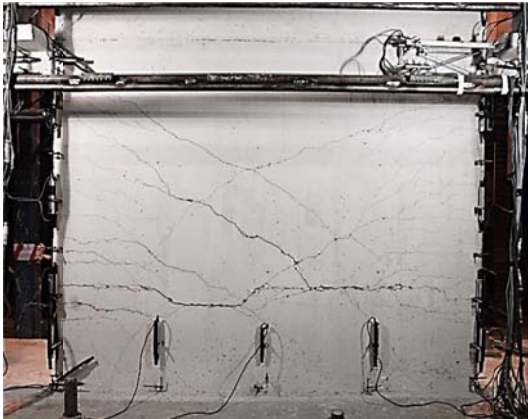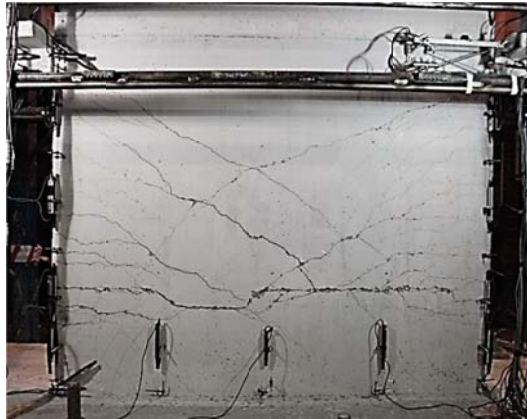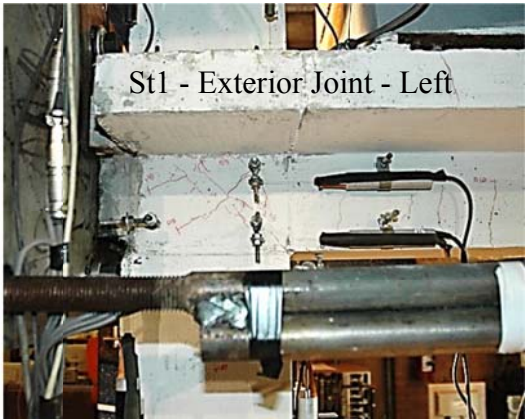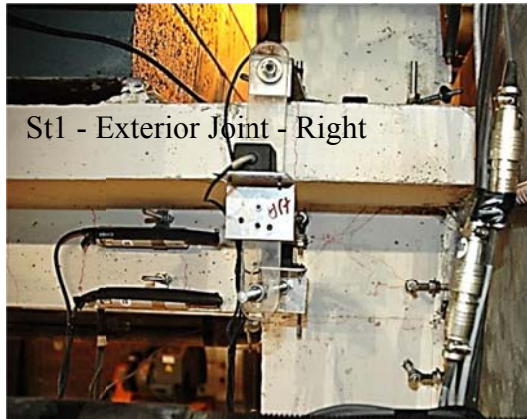
f (45 mm)

f (45 mm)

Figure 3.20 Damage states in RC-SW1 associated with the points marked in
Figure 3.17 (cont'd)

f (45 mm)

g (54 mm)

g (54 mm)
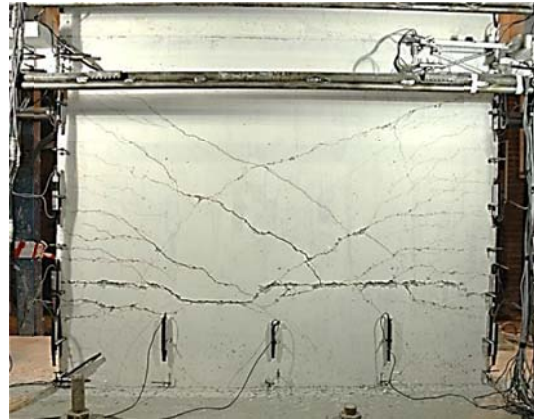
g (54 mm)

i (72 mm)
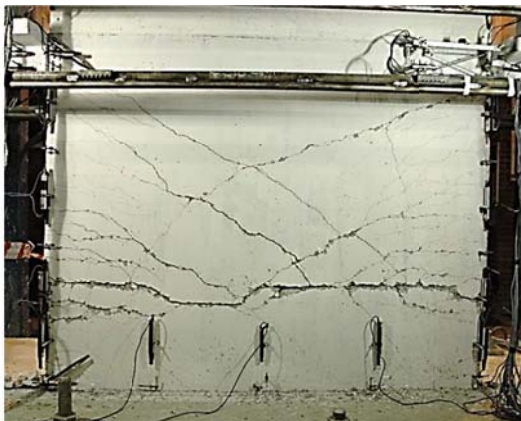
h (63 mm)

i (72 mm)

Figure 3.20 Damage states in RC-SW1 associated with the points marked in
Figure 3.17 (cont'd)

65

Figure 3.20 Damage states in RC-SW1 associated with the points marked in

Figure 3.17 (cont'd)

i (72 mm) i (72 mm)

i (72 mm) i (72 mm)

i (72 mm)

Figure 3.20 Damage states in RC-SW1 associated with the points marked in
Figure 3.17 (cont'd)

Location of failure surface on RC-SW1 wall at the end of the test is shown in Figure 3.21. In order to illustrate a clear view of the failure surface, cover concrete was removed from the surface very gently. Moreover, to show the height of the failure surface relative to the anchorage dowels end concrete around two neighboring dowels, one bar representing the anchorage dowels in boundary region and another one representing dowels in wall web, were taken out. It can be clearly seen that a sliding surface formed at the level just above the anchorage dowels.
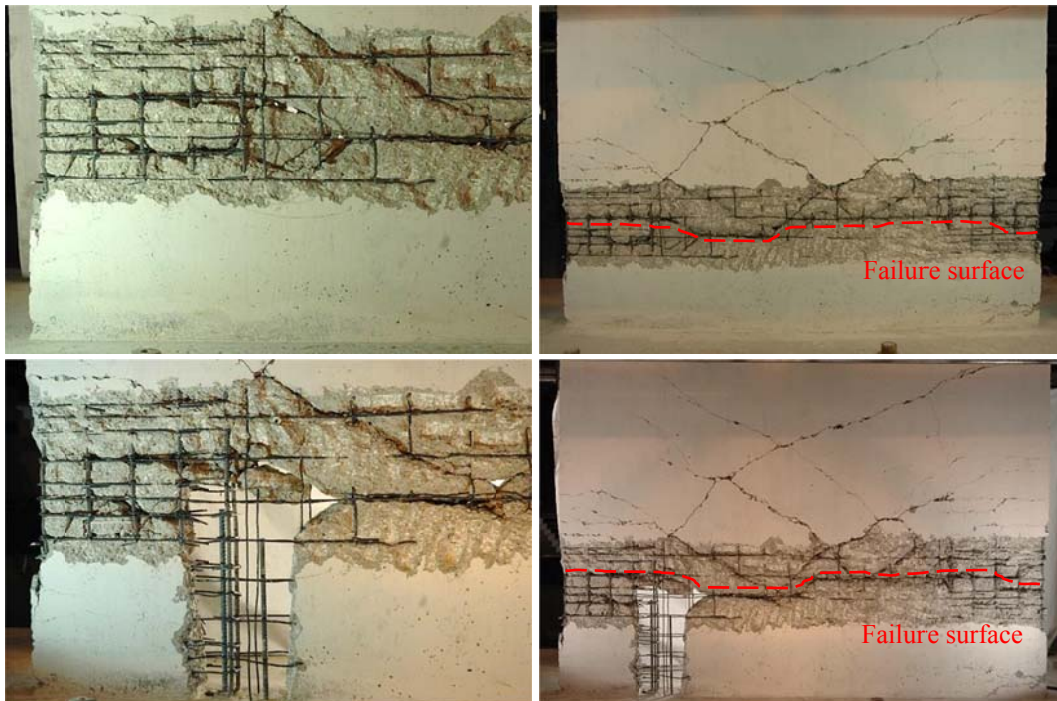
Figure 3.21 Location of failure surface on RC-SW1 wall

3.4.1.2. Specimen RC-SW2

This specimen had the same geometrical properties as the previous specimen (RC-SW1) while having differences in reinforcement detailing of structural members. RC-SW2 test frame was designed according to the Turkish reinforced concrete practice code (TS500) -1981 and Turkish Earthquake Code (TEC) -1975. There are minor changes between TS500-2000 which is the latest version and TS500-1981. However, major differences can be found between TEC-2007 and TEC-1975. The major differences are listed as follows. In comparison with TEC-2007, in TEC-1975;

- Stirrup and tie volumetric ratio in confined and non-confined regions of beams and column is lower.

- Transverse and longitudinal reinforcement spacing is wider.

- There is no special transverse reinforcement requirement in boundary regions of RC shear walls.

- There is no strong column-weak beam check.

This specimen was tested under lateral loads using quasi-static reversed cyclic loading protocol. To do this, a lateral load profile in accordance with first vibrating mode shape with increasing top displacement was applied to the frame. During the experiment, top displacement was adjusted to reversed cycles with increasing magnitudes of amplitude by utilizing displacement control algorithm. Figure 3.22 shows the history of applied displacement at third story level.

By employing load control algorithm, actuators forces at the first and second stories were fixed to 20 and 58 (compatible with first vibrating mode) percent of applied force at third story level, respectively, for each point in displacement history of third story. Doing this, actually, reversed cyclic push over loading was carried out on frame which enabled to make comments on system ductility, shear force bearing capacity and damage-displacement correlations.
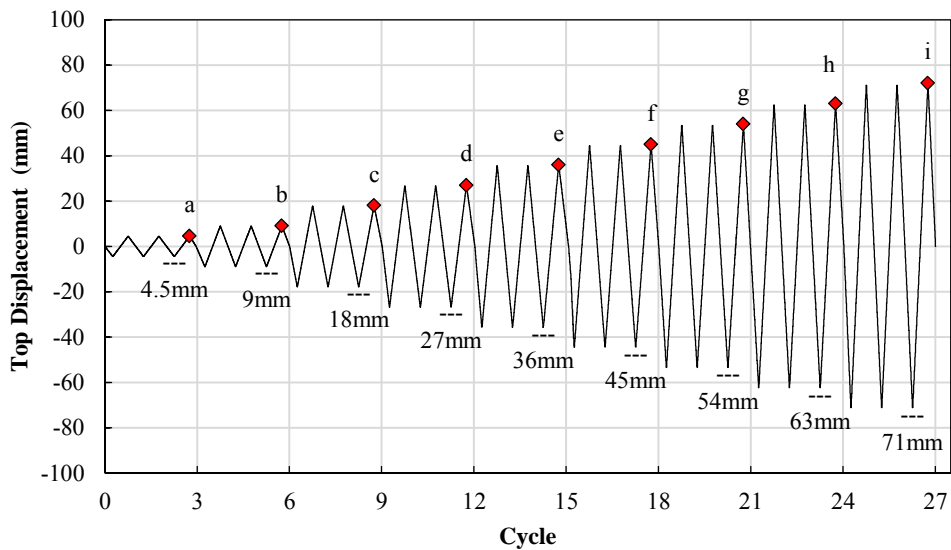
Figure 3.22 Loading cycles with increasing amplitudes of displacement applied on RC-SW2

Story displacement and force histories which were recorded during the test are provided separately in Figure B.20 in Appendix B.

Hysteresis behavior of the specimen under the applied loads is presented in Figure 3.23 and Figure 3.24. Figure 3.23 shows story shear versus inter-story drift diagram of each stories for RC-SW2. In this figure, Inter-story drift ratio histories are also provided. Overall response of frame is illustrated in Figure 3.24 demonstrating base shear-top displacement/overall drift ratio relationship.
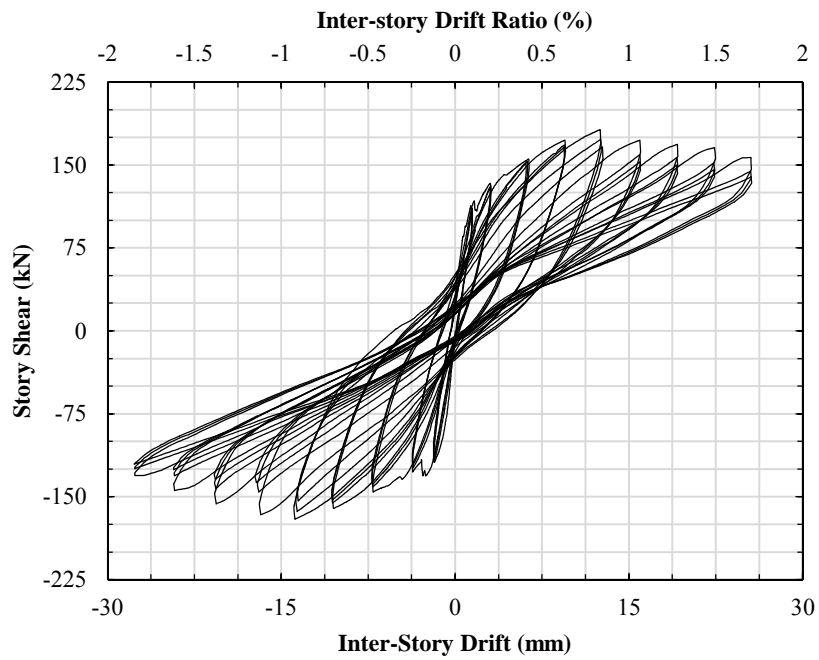
70

a)

b)

Figure 3.23 Story shear versus Inter-story displacement response of RC-SW2; a) first story, b) second story 3), third story

c)
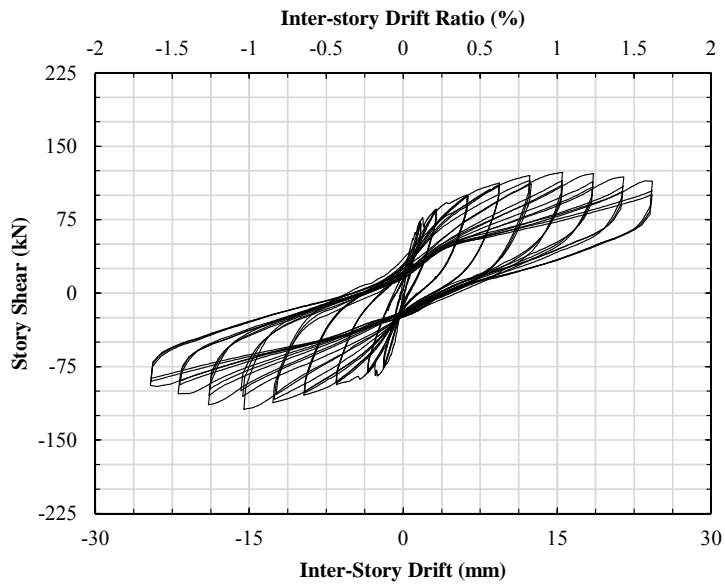
Figure 3.23 Story shear versus Inter-story displacement response of RC-SW2; a)
first story, b) second story 3), third story (cont'd)
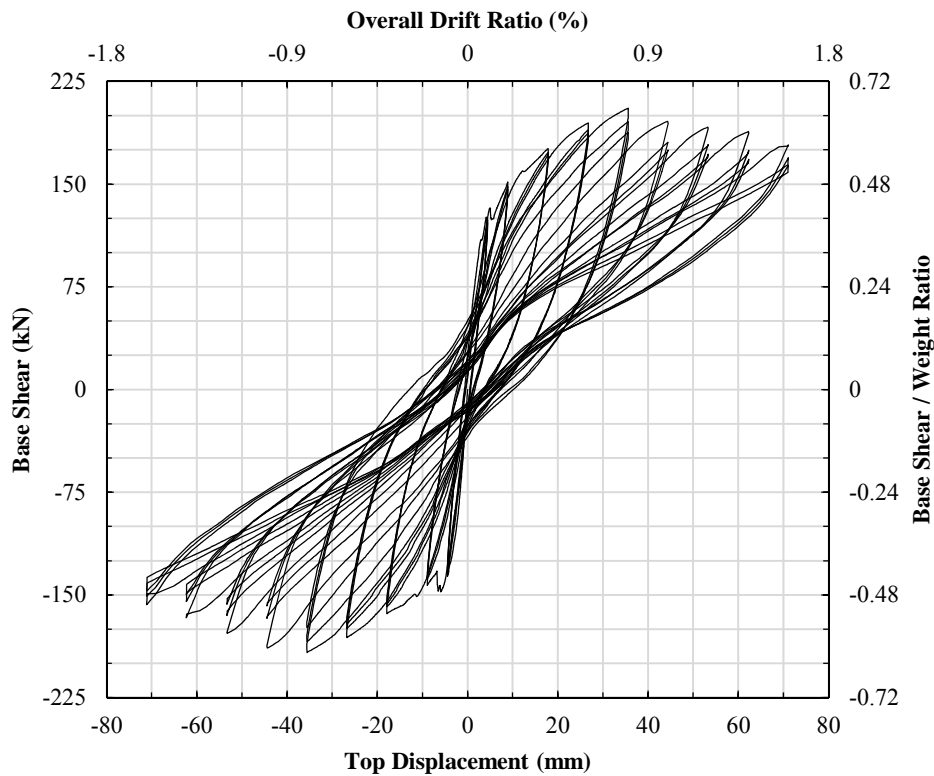
Figure 3.24 Base shear versus top displacement hysteretic response of RC-SW2

The observed damage states at the end of every set of displacement cycles with same amplitude are also presented in Figure 3.25. The points at which the damage were reported are marked as points a, b, c, d, e, f, g, h and i in Figure 3.22.

First crack on the wall took place at wall base at first story drift ratio of 0.06 %. This crack was followed by a horizontal flexure crack at the height of about 300 mm from wall base where the anchorage dowels were ended. At this instance, first story drift ratio was about 0.08 % (about 0.09 % of overall drift ratio and 126 kN of base shear).

After a number of displacement cycles, a couple of horizontal flexural cracks were formed at lower part of the wall until point "c" (Figure 3.22). Some of these horizontal cracks which were started from the edge of the wall rotated and inclined towards the wall width. In addition, two major horizontal cracks which were formed in opposite directions in load reversals met each other and formed a failure plane, see Figure 3.25. At point "c" overall drift ratio was 0.4% (corresponding to about 0.3% and 0.4% of first story drift ratio in positive and negative directions, respectively).

Beyond this drift ratio, damage concentrated at the level of the major horizontal continuous crack which was formed previously. Cover spall and bar buckling in compression zone and opening tension cracks (point "d") indicated flexural failure. Finally, RC-SW2 reached its shear capacity of about 205.4 kN at overall drift ratio of 0.8% in positive direction (about 0.75% of first story drift ratio) and 192 kN in negative direction (about 0.65% of first story drift ratio). Observed damage at point "e" corresponding to this level of overall drift ratio were concrete crushing in compression region in wall edge, extensive buckling of longitudinal bars in wall boundary, a wide flexural crack in tension zone of the wall, hairline shear cracks in beam to column joints and hairline flexural cracks in exterior columns.

73

After point "e", by increasing the amplitude of the displacement cycles, shear strength deterioration started due to the cumulative damage in RC wall which was the main lateral load bearing element. A rocking failure mechanism started to form at the height just above the wall anchorage dowels. Lateral load bearing capacity of the frame reduced by 13% and was 178.7 kN in positive direction at overall drift ratio of 1.6% (about 1.5% of first story drift ratio) and reduced by 18% and was 157 kN in negative direction at 1.6% of overall drift ratio corresponding to 1.3% of first story drift ratio in that direction. State of damage at point "i" which was the last peak of applied cycles is shown in Figure 3.25. Flexural plastic hinging with extensive spalling in beam ends close to the wall, slight flexural yielding in column ends at the base level, and shear cracking in beam-column joint representing moderate to heavy damage level were the major perceived damage level.

An extensive pinched behavior was observed in hysteresis diagram of RC-SW2. As it is apparent in Figure 3.24, after the point that maximum base shear was reached, hysteresis cycles started to pinch. This behavior is well-matched with the observed damages. Shear strength deterioration in wall is mainly due to the concrete strength deterioration during crack opening and closure, rocking type mechanism and closure of wide flexure crack with very low strength due to buckled and/or ruptured longitudinal bars. During test observations visible major diagonal shear crack were not detected.

a (4.5 mm)

b (9 mm)

c (18 mm)

d (27 mm)

e (36 mm)

Buckling

d (27 mm)
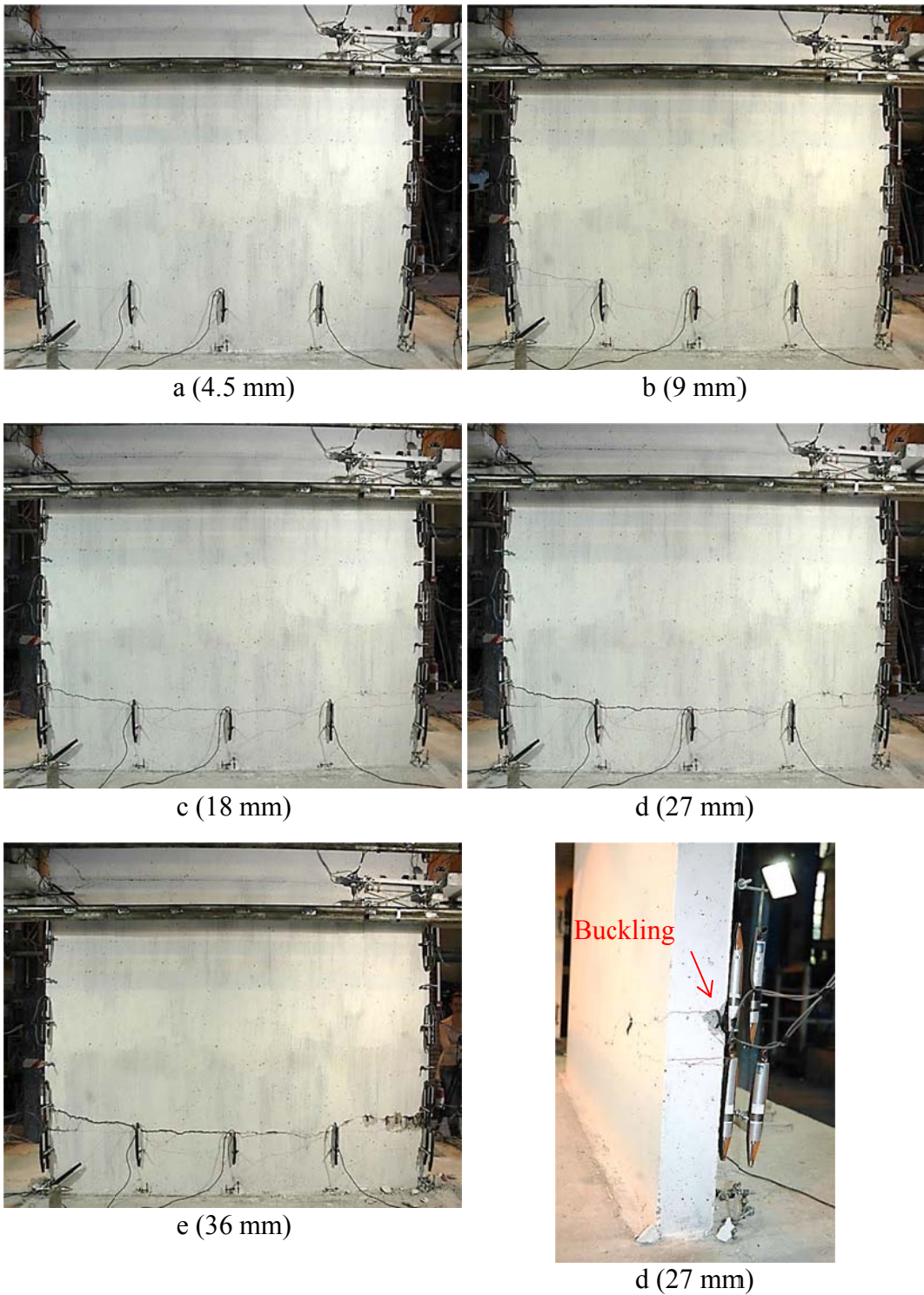
Figure 3.25 Damage states in RC-SW2 associated with the points marked in Figure 3.22

e (36 mm)

e (36 mm)

e (36 mm)
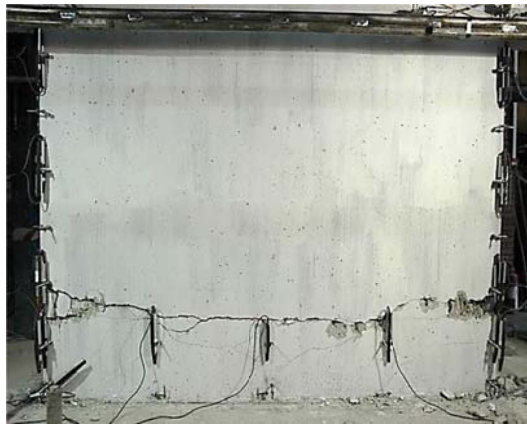
f (45 mm)

f (45 mm)
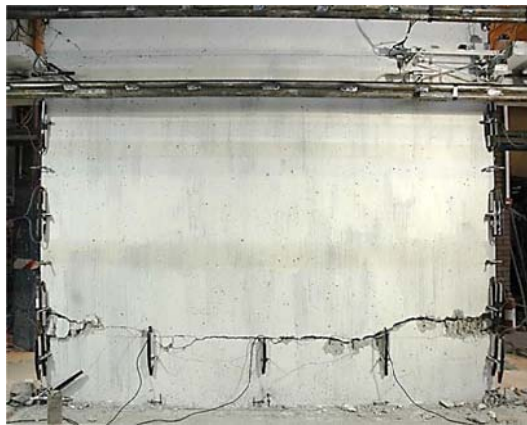
g (54 mm)

Figure 3.25 Damage states in RC-SW2 associated with the points marked in Figure 3.22 (cont'd)

g (54 mm)

h (63 mm)

St2 - Beam to Wall - Right

h (63 mm)

St2 - Beam to Wall - Left

h (63 mm)

St1 - Exterior Joint - Left
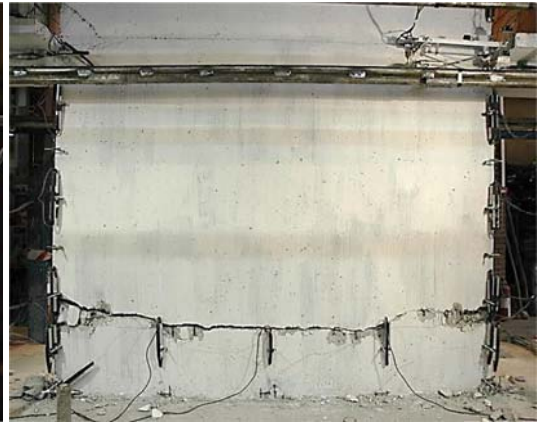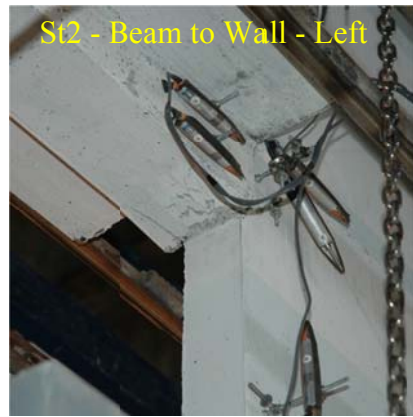
h (63 mm)

St1- Right Column

h (63 mm)

Figure 3.25 Damage states in RC-SW2 associated with the points marked in Figure 3.22 (cont'd)

77
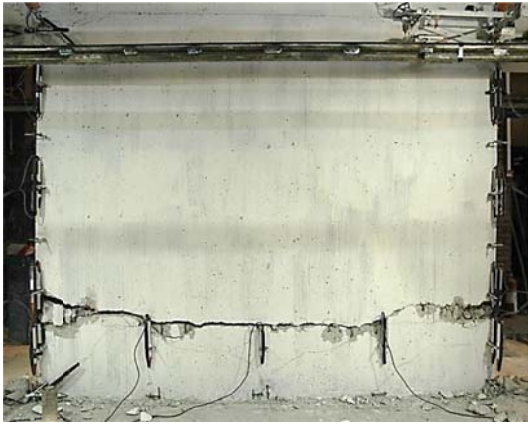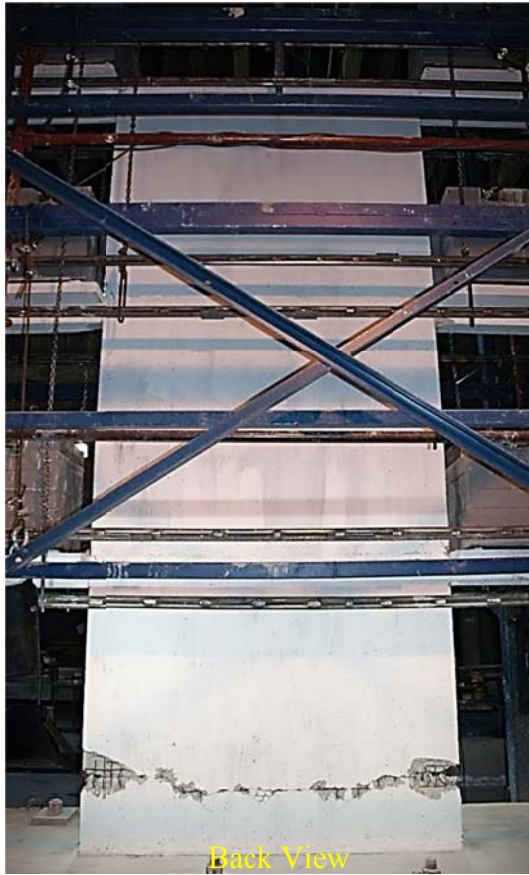
i (71 mm)

i (71 mm)

i (71 mm)

Back View

St1 - Right Column

i (71 mm)

St1 - Left Column

i (71 mm)

Figure 3.25 Damage states in RC-SW2 associated with the points marked in
Figure 3.22 (cont'd)
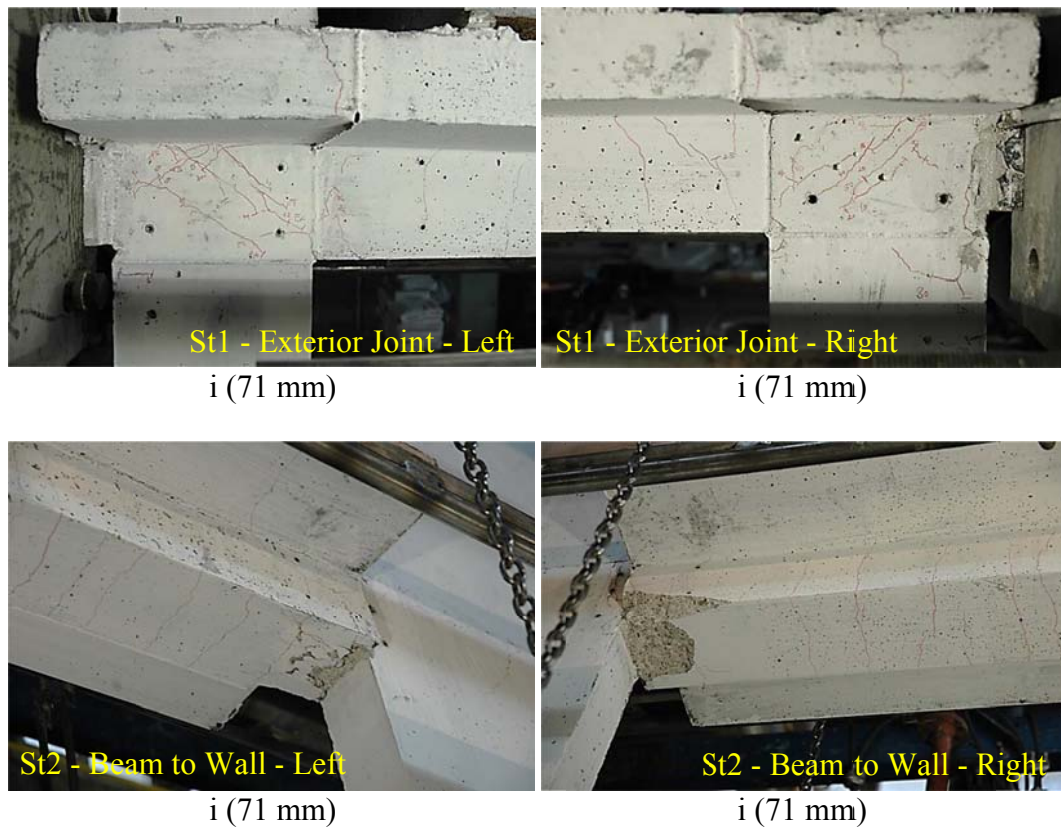
Figure 3.25 Damage states in RC-SW2 associated with the points marked in Figure 3.22 (cont'd)

Figure 3.26 exhibits final damage state of RC-SW2 wall at the end of test. Formation of a sliding surface just above the dowels at a height about 300 mm from the wall bottom is clearly obvious. The cover concrete of the wall was taken out to show the failure surface clearly. Moreover, to show the height of the failure surface relative to the anchorage dowels end concrete around two anchorage dowels, one in boundary region and other in wall web, were taken out.
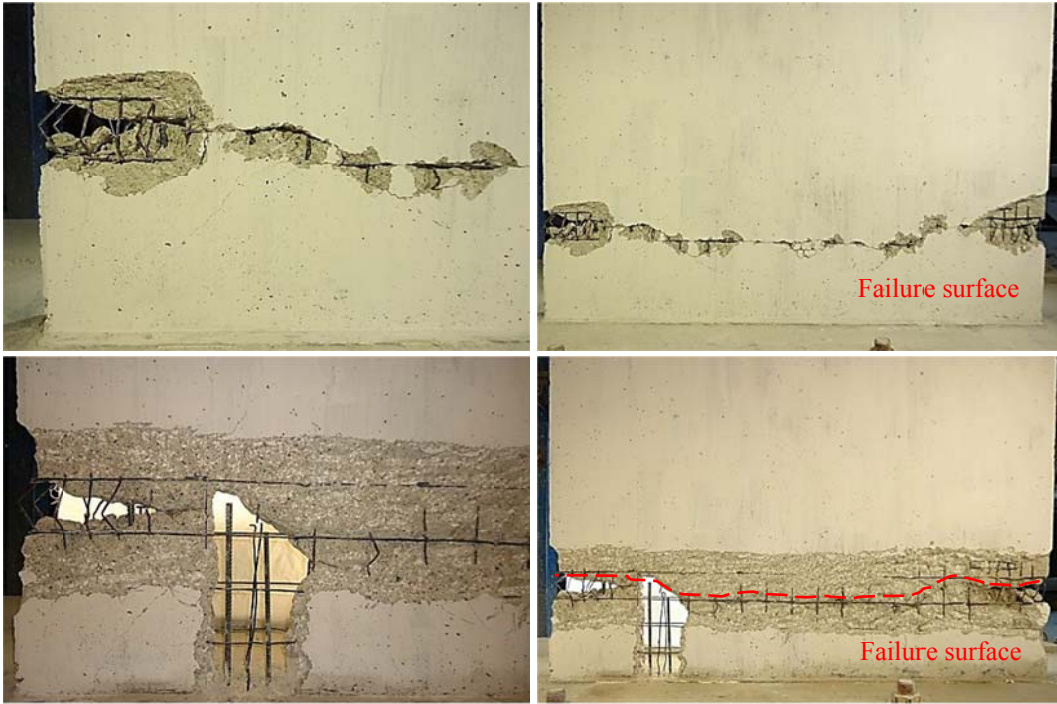
Figure 3.26 Location of failure surface on RC-SW2 wall

3.4.2. Overall ductility

In the concept of seismic design of structures to withstand severe earthquakes, ductility plays an important role. Ductility in a structure is the ability of a structure to resist large cyclic deformations without significant strength loss. In seismic design of structures, ductility factor, unlike maximum deformation, is a non-dimensional factor which indicates inelastic deformation capacity of structures. As illustrated in Figure 3.27, displacement ductility factor is defined as

$$\mu = \frac{\Delta_{max}}{\Delta_y}$$
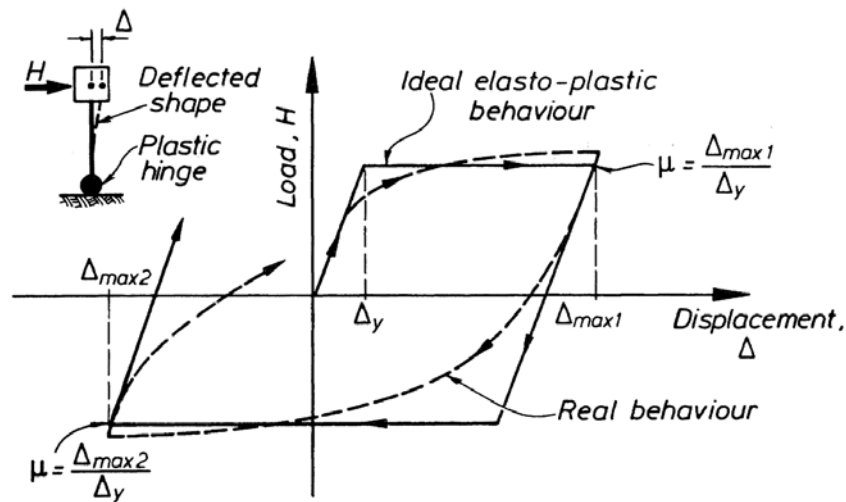
Figure 3.27 Displacement ductility factor (Park, 1989)

and ranged from 1 for elasic structures to 6 for ductile structures (Park, 1989). To evaluate the displacement ductility of tested specimens, the hysteretic behavior of the structure needs to be idealized. The method described in Park (1989) was utilized to idealize envelope curve of hysteresis diagram. According to Park (1988), yield displacement of the equivalent elastic-perfectly plastic system is found as the intersection of a line going through the origin and first yield point or the point corresponding to 75% of the ultimate lateral load, whichever occurs first,

and a horizontal line going through ultimate strength point. The first yield point is defined as the point in which the outer edge reinforcements of the member are yielded or the strain at outer edge of compressive concrete reaches 0.002, whichever reaches first (Priestley and Kowalsky, 1998). However, since the considered hysteretic curve corresponds to overall response of the whole frame, the yield criterion which is associated with member response was not considered. Ultimate or maximum available deformation is the point that corresponds to the maximum of 20% reduction in strength or first fracture of longitudinal or transvers reinforcement or buckling of longitudinal reinforcement or core concrete crushing. For the same reason stated for yield criterion, maximum of 20% reduction in strength was considered as the first limiting criteria.
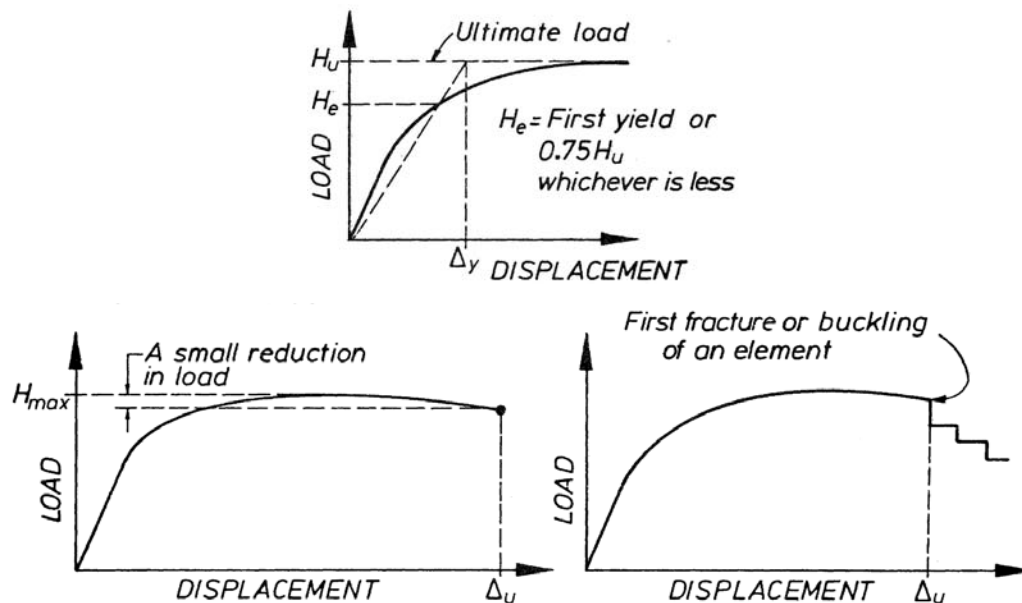
Figure 3.28 Definitions of yield and ultimate deformations (Park, 1989)

The same method was employed for both positive and negative directions.

82
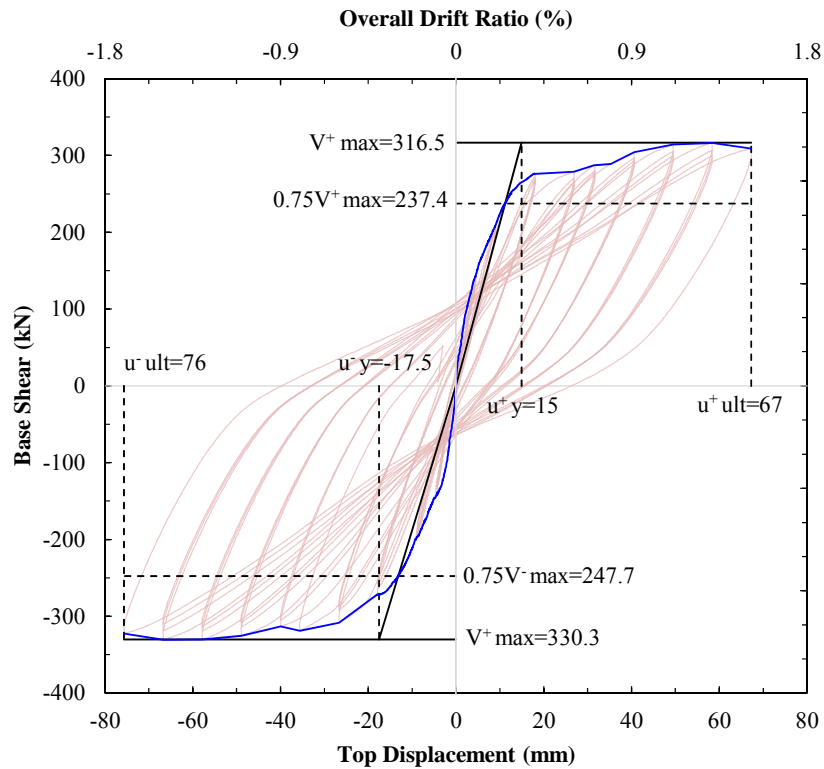
Figure 3.29 Idealized bilinear hysteretic response; RC-SW1

Ultimate lateral load bearing capacity of specimen RC-SW1 was 316.5 kN in positive direction and 330.3 kN in negative direction, Figure 3.29. These amount of base shears were reached at the points corresponding to about 1.3% overall drift ratio (displacement ductility factor of 3.9, 59 mm of top displacement and about 1.5% of first story drift ratio) in positive direction and 1.5% overall drift ratio (ductility factor of 3.8, 67 mm of top displacement and 1.5% of first story drift ratio) in negative direction. At the end of cycles in which specimen RC-SW1 reached its shear capacity (average displacement ductility factor of about 4 in push and pull directions) extensive and evenly distributed flexure, flexure-shear and shear cracks over the wall critical height, cover spalling in wall boundary regions, edge bar buckling and concrete deterioration due to opening and closing of flexural cracks in boundary regions and due to shear sliding were observed. After this point, base shear capacity started to degrade slightly.

83
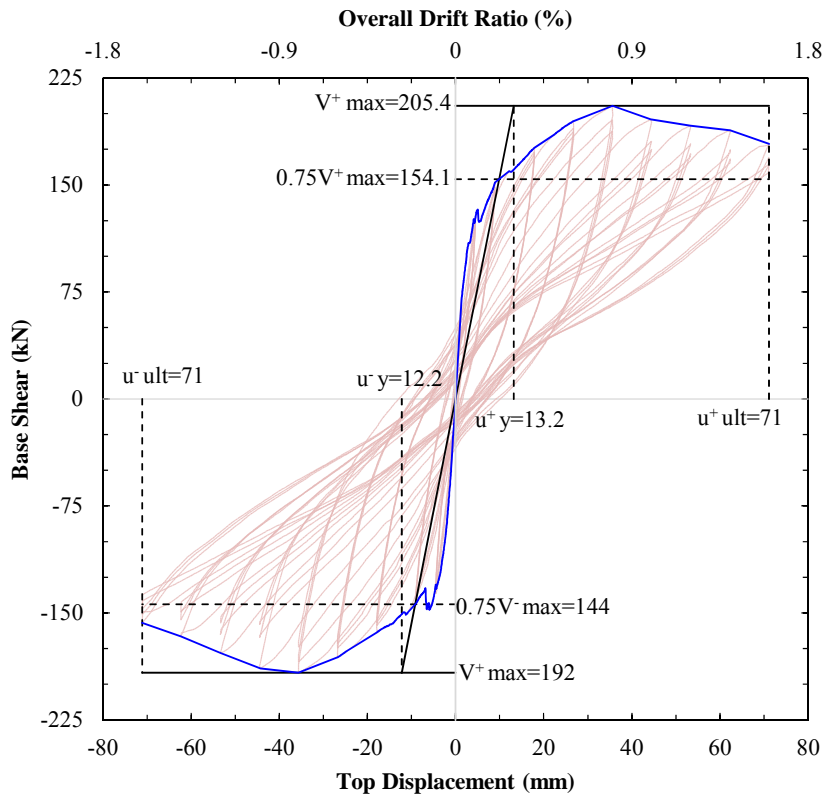
Figure 3.30 Idealized bilinear hysteretic response; RC-SW2

At the end of displacement cycles with 27 mm of amplitude, corresponds to 0.6% of overall drift ratio, 0.56% of first story drift ratio and displacement ductility factor of about 2, major reported damage was buckling of some longitudinal bars in RC-SW2 (Figure 3.25). However base shear increased in following cycles and toped at the first cycle with 36 mm of amplitude reaching 205.4 kN in positive and 192 kN in negative directions, Figure 3.30. These points match with overall drift ratio of 0.8%, displacement ductility of 2.7 and 0.75% of first story drift ratio in positive and overall drift ratio of 0.8%, displacement ductility of 3 and 0.65% of first story drift ratio in negative directions. At the end of cycles corresponding to average (of negative and positive directions) displacement ductility factor of about 3, extensive damage was developed in RC wall comprising concrete core crushing in wall edges due to compressive stresses and buckling of larger number

of longitudinal bars in these regions (Figure 3.25). As a result of extensive damage in RC wall, shear capacity of the specimen decreased after this point. Due to safety concerns, cyclic test was not continued to higher drifts for both specimens, ultimate displacement ductility capacity of both frames could not be obtained and compared.

3.4.3. Energy dissipation

Energy dissipation is a fundamental structural characteristic of RC elements subjected to cyclic load demands. According to the seismic design concept, RC structures designed to seismic codes are intended to accommodate earthquake induced damage without collapse through dissipating input energy by members hysteretic response, without a significant reduction in strength (Rodrigues, Varum, Arêde and Costa, 2012).

RC structures dissipate energy by internal friction mechanism and yielding in structural members under cyclic loadings. Hysteretic dissipated energy, E_h, is defined as the area enclosed by each hysteretic loop of structures during earthquake cycles. The energy dissipation capacity of tested specimens were evaluated in terms of cumulative hysteretic energy dissipation, E_{cum}, which can be determined as the total area of all hysteresis loops until ultimate cyclic displacement. Accumulated hysteretic energy which is associated with accumulated damage increases with increasing displacement amplitudes of earthquake cycles. Due to simplicity, this parameter was used in damage models defined by different researches (e.g. Park and Ang, 1985) for performance assessment purposes. It is noticeable in Figure 3.31 that cumulative hysteretic energy increases with increasing number of cycles for both RC-SW1 and RC-SW2 specimens. The rate of increase in cumulative hysteretic energy increased rapidly by formation of cracks and yielding in members before maximum load bearing capacity of frames was reached. After this point, however, strength

degradation started and due to the significant pinching in hysteresis behavior of RC-SW2 this rate decreased slightly which means that in the cycles after formation of extensive damage, cycle energy absorption decreases, Figure 3.31b. Diagonal shear cracks closure, reinforcement Bauschinger effect and shear slip causes hysteresis loops to shrink and pinch which reduces energy absorbtion capacity (Li and Li, 2012). In the first cycle of each set of displacement cycles with constant amplitudes, energy absorption was slightly higher than the energy dissipated in subsequent cycle with the same peak displacement. This reduction was more pronounced after formation of failure mechanism which was associated with the cycles in which maximum strength was reached.
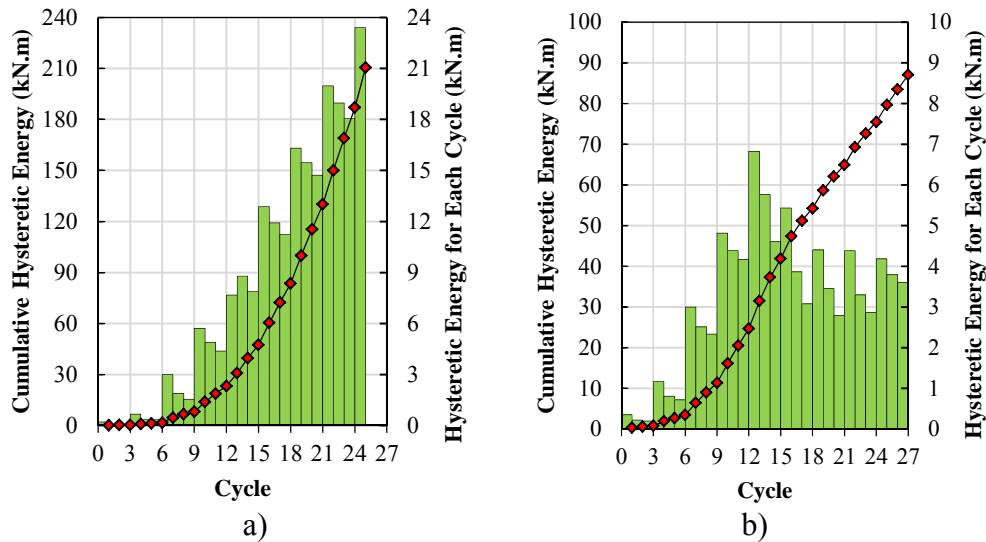
Figure 3.31 Hysteretic energy dissipation in for each cycle along with cumulative hysteretic energy dissipation; a) Specimen RC-SW1, b) Specimen RC-SW2

Quantitative comparison of hysteretic energy dissipation of RC members or structures is not meaningful as different structures may differ in lateral stiffness, yield strength, ductility, degradation characteristics and loading histories. To overcome this problem and make a representative and meaningful comparison of hysteretic energy dissipation as a sign of damage in tested specimens, normalized cumulative hysteresis energy dissipation, NE_{cum}, is used (Erberik and Kurtman,

86

2010). Mahin and Bertero (1976) defined normalized cumulative hysteretic energy for the first time for single degree structures. Normalized dissipated hysteretic energy can be used as a damage indicator as it is directly related to stiffness and strength degradation in a structure subjected to earthquake load. Cumulative hysteresis energy is normalized according to Eq (3.1).

$$NE_{cum} = \frac{E_{cum}}{F_y \times u_x} \qquad (3.1)$$

In this equation; NE_{cum} is normalized cumulative hysteresis energy, E_{cum} stands for cumulative hysteresis energy; and f_y and u_y is the averaged base shear and displacement at yield point in idealized elastic-perfectly plastic envelop for positive and negative directions. Figure 3.32 shows normalized cumulative absorbed hysteretic energy associated with different levels of displacement ductility. Non-dimensional displacement ductility is used instead of cycle number or top displacement in Figure 3.32.
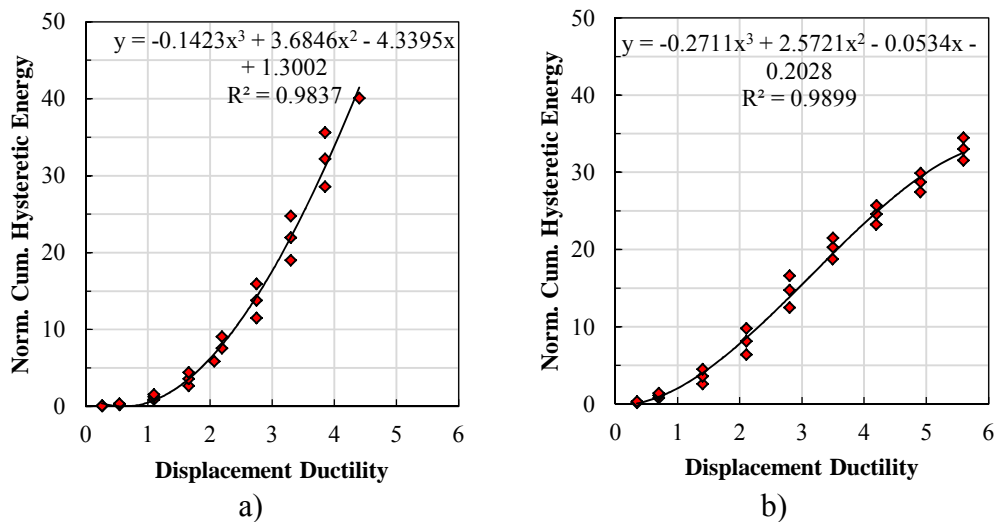
Figure 3.32 Normalized cumulative hysteretic energy associated with different displacement ductility level; a) Specimen RC-SW1, b) Specimen RC-SW2

In lower drift ratios, normalized cumulative hysteresis energy of RC-SW2 was slightly higher than RC-SW1. This implies that the more damage such as concrete cracking or steel yielding was developed in RC-SW2 compared with RC-SW1in lower drift ratios. In higher ductility levels, however, normalized cumulative hysteresis energy of RC-SW2 is lower than RC-SW1 due to considerably reduced hysteresis energy absorption after the formation of failure mechanism at displacement ductility level close to 3.

3.4.4. Stiffness degradation

To investigate the effect of consecutively applied lateral displacement cycles associated with constant or increasing amplitudes and effect of developed damages in shear walls, in stiffness degradation characteristics of tested RC shear walls, system stiffness for each half cycles and effective cycle stiffness (K_{eff}) were calculated. The average value of effective half-cycle stiffness for the positive and negative directions (push and pull directions) in a full cycle is used as effective stiffness for each cycle. The procedure employed to calculate cycle stiffness is illustrated in Figure 3.33 and Eq (3.2) and Eq (3.3).

$$K_{eff1} = \frac{F_1}{\Delta_{m1}} \quad , \quad K_{eff2} = \frac{F_2}{\Delta_{m2}} \tag{3.2}$$

$$K_{eff} = \frac{K_{eff1} + K_{eff2}}{2} \tag{3.3}$$

In Eq (3.2) and Eq (3.3), K_{eff}, Δ_m and F are half-cycle stiffness, maximum displacement and base shear corresponding to Δ_m ,respectively. Subscript 1 and 2 stands for positive and negative directions, respectively. Effective cycle stiffness (K_{eff}) change in consecutive displacement cycles for RC-SW1 and RC-SW2 are presented in Figure 3.34.
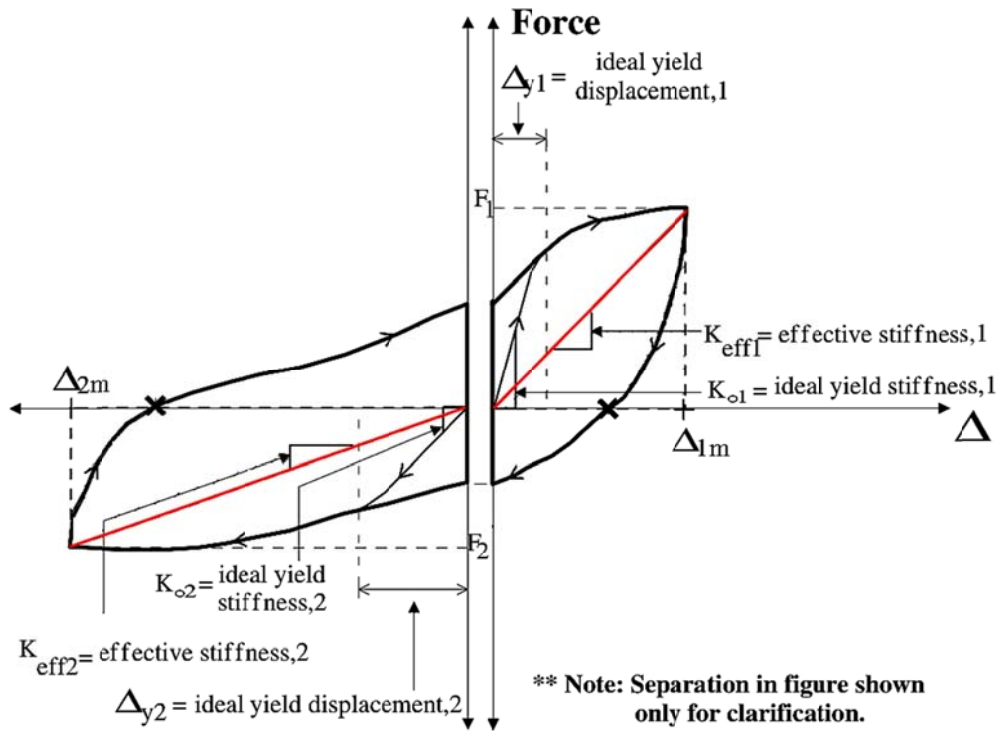
Figure 3.33 Effective stiffness (K_{eff}) for hysteresis loops (modefied from Hose and Seible, 1999)

a)   b)
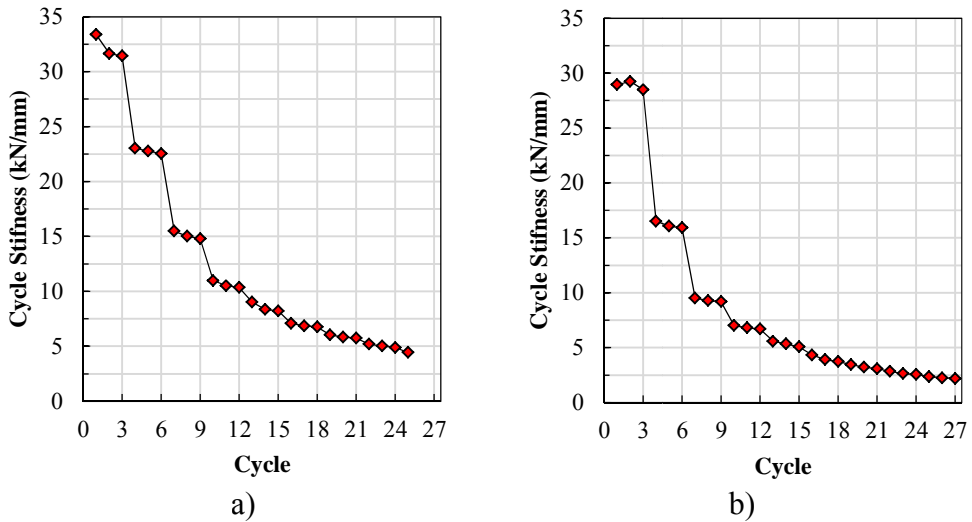
Figure 3.34 Effective cycle stiffness (K_{eff}) for each displacement cycle; a) Specimen RC-SW1, b) Specimen RC-SW2

As it is evident in Figure 3.34, no considerable stiffness degradation in cycles with constant displacement amplitude was observed for both specimens under applied loading. Conversely, as it was expected, cycle stiffness reduced as displacement amplitude increased. This reduction was more prominent for earlier cycles of loading.

In order to eliminate effect of some factors such as different mechanical properties of materials, yield and maximum lateral strength of system, yield and maximum drifts of two different test specimens and making a relevant comparison between tested frames with different characteristic, effective cycle stiffness were normalized with respect to lateral elastic cracked stiffness of system or simply initial stiffness at ideal yield, K_0, obtained from idealized elastic-perfectly plastic hysteretic behavior. The average value of normalized effective half-cycle stiffness for the positive and negative directions (push and pull directions) in a full cycle was used as normalized effective cycle stiffness for each cycle. Normalized effective cycle stiffness is calculated using the Eq (3.4), as follows;

$$\frac{K_{eff}}{K_0} = \frac{1}{2}\left(\frac{K_{eff1}}{K_{01}} + \frac{K_{eff2}}{K_{02}}\right) \tag{3.4}$$

In this equation, K_{eff} parameters with subscripts 1 and 2 are effective half-cycle stiffness for positive and negative directions, respectively. Similarly, K_0 parameters with subscripts 1 and 2 stand for initial stiffness at ideal yield for positive and negative directions, respectively. Figure 3.35 shows normalized effective cycle stiffness, K_{eff}/K_0, versus displacement ductility factor. It should be reminded that for the very earlier sets of cycles with constant amplitude, cycle stiffness is larger than K_0 (initial stiffness of bilinear envelope curve) since K_0 represents estimated cracked stiffness of system at the end of elastic region. However, during the very earlier sets of cycles of experiment the whole system is

90

approximately behaved almost uncracked in a global sense. It can be concluded from Figure 3.35 that, normalized cycle stiffness drops tremendously with increasing displacement until displacement associated with displacement ductility of 1 for both specimens. The trend of stiffness degradation was very close for both tested specimens. It is worth noting that at the cycles corresponding to maximum lateral load bearing capacity (agrees to displacement ductility factor of around 4 and 3 for RC-SW1 and RC-SW2, respectively) after which strength deterioration starts, effective cycle stiffness was around 25% of ideal elastic stiffness for RC-SW1 and about 35% of ideal elastic stiffness for RC-SW2.
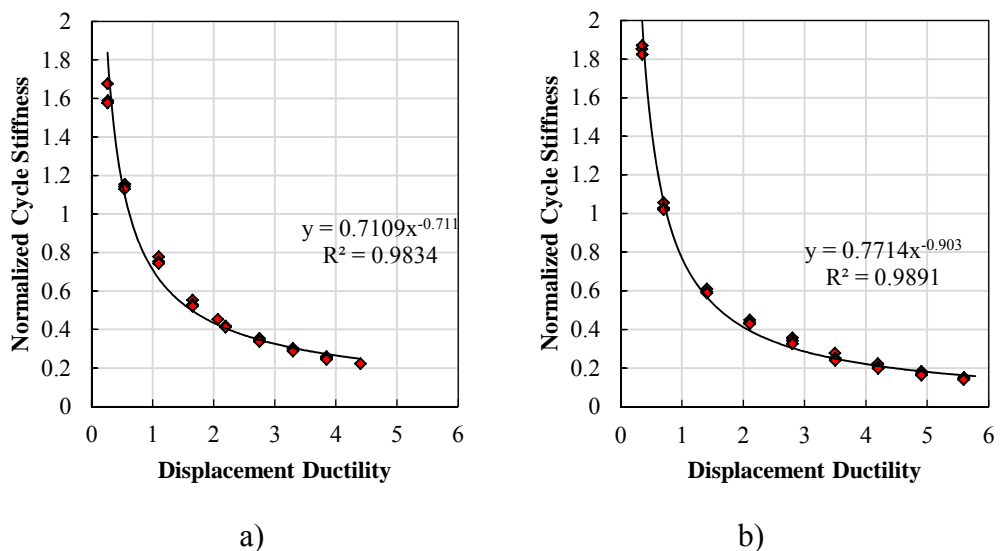
Figure 3.35 Normalized cycle stiffness (K_{eff}) for each displacement cycle; a) Specimen RC-SW1, b) Specimen RC-SW2

3.4.5. Equivalent viscos damping

Equivalent viscos damping actually represents ductility and energy dissipation capacity of a MDOF system in idealized single degree of freedom representative system. The effective damping depends on the structural system and displacement

ductility demand. It should be reminded that the energy absorption capacity of structural members at failure is strongly path dependent. Thereafter, different cyclic loading protocols may result in different energy absorption capacities (Kunnath et al. 1997). Equivalent viscos damping in structures is characterized by combination of elastic damping, which is generally agreed as 5% of critical damping for RC structures and the hysteretic energy absorbed during inelastic response or simply hysteretic damping, Eq (3.5). However, these two types of damping are not simply summed up but superimposed upon each other (Priestley, Calvi, and Kowalsky, 2007).

$$\xi_{eq} = \xi_{el} + \xi_{hyst} \tag{3.5}$$

In this equation, ξ_{el} represents elastic damping and ξ_{hyst} stands for hysteretic damping. For the symmetric hysteresis response with pure harmonic loading, hysteretic component of equivalent viscous damping is defined as by Eq (3.6).

$$\xi_{hyst} = \frac{1}{4\pi}\left(\frac{E_D}{E_{SO}}\right) = \frac{FA_h}{2\pi F\Delta_m} \tag{3.6}$$

All parameters used in Eq (3.6) are illustrated in Figure 3.36. E_D denotes dissipated energy in one complete cycle, E_{SO} symbolizes the elastic strain energy stored in an equivalent linear elastic system at maximum displacement. A_h is the area enclosed in one complete cycle of stabilized force-displacement response, and Δ_m is the maximum displacement achieved in a stabilized loop and F is the force corresponds to the maximum displacement Δ_m.
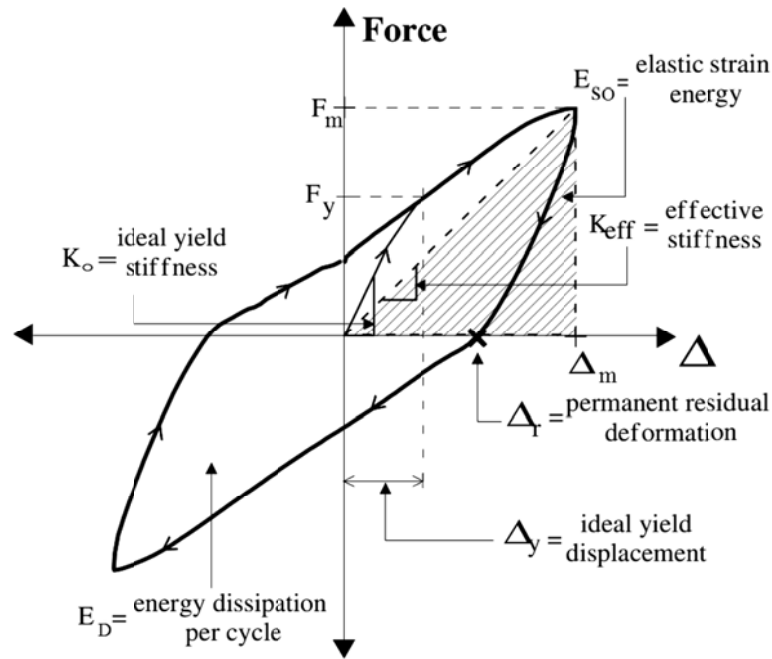
Figure 3.36 Equivalent viscous hysteresis damping for symmetric hysteresis loops
(Hose and Seible, 1999)

In earthquakes or some load controlled quasi-static loadings hysteretic response may not be symmetric. Thus, the equivalent hysteretic equivalent damping which is developed based on harmonic loading and symmetric hysteretic response may include some errors with respect to the pure harmonic and symmetric responses. For these cases, using Eq (3.7) average hysteretic damping of positive and negative parts of hysteretic loop is derived (Hose and Seible, 1999). Figure 3.37 shows the definition of the parameters used in Eq (3.7).

$$\xi_{hyst} = \frac{\xi_{hyst1} + \xi_{hyst2}}{2} = \frac{1}{2}\left(\frac{2E_{D1}}{4\pi E_{SO1}} + \frac{2E_{D2}}{4\pi E_{SO2}}\right)$$
$$= \frac{1}{4\pi}\left(\frac{E_{D1}}{E_{SO1}} + \frac{E_{D2}}{E_{SO2}}\right)$$

(3.7)
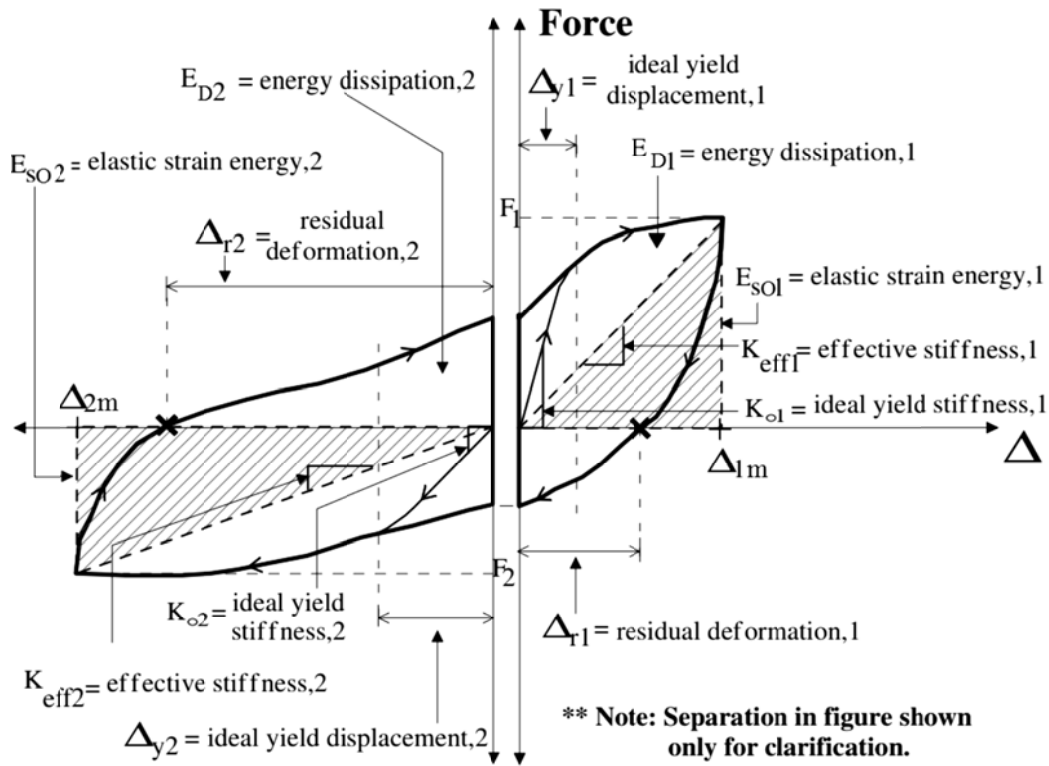
Figure 3.37 Equivalent hysteresis damping for asymmetric hysteresis loops (Hose and Seible, 1999)

a)

b)
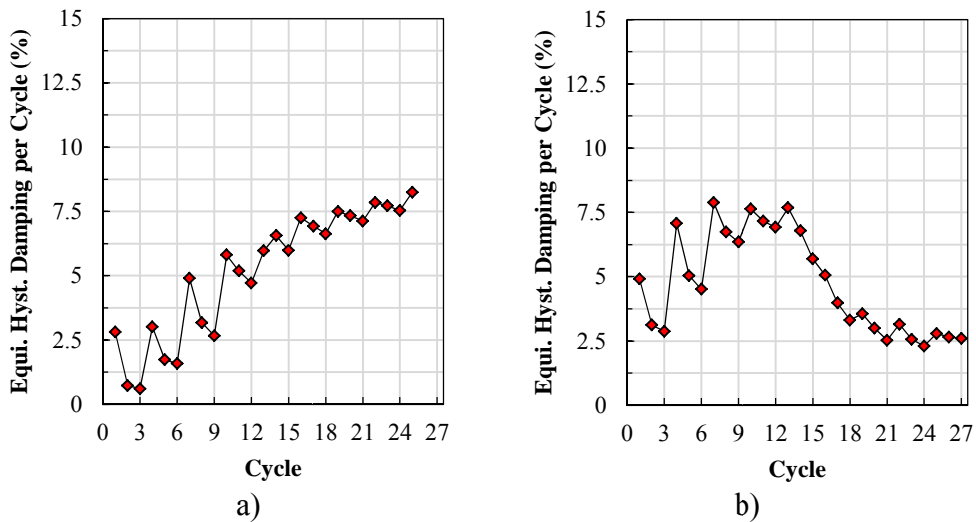
Figure 3.38 Equivalent hysteresis damping change for applied displacement cycles

94

Figure 3.38 shows equivalent hysteresis damping change for applied displacement cycles. As it is illustrated in this figure, hysteresis damping for very early cycles was larger for RC-SW2 compared with RC-SW1, which indicates that level of nonlinearity (due to concrete cracking and some yielding in steel) in small drifts are higher for RC-SW2.

Equivalent hysteresis damping ratios associated with different levels of displacement ductility for RC-SW1 and RC-SW2 are presented in Figure 3.39. Equivalent hysteresis damping ratios increased with a logarithmic trend with increasing displacement ductility until maximum shear capacity was reached. After this point (displacement ductility close to 3) hysteresis damping of RC-SW2 reduced with quadratic trend as a result of extensive pinching in hysteresis behavior.

a)   b)
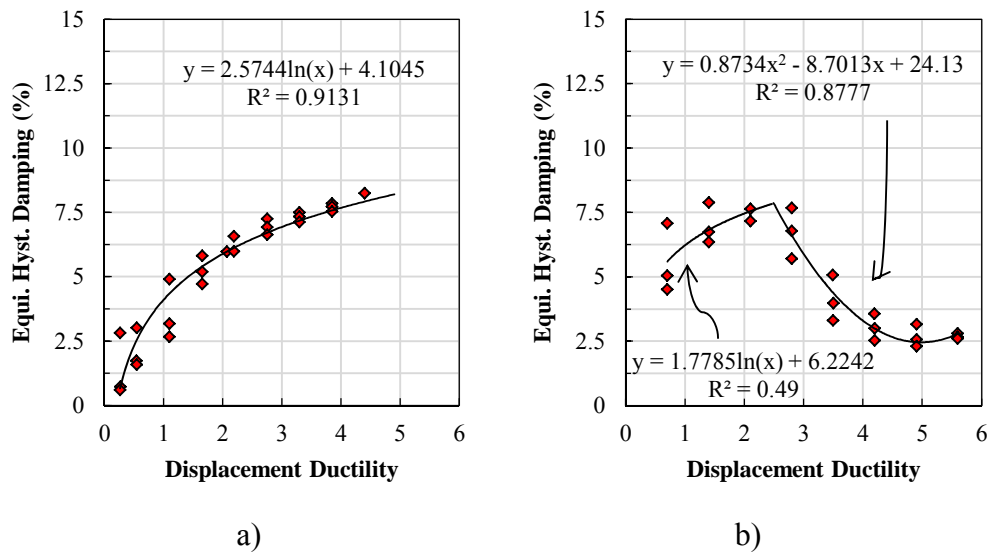
Figure 3.39 Equivalent hysteresis damping versus displacement ductility

3.4.6. Wall shear and flexure response

Shear force at the base of the RC wall is obtained as total applied lateral load minus sum of shear force at the base of exterior columns. Base reactions at the lower end of exterior columns were measured using special force transducers (Canbay et al, 2004). However the data acquired by the force transducers installed under the left column was not reliable due to damage in strain gages used in this transducer. Shear force and bending moment measured by the other transducer at the base of right column are shown in Figure 3.40.

a)
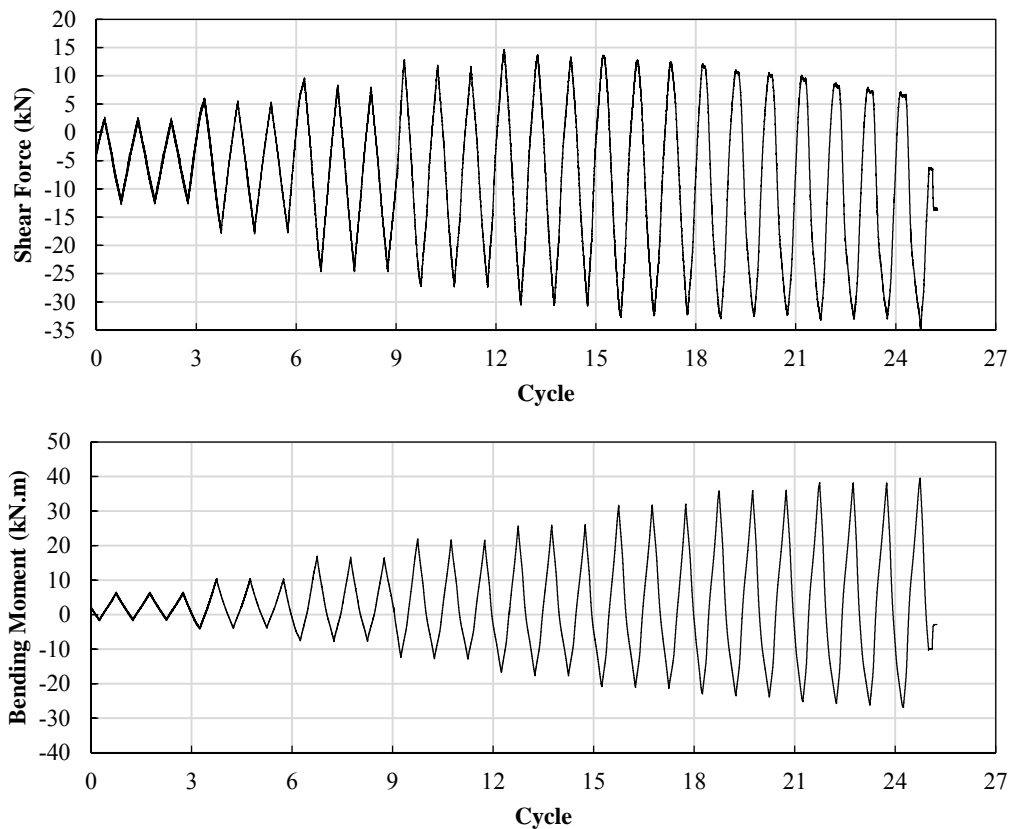
Figure 3.40 Shear force and bending moment at the base of the right column extracted from experiment; a) RC-SW1 b) RC-SW2

96

b)
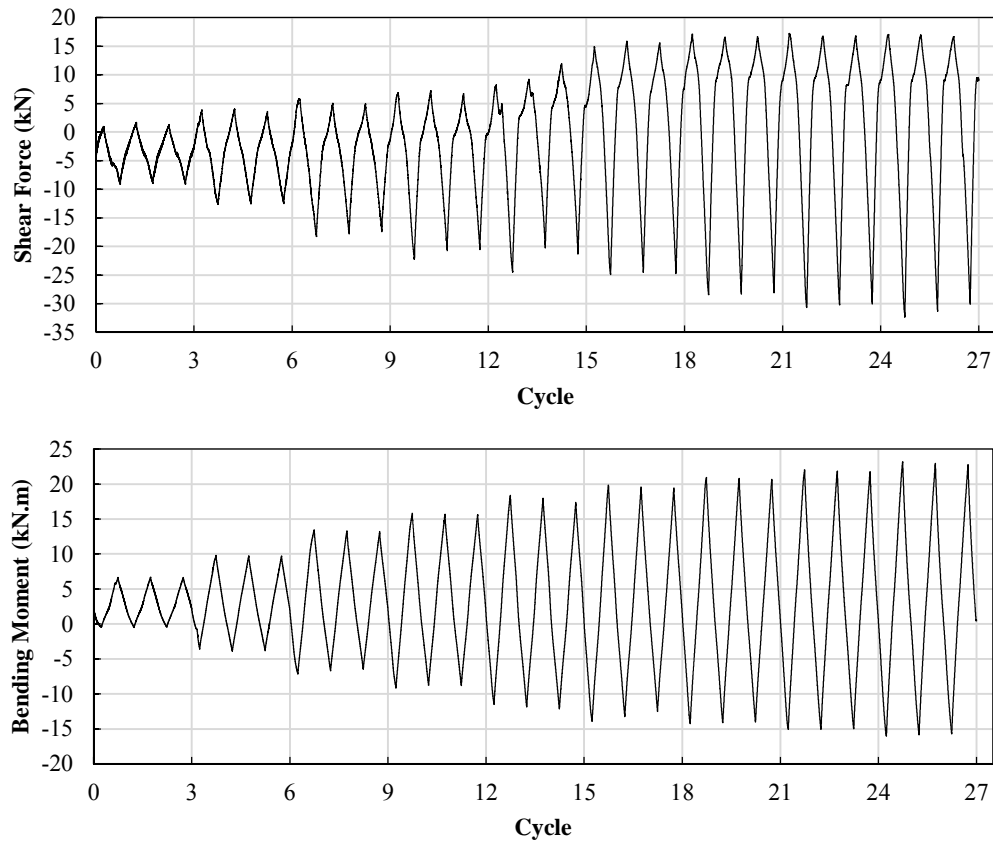
Figure 3.40 Shear force and bending moment at the base of the right column
extracted from experiment; a) RC-SW1 b) RC-SW2 (cont'd)

As the data recorded by one of force transducers was not reliable, in order to find
the shear force at the base of the RC wall total force applied on the specimen by
hydraulic actuators was subtracted by twice of the right column base shear. It was
assumed that base shear force at both columns are close with some
approximations. Figure 3.41 presents shear wall base shear history of tested walls
during experiment. The shear force resisted by RC walls in the middle bay of the
RC-SW1 changed from 80% to 93% of total applied lateral load. This ratio ranged
from 74% to 93% during the loading history.

a)

b)
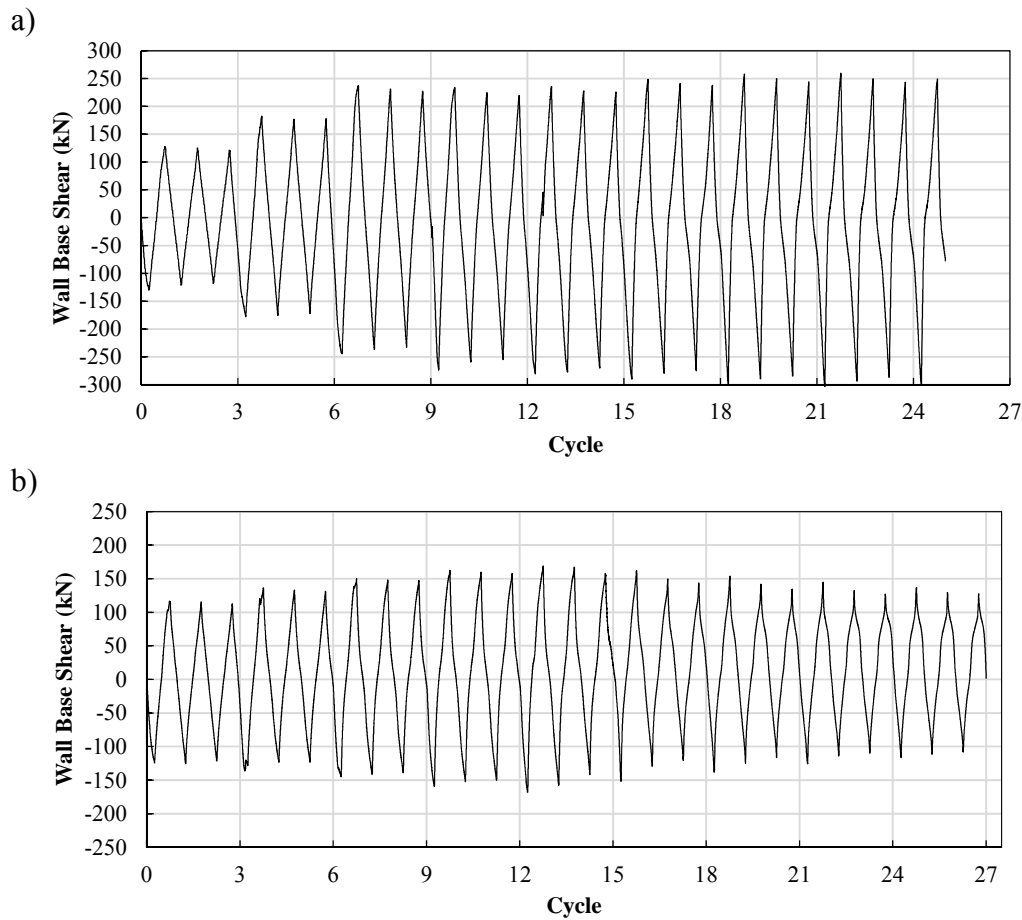
Figure 3.41 Shear force at the base of RC wall obtained from experiment; a) RC-SW1 b) RC-SW2

To better investigate visually inspected wall behavior of tested shear walls and to verify failure modes, contribution of shear and flexural deformations on total lateral drift was extracted utilizing the procedure introduced by Massone and Wallace (2004) (Appendix E) using measurements recorded by grid of installed LVDTs. Figure 3.42a and Figure 3.43a illustrate wall base shear (total base shear subtracted by shear at the base of exterior columns) against wall first-story shear displacement of RC-SW1 and RC-SW2 walls respectively. Similarly, wall shear versus first-story flexural displacement relation was extracted and presented in Figure 3.42b and Figure 3.43b for specimens RC-SW1 and RC-SW2 respectively.

98
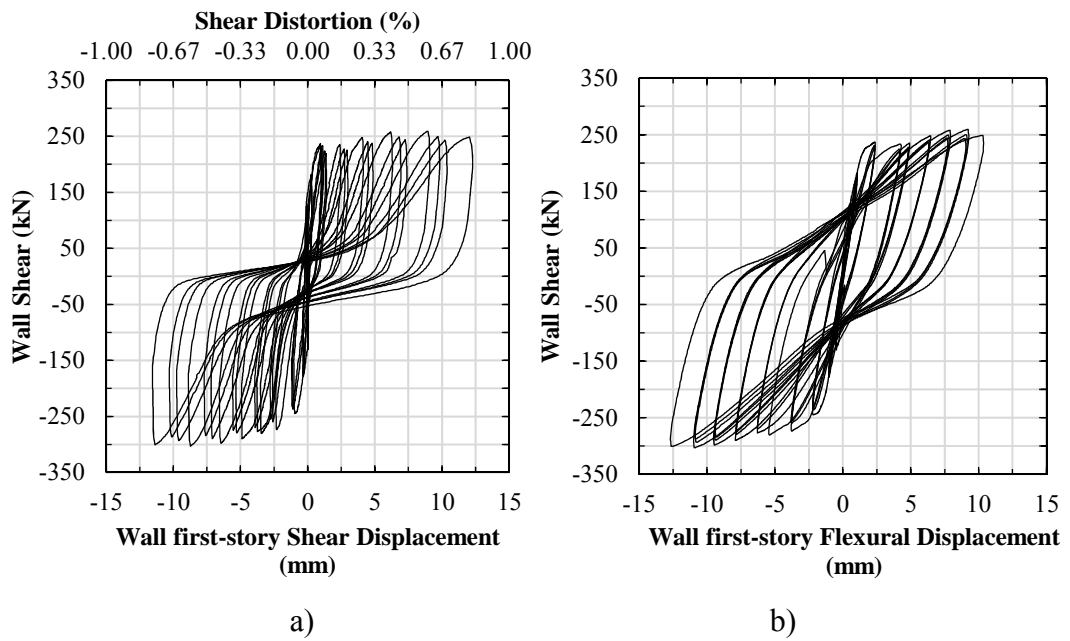
Figure 3.42 RC-SW1 first story hysteresis behavior; a) Shear b) Flexure
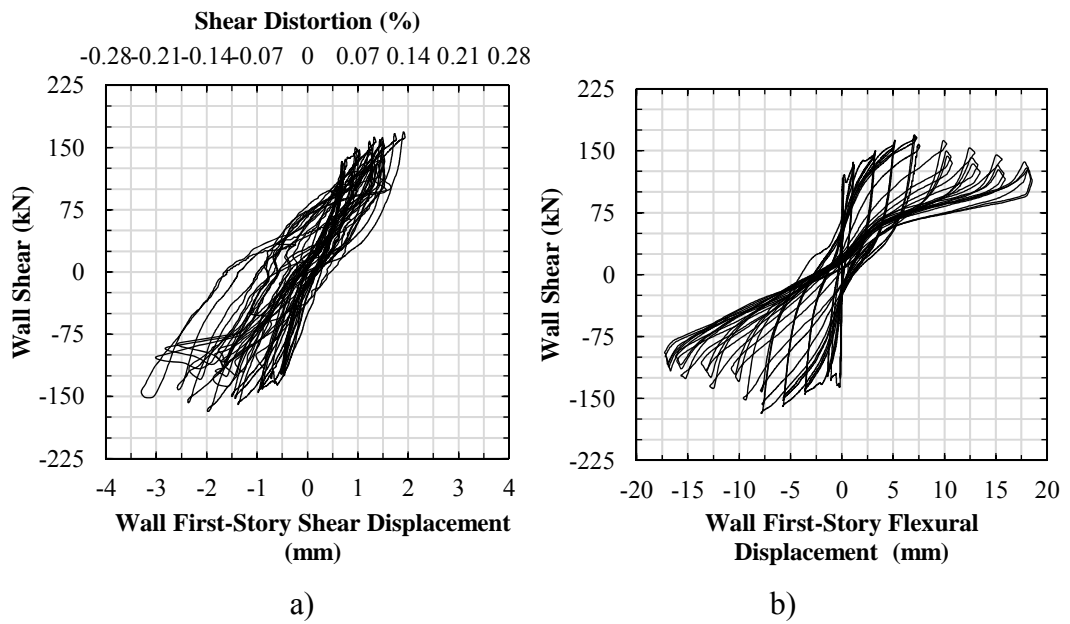
Figure 3.43 RC-SW2 first story hysteresis behavior; a) Shear b) Flexure

Figure 3.42a demonstrates shear response of RC-SW1. For this specimen with confined boundary elements shear deformations significantly contributed to the total lateral displacement owing to the boundary elements which controlled flexural and shear damage effectively. Despite large flexural and shear cracks in shear wall of RC-SW1in higher drifts, there was no strength degradation in lateral load capacity reaching 259 kN and 303 kN in positive and negative directions respectively, see Figure 3.42a and Figure 3.42b.

Looking at Figure 3.42a which shows shear behavior and Figure 3.42b which presents flexural behavior, it can be seen that inelasticity in shear and flexure behavior took place almost at the same level of wall shear force which was around 250 kN and smaller than nominal shear capacity of walls. Similar behaviors were reported earlier by other researchers such as Ozcebe and Saatcioglu (1989), Massone and Wallace (2004) and Beyer et al. (2011).

As it is evident in Figure 3.43a, following an elastic shear behavior during early cycles, RC-SW2 shear wall showed a slight inelastic shear response at higher levels of lateral drift. In Figure 3.43b flexural behavior of the RC-SW2 wall also displayed an inelastic response during the test which matched well with large flexural cracks over the height of the wall. Additionally Figure 3.43b reveals that shear capacity of the RC wall in flexural mode exhibited degrading trend after the RC wall reached its ultimate load bearing capacity which was 169 kN and 168 kN in positive and negative directions respectively. This response matched well with strength deterioration due to extensive flexural type damage in wall including bar rupture and bucking at wall boundary region, core crushing in compression region at wall boundaries and finally rocking type failure. Extensive pinching in Figure 3.43b is a sign of extensive rocking failure.

Similar to RC-SW1, inelasticity in shear and flexure behavior of RC-SW2 took place almost at the same level of wall shear force which is around 135 kN.

Despite the slight inelasticity in shear behavior, dominant failure mode was flexure with rocking of wall at higher displacement levels.

Comparing the two shear responses, Figure 3.42a and Figure 3.43a shows that shear displacements in RC-SW1 were larger than wall shear displacements in RC-SW2 due to higher level of shear stress in RC-SW1 compared to RC-SW2.

It is worth noting that web detailing of both specimens are fairly close to each other and the main difference was boundary region detailing. Minimum code requirements in boundary region dominated longitudinal reinforcement detailing. Thus, lateral strength of wall in RC-SW1, designed to TEC-2007, was considerably larger than RC-SW2, designed to TEC-1975, mainly due to the larger amount of longitudinal reinforcement in boundary region of RC-SW1 compared to RC-SW2. It is fairly impossible to separately examine the effect of confinement reinforcements and longitudinal steel in boundary elements of tested specimens as both parameters were different in RC-SW1 and RC-SW2. More specimens must be tested through parametric study by changing one parameter while keeping the others same to investigate the effect of considered parameters separately. However, considering conducted tests as verification tests to examine code criteria, it can be concluded that the specimen designed to TEC-2007, which had a heavy boundary region, had much better flexural hysteresis behavior and larger shear displacement capacity (Figure 3.42 and Figure 3.43).

3.5. Shear strength capacities for different failure modes

As stated in previous sections observed failure mode of tested wall specimens was flexural mode. In order to check the observed failure mode of tested shear walls, wall shear strength corresponding to flexural failure was compared with shear strength associated with some shear failure modes such as diagonal tension, diagonal compression and sliding shear. Maximum lateral loads bearing capacity

of the tested specimens which corresponded to formation of flexural failure was an average value of about 281 kN for shear wall of RC-SW1 in positive and negative directions and 168 kN for RC-SW2. This flexural strength was compared with shear strength corresponding to some shear type failure modes.

Sliding shear or shear friction strength was calculated using the equation 22.9.4.2 in ACI318-14. This equation, Eq (3.8), conservatively estimate the shear transfer strength.

$$V_n = \mu A_{vf} f_y \qquad (3.8)$$

Where the A_{vf} is the area of reinforcement crossing the assumed shear plane to resist shear. f_y is reinforcement yield strength and μ stands for shear-friction coefficient which is equal to 1.4 for monolithically constructed member. Coefficient of friction, μ, in this formula is specified unrealistically higher to account for neglecting of dowel action. Sliding shear strength was obtained for the section above the anchorage dowels where the failure surface was formed during the test. It must be mentioned that the total cross section area of anchorage steel was larger than wall longitudinal reinforcement cross section area. Turkish reinforced concrete practice code (TS500-2000) uses same equation to calculate shear-friction strength. The calculated sliding shear strength was about 790 kN and 230 kN for shear wall of RC-SW1 and RC-SW2, respectively. These values are larger than shear forces corresponding to observed flexural failure mode during the tests.

In order to calculate diagonal compression capacity of tested walls method stated in Paulay and Priestley (1992) was utilized. According to this method diagonal compression capacity of RC walls can be obtained by Eq (3.9).

$$V_i = (0.8 L_w b_w) v_{i,max} \tag{3.9}$$

where L_w and b_w are wall length and thickness, respectively. $v_{i,max}$ is the maximum shear stress in wall section which is limited as follows.

$$v_{i,max} \leq \left(\frac{0.22 \phi_{0,w}}{\mu_\Delta} + 0.03 \right) f_c' < 0.16 f_c' \leq 6 \, MPa \tag{3.10}$$

Where the $\phi_{0,w}$ is flexural over strength factor which is obtained as the ratio of flexural over strength or maximum flexural strength that could be developed in the wall over the moment resulting from code forces. This factor was approximately assumed as 1.4. The Parameter μ_Δ denotes for displacement ductility ratio which was taken as the maximum overall displacement ductility factor of tested specimens under applied loading cycles (μ_Δ is 4.5 and 5.5 for RC-SW1 and RC-SW2, respectively). The term $0.16 f_c'$ is to limit the shear stress in plastic region to 80% of maximum shear stress limit in elastic region to prevent diagonal compression failure. However experimental tests conducted by Portland Cement Association and the University of California at Berkley revealed that web crushing still may happen in wall webs with limited shear stress in displacement ductility levels higher than 4. Thus the term including μ_Δ is an additional limit to reduced the shear stresses to account for displacement ductility ratio of 4 or more. Estimated diagonal compression or web-crushing strength of tested walls based on Eq (3.9) was 458 kN for RC-SW1 and 487 for RC-SW2. Comparing these values with flexural capacity of tested walls, diagonal compression strength of each wall is higher than flexural strength of that wall.

Diagonal tension strength of tested wall can be calculated according to the equation by 18.10.4.1 in ACI318-14, see Eq (3.11).

$$V_n = A_{cv}(\alpha_c \lambda \sqrt{f_c'} + \rho_t f_y) \qquad (3.11)$$

In this equation, the A_{cv} is gross area of wall section bounded by web thickness and length of section in the direction of shear force. Parameter α_c is a coefficient defining the relative contribution of concrete strength to nominal wall shear strength which equals to 2 in psi units (0.17 in MPa units) for walls with $h_w/l_w \geq$ 2.0. For normal weight concrete λ equals to 1. f_y is reinforcement yield strength and ρ_t represents transverse reinforcement ratio. RC wall shear strength computed using the ACI318-14 equation was 358.4 kN for shear wall of RC-SW1 and 332.7 kN for shear wall RC-SW2.

Turkish Earthquake Code (TEC-2007) has also similar equation to determine shear capacity of reinforced concrete walls. According to 3.6.7.1 in TEC-2007 wall shear strength is calculated using equation Eq (3.12).

$$V_n = A_{ch}(0.65 f_{ct} + \rho_{sh} f_{yw}) \qquad (3.12)$$

Where the A_{cv} is gross area of wall section. f_{ct} and f_{yw} are concrete tensile strength and horizontal reinforcement yield strength, respectively. Concrete tensile strength is calculated using the equation 3.1 ($f_{ct} = 0.35\sqrt{f_c}$) in TS500-2000. ρ_{sh} is volumetric ratio of web horizontal reinforcement. Shear strength obtained by Eq (3.12) was 419.5 kN and about 400 kN for shear walls of RC-SW1 and RC-SW2, respectively. Wall shear capacities calculated for both RC-SW1 and RC-SW2 specimens using equations proposed by ACI318-14 and TEC-2007 are larger than maximum wall base shear obtained from the tests, see Table 3.3.

Table 3.3 Wall shear capacities for different failure modes

Failure Modes	Shear strength (kN)	
	RC-SW1	RC-SW2
Sliding shear (ACI318-14)	790	230
Diagonal compression (Paulay & Priestley, 1992)	458	487
Diagonal tension (ACI318-14)	358.4	332.7
Diagonal tension (TEC-2007)	419.5	400
Flexural yielding (Initial failure mode during the test)	281	168

Considering that all calculated shear capacities associated with shear types of failure were larger than the maximum measured wall base shear, observed flexural failure mode was verified.

CHAPTER4

ANALYTICAL MODELING OF TEST SPECIMENS

4.1. General

In the context of this chapter performance limits and generalized force-deformation relations for RC shear walls proposed by ASCE/SEI 41-13 and TEC-2007 which are used in nonlinear analysis and performance evaluations were investigated. To achieve this, nonlinear pushover analysis was performed and analytical models were calibrated to capture the envelope of the overall hysteresis response of tested frame specimens. Through the nonlinear pushover analysis it was aimed to find inflection point over the wall height. Then wall base shear history which was measured during the test converted to base moment history which could not be directly calculated from experiments. Analytically obtained moment capacities and corresponding shear forces, along with code specified modeling parameters are used in construction of wall member response backbone curve. Analytical model of tested frames was constructed in SeismoStructs v7.0 software package. Structural elements comprising beams, columns and walls were modeled with beam-column line elements which were discretized to fibers in cross section.

4.2. Model description

Analytical model constructed in SeismoStruct v7.0 software is presented in Figure 4.1. Frame members were represented with one distributed plasticity line elements with force-based formulation except for first story shear wall which was

modeled with two elements. As longitudinal bars of boundary columns were welded to the base plate provided on the foundation of wall, they effectively contributed to the flexure capacity of the wall. Moreover, anchorage dowels at lower sections up to about 300 and 360 mm are the additional members which transfer loads from wall to foundation. Thus, increased moment capacity at wall lower sections shifted up the failure surface just above the surface at which anchorage dowels ended. Two elements with different section details were used to model the first story wall to match the model to the tested specimen as much as the software allows. One element with 300 mm length and displacement-based formulation was used in the analysis to model lower part of the shear wall which includes anchorage dowels.
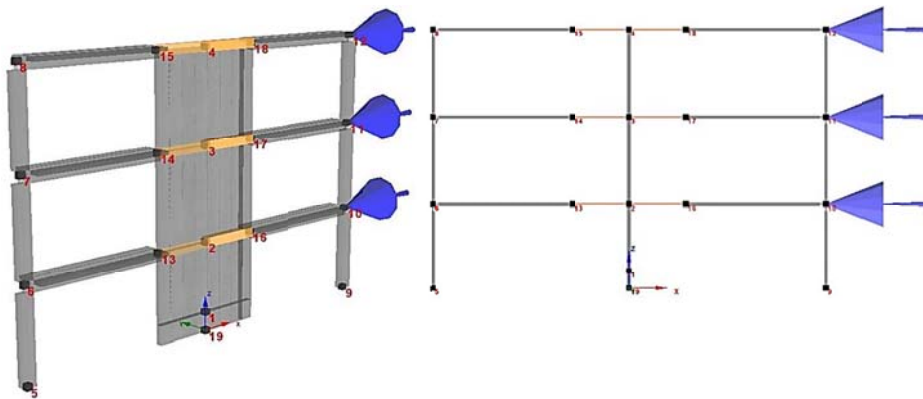
Figure 4.1 Analytical model constructed in SeismoStruct v7.0

Cross section of this element was discretized with fibers representing wall longitudinal reinforcements welded to the base plate in boundary regions and anchorage dowels assuming perfect bond between reinforcement and concrete. Wall element above this base element was discretized according to wall section detail above the anchorage dowels. The element response is evaluated by integration of uniaxial stress-strain relationship on the sections comprising individual fibers at integration point locations over the length of elements (Figure 4.2).
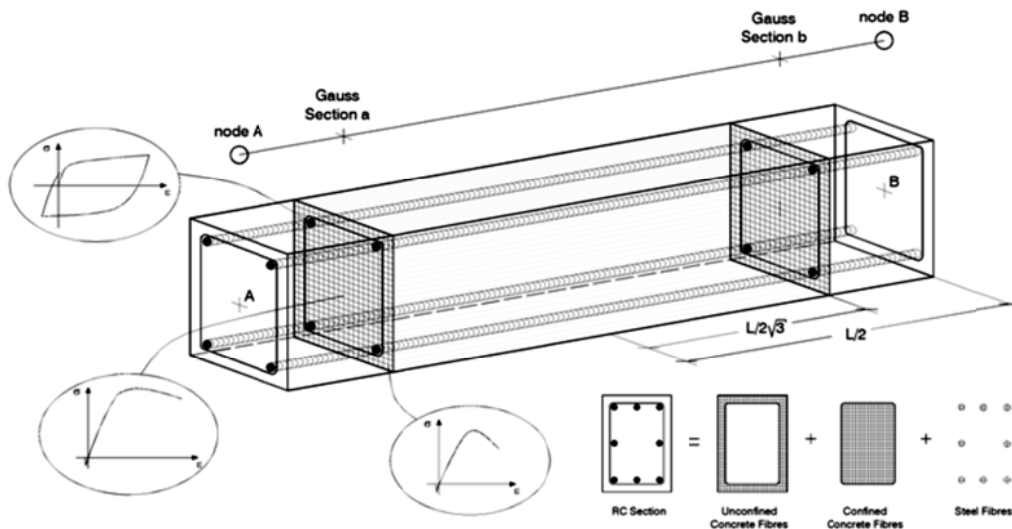
Figure 4.2 Discretization of a typical reinforced concrete cross-section (from SeismoStruct v7.0 user manual)

Number of integration points was three along beam length and shear wall height. This amount was four for columns. Each fiber is assigned a nonlinear uniaxial material behavior.

Modeling each structural member with one forced-based element having multiple numbers of integration points eliminates the need for discretizing members to a couple of elements as for displacement-based elements. The reason displacement-based element was selected for lower element of the wall is that very short forced-based element (element with length considerably smaller than its cross section width) imposes convergence difficulties to analysis.

Member gravity loads are automatically calculated as permanent gravity loads. Weight of steel blocks are automatically calculated and applied as permanent loads by defining distributed mass on beams. Geometric nonlinearities along with material nonlinearities were considered in analysis.

109

Nonlinear pushover analysis with the same displacement history of the experiment at third story was applied on the analytical models using displacement control approach. Similar to the experimental loading scheme, lateral loads of 0.58P and 0.20P were applied to the second and first story levels, respectively, during the push over analysis. The load P is the force applied on the model at the control point (which is top third story) corresponding to each applied displacement value. It was aimed to obtain bending moment diagram throughout the height of the wall and determine approximate location of inflection point developing along the wall height. Through this analysis the wall shear force corresponding to nominal moment capacity of wall members can be obtained more accurately using the exact lateral load pattern as it was in experiment.

4.3. Material models properties

4.3.1. Concrete material model

Nonlinear hysteretic constitutive model presented by Chang and Mander (1994) was used to define stress-strain relationship of concrete material. The ascending and descending branches of tension and compression parts can be controlled separately through changing some parameter (SeismoStruct user Manual, 2014). Descending branch of tension and compression parts of concrete stress-strain curve was calibrated to obtain a backbone capacity curve as close as possible to the envelope of the experimental hysteresis curve of frames (Appendix C).

4.3.2. Steel material model

The hysteresis steel model proposed by Dodd and Restrepo (1995) steel model was used as the steel constitutive model in all members.

It must be mentioned that as there were no visible flexural crack and flexural damage in lower 300 mm of the RC wall in RC-SW1, the yield strength of

reinforcement steels in the fiber element representing the lower 300 mm of the RC wall was intentionally increased in such a way that the steel bars remain in elastic region (Appendix D).

4.4. Analysis results

Total base shear-top displacement hysteresis relationship of tested frames is given in Figure 4.3. Base shear-top displacement backbone curve obtained from the nonlinear pushover analysis is provided in same figure as well. Looking at the Figure 4.3, it is clearly seen that there is a good match between analytical backbone curve and envelope of experimental overall hysteretic behavior.
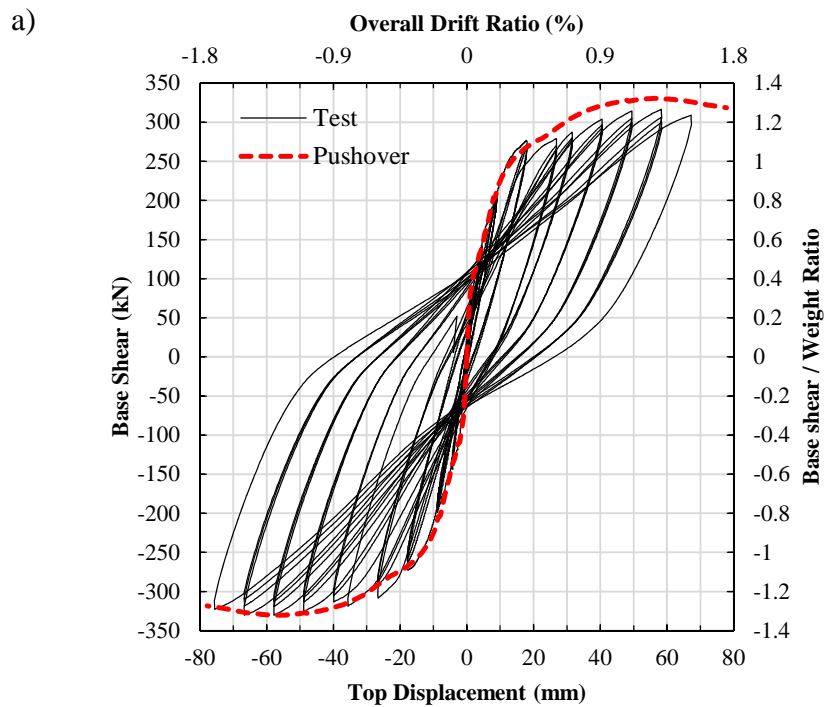
Figure 4.3 Base shear-top displacement relationship obtained from analysis and experiment; a) RC-SW1 b) RC-SW2

b)
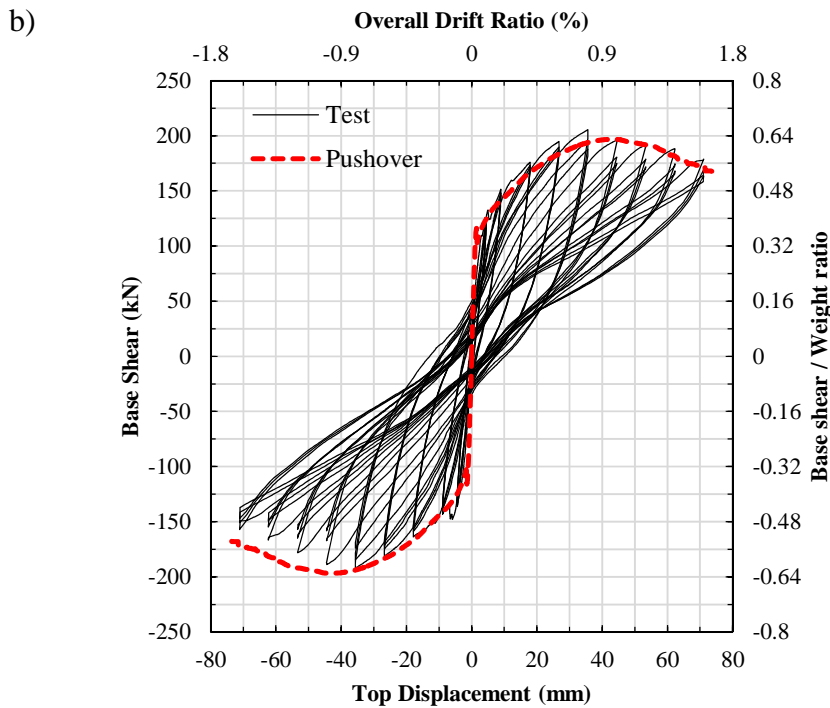
Figure 4.3 Base shear-top displacement relationship obtained from analysis and experiment; a) RC-SW1 b) RC-SW2 (Cont'd)

Ultimate moment capacity of RC walls obtained from pushover analysis on both specimens was used to construct the analytical backbone proposed by ASCE/SEI 41-13 and TEC-2007. Also, bending moment history at the base of the walls was calculated using $M = V.h_{eff}$ in which h_{eff} is approximately equal to $\frac{2}{3}h_s$ (h_s is the wall shear span length). Figure 4.4 shows the bending moment diagram of the RC walls in RC-SW1 and RC-SW2.
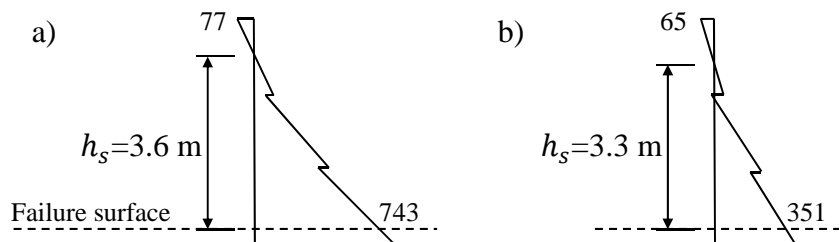
Figure 4.4 Wall moment diagram; a) RC-SW1 b) RC-SW2

4.5. Deformation performance limits and modeling parameters

4.5.1. ASCE/SEI41-13

Seismic performance evaluation standard of ASCE/SEI 41-13 prescribes generalized force-deformation relationships which are used to represent deformation-controlled structural elements behavior. These idealized responses are used to model structural elements in nonlinear analysis for seismic performance evaluations. Multilinear curves in Figure 4.5 are idealized force-deformation relationship of reinforced concrete members for deformation-controlled actions. More specifically, for reinforced concrete shear walls, when inelastic behavior is governed by flexure, backbone curve (a) is used to define inelastic response. Backbone curves (b) and (c) represent inelastic behavior of shear walls with shear dominant behavior. As the failure mode of RC-SW1 was initially flexure followed by sliding shear, and flexure for RC-SW2, the backbone curve for flexure mode was constructed. Parameters a, b, and c in these curves are the modeling parameters for shear walls which are specified in Table 4.1 for flexural controlled shear walls. In addition to modeling parameters, member's performance acceptance criteria as limiting values, shown in Figure 4.6, are also provided in this table. According to Table 4.1, different modeling parameters and rotation limits which are presented in terms of plastic hinge rotations are introduced for different levels of axial load and maximum average shear stresses.

In order to evaluate the ASCE/SEI 41-13 suggested backbone curve in representing nonlinear response of tested RC shear walls, idealized force-deformation relationship of shear walls was constructed using the procedure described in ASCE/SEI 41-13. To do this, nominal flexural strength (M_n) and flexural yield strength (M_y) of RC walls were calculated according to 10.7.2.3 provision of ASCE/SEI 41-13. Nominal flexural strength was calculated using

section analysis considering all of the longitudinal steel (including web reinforcement). Moment capacity corresponding to compressive strain of 0.003 in outer compressive edge of the wall was assumed as the nominal flexural strength.
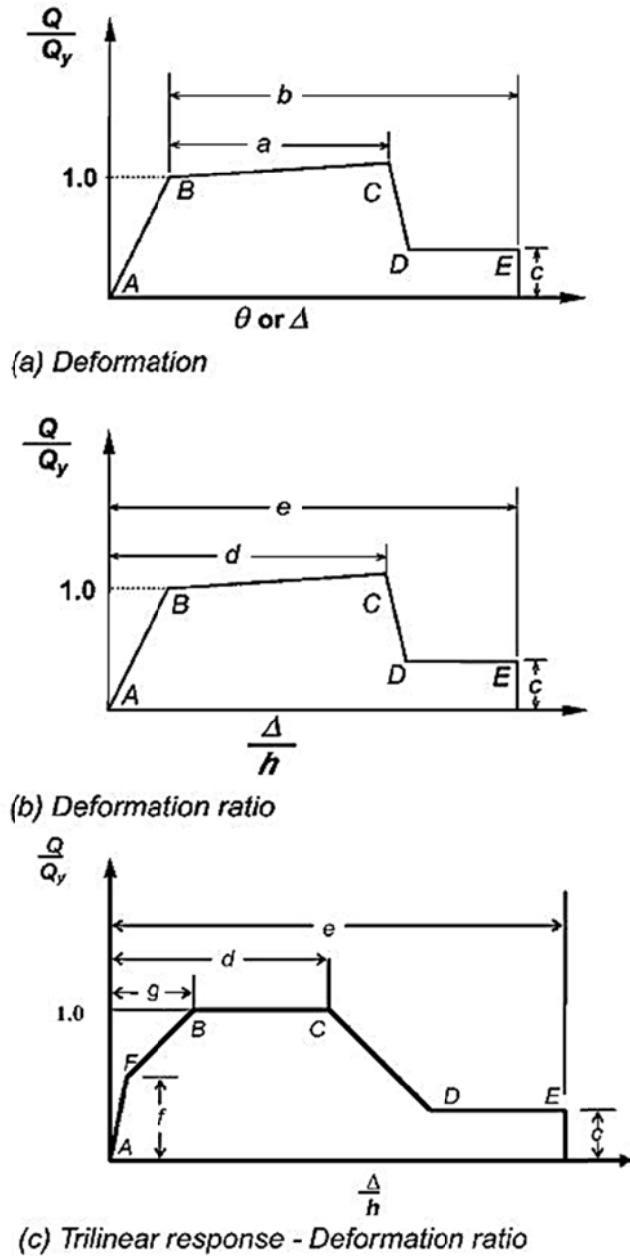
Figure 4.5 Generalized component force-deformation relations for concrete elements or components (ASCE/SEI 41-13)

Only longitudinal reinforcements in wall boundary members were included in flexural yield strength calculations. Moment strength corresponding to strain equals to steel yield strain at center of area of boundary reinforcements was selected for yield moment. Yield rotation in backbone curve was calculated as $\theta_y = \frac{M_y}{E_c I_{cr}} L_p$. Secant modulus of elasticity of concrete is $E_c = 4730\sqrt{f_c'}$. I_{cr} is the cracked moment of inertia ($I_{cr} = 0.5 I_g$). Plastic hinge length (L_p) was assumed to be equal to $0.5 L_w$ (L_w is wall depth). Axial load was assumed equal to gravity loads in section analysis. The same steel and concrete material models as used in pushover analysis were used in section analysis except the tensile strength of the concrete which was neglected in ultimate moment capacity calculations.

Table 4.1 Modeling parameters and numerical acceptance criteria for nonlinear procedures—RC shear walls and associated components controlled by flexure (ASCE/SEI 41-13)

Conditions			Plastic Hinge Rotation (radians)		Residual Strength Ratio	Acceptable Plastic Hinge Rotation[a] (radians) Performance Level		
			a	b	c	IO	LS	CP
i. Shear walls and wall segments								
$\frac{(A_s - A_s')f_y + P}{t_w l_w f_c'}$	$\frac{V}{t_w l_w \sqrt{f_c'}}$	Confined Boundary[b]	0.015					
≤0.1	≤4	Yes	0.010	0.020	0.75	0.005	0.015	0.020
≤0.1	≥6	Yes	0.009	0.015	0.40	0.004	0.010	0.015
≥0.25	≤4	Yes	0.005	0.012	0.60	0.003	0.009	0.012
≥0.25	≥6	Yes	0.008	0.010	0.30	0.0015	0.005	0.010
≤0.1	≤4	No	0.006	0.015	0.60	0.002	0.008	0.015
≤0.1	≥6	No	0.003	0.010	0.30	0.002	0.006	0.010
≥0.25	≤4	No	0.002	0.005	0.25	0.001	0.003	0.005
≥0.25	≥6	No	0.002	0.004	0.20	0.001	0.002	0.004
ii. Shear wall coupling beams[c]								
Longitudinal reinforcement and transverse reinforcement[d]	$\frac{V}{t_w l_w \sqrt{f_c'}}$			0.050				
Conventional longitudinal reinforcement with conforming transverse reinforcement	≤3		0.025	0.040	0.75	0.010	0.025	0.050
	≥6		0.020	0.035	0.50	0.005	0.020	0.040
Conventional longitudinal reinforcement with nonconforming transverse reinforcement	≤3		0.020	0.025	0.50	0.006	0.020	0.035
	≥6		0.010	0.050	0.25	0.005	0.010	0.025
Diagonal reinforcement	NA		0.030	0.050	0.80	0.006	0.030	0.050

[a]Linear interpolation between values listed in the table shall be permitted.
[b]A boundary element shall be considered confined where transverse reinforcement exceeds 75% of the requirements given in ACI 318 and spacing of transverse reinforcement does not exceed $8d_b$. It shall be permitted to take modeling parameters and acceptance criteria as 80% of confined values where boundary elements have at least 50% of the requirements given in ACI 318 and spacing of transverse reinforcement does not exceed $8d_b$. Otherwise, boundary elements shall be considered not confined.
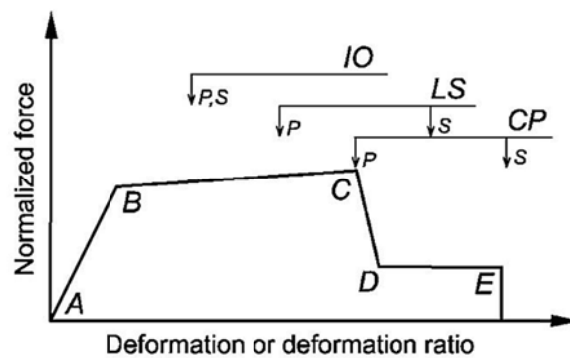
Figure 4.6 Element deformation acceptance criteria (ASCE/SEI 41-13)

There were no bending moment measurements at the base of shear walls during the experiments. However, wall base shear history can be calculated from experimental measurements of total applied loads and exterior columns base shear. Hence, wall base shear history was converted to wall base bending moment history using shear span length obtained from pushover analysis at the point of ultimate moment capacity. Then the backbone curve was compared with experimental wall bending moment-plastic hinge rotation history. Wall rotation history over the plastic hinge was calculated using the vertical displacements of the outer edges of shear wall recorded by vertically installed LVDTs. Wall Plastic hinge region was assumed from the base to up to a distance equals to 50 percent of flexural depth of wall. In the calculation of wall base bending moment history, shear forces were multiplied by effective shear span. Effective shear span was assumed as $\frac{2}{3}$ of shear span length (the distance between maximum and zero moment or inflection point). Figure 4.7 illustrates the obtained backbone curve and response history of first story shear wall simultaneously. Deformation performance limits corresponding to Immediate Occupancy (IO), Life Safety (LS) and Collapse Prevention (CP) performance levels are also marked on the backbone curve.

116

a)
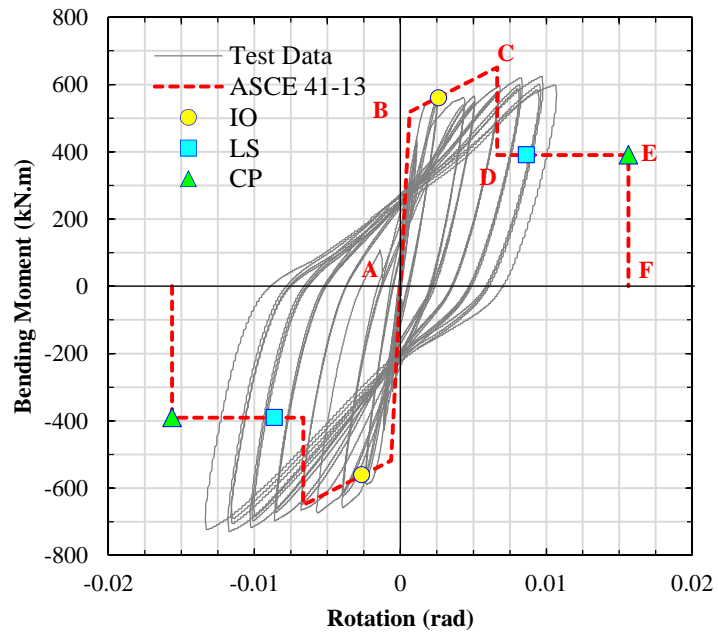
b)
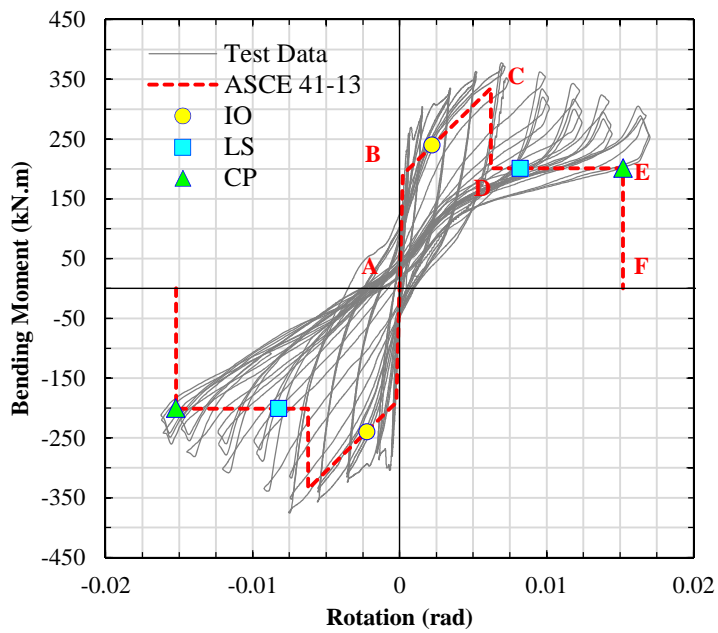
Figure 4.7 Shear wall flexural response history and backbone curve and
performance limits predicted by ASCE/SEI 41-13; a) RC-SW1, b) RC-SW2

Figure 4.7a and Figure 4.7b show that ASCE/SEI 41-13 backbone curve can predict wall flexural behavior of RC-SW1 and RC-SW2 with acceptable level of safety. As indicated in ASCE/SEI41-13, a linear degradation in strength from point C to E (Figure 4.7) in capacity backbone curve would represent the behavior more realistically. Comparing the test data and backbone curve, a sudden drop in resistance after point C is a conservative assumption for both specimens. In RC-SW1, deformation level of life safety performance level (LS) is conservatively predicted on the safe side. However, this level of deformation matches with the point in test response corresponding to slight reduction in strength for RC-SW2. Due to safety concerns, the test of RC-SW1 was stopped at an early cycle without softening in hysteresis response. However, looking at the observed damage levels and other hysteresis characteristics of this specimen such as energy dissipation, cycle stiffness and in-cycle behavior histories, it can be expected that if the test would be continued, collapse prevention deformation limit would be on the safe side. In RC-SW2 predicted deformation for collapse prevention limit state is very close to the deformation capacity of the wall.

4.5.2. TEC-2007

Turkish Earthquake Code (TEC-2007) requires a strain based performance evaluation method. In this method member performance limits are specified by concrete and steel strain limits. According to TEC-2007, three limit stats are Minimum Damage Level (MN), Safety Limit (GV) and Collapse Limit (GÇ). Table 4.2 illustrates steel and concrete strain limits in reinforced concrete sections for different performance limit states.

This code permits using one of idealized plastic moment-plastic rotation relationships to simulate flexural response of reinforced concrete members in nonlinear analysis. Figure 4.8a and b show a backbone curves without and with hardening parts respectively.

Table 4.2 Steel and concrete strain limits in reinforced concrete section for
different sectional damage states

Damage States	Strain limits		
	ε_s	$\varepsilon_{c\ (core)}$	$\varepsilon_{c\ (cover)}$
MN	0.01	-	0.0035
GV	0.04	$0.0035 + 0.01(\rho_s/\rho_{sm}) \leq 0.0135$	-
GÇ	0.06	$0.004 + 0.014(\rho_s/\rho_{sm}) \leq 0.018$	-

ρ_s: Existing confinement reinforcement volumetric ratio; ρ_{sm}: required confinement reinforcement volumetric ratio according to TEC-2007
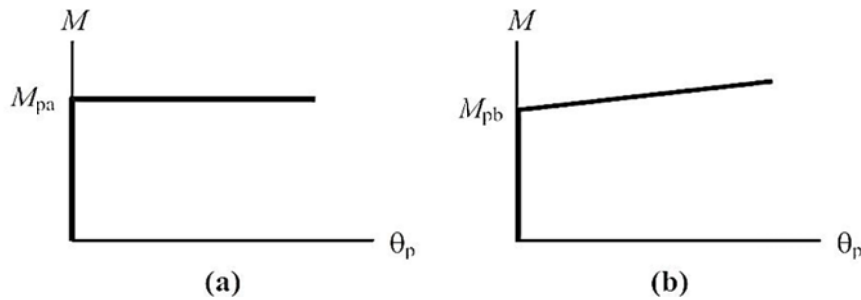
Figure 4.8 Idealized plastic moment-rotation relationships in TEC-2007

In this study the backbone curve which is shown in Figure 4.8a without hardening was considered. No strength degradation is considered in TEC-2007 proposed backbone curve. Based on TEC-2007, M_p (plastic moment capacity) can be calculated using detailed moment-curvature analysis considering material characteristic strength and strain hardening of steel. The same procedure as in ASCE/SEI 41-13 was used to calculate M_p assuming 0.003 of ultimate strain in extreme fiber of cross section. Similar to ASCE/SEI 41-13, yield rotation was

calculated as $\theta_y = \frac{M_y}{(EI)_e} L_p$ using cracked flexural rigidity. For columns and shear walls with low axial load ($N_D/(A_c\, f_{cm}) \leq 0.10$), cracked flexural rigidity is $(EI)_e = 0.4(EI)_0$. Plastic hinge length (L_p) is specified as $0.5h$ (h is the wall dimension in the direction of loading) by TEC-2007.

Constructed moment-rotation backbone curve for RC-SW1 and RC-SW2 according to TEC-2007 are shown in Figure 4.9. Experimental Moment-rotation history of the wall base over the plastic hinge which was obtained and described in previous part is provide in the same figure, simultaneously. Figure 4.9 indicates that TEC-2007 significantly overestimate deformation capacity limits of the investigated shear walls.

a)
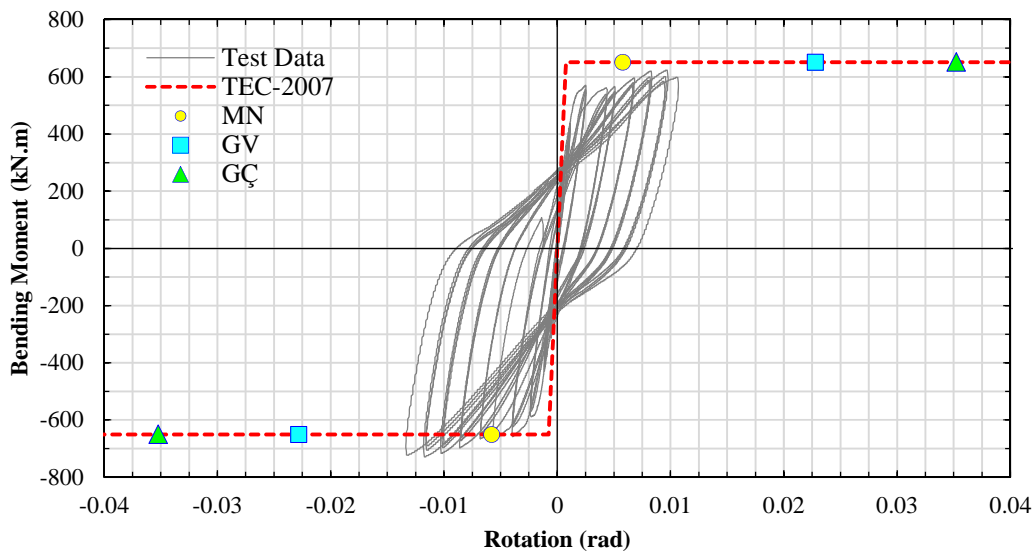
Figure 4.9 Shear wall flexural response history and backbone curve and performance limits predicted by TEC-2007; a) RC-SW1, b) RC-SW2

b)
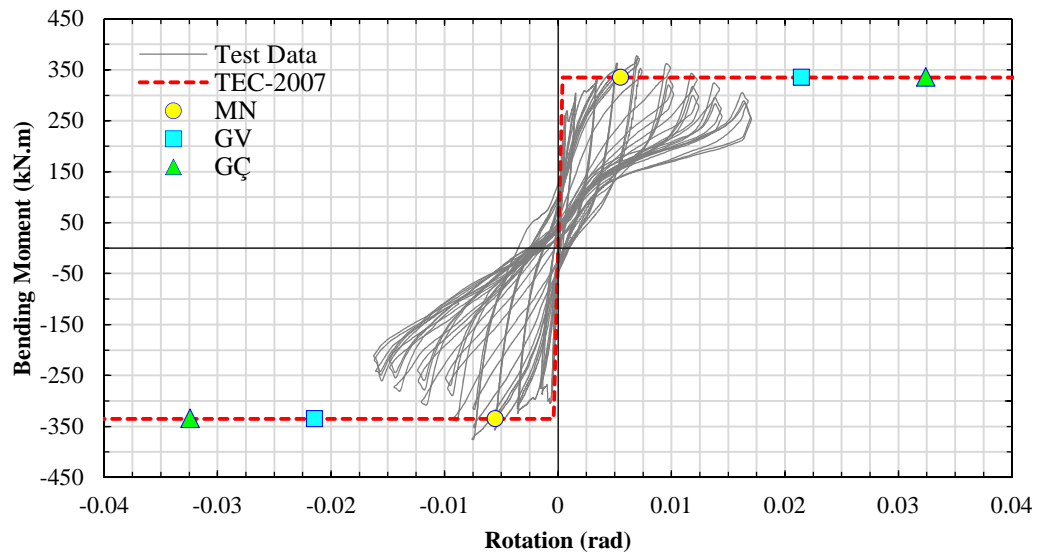
Figure 4.9 Shear wall flexural response history and backbone curve and performance limits predicted by TEC-2007; a) RC-SW1, b) RC-SW2 (Cont'd)

CHAPTER5

CONCLUSION

5.1. Summary

In the context of this dissertation, seismic performance of 2 large scale RC shear walls surrounded by frame elements was investigated through quasi–static reversed cyclic loading tests. Most of the available experimental studies within the relevant literature were conducted on isolated cantilever RC walls. There are very few number of large scale experimental tests on frame-wall specimens. Specimens composed of wall surrounded with frame in this study provided realistic lateral load flow through structural elements. Experimentally observed damage, distributed in structural elements, shed light to make a relevant judgment about performance of the whole system. Thus, these tests can be considered as verification large scale tests in order to examine the behavior of walls in low- to mid-rise buildings RC structures.

Furthermore, owing to very detailed experimental measurements provided in this thesis, the conducted tests can be used as benchmark and calibration tests for further analytical studies.

Two ½ scaled three-story three-bay RC test frames with RC shear wall in middle bay were tested. These two specimens are identical in geometrical dimensions and represent internal frames of a prototype three-story residential building constructed in different time periods in Turkey. One of the prototype buildings was designed, detailed and constructed according to the last generation of Turkish

123

earthquake code (TEC-2007) and Turkish reinforced concrete practice code (TC500-2000). For the other building, reinforcement detailing and seismic requirements were determined based on one of the earliest generations of Turkish earthquake code (TEC-1975) and Turkish reinforced concrete practice code (TC500-1981). Some rigid criteria such as low spaced stirrups and large longitudinal and transvers reinforcement ratio for detailing of boundary regions in RC shear walls are given by TEC-2007. However, TEC-1975 specifies minor requirements without confinement reinforcements for boundary regions of shear walls. The effect of confinement requirements of boundary regions in behavior of RC shear walls was verified through comparing one more detailed and one lightly detailed boundary regions.

Experimental observations during the tests were reported and discussed in detail for both specimens. Seismic behavior in terms of actual deformation and lateral load strength obtained through implementation of reversal cyclic quasi-static loading tests was examined. Fundamental seismic characteristics of lateral load bearing elements such as ductility, energy dissipation, stiffness and strength degradation aspects and equivalent viscos damping were assessed during loading cycles and their correlation with observed damages were discussed.

Finally, analytical models of tested frames were constructed in SeismoStructs v7.0 software package and nonlinear pushover analysis was performed. Analytical models were accurately calibrated to capture the envelope of the overall hysteresis response of tested frame specimens. Through the nonlinear pushover analysis it was aimed to estimate inflection point over the wall height to convert wall base shear history which was measured during the test to base moment history which could not be directly calculated from experiments. Analytically obtained moment capacities and corresponding shear forces, along with code specified modeling parameters are used in construction of wall member response backbone curve used in nonlinear analysis. Then performance limits and generalized force-

deformation relations for RC shear walls members proposed by ASCE/SEI 41-13 and TEC-2007 which are used in nonlinear analysis and performance evaluations were investigated.

Furthermore, owing to the grid of LVDTs installed on the walls, contribution of shear and flexure deformations in total lateral displacement were extracted and discussed.

The specimen design to TEC-2007 (RC-SW1) exhibited very satisfactory behavior under applied lateral forces showing ductile flexural failure mode. For this specimen failure mechanism started with flexural cracks over the plastic hinge region followed by corner to corner diagonal shear cracks. Then, sliding shear mechanism formed at first-story drift ratio as high as 1.5% which is normally selected as a design drift for shear walls. Even at 1.8% of first-story drift ratio, there was very slight reduction in lateral load bearing capacity of the frame-wall specimen. Damage in other structural elements at this level of drift ratio were flexural cracking in exterior columns, moderate damage in joints due to shear cracking, cover spall and hinging in beam ends at wall side. The specimen designed according to TEC-1975 (RC-SW2), in contrast to RC-SW1, had concentrated failure surface. Plastic deformations concentrated at two major horizontal cracks which formed at the opposite sides of the wall due to reversed cyclic loading and merged together at about 0.7% first story drift ratio. This ratio of drift corresponds to the lateral load capacity of the wall. After this point due to rocking mechanism lateral load bearing capacity degraded considerably. Although failure mechanism of RC-SW2 was flexural type, there was extensive pinching in overall hysteresis behavior. Shear strength deterioration in wall was mainly due to the concrete strength deterioration during crack opening and closure, rocking type mechanism due to buckled and/or ruptured longitudinal bars. Flexural plastic hinging with extensive spalling in beam ends close to the wall, slight flexural yielding in column ends at the base level, and shear cracking in beam-column

joint representing moderate to heavy damage level were the major perceived damage level in other frame elements.

5.2. Conclusions

Following conclusions are made through experimental and analytical work done.

- The specimen design to TEC-2007 (RC-SW1) in comparison with the specimen designed according to TEC-1975 (RC-SW2) exhibited very satisfactory shear and flexure behavior under applied lateral forces showing ductile flexural failure mode.

- In both wall specimens sliding and failure surface was formed just above the anchorage dowels at a height about 300 mm from the wall base where the moment capacity dramatically changes. It is believed that providing staggered starter bars or anchorage dowels can cause the damage to be distributed over a larger distance along the wall height and may prevent formation of preemptive failure surface.

- Considering the tests as code requirements' verification tests it can certainly be concluded that the boundary reinforcement requirements (confinement and longitudinal reinforcements) have significant effect on improving flexural and shear hysteresis behavior of RC walls.

- Overall displacement ductility factor associated with maximum lateral load bearing capacity (first story drift ratio of about 1.5%) of RC-SW1 with special boundary detailing was about 4. This amount was around 3 for RC-SW2 without special wall boundary element which was calculated at the point when base shear was topped (first story drift ratio of about

0.7%). Due to safety concerns cyclic test was not continued to higher overall drift ratio for both specimens. However, considering damage level, failure mechanism and overall hysteresis behavior of the specimens if lateral loading was continued to larger displacement cycles, ultimate displacement ductility factors larger than 3 or 4 would have been expected for this specimens.

- In the first cycle of each set of displacement cycles with constant amplitudes, energy absorption of both specimens was slightly higher than the energy dissipated in subsequent cycles. This reduction was more pronounced after formation of failure mechanism which was associated with the cycles in which maximum strength was reached. Cumulative hysteretic energy increased with increasing amplitudes of cycles due to formation of cracks and yielding in members before maximum load bearing capacity of frames was reached for both RC-SW1 and RC-SW2 specimens. However, this rate was lower for the cycles after formation of extensive damage. In lower drift ratios, normalized cumulative hysteresis energy of RC-SW2 was slightly higher than RC-SW1. This implies that the more damage such as concrete cracking or steel yielding was developed in RC-SW2 compared with RC-SW1 in lower drift ratios. However, at higher ductility levels, normalized cumulative hysteresis energy of RC-SW2 is lower than RC-SW1.

- No considerable stiffness degradation in cycles with constant displacement amplitude was observed for both specimens under applied loading. Conversely, as it was expected, cycle stiffness reduced as displacement amplitude increased. This reduction was more prominent for earlier cycles of loading. The trend of normalized cycle stiffness degradation was very close for both tested specimens. For the cycles corresponding to maximum

lateral load bearing capacity, effective cycle stiffness was around 25% and 35% of ideal elastic stiffness for RC-SW1 and RC-SW2, respectively.

- Equivalent hysteresis damping for very early cycles was larger for RC-SW2 compared with RC-SW1, which indicates that level of nonlinearity (due to concrete cracking and some yielding in steel) in small drifts are higher for RC-SW2. However, unlike RC-SW1, there was a decreasing trend in equivalent hysteresis damping due to formation of rocking mechanism after the point maximum shear capacity was reached.

- ASCE/SEI 41-13 uses rotation based approach in member performance evaluation and performance criteria. Modeling parameters which is used in nonlinear analysis are also in terms of rotations. ASCE/SEI 41-13 backbone curve can predict wall flexural behavior of RC-SW1 and RC-SW2 with acceptable level of safety. Moreover, immediate occupancy and life safety performance acceptance levels are conservatively predicted on the safe side by this code. While ASCE/SEI 41-13 introduces collapse prevention deformation limit on the safe side for RC-SW1, this deformation limit is very close to the deformation capacity of the wall in RC-SW2.

- Unlike ASCE/SEI 41-13, TEC-2007 requires a strain based performance evaluation method and member performance limits are specified by concrete and steel strain limits. Another major difference between ASCE/SEI 41-13 and TEC-2007 is that there is no descending branch in member behavior backbone curve predicted by TEC-2007. Based on the performance limit criteria specified for different performance states, TEC-2007 significantly overestimates deformation capacity limits of the investigated shear walls of RC-SW1 and RC-SW2.

128

REFERENCES

ACI 318-14. (2014). *Building code requirements for structural concrete (ACI 318-14) and commentary*. American Concrete Institute.

Alexander, C. M., Heidebrecht, A. C., & Tso, W. K. (1973). Cyclic load tests on shear wall panels. In *Proceedings, fifth world conference on earthquake engineering, Rome* (pp. 1116-1119).

ASCE/SEI 41-13. (2014). *Seismic Evaluation and Retrofit of Existing Buildings (41-13)*. Reston: American Society of Civil Engineers.

Barda, F., Hanson, J. M., & Corley, W. G. (1977). Shear strength of low-rise walls with boundary elements. *Special Publication*, *53*, 149-202.

Bekő, A., & Roško, P. (2013). Testing of Stiff Shear Walls. In *Industrial Safety and Life Cycle Engineering - IRIS Book* (pp. 213–234). Vienna, Austria: VCE Vienna Consulting Engineers ZT GmbH.

Beyer, K., Dazio, A. & Nigel Priestley, M.J., (2011). Shear deformations of slender reinforced concrete walls under seismic loading. *ACI Structural Journal, 108(108),* pp.167–177.

Canbay, E., Ersoy, U., & Tankut, T. (2004). A three component force transducer for reinforced concrete structural testing. *Engineering Structures*, 26(2), 257-265.

Dazio, A., Beyer, K., & Bachmann, H. (2009). Quasi-static cyclic tests and plastic hinge analysis of RC structural walls. *Engineering Structures, 31*(7), 1556-1571. doi:10.1016/j.engstruct.2009.02.018

Dillon, P. (2015). *Shear Strength Prediction Methods for Grouted Masonry Shear Walls*. Brigham Young University.

Dodd, L., & Restrepo-Posada, J. (1995). Model for predicting cyclic behavior of reinforcing steel. *J. Struct. Eng.*, 121, 433–445.

Erberik, M., & Kurtman, B. (2010). A detailed evaluation on degrading behavior of structural systems. *In Proceedings of the 9th U.S. National and 10th Canadian Conference on Earthquake Engineering*. Toronto.

FEMA 306. (1998). *Evaluation of Earthquake Damaged Concrete and Masonry Wall Buildings, Basic Procedures Manual*. Washington, DC: Federal Emergency Management Agency.

Fintel, M., & Fintel, M. (1995). Performance of buildings with shear walls in earthquakes of the last thirty years. *PCI journal*, *40*(3), 62-80.

Greifenhagen, C., & Lestuzzi, P. (2005). Static cyclic tests on lightly reinforced concrete shear walls. *Engineering Structures*, *27*(11), 1703-1712.doi:10.1016/j.engstruct.2005.06.008

Gulec, C. K., & Whittaker, A. S. (2009). *Performance-based assessment and design of squat reinforced concrete shear walls*. (Tech. Rep. No. MCEER-09-0010). Multidisciplinary Center for Earthquake Engineering Research MCEER.

Hidalgo, P. A., Jordan, R. M., & Martinez, M. P. (2002). An analytical model to predict the inelastic seismic behavior of shear-wall, reinforced concrete structures. *Engineering Structures*, *24*(1), 85-98. doi:10.1016/S0141-0296(01)00061-X

Hirosawa, M. (1975). *Past Experimental Results on Reinforced Concrete Shear Walls and Analysis on Them*. In *Kenchiku Kenkyu Shiryo, No. 6* (p. 277). Building Research Institute, Ministry of Construction. (In Japanese).

Hose, Y. D., & Seible, F. (1999). *Performance Evaluation Database for Concrete Bridge Components and Systems under Simulated Seismic Loads*. (Tech. Rep. No. PEER Report 1999/11). Berkeley, CA.: Pacific Earthquake Engineering Research Center College of Engineering University of California.

Kappos, A., & Penelis, G. G. (2010). *Earthquake Resistant Concrete Structures*. CRC Press.

Kolozvari, K., Orakcal, K., & Wallace, J. (2015). *Shear-Flexure Interaction Modeling for Reinforced Concrete Structural Walls and Columns under Reversed Cyclic Loading*. (Tech. Rep. No. PEER Report 2015/12). Berkeley, CA.: University of California, Pacific Earthquake Engineering Research Center

Kuang, J. S., & Ho, Y. B. (2008). Seismic Behavior and Ductility of Squat Reinforced Concrete Shear Walls with Nonseismic Detailing. *ACI Structural Journal*, *105*(2), 225–231.

Li, W., & Li, Q. (2012). Seismic performance of L-shaped RC shear wall subjected to cyclic loading. *The Structural Design of Tall and Special Buildings*, *21*(13), 855–866. doi:10.1002/tal

Maekawa, K., Okamura, H., & Pimanmas, A. (2003). *Non-linear mechanics of reinforced concrete*. CRC Press.

Mahin, S. A., & Bertero, V. V. (1976). Problems in establishing and predicting ductility in aseismic design. In *Proceedings, International Symposium on Earthquake Structural Engineering* (pp. 613 – 628). St. Luis, Missouri.

Maier, J., & Thurlimann, B. (1985). *Bruchversuche an Stahlbetonscheiben*.

Massone, L. M., & Wallace, J. W. (2004). Load-deformation responses of slender reinforced concrete walls. *ACI Structural Journal-American Concrete Institute*, *101*(1), 103-113.

OECD. (1996). *Seismic shear wall ISP, NUPEC's seismic ultimate dynamic response test*. (Comparison Report, NEA/CSNI/R(96)10), Paris, France.

Oesterle, R.G., Aristizabal-Ochoa, J. D., Shiu, K.N., & Corley, W.G., & A.-O. (1984). Web Crushing of Reinforced Concrete Structural Walls. In *ACI Journal Proceedings*, *81*(3). doi:10.14359/10679

Ozcebe, G., & Saatcioglu, M. (1989). Hysteretic shear model for reinforced concrete members. *Journal of Structural Engineering*, *115*(1), 132-148.

Park, R. (1988). Ductility evaluation from laboratory and analytical testing. In *Proceedings of the 9th World Conference on Earthquake Engineering, Tokyo-Kyoto, Japan* (Vol. 8, pp. 605-616).

Park, R. (1989). Evaluation of ductility of structures and structural assemblages from laboratory testing. *Bulletin of the New Zealand National Society for Earthquake Engineering*, *22*(3), 155–166.

Paulay, T. (1972). Some Aspects of Shear Wall Design. *Bulletin of New Zealand Society for Earthquake Engineering*, *5*(3).

Paulay, T., & Priestley, M. J. N. (1992). *Seismic Design of Reinforced Concrete and Masonry Buildings*. John Wiley & Sons, Inc., New York.

Paulay, T., Priestley, M. J. N., & Synge, A. J. (1982, July). Ductility in earthquake resisting squat shear walls. In *ACI Journal Proceedings* (Vol. 79, No. 4, pp. 257-269). doi:10.14359/10903

Pilakoutas, K., & Elnashai, A. (1995). Cyclic behavior of reinforced concrete cantilever walls. I: Experimental results. *ACI Structural Journal*, *92*(3), 271-281.

Priestley, M. J. N., Calvi, G. M., & Kowalsky, M. J. (2007). *Displacement-Based Seismic Design of Structures. IUSS Press*.

Priestley, M. J. N., & Kowalsky, M. J. (1998). Aspects of drift and ductility capacity of rectangular cantilever structural walls. *Bulletin of the New Zealand National Society for Earthquake Engineering*, *31*(2), 73-85.

Rodrigues, H., Varum, H., Arêde, A., & Costa, A. (2012). A comparative analysis of energy dissipation and equivalent viscous damping of RC columns subjected to uniaxial and biaxial loading. *Engineering Structures*, *35*, 149–164. doi:10.1016/j.engstruct.2011.11.014

Salonikios, T. N., Kappos, A. J., Tegos, I. A., & Penelis, G. G. (1999). Cyclic load behavior of low-slenderness reinforced concrete walls: Design basis and test results. *ACI Structural Journal*, *96*(4), 649–660.

SeismoStruct user Manual. (2016). Version 7.0. *Pavia, Italy. Seismo-Soft Inc. Supporting Services*.

Shirai, K., Matsumori, T., & Kabeyasawa, T. (2007). 3-D Dynamic Collapse Test of a Six-Story Full-Scale RC Wall-Frame Building. *Structural Engineering Research Frontiers*, 1–10. doi:10.1061/40944(249)12

Tegos, I. A., Psarras, K. T., Kalkinis, D., Papadopoulos, I. C., & Legbelos, N. (2012). Experimental Evaluation of Transverse Reinforcement Configurations of Earthquake – resistant R / C. In *15th World Conference Earthquake Engineering*. Lisbon, Portugal.

Tran, T. A., & Wallace, J. W. (2012). *Experimental Study of the Lateral Load Response of Moderate Aspect Ratio Reinforced Concrete Structural Walls*. (Tech. Rep. No. UCLA SGEL 2012/12). Los Angeles, CA: Department of Civil Engineering, University of California.

TS500. (1981). *Requirements for design and construction of reinforced concrete structures*. Turkish Standard Institute, Necatibey Street No. 112, Bakanliklar, Ankara.

TS500. (2000). *Requirements for design and construction of reinforced concrete structures*. Turkish Standard Institute, Necatibey Street No. 112, Bakanliklar, Ankara.

Turkish Earthquake Code. (1975). *Specification for structures to be built in disaster areas*. Ministry of Public Works and Settlement Government of Republic of Turkey.

Turkish Earthquake Code. (2007). *Specification for structures to be built in disaster areas*. Ministry of Public Works and Settlement Government of Republic of Turkey.

Wallace, J. W. (2012). Behavior, design, and modeling of structural walls and coupling beams — Lessons from recent laboratory tests and earthquakes. *International Journal of Concrete Structures and Materials*, 6(1), 3–18. doi:10.1007/s40069-012-0001-4

Whyte, C. A., & Stojadinovic, B. (2013). *Hybrid Simulation of the Seismic Response of Squat Reinforced Concrete Shear Walls*. (Tech. Rep. No. PEER Report 2013/02). Berkeley, CA.: University of California, Pacific Earthquake Engineering Research Center.

APPENDIX A

MEASURED MEMBER LOCAL DEFORMATIONS FOR SPECIMEN RC-SW1

RC-SW1 member local deformations such as beams and columns plastic hinge rotations and curvatures, wall rotation and curvature profile over the wall height, story displacements and forces which were measured during the quasi-static (QS) test are presented in this appendix. Rotations and average curvatures were calculated using the procedure given below.
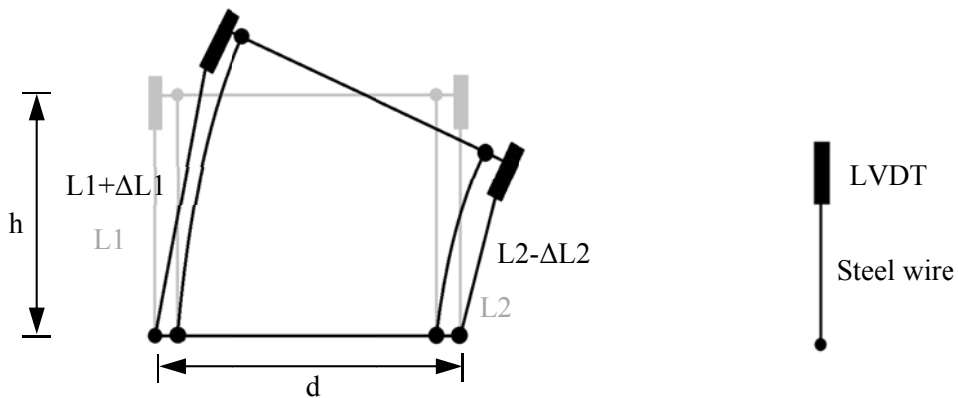
Figure A.1 Schematic illustration of rotation calculation

$$\theta = \frac{\Delta L1 + \Delta L2}{d} \qquad (A.1)$$

$$\xi_{avg} = \frac{\theta}{h} \qquad (A.2)$$

Figure A.2 illustrates the location and number of each measurement tool and the name which are assigned to each structural member

Figure A.2 Layout of instrumentation

136
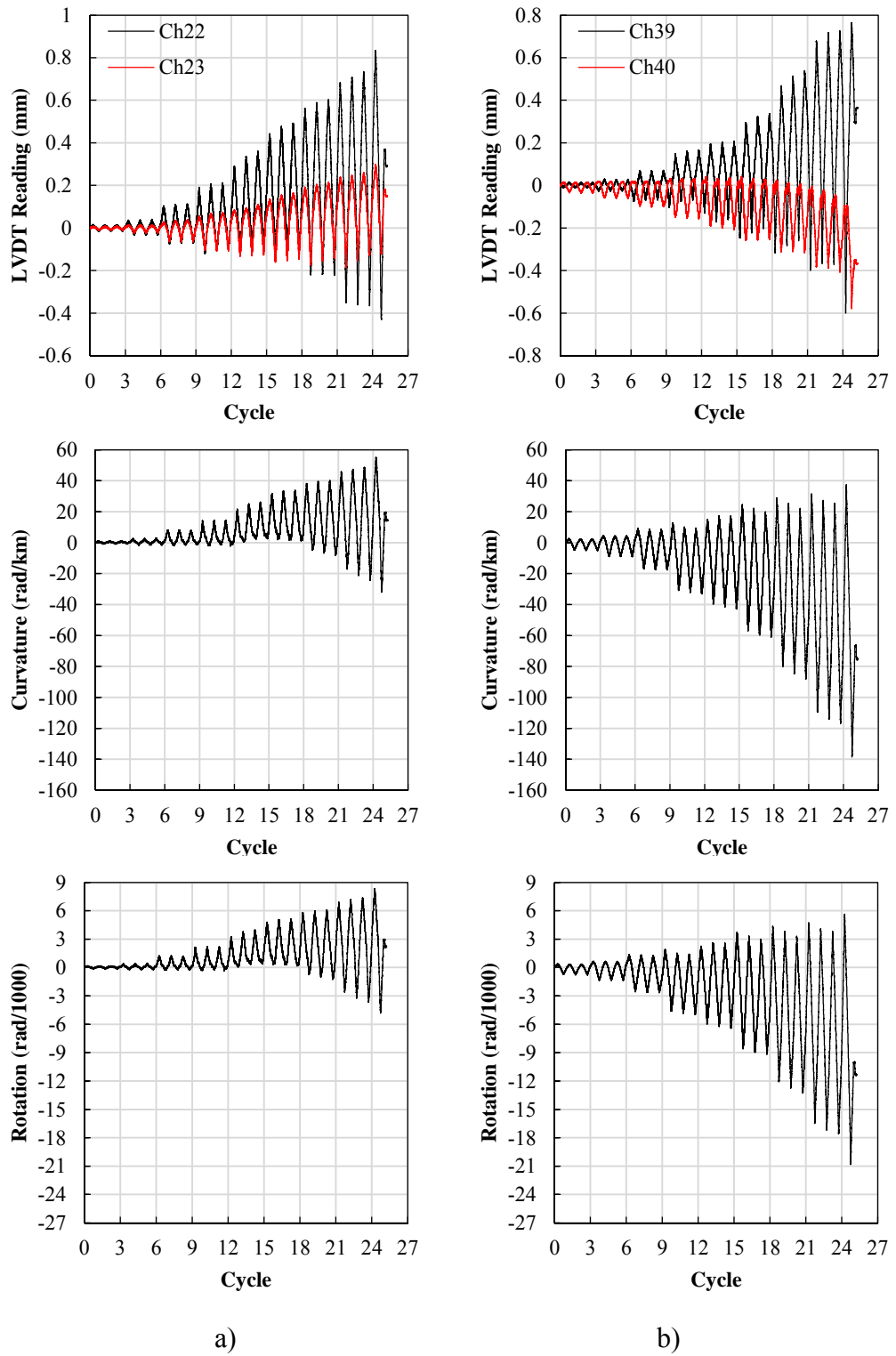
Figure A.3 Beam local deformations obtained from QS test; a) B11L, b) B11R
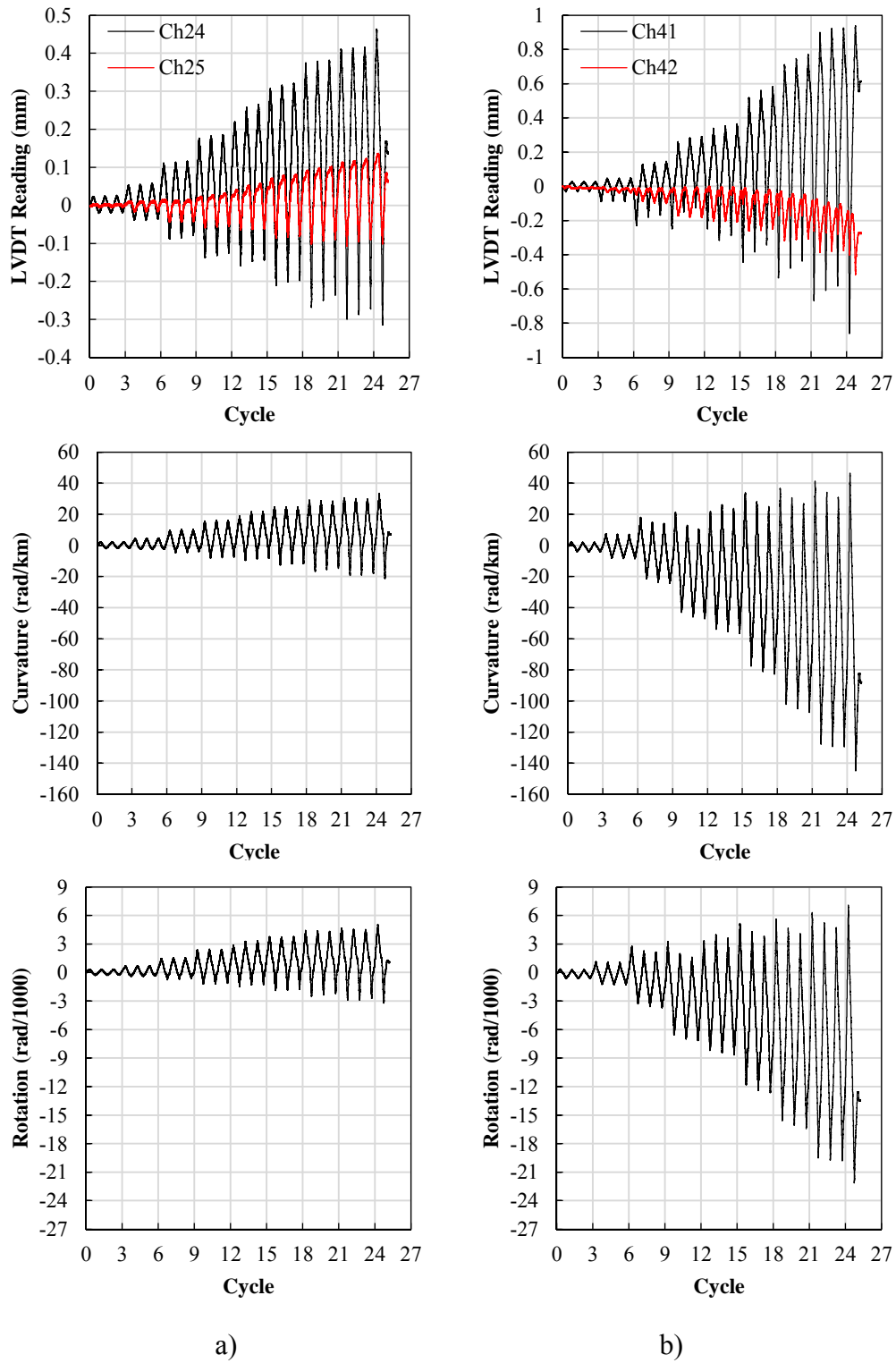
Figure A.4 Beam local deformations obtained from QS test; a) B21L, b) B21R
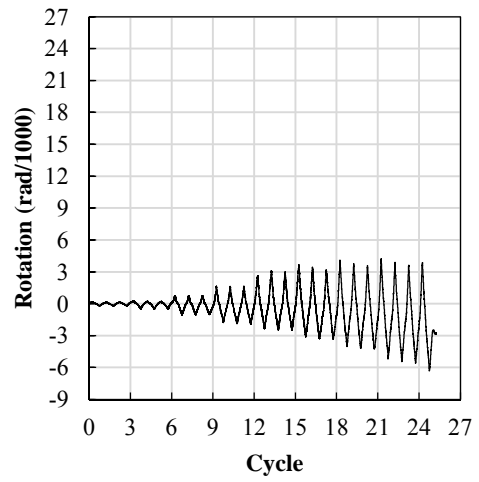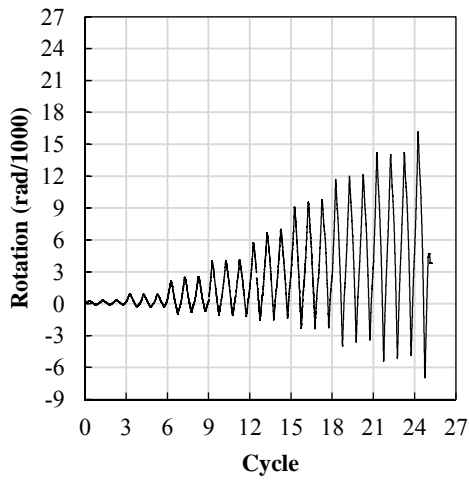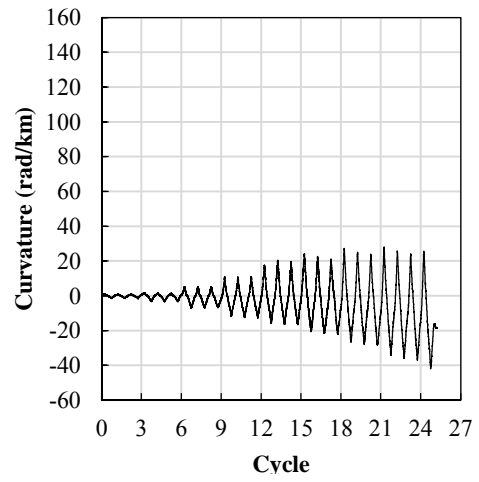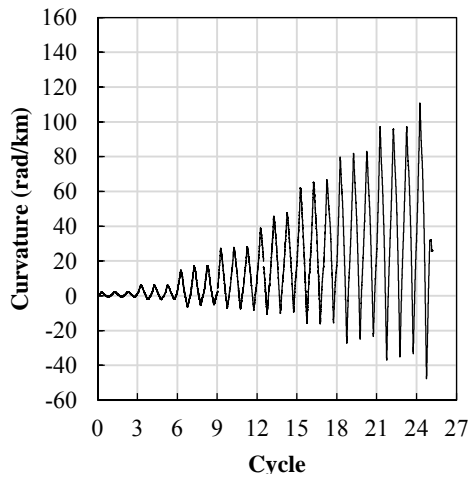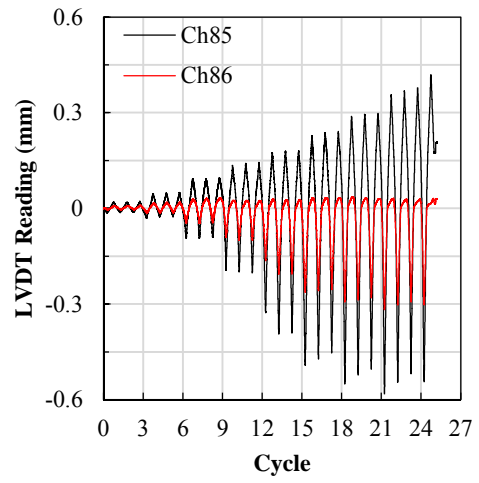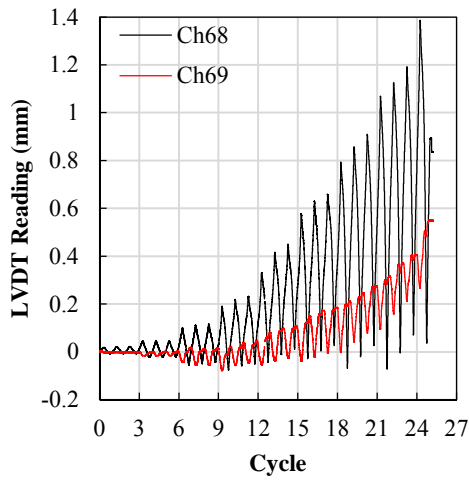
Figure A.5 Beam local deformations obtained from QS test; a) B13L, b) B13R
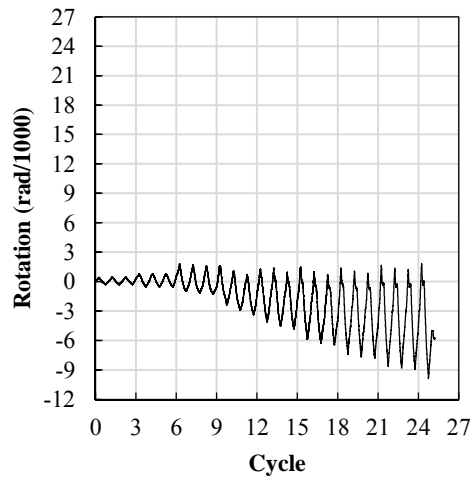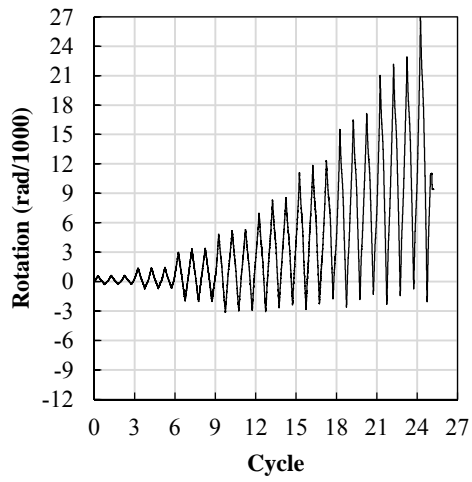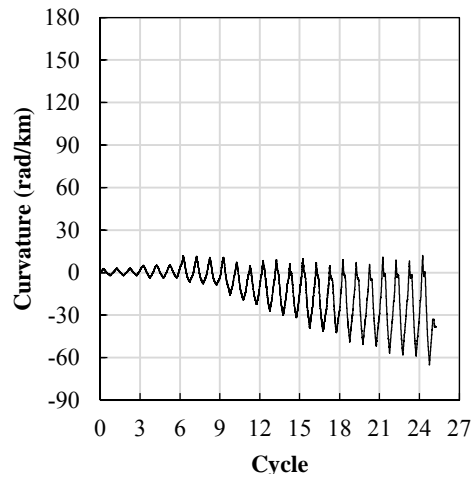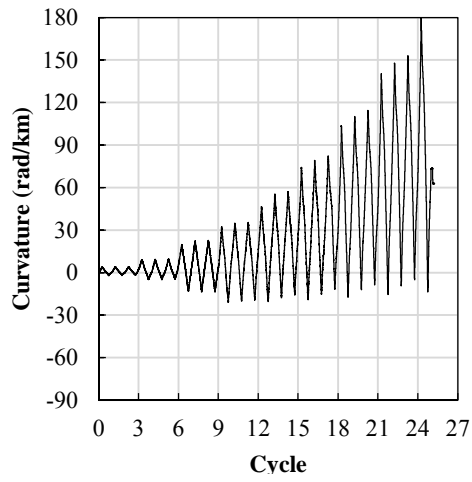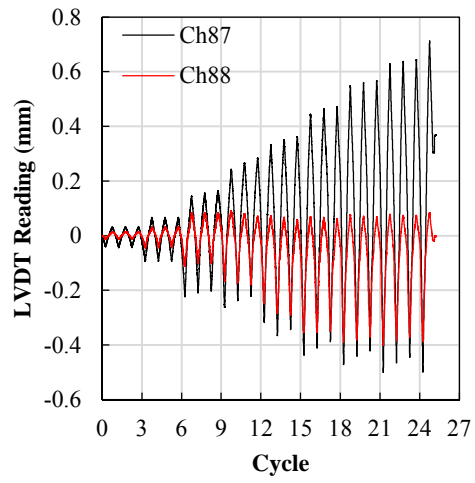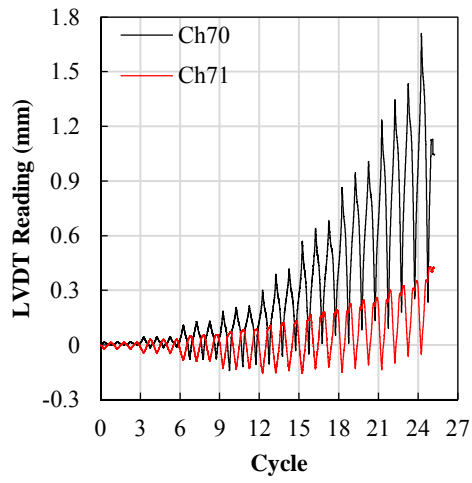
Figure A.6 Beam local deformations obtained from QS test; a) B23L, b) B23R

140
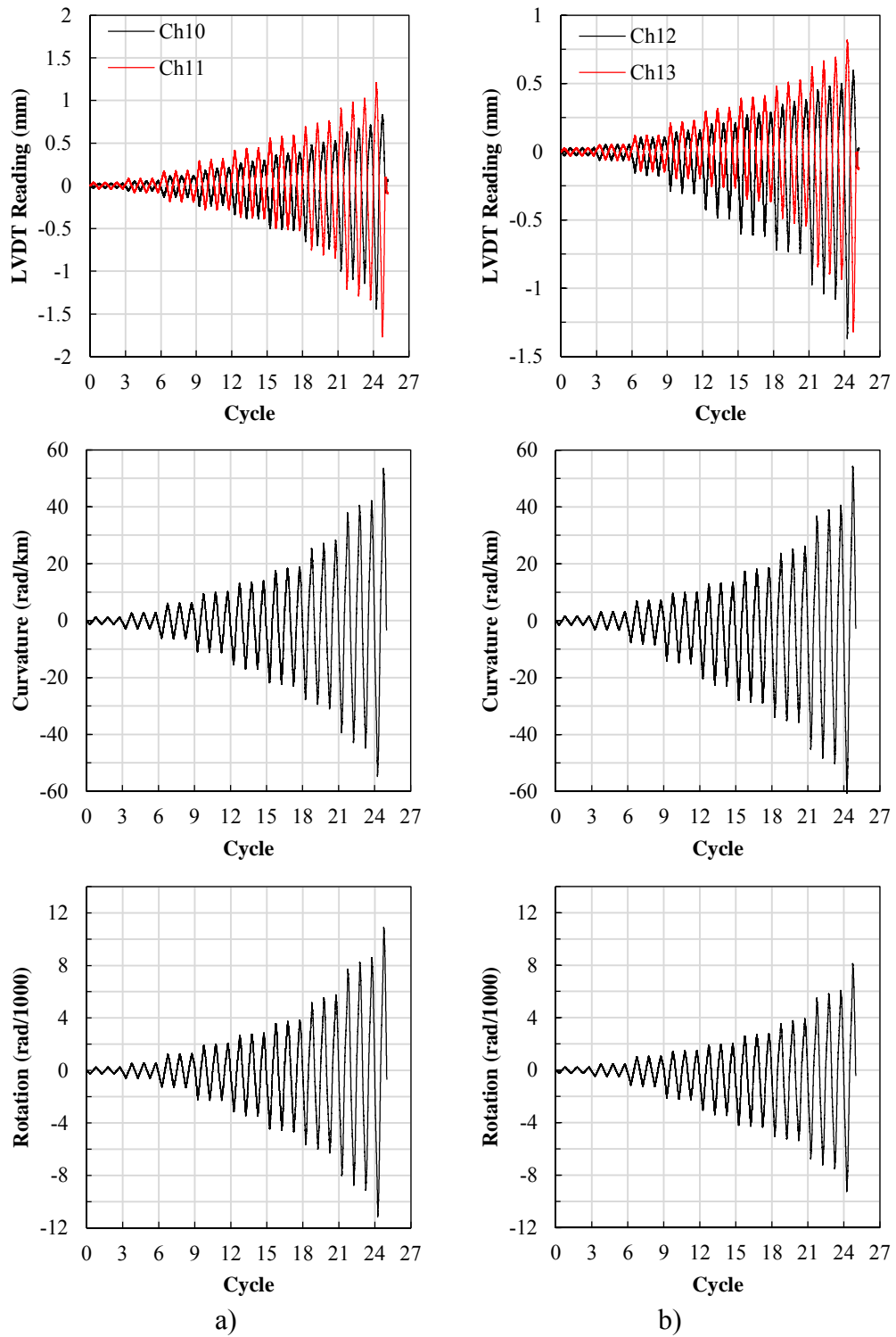
Figure A.7 Beam local deformations obtained from QS test; a) C1BL-Long, b) C1BL-Short
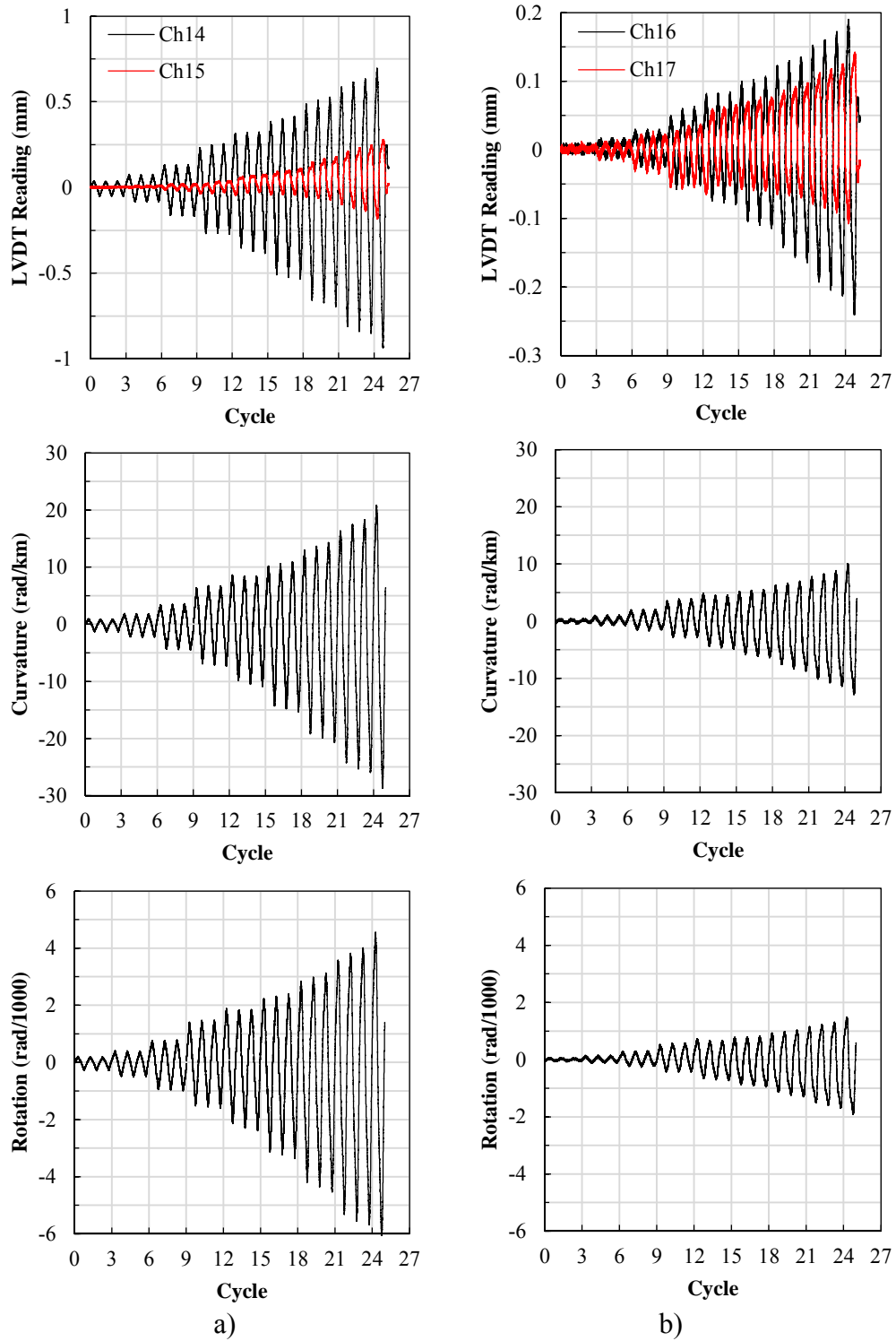
Figure A.8 Column local deformations obtained from QS test; a) C1TL-Long, b) C1TL-Short
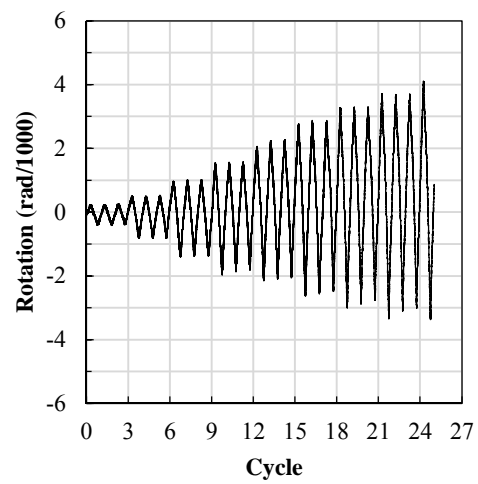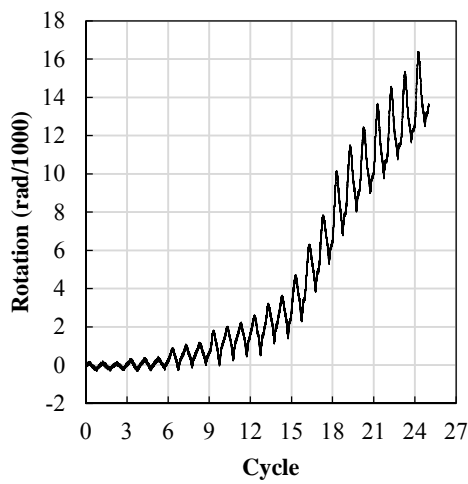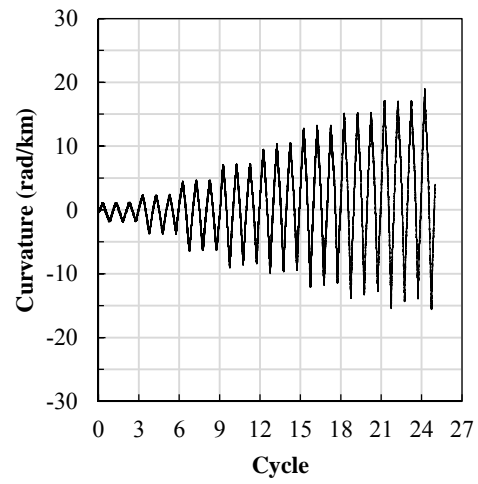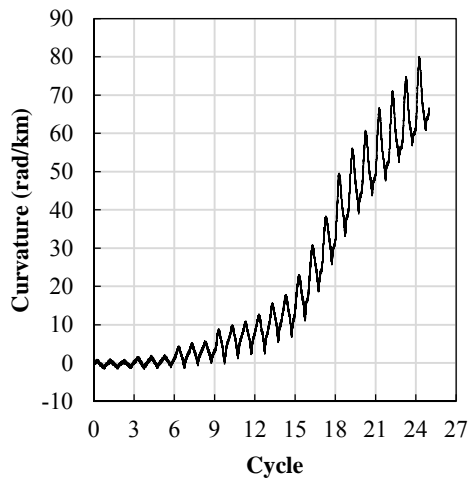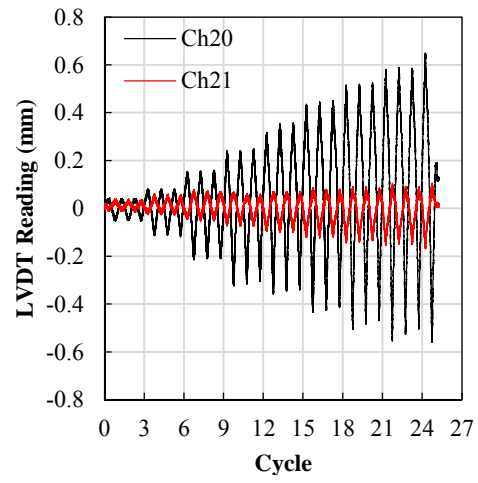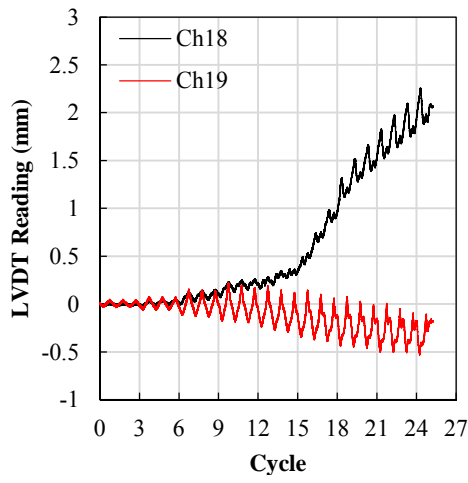
Figure A.9 Column local deformations obtained from QS test; a) C2BL, b) C2TL
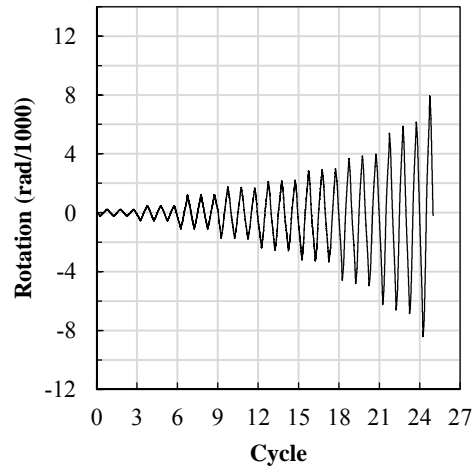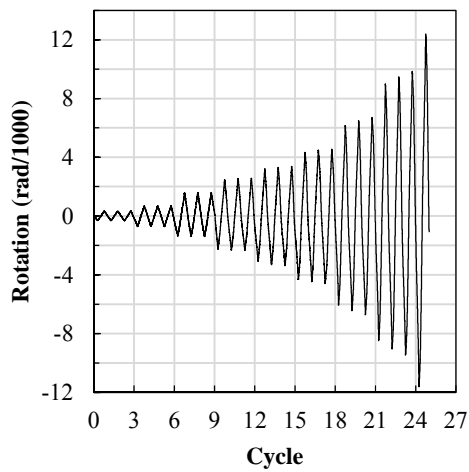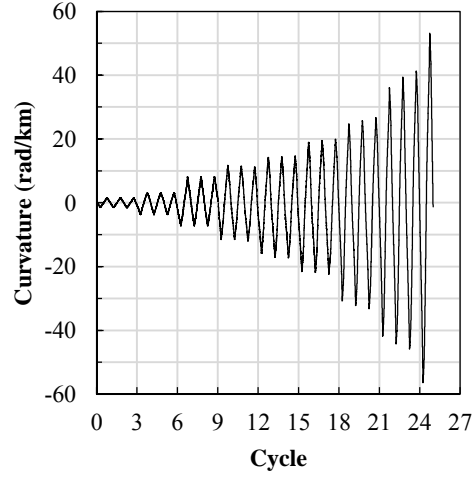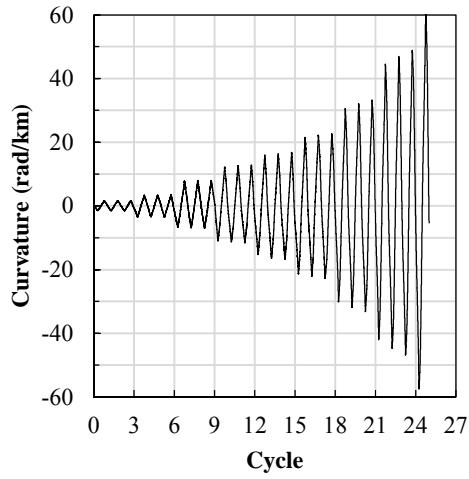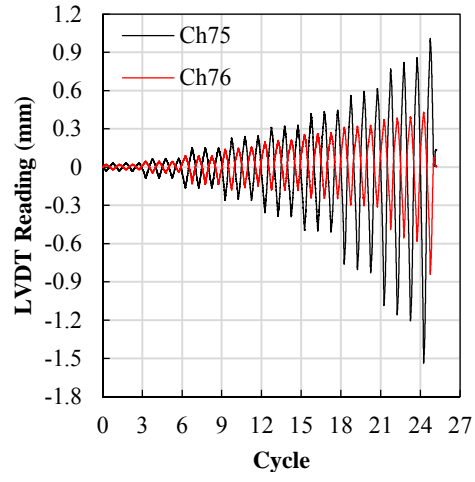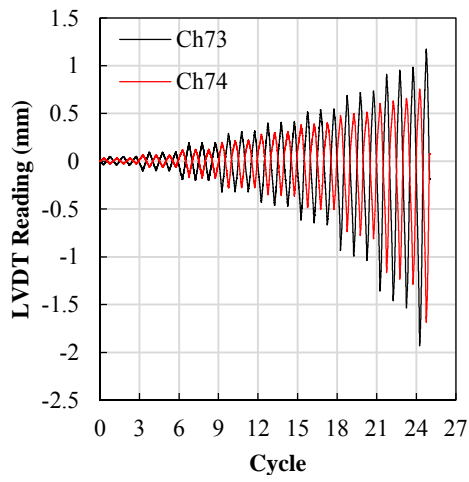
Figure A.10 Column local deformations obtained from QS test; a) C1BR-Long, b) C1BR-Short
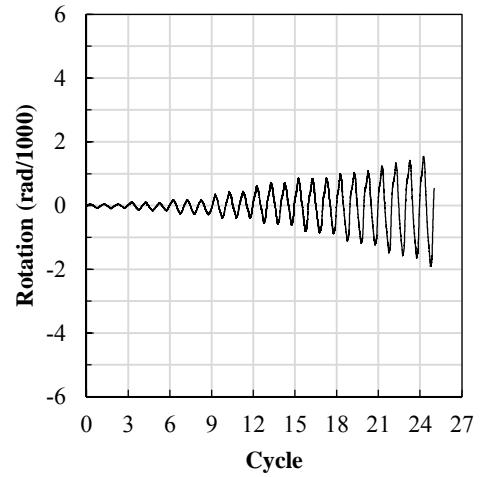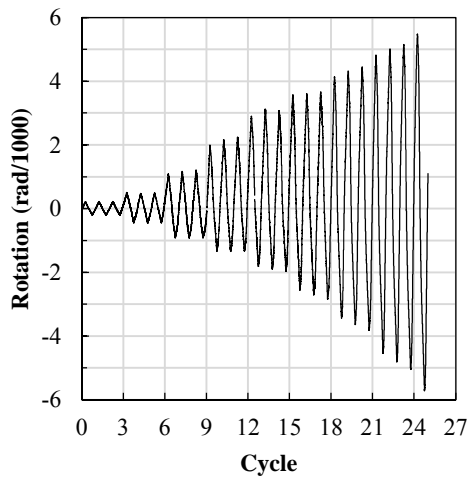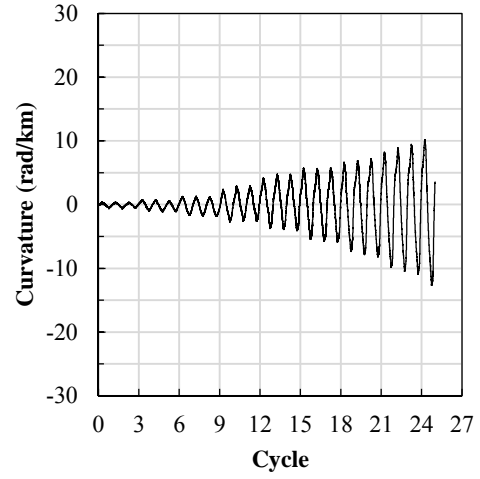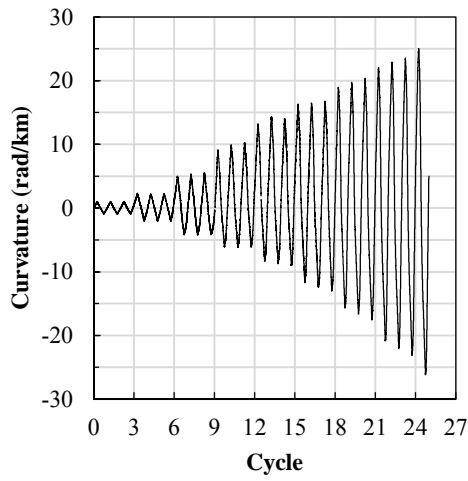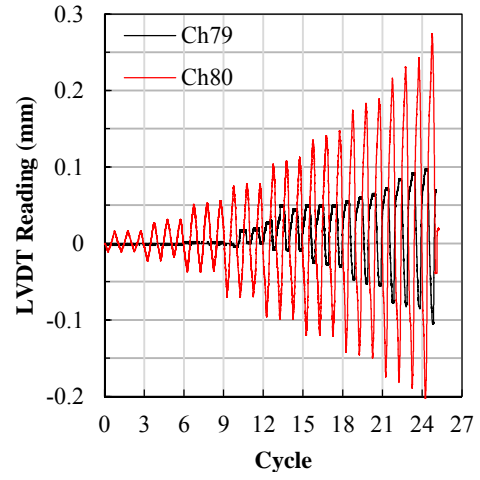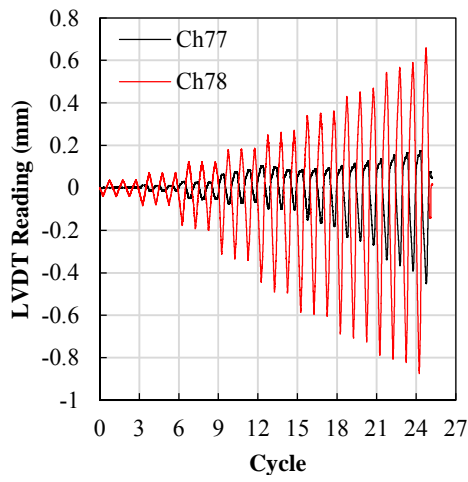
Figure A.11 Column local deformations obtained from QS test; a) C1TR-Long, b) C1TR-Short
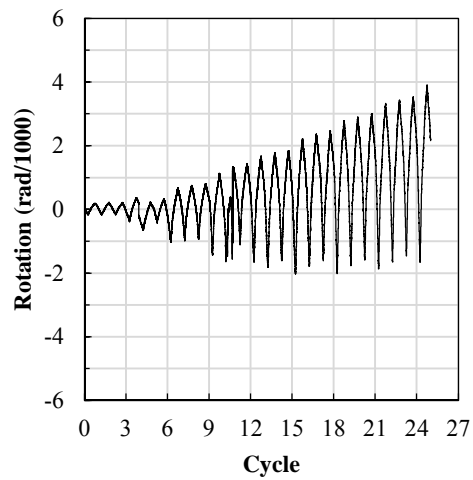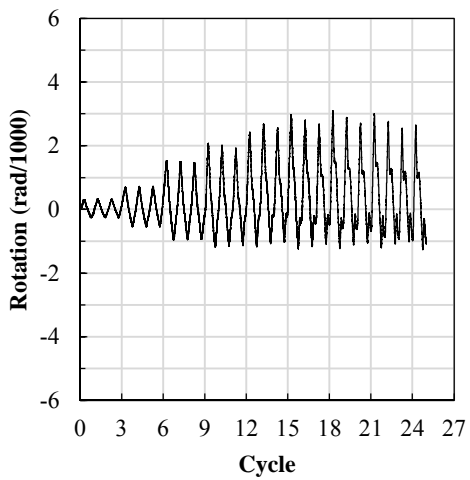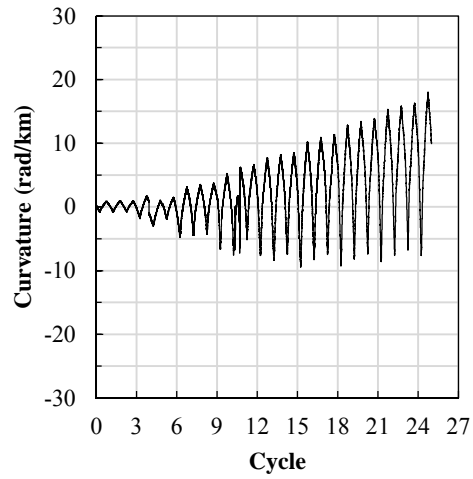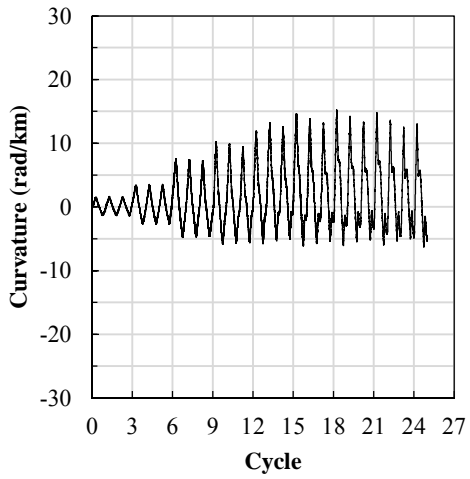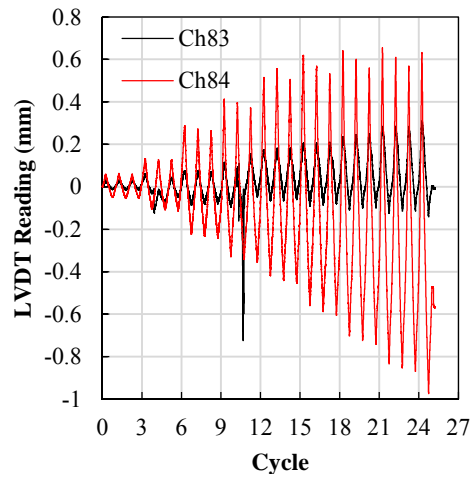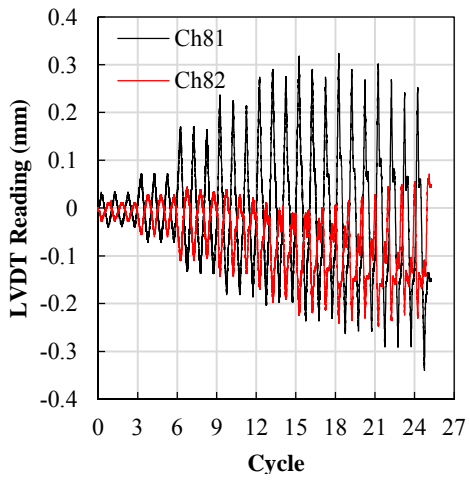
Figure A.12 Column local deformations obtained from QS test; a) C2BR, b) C2TR
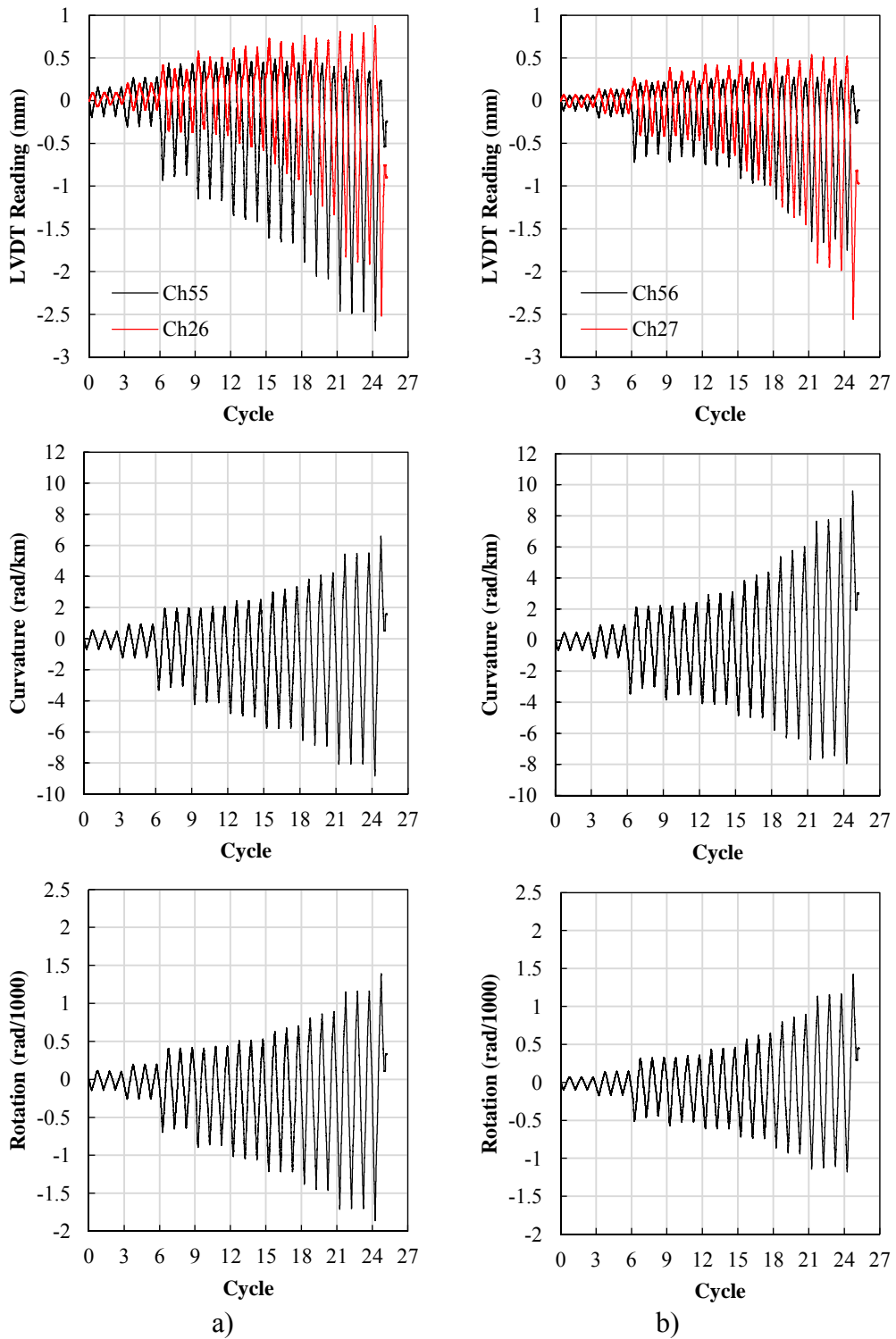
Figure A.13 Wall local deformations obtained from QS test; a) W1-Long, b) W1-Short
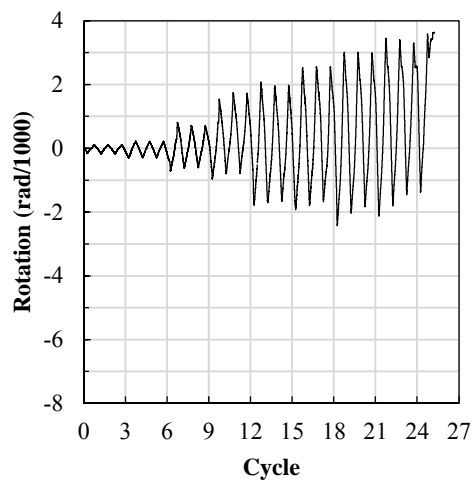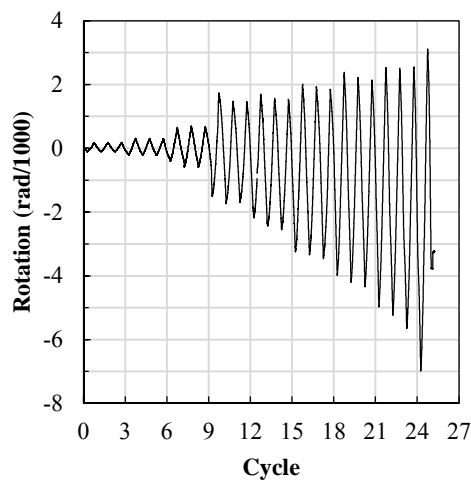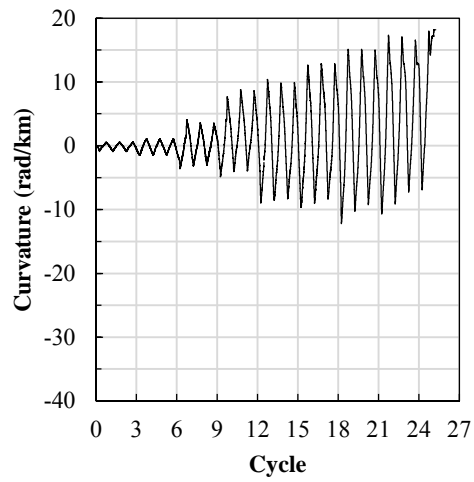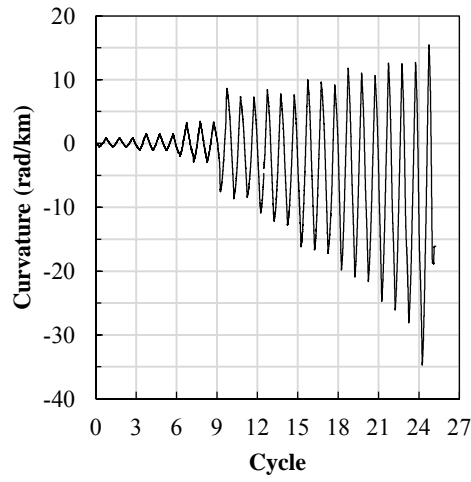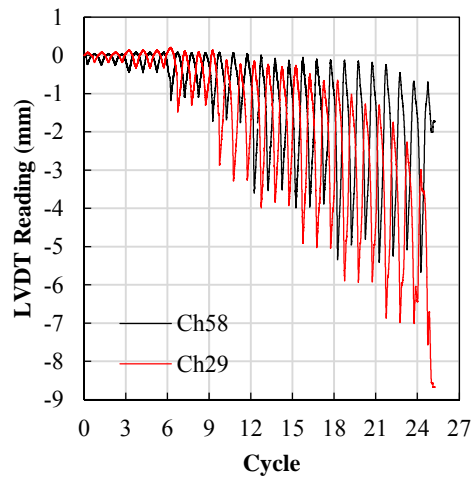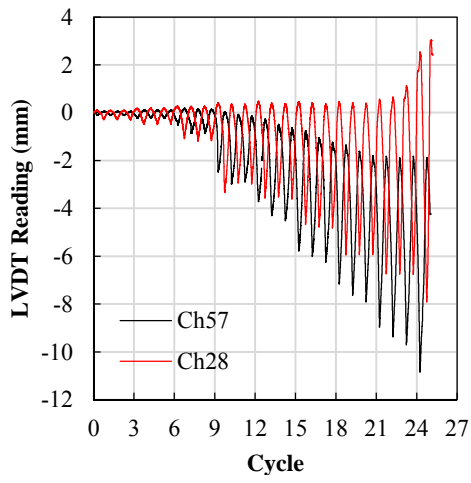
Figure A.14 Wall local deformations obtained from QS test; a) W2, b) W3

148
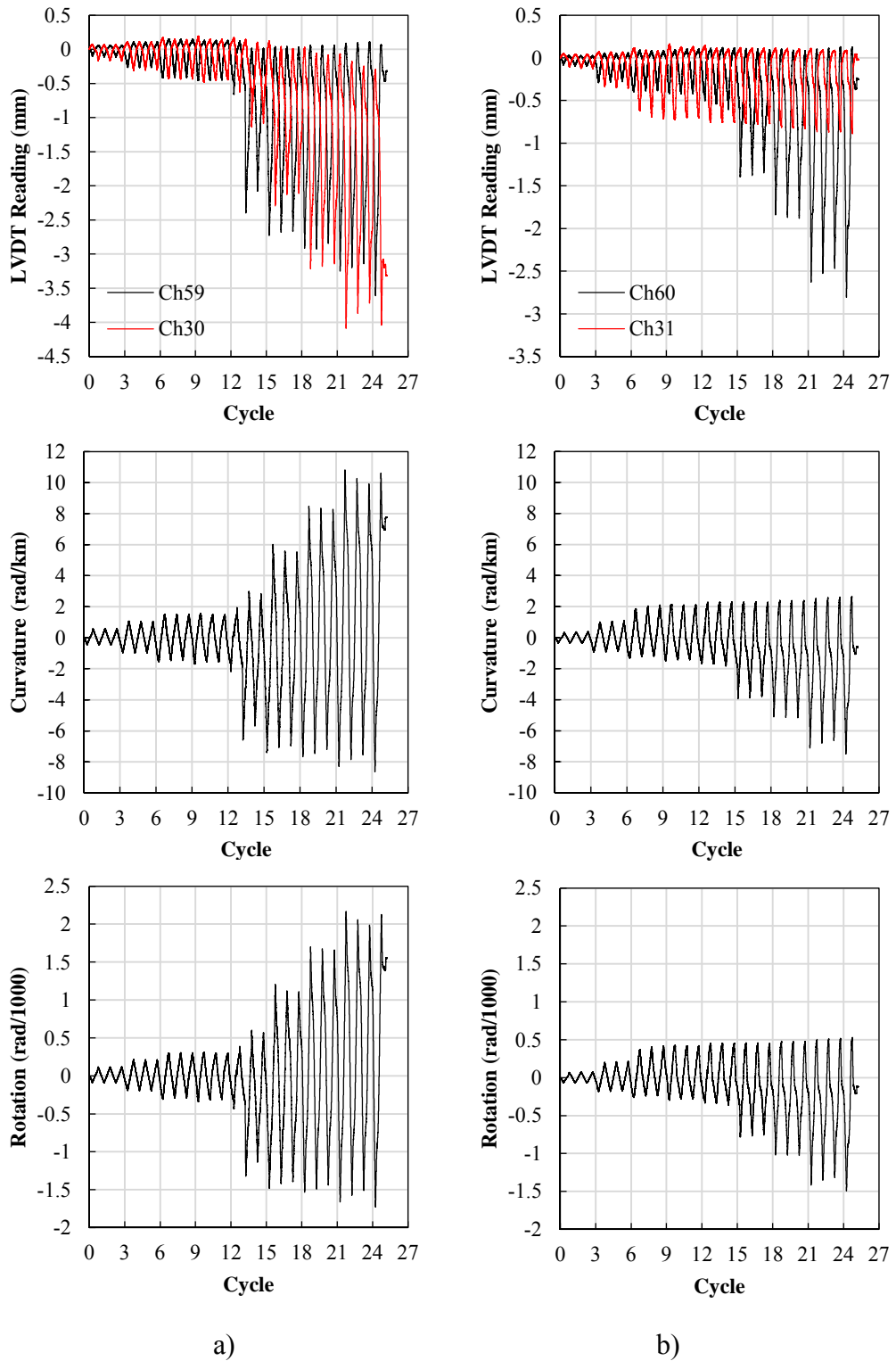
Figure A.15 Wall local deformations obtained from QS test; a) W4, b) W5
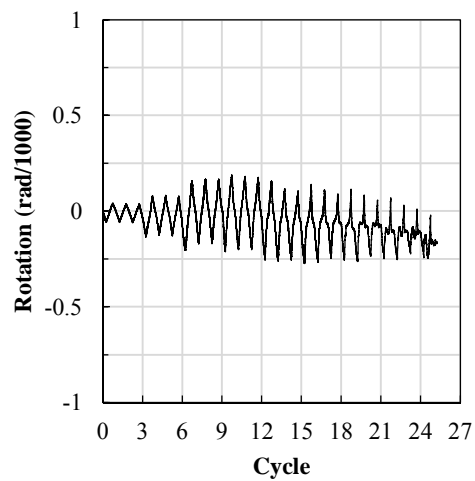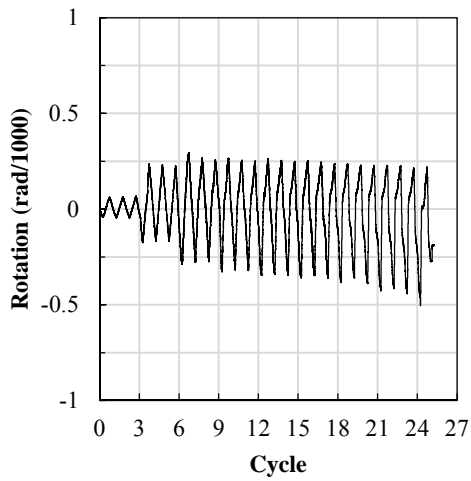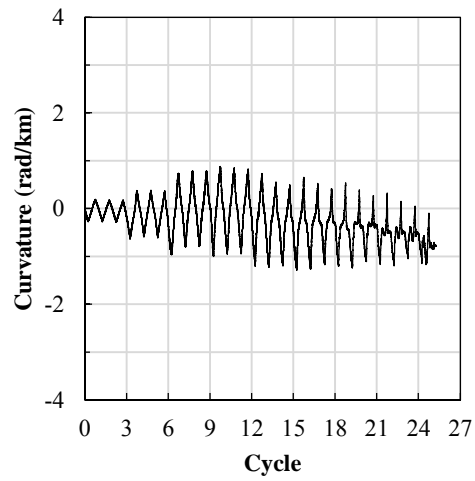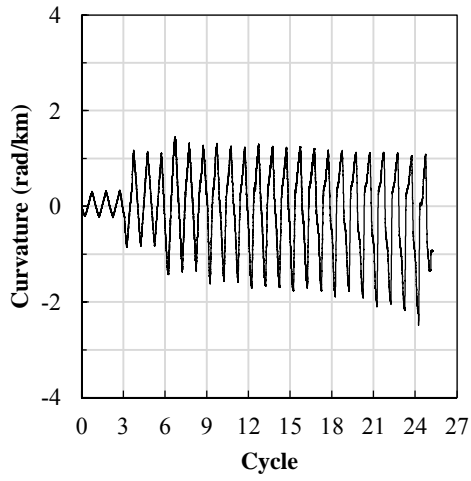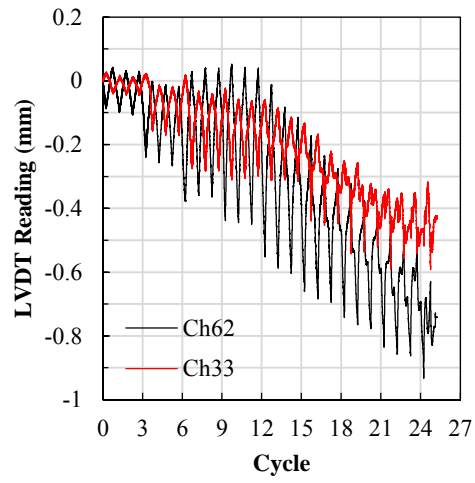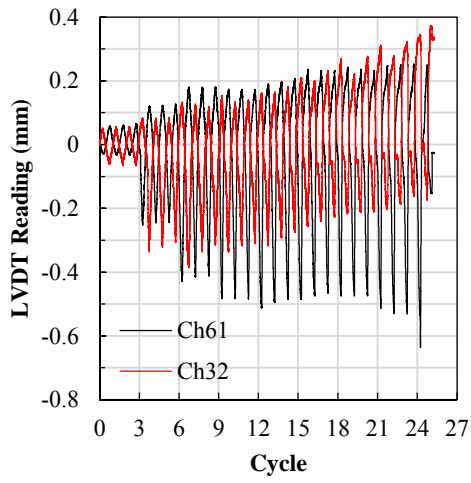
Figure A.16 Wall local deformations obtained from QS test; a) W6, b) W7
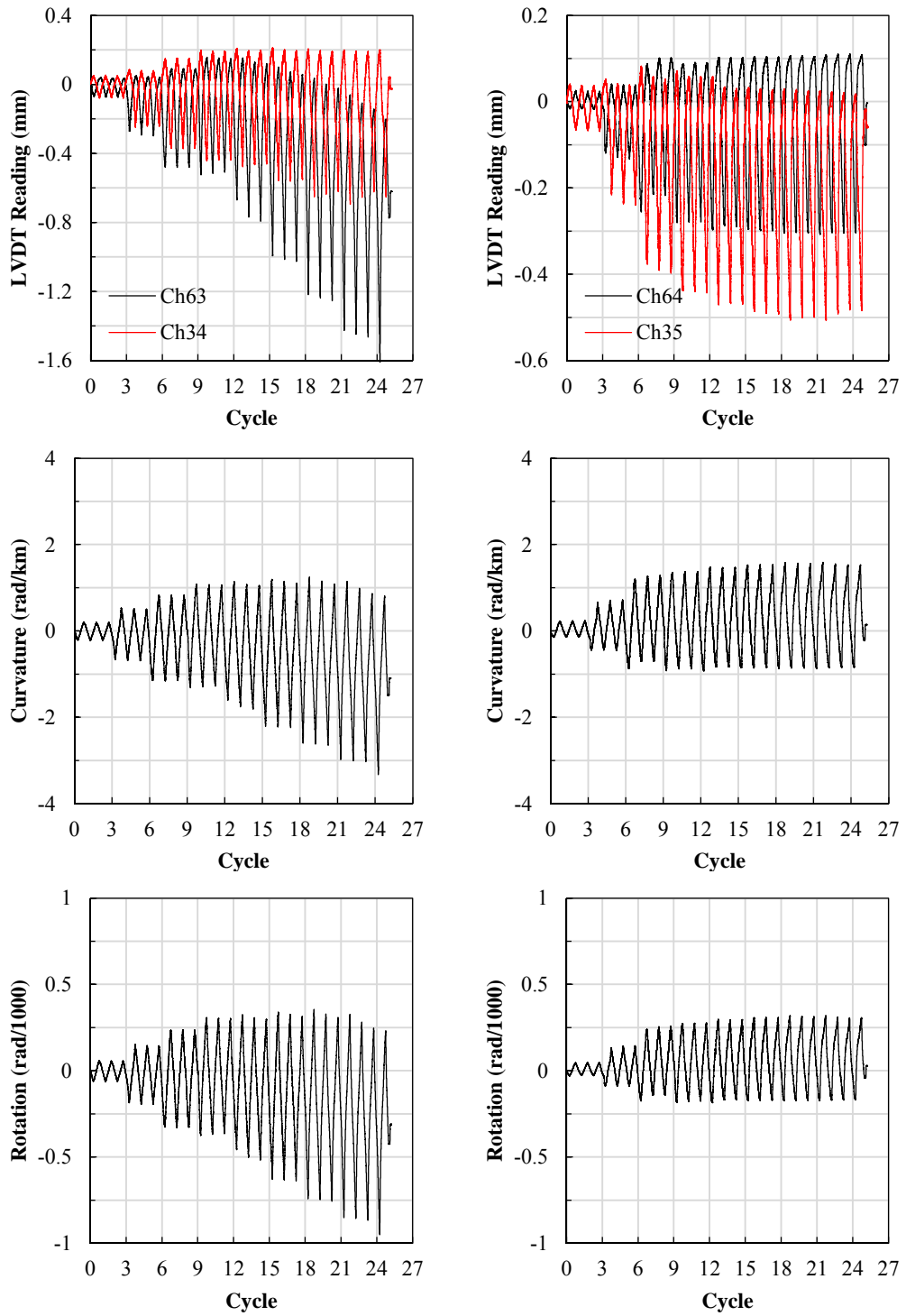
Figure A.17 Wall local deformations obtained from QS test; a) W8, b) W9
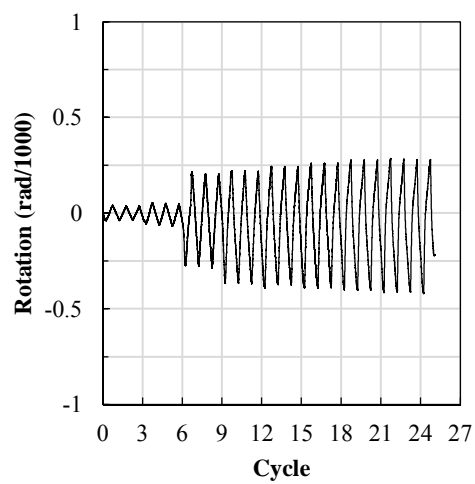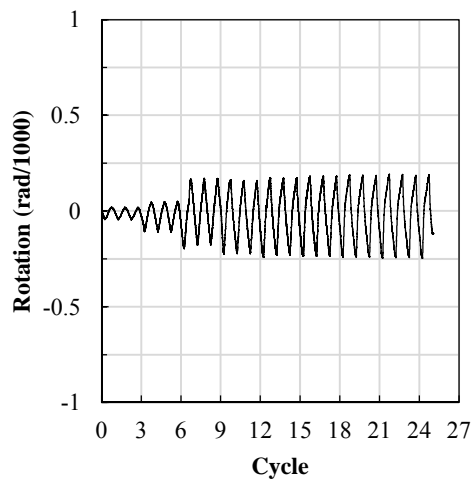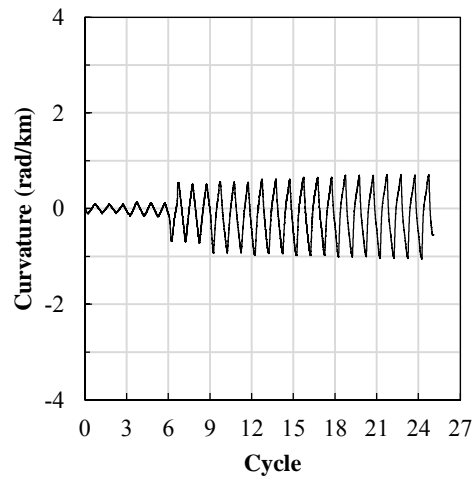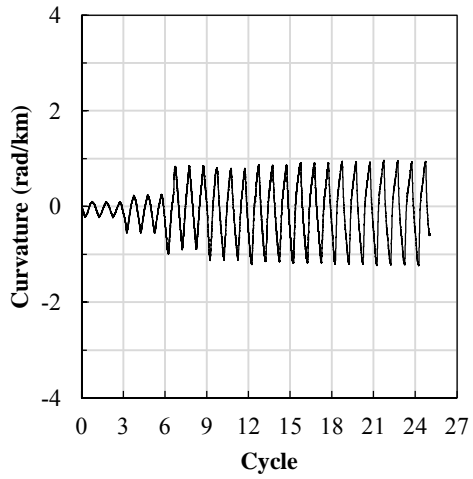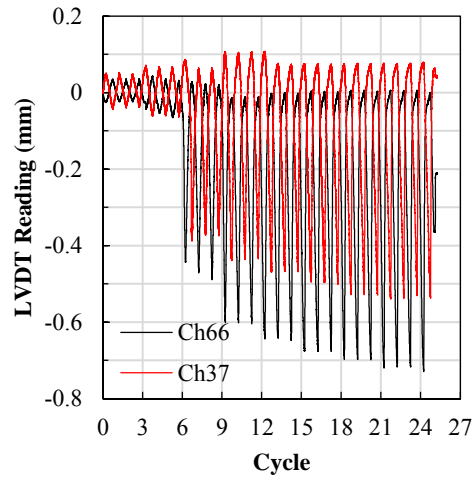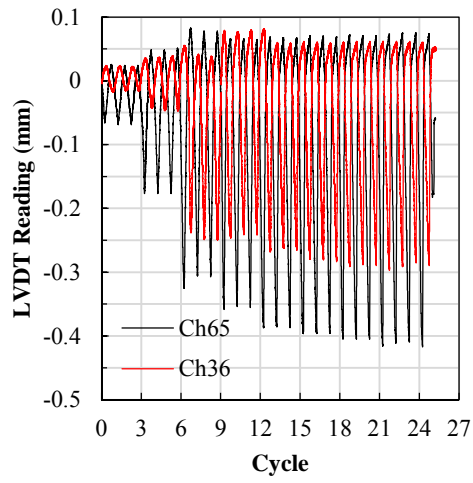
Figure A.18 Wall local deformations obtained from QS test; a) W10, b) W11
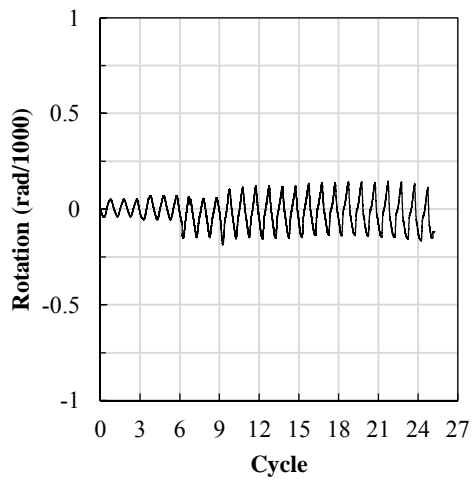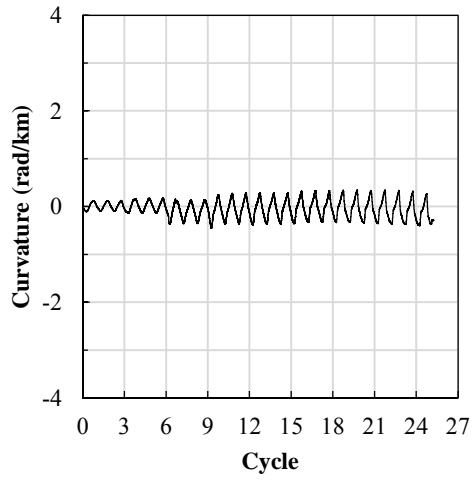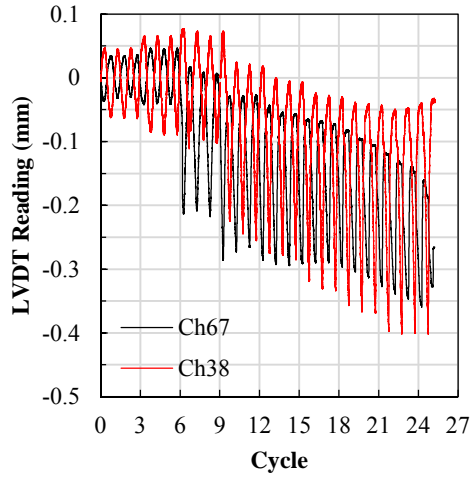
Figure A.19 Wall local deformations obtained from QS test; Segment W12
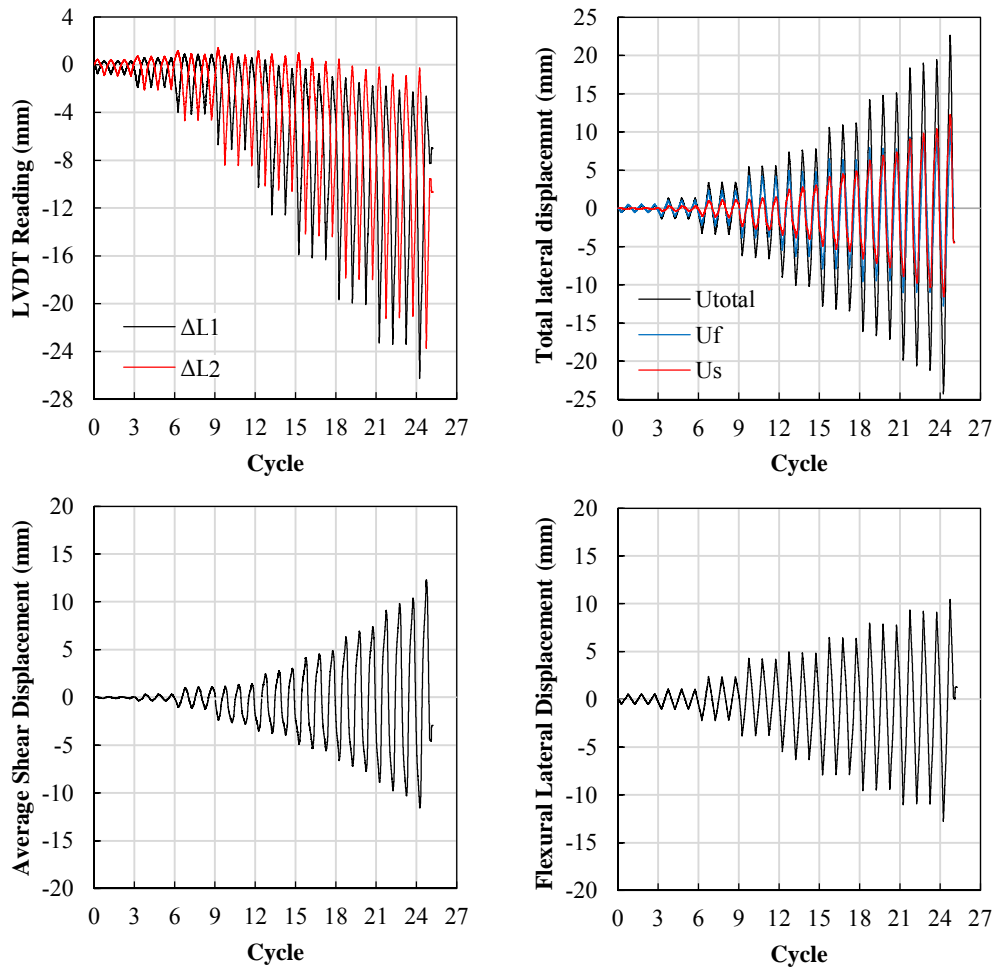
Figure A.20 Wall displacement components due to shear and flexural deformations and wall deformation because of base rotation (base crack) at first story level
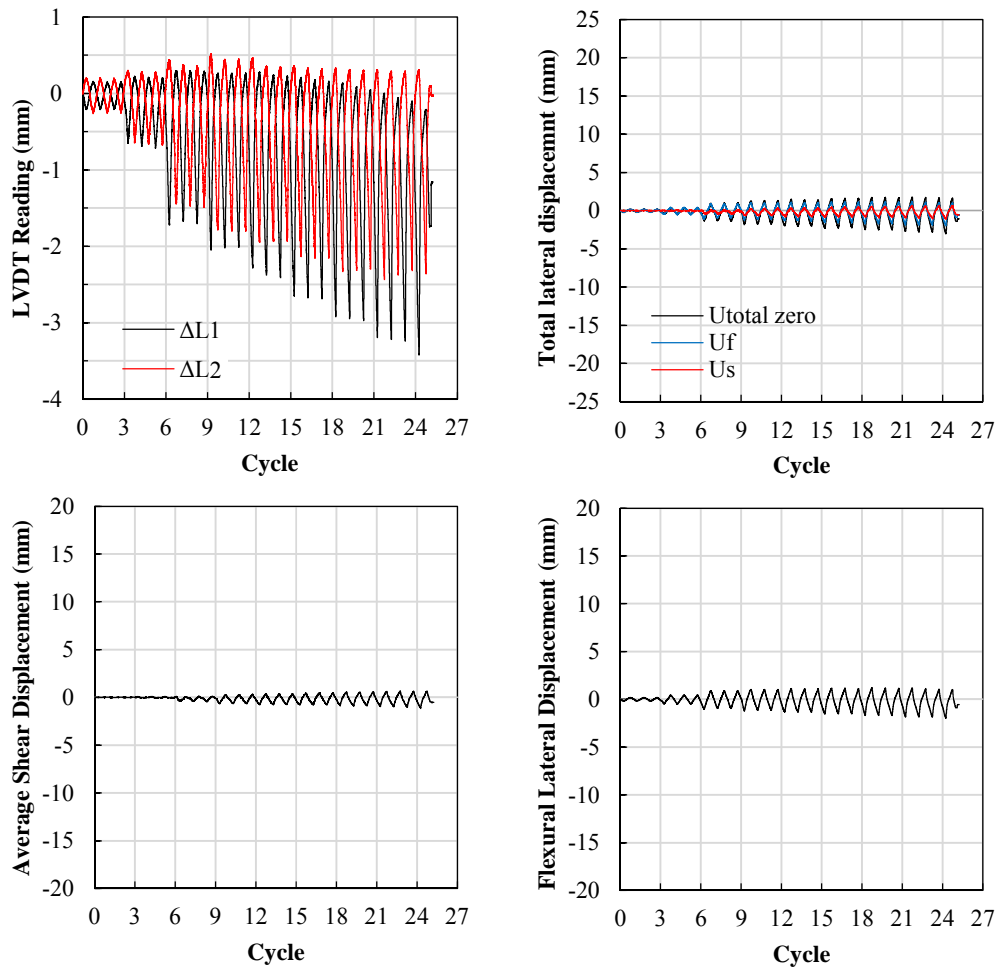
Figure A.21 Wall displacement components due to shear and flexural
deformations at second story level
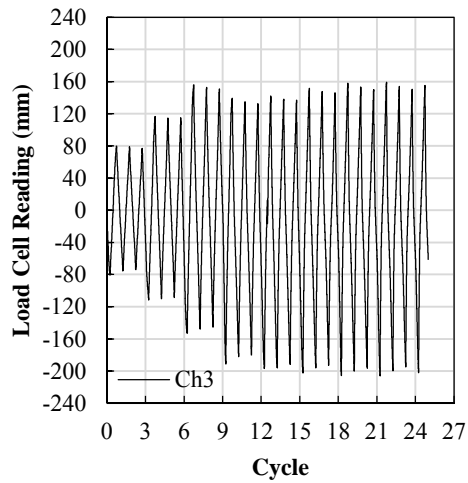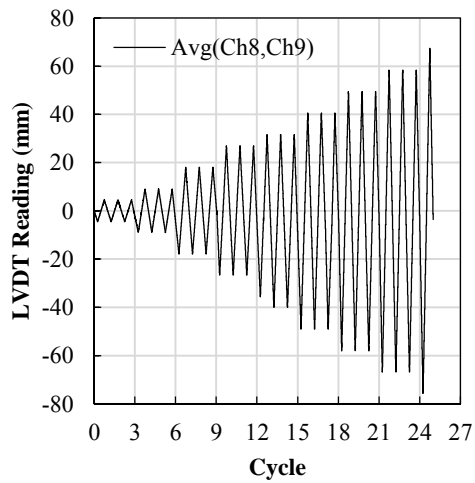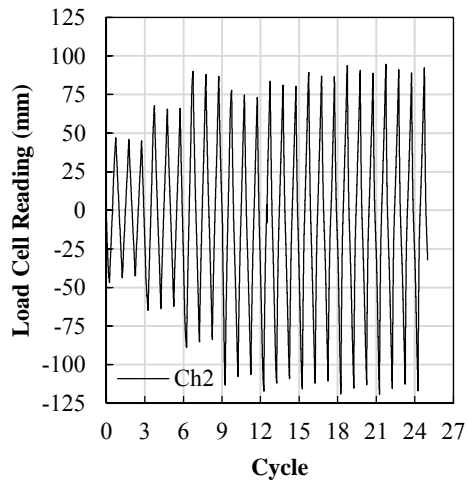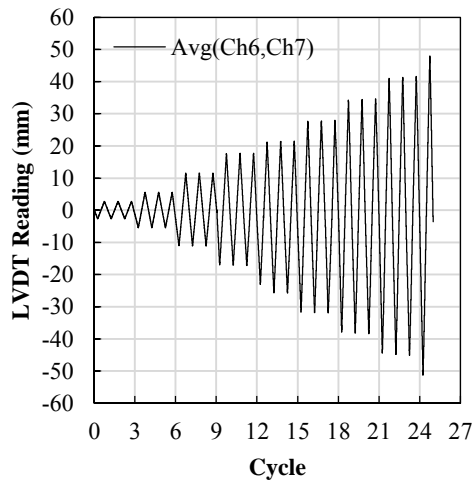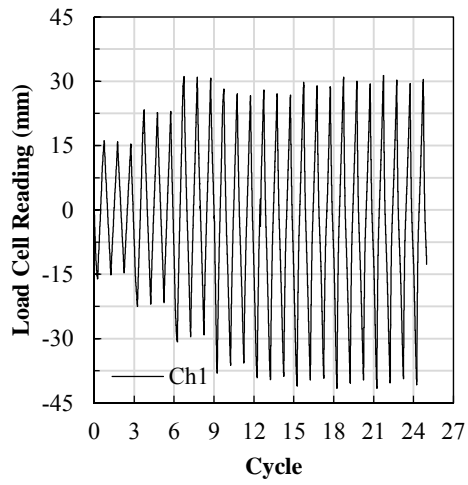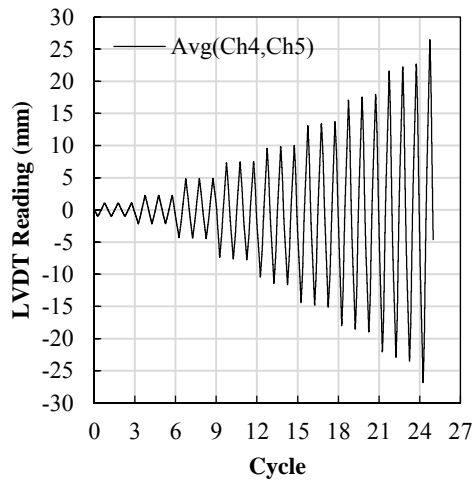
Figure A.22 RC-SW1 story displacements and forces

APPENDIX B

MEASURED MEMBER LOCAL DEFORMATIONS FOR SPECIMEN RC-SW2

RC-SW2 member local deformations such as beams and columns plastic hinge rotations and curvatures, wall rotation and curvature profile over the wall height, story displacements and forces which were measured during the quasi-static (QS) test are presented in this appendix. Local member deformations for specimen RC-SW2 was calculated using the procedure illustrated in Figure A.1 in Appendix A. The same layout of instrumentation as RC-SW1 was used for RC-SW2.
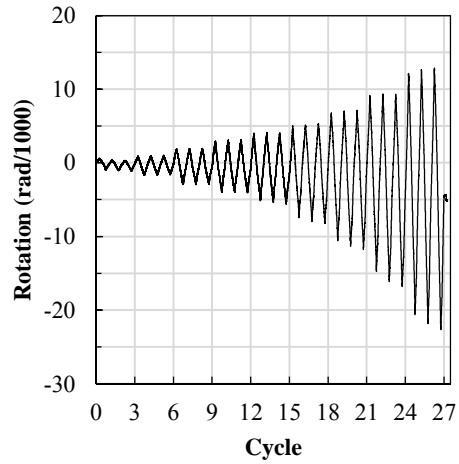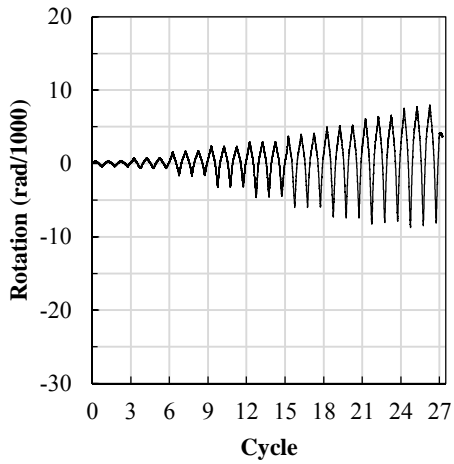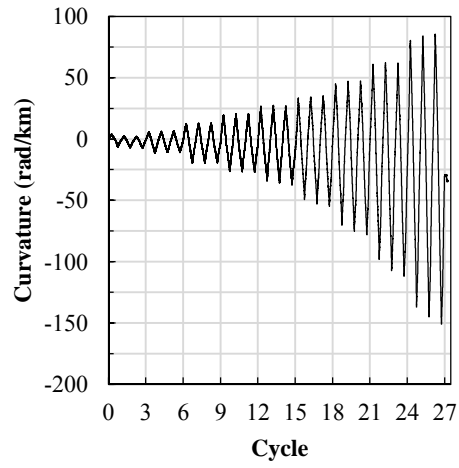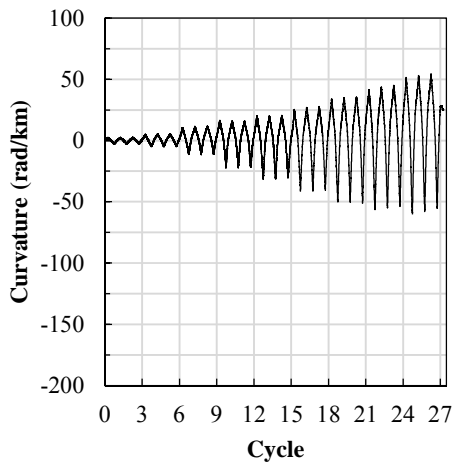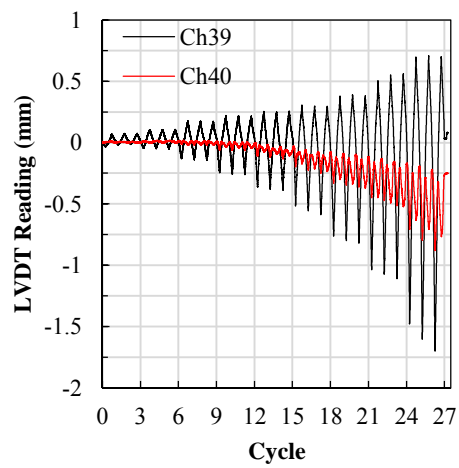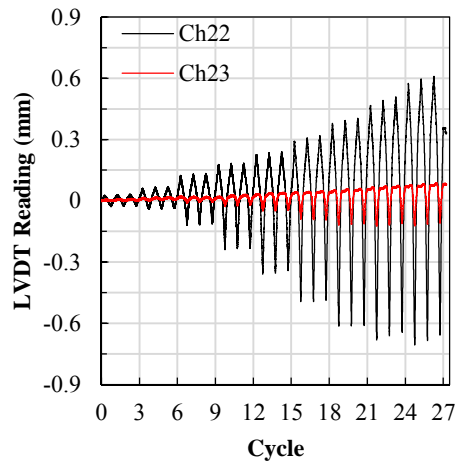
Figure B.1 Beam local deformations obtained from QS test; a) B11L, b) B11R

158
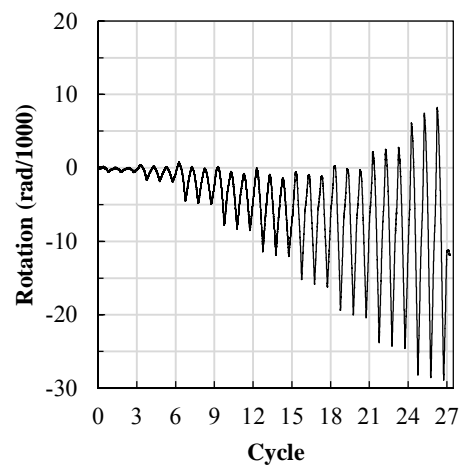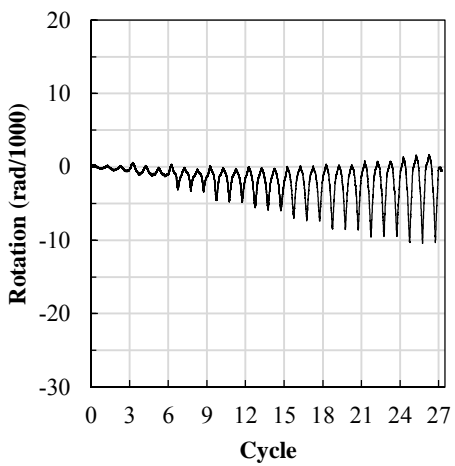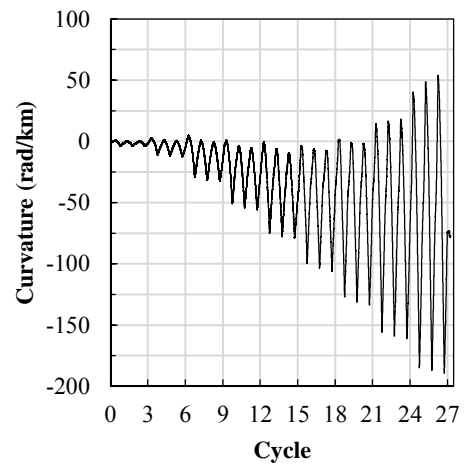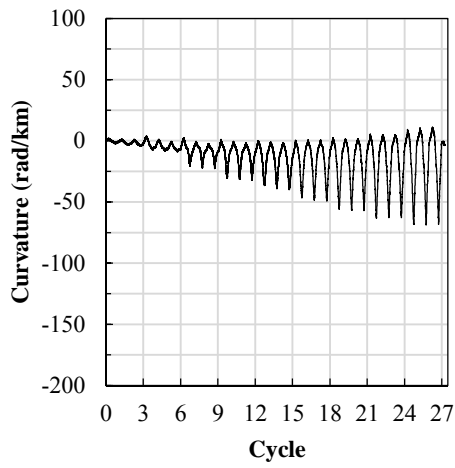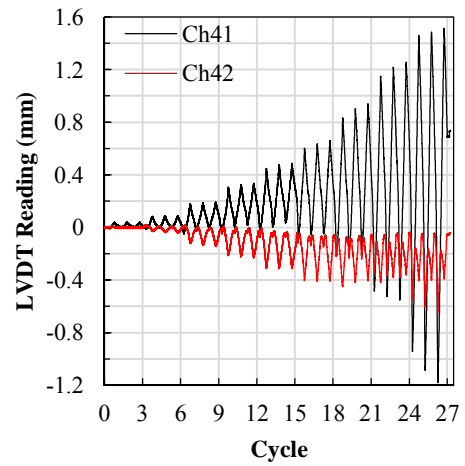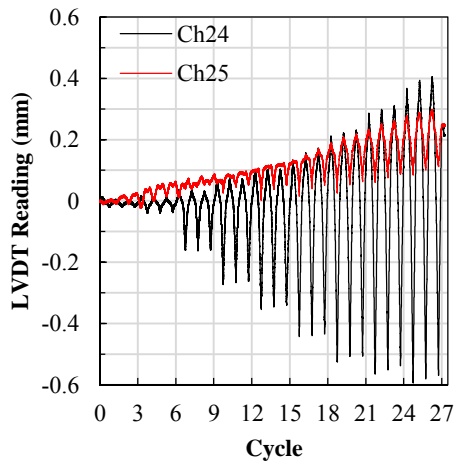
Figure B.2 Beam local deformations obtained from QS test; a) B21L, b) B21R
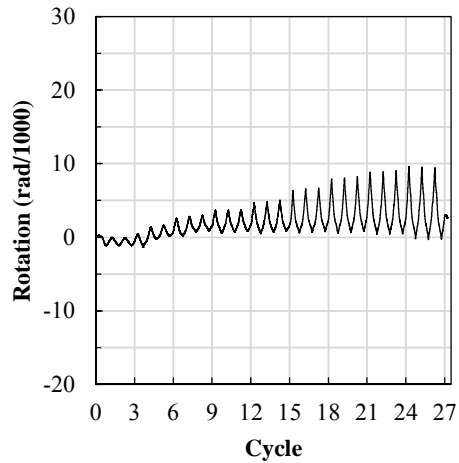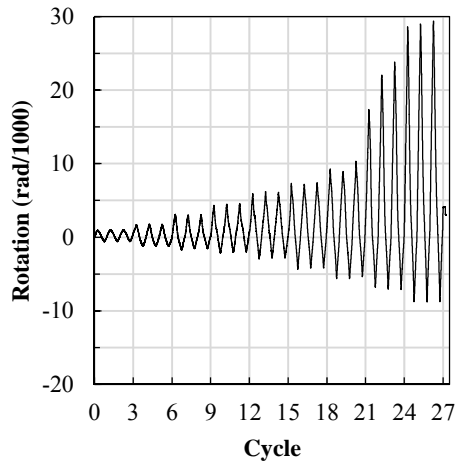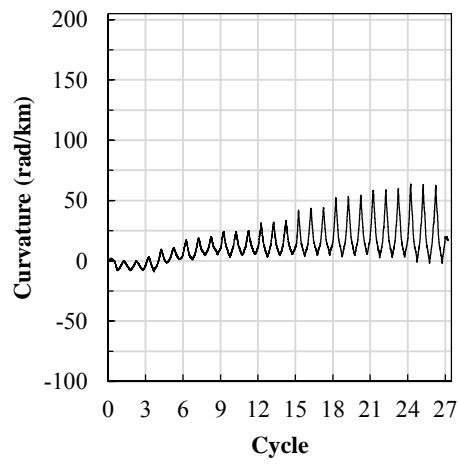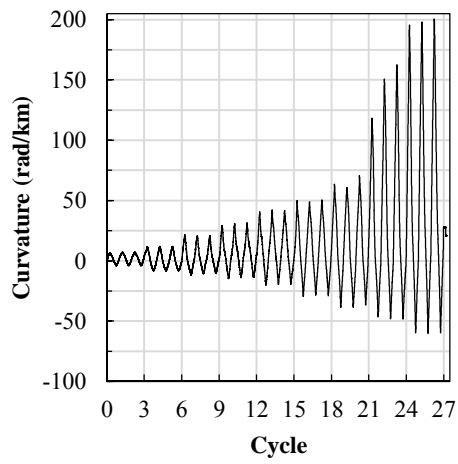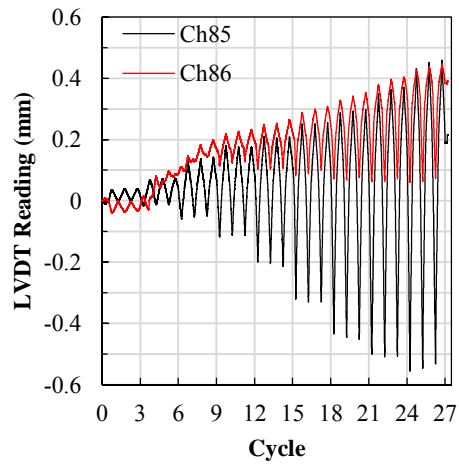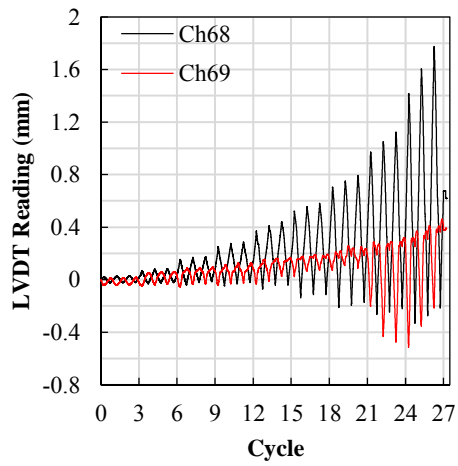
Figure B.3 Beam local deformations obtained from QS test; a) B13L, b) B13R
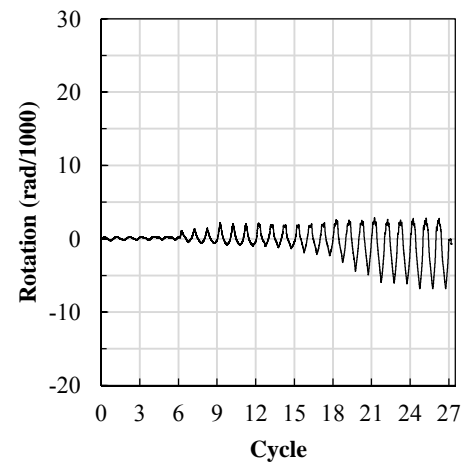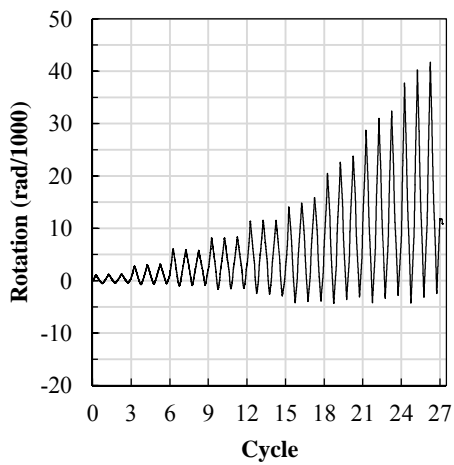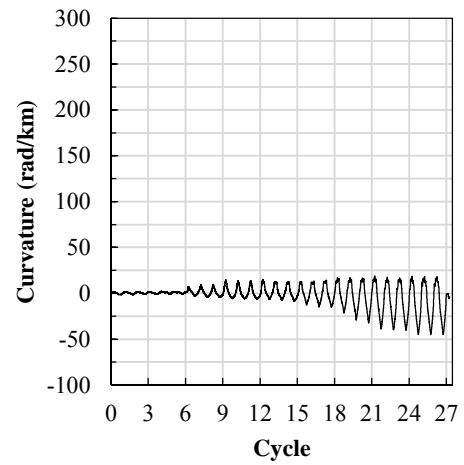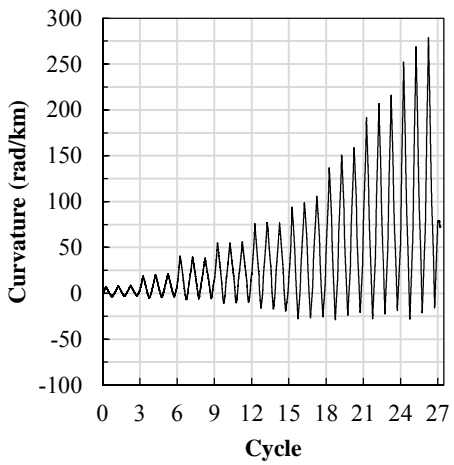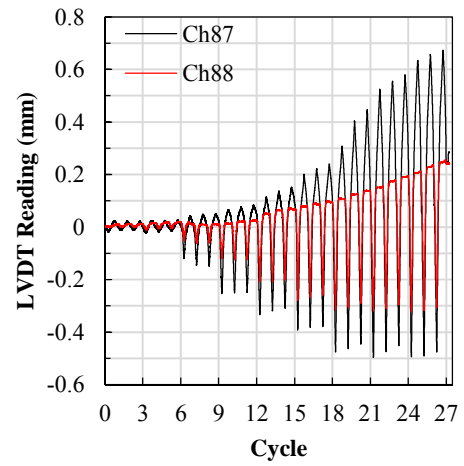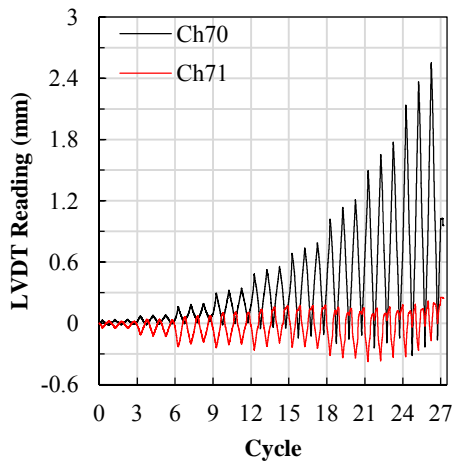
Figure B.4 Beam local deformations obtained from QS test; a) B23L, b) B23R
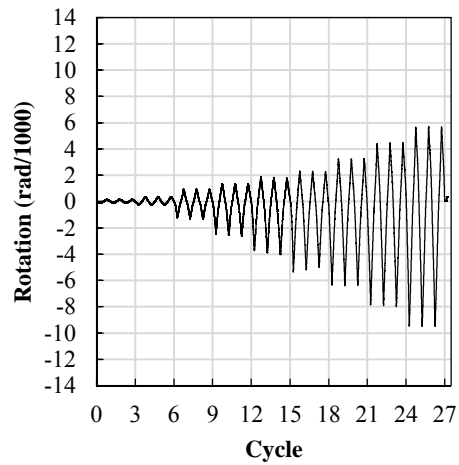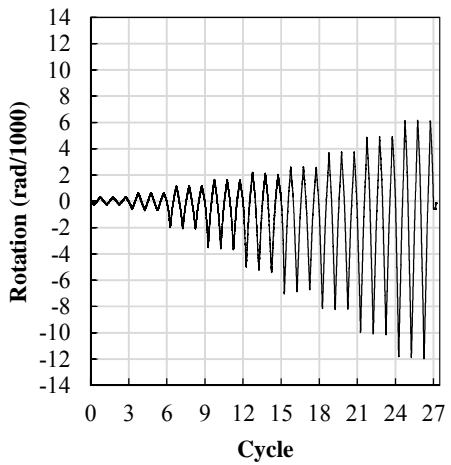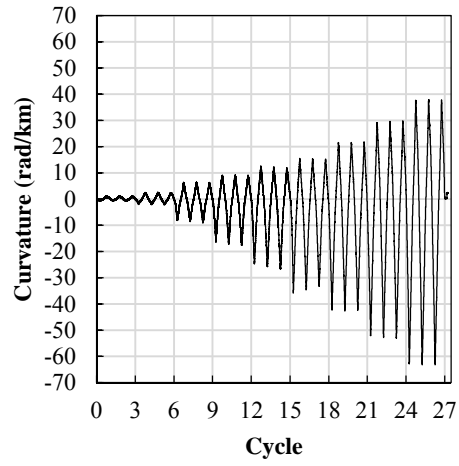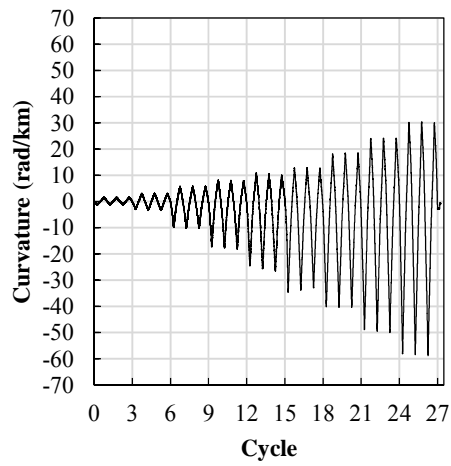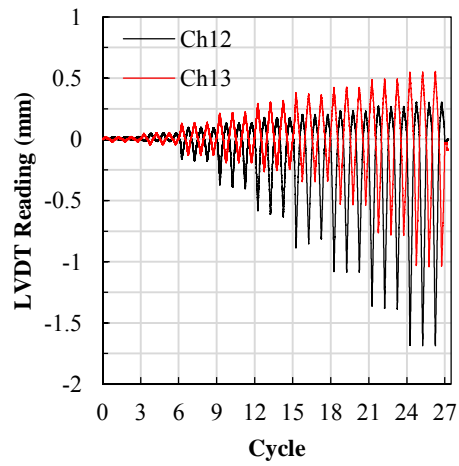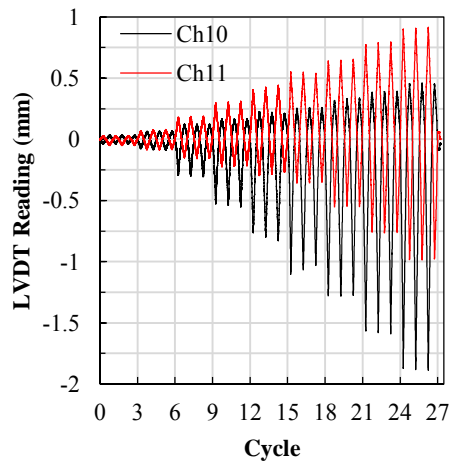
Figure B.5 Beam local deformations obtained from QS test; a) C1BL-Long, b) C1BL-Short
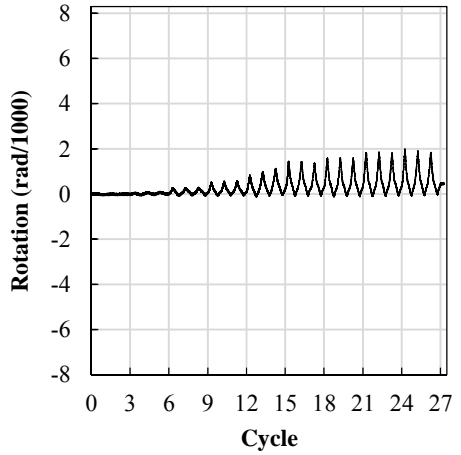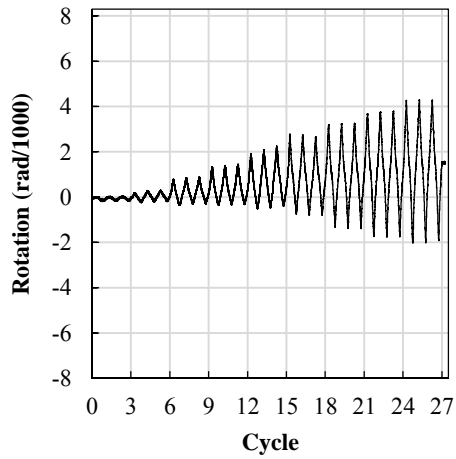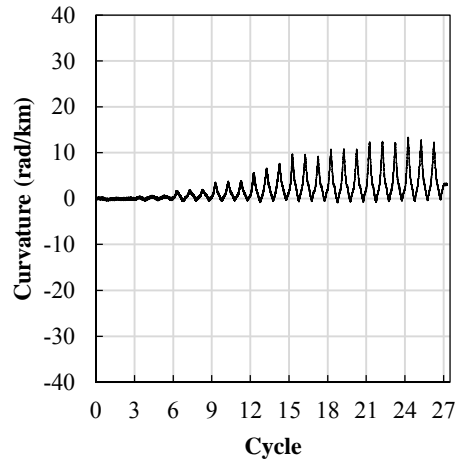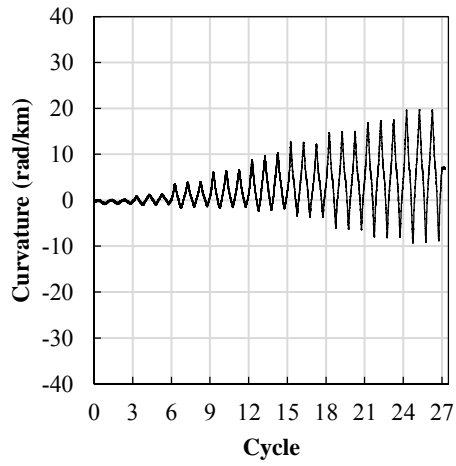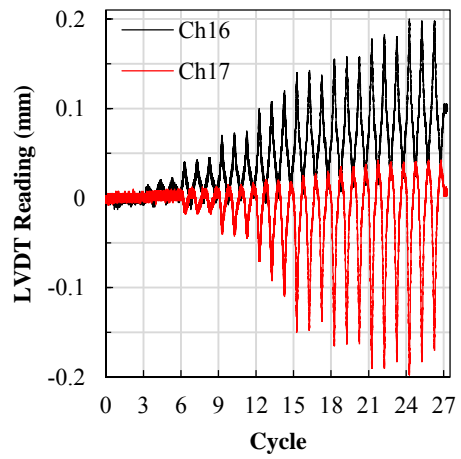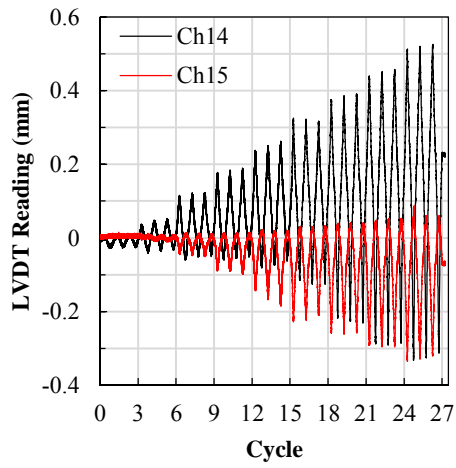
Figure B.6 Column local deformations obtained from QS test; a) C1TL-Long, b) C1TL-Short

163
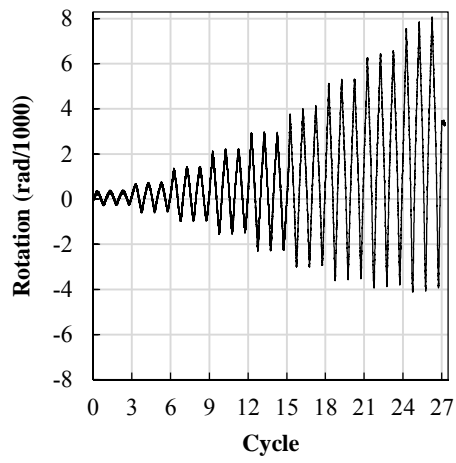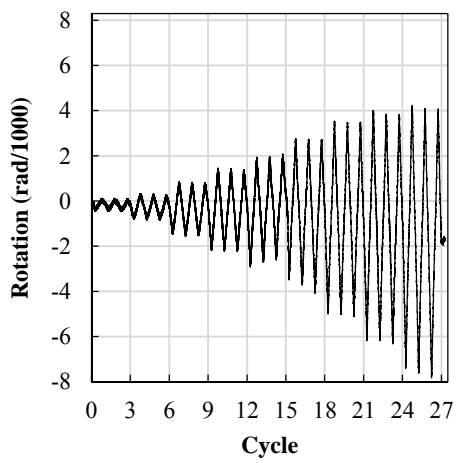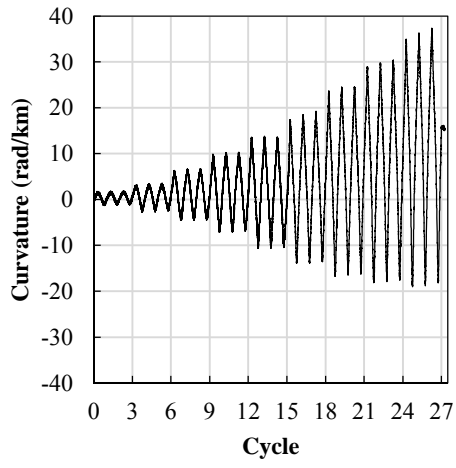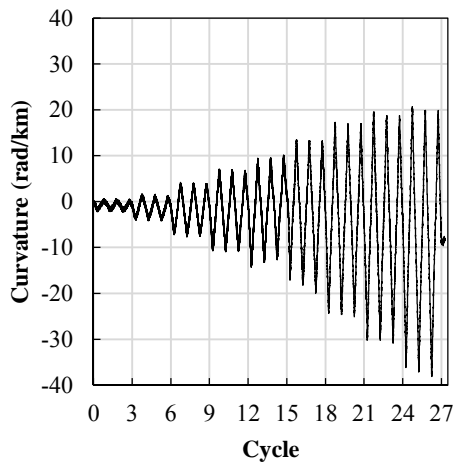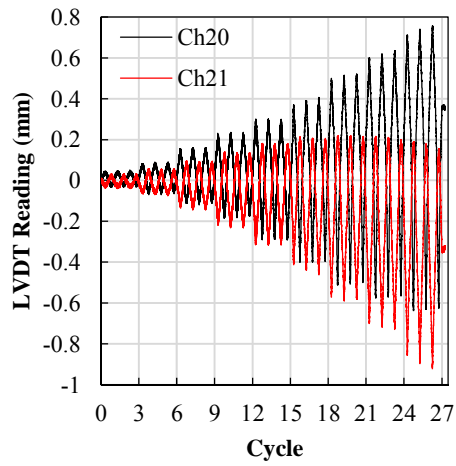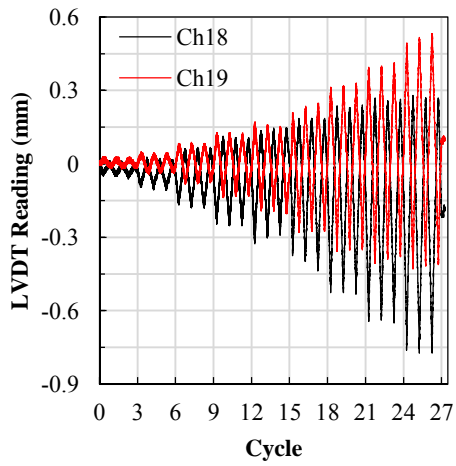
Figure B.7 Column local deformations obtained from QS test; a) C2BL, b) C2TL
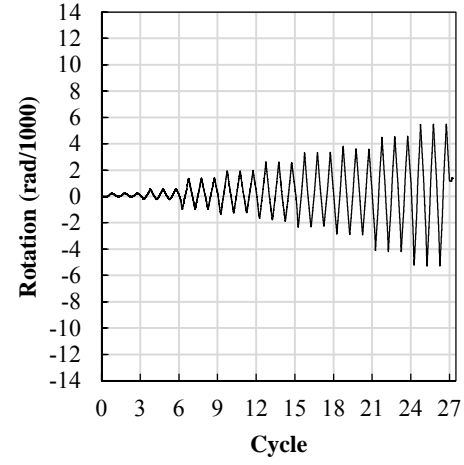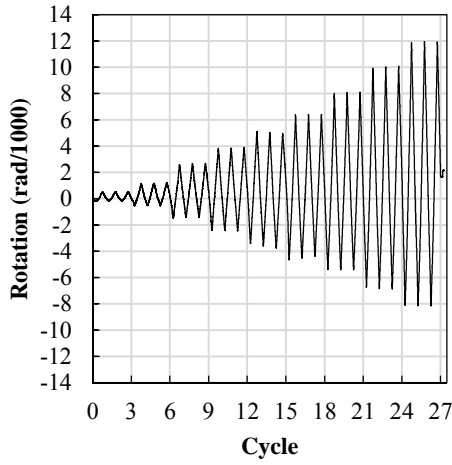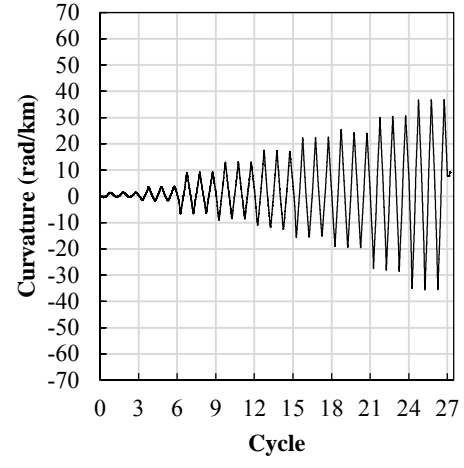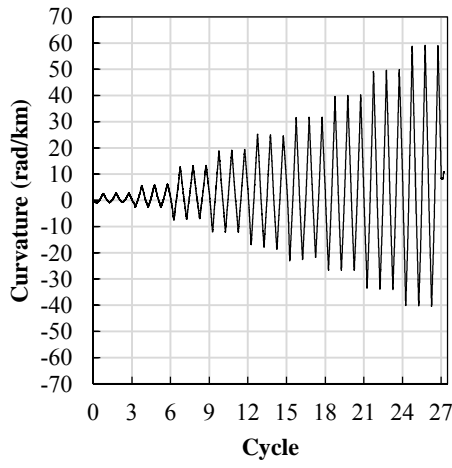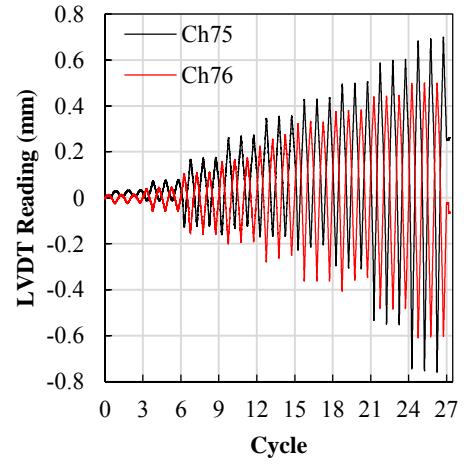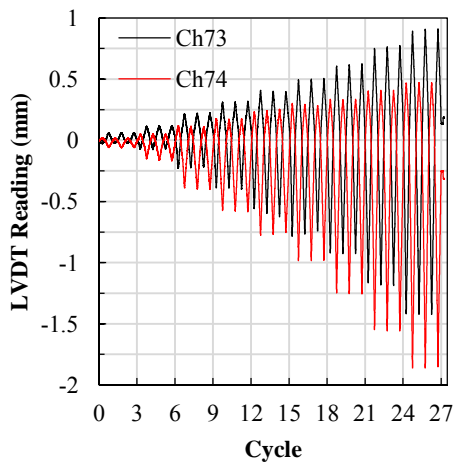
Figure B.8 Column local deformations obtained from QS test; a) C1RB-Long, b) C1RB-Short
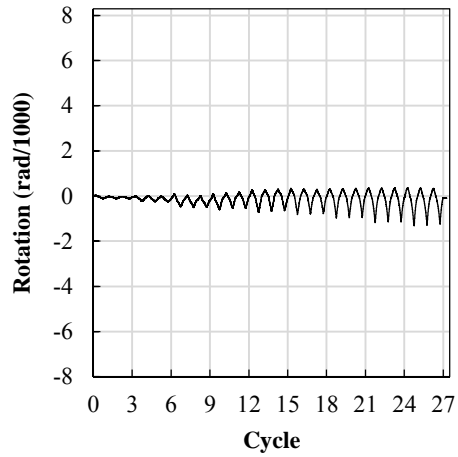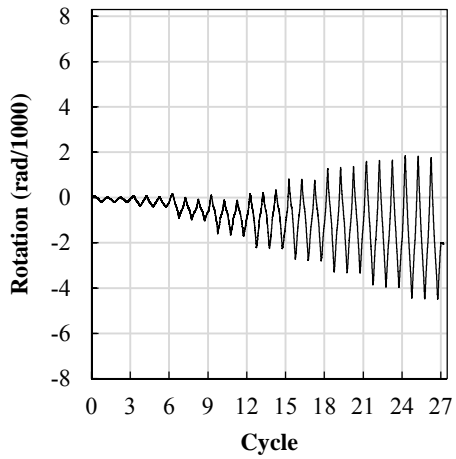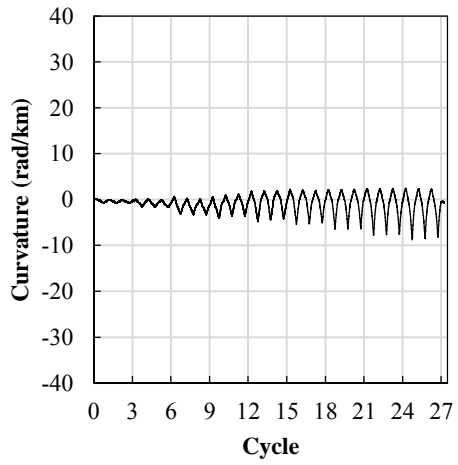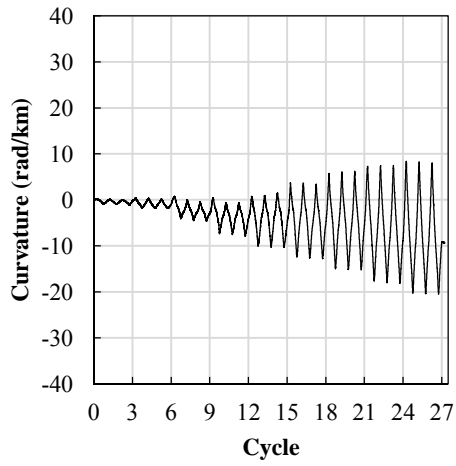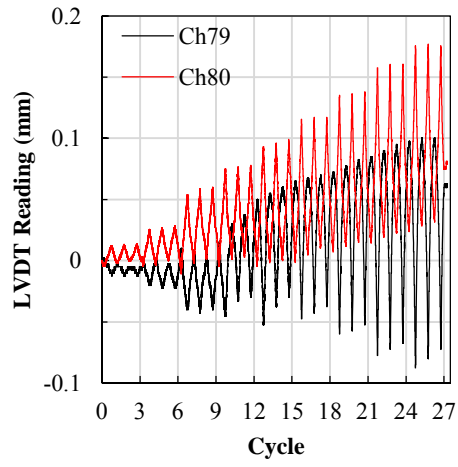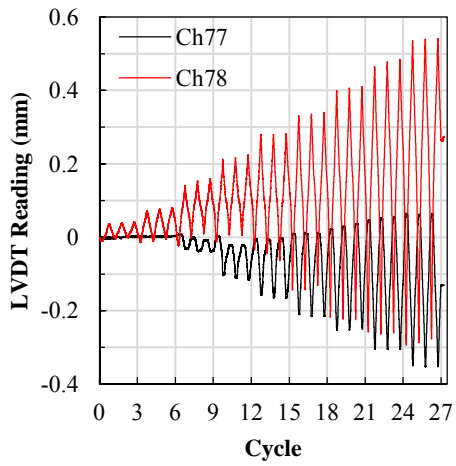
Figure B.9 Column local deformations obtained from QS test; a) C1RT-Long, b) C1RT-Short

166
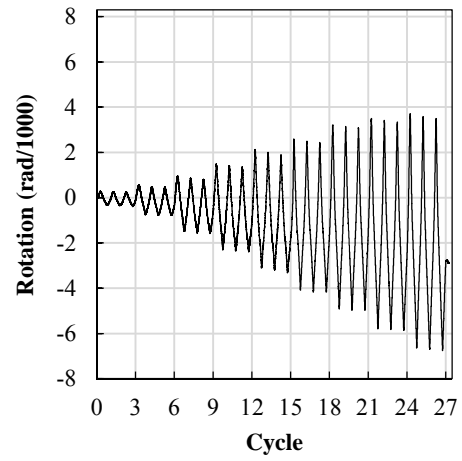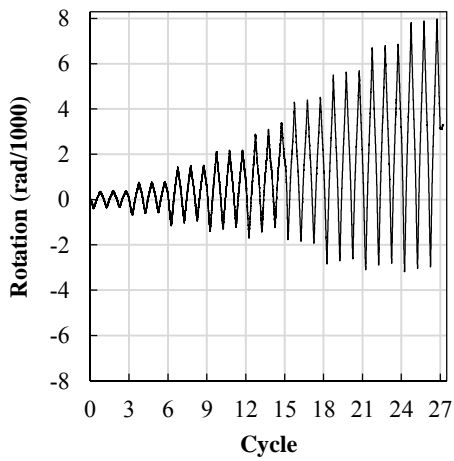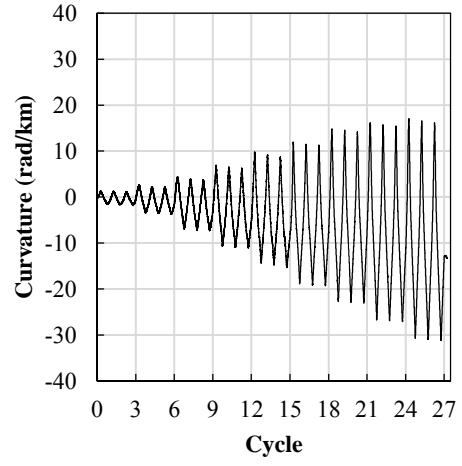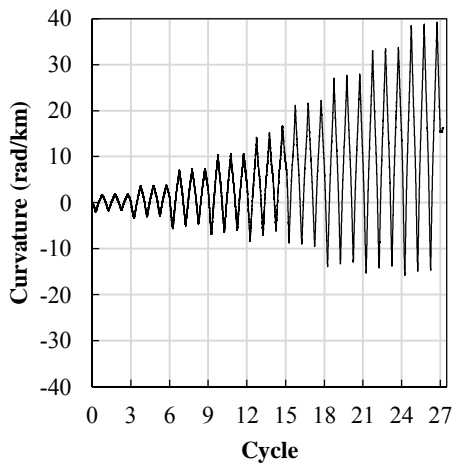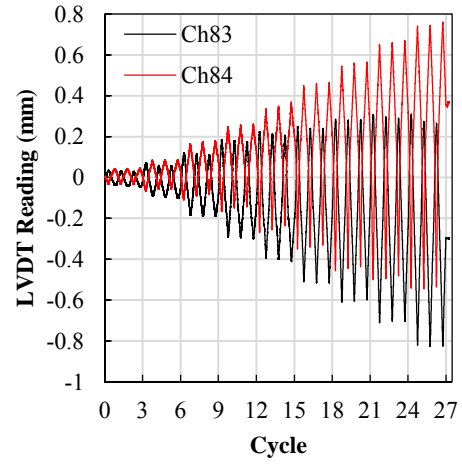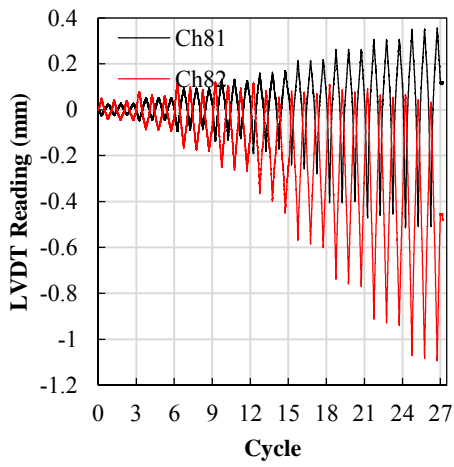
Figure B.10 Column local deformations obtained from QS test; a) C2RB, b) C2RT
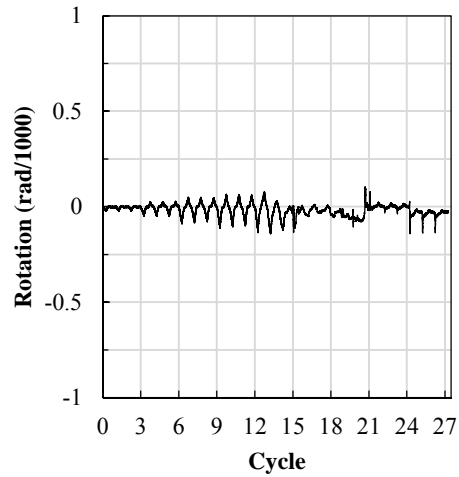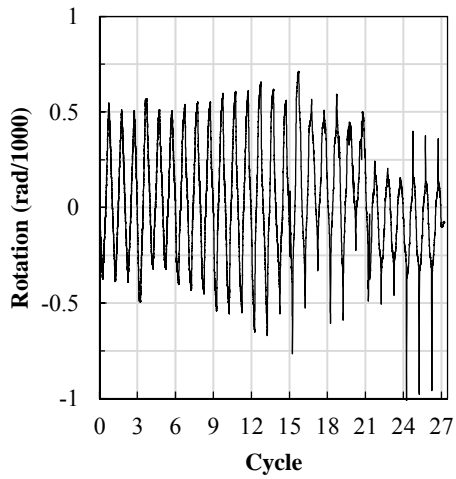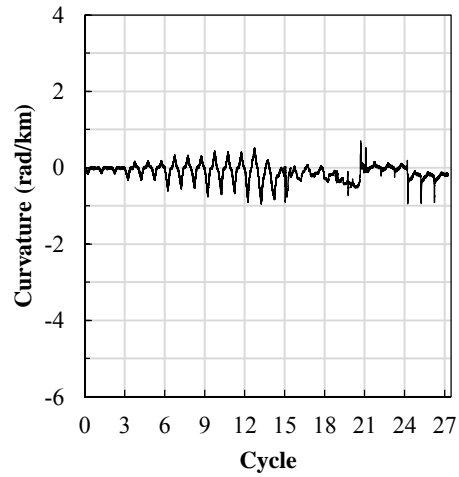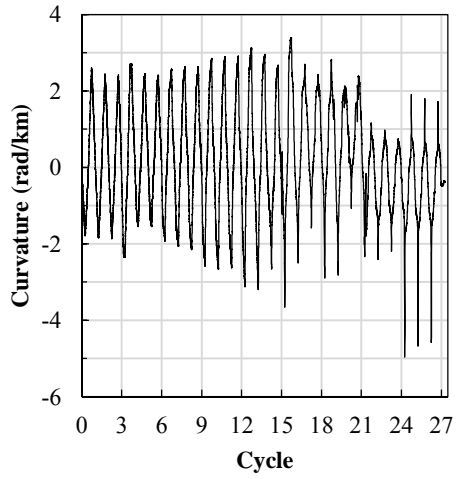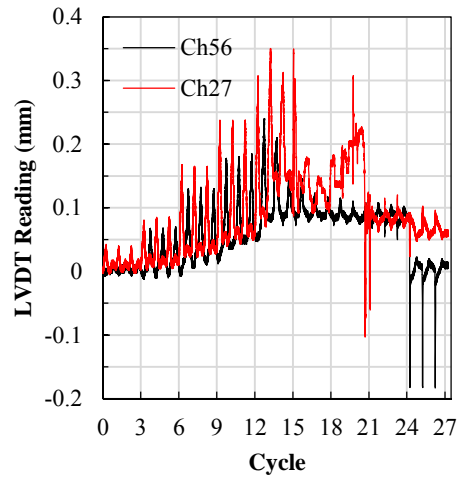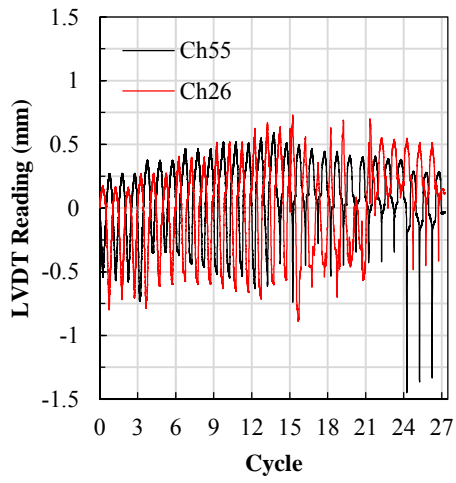
Figure B.11 Wall local deformations obtained from QS test; a) W1-Long, b) W1-Short
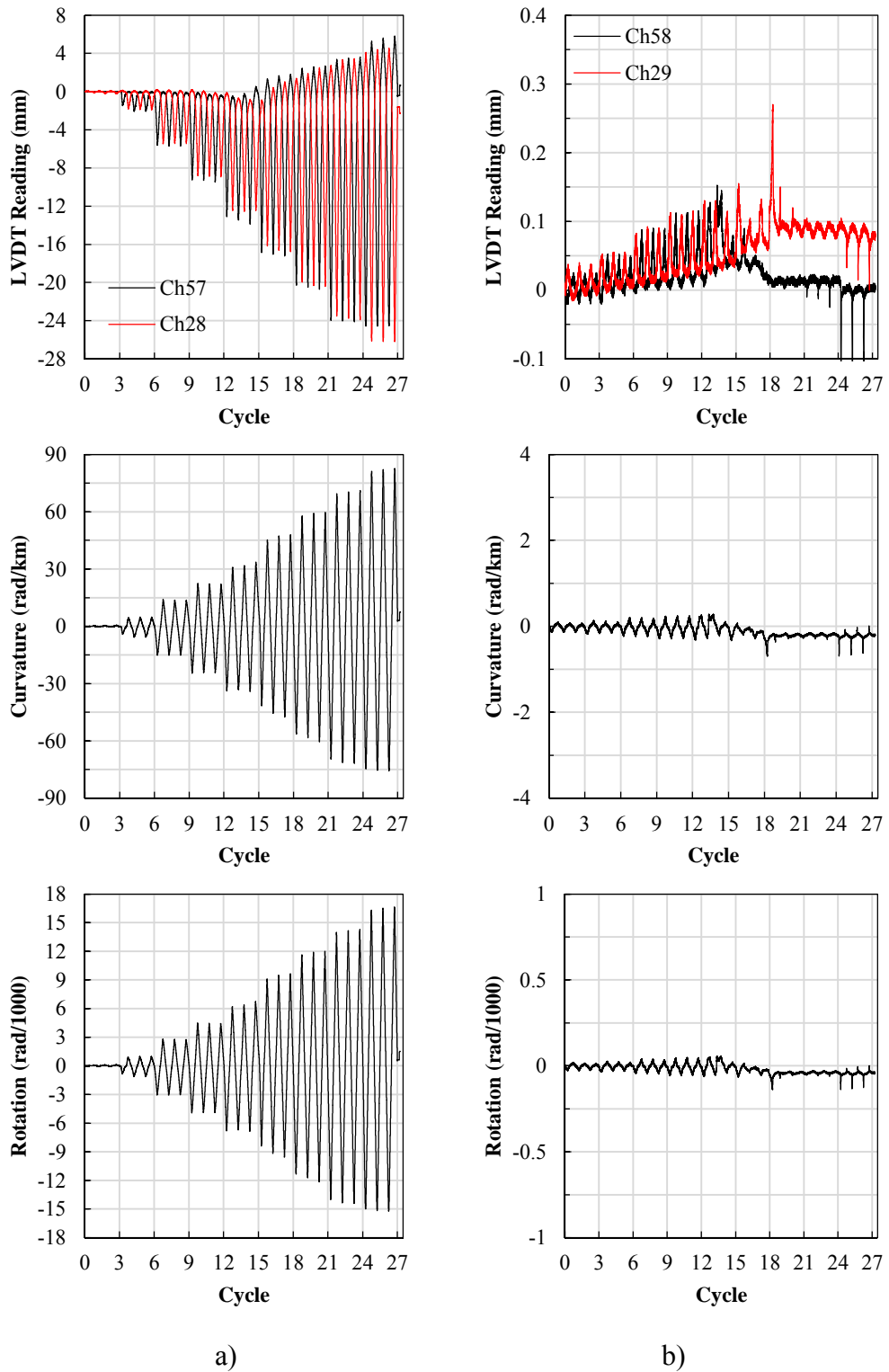
Figure B.12 Wall local deformations obtained from QS test; a) W2, b) W3
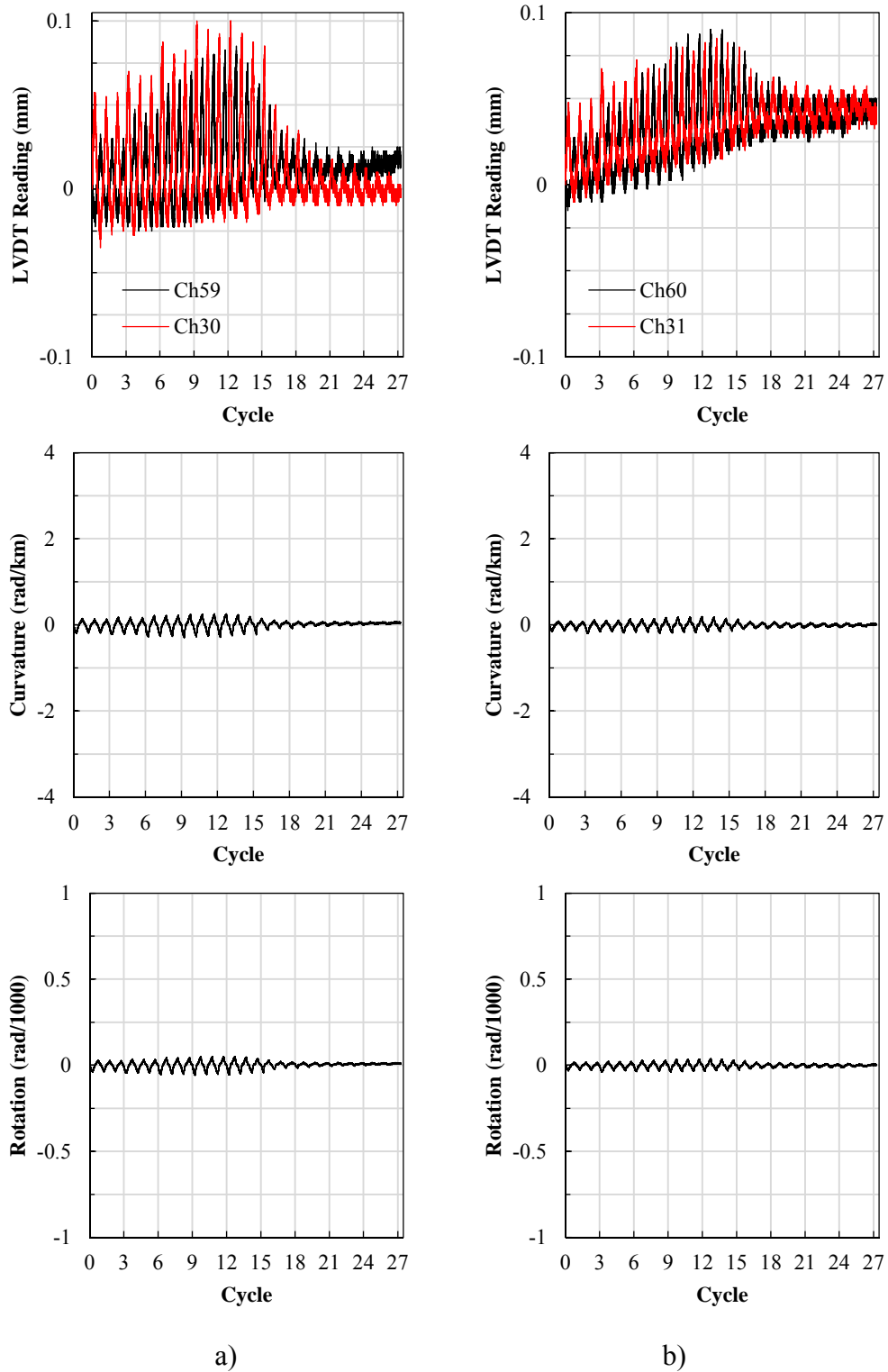
Figure B.13 Wall local deformations obtained from QS test; a) W4, b) W5
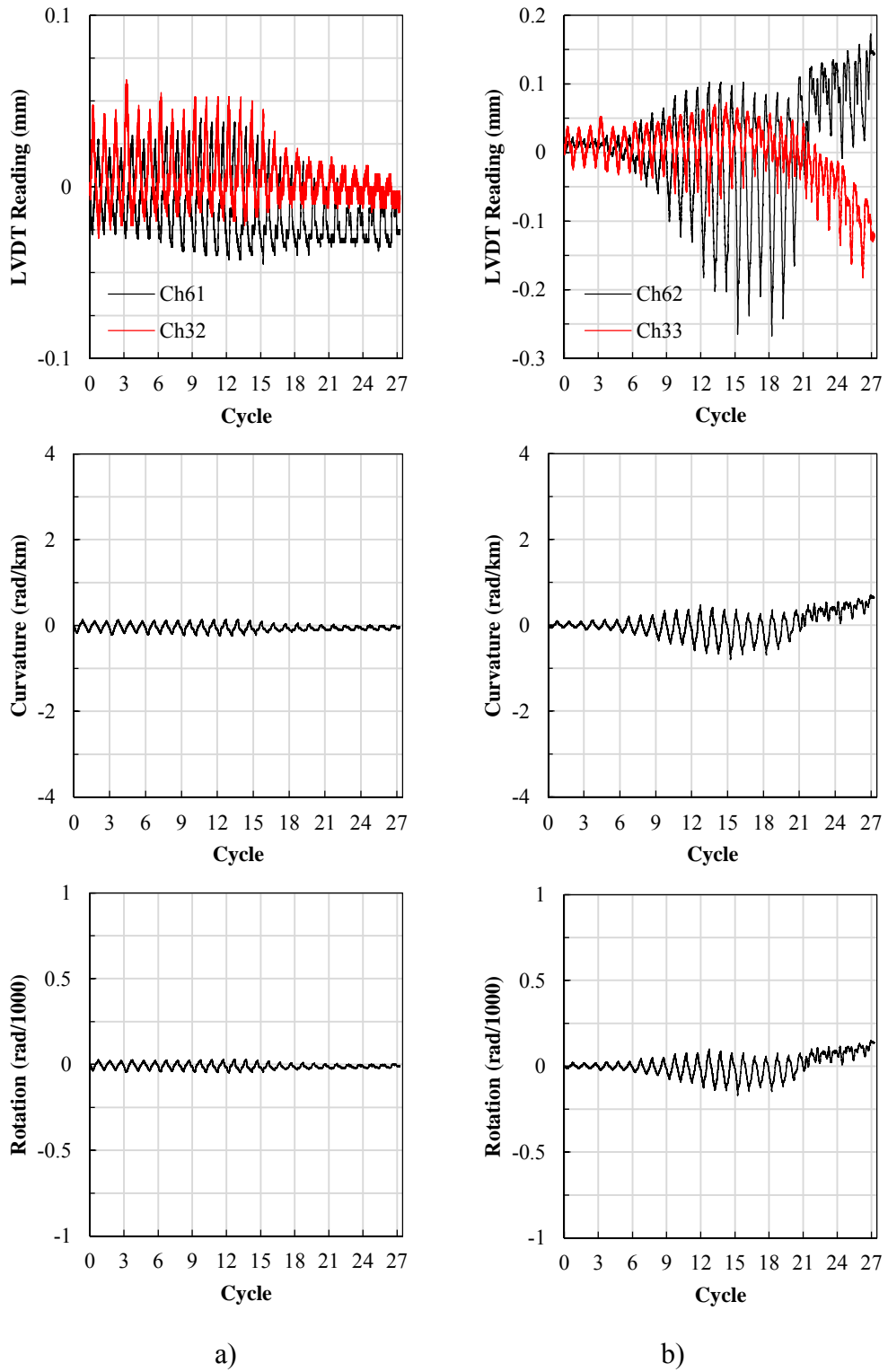
Figure B.14 Wall local deformations obtained from QS test; a) W6, b) W7
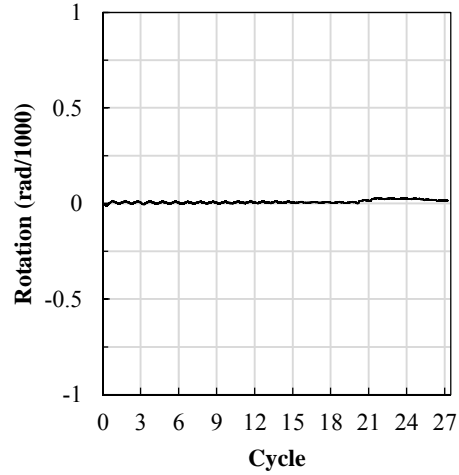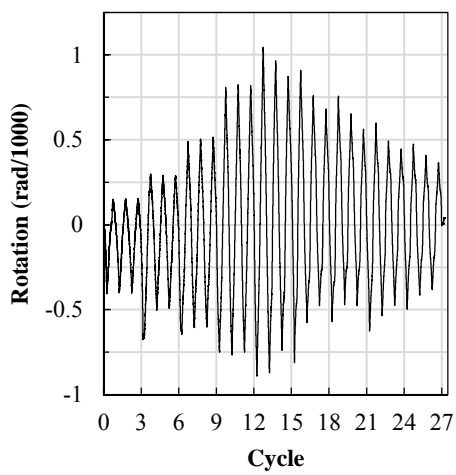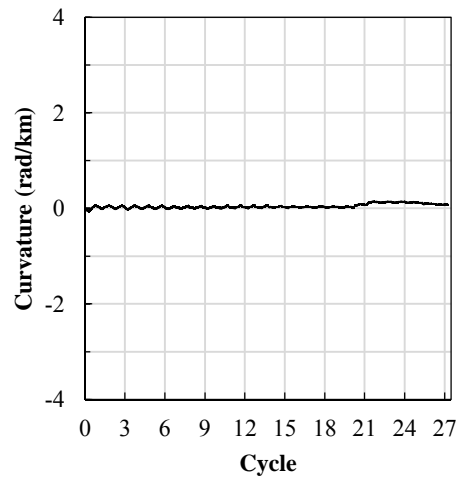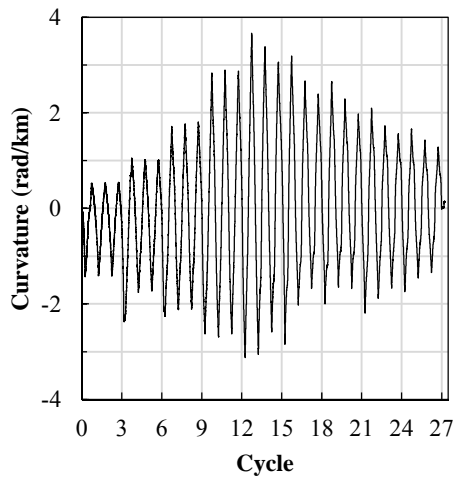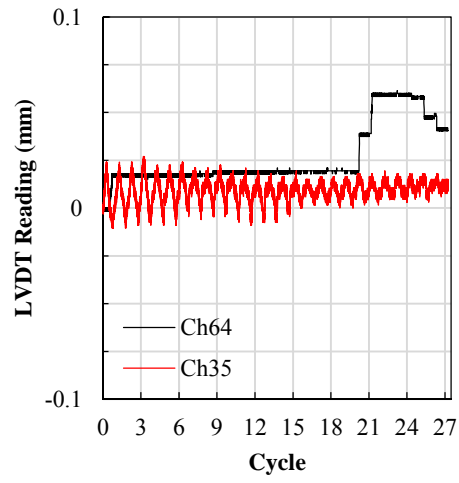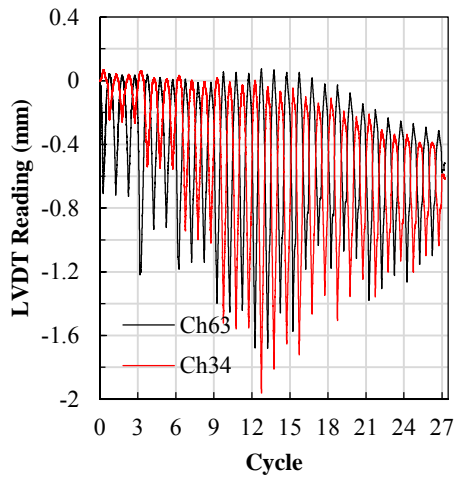
Figure B.15 Wall local deformations obtained from QS test; a) W8, b) W9
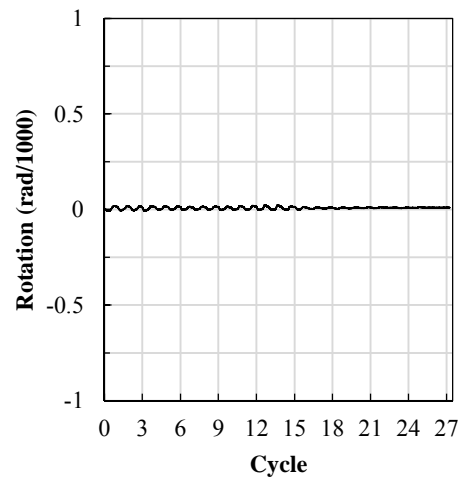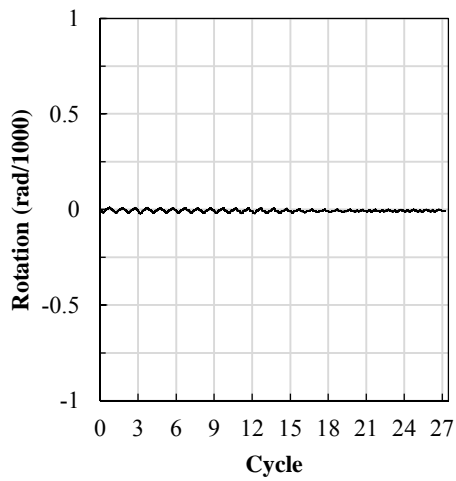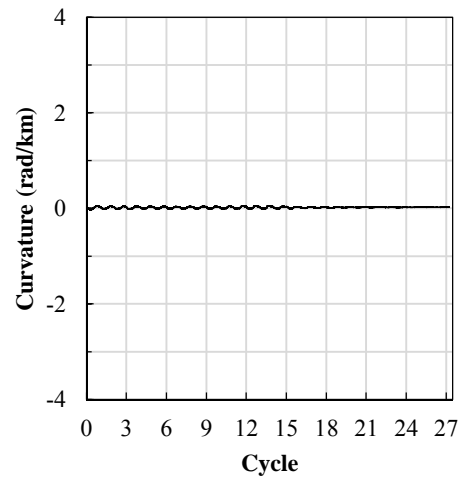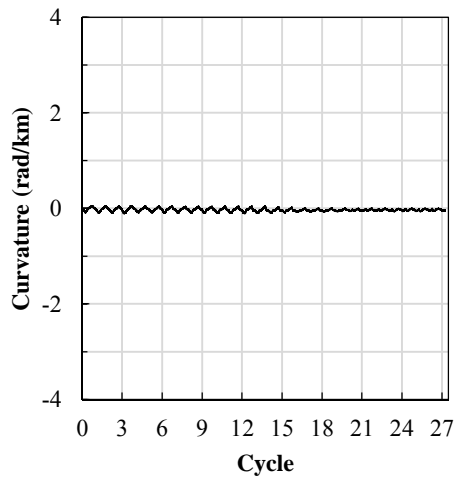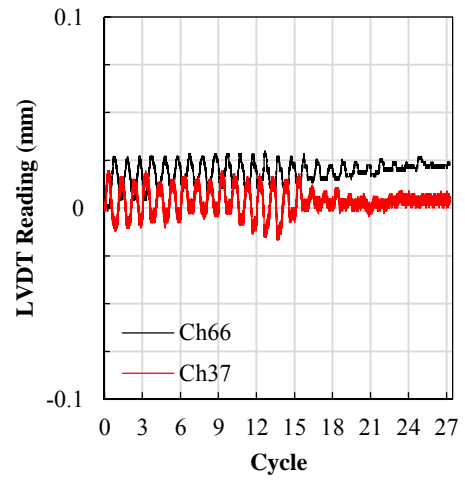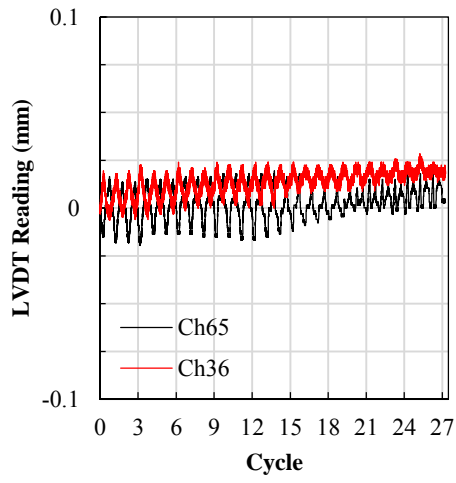
Figure B.16 Wall local deformations obtained from QS test; a) W10, b) W11
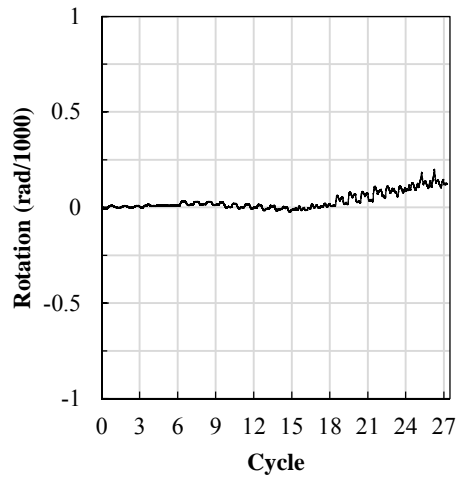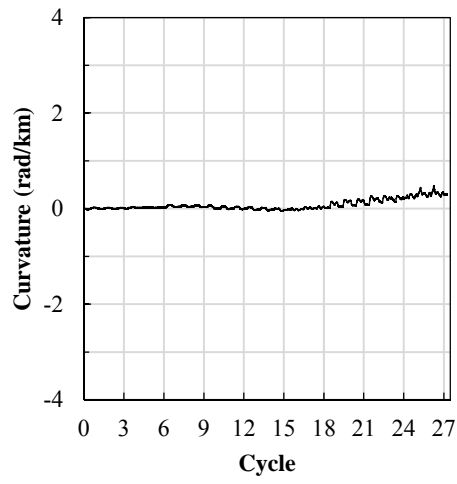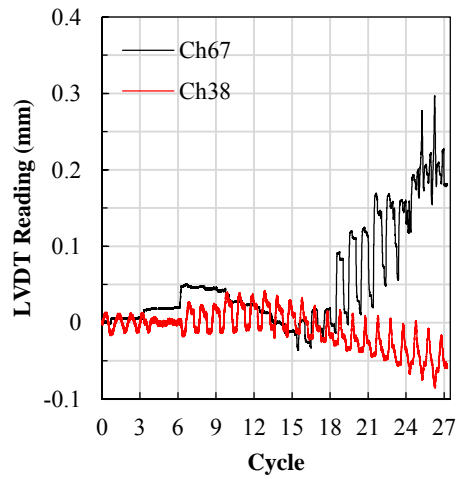
Figure B.17 Wall local deformations obtained from QS test; Segment W12
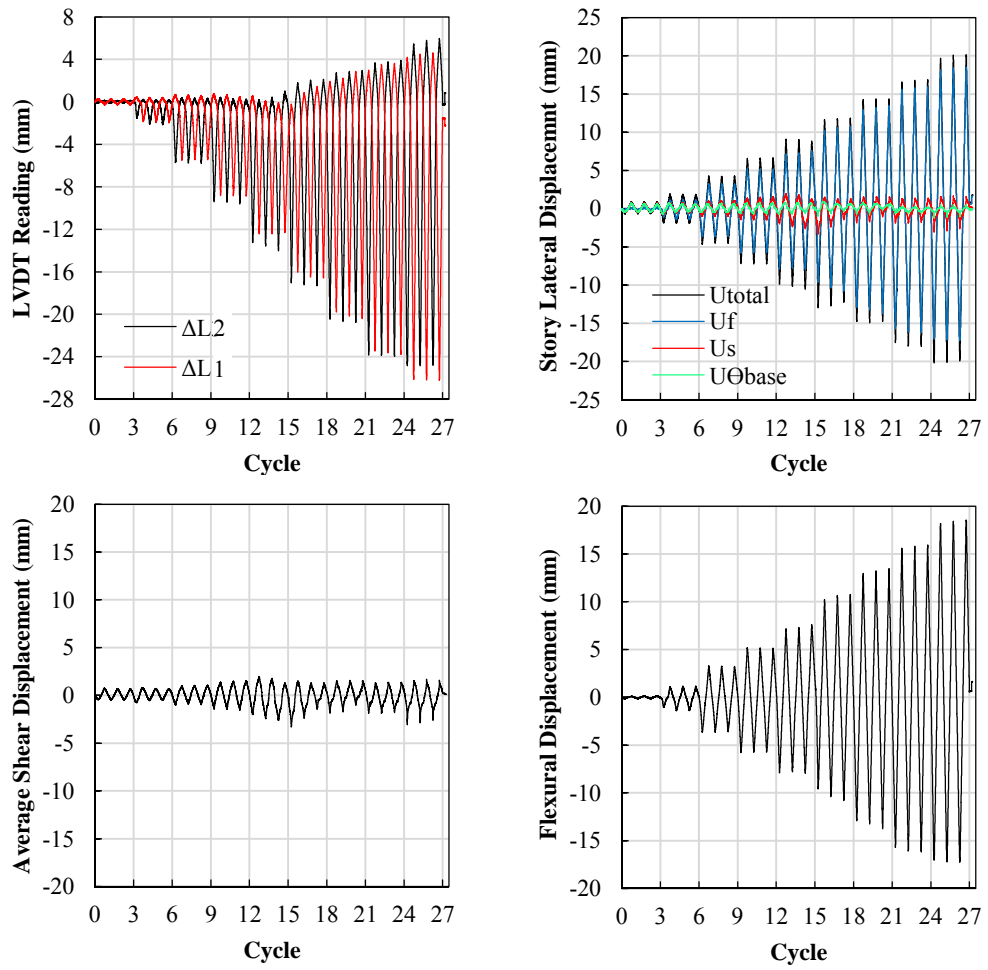
Figure B.18 Wall displacement components due to shear and flexural deformations and wall deformation because of base rotation (base crack) at first story level
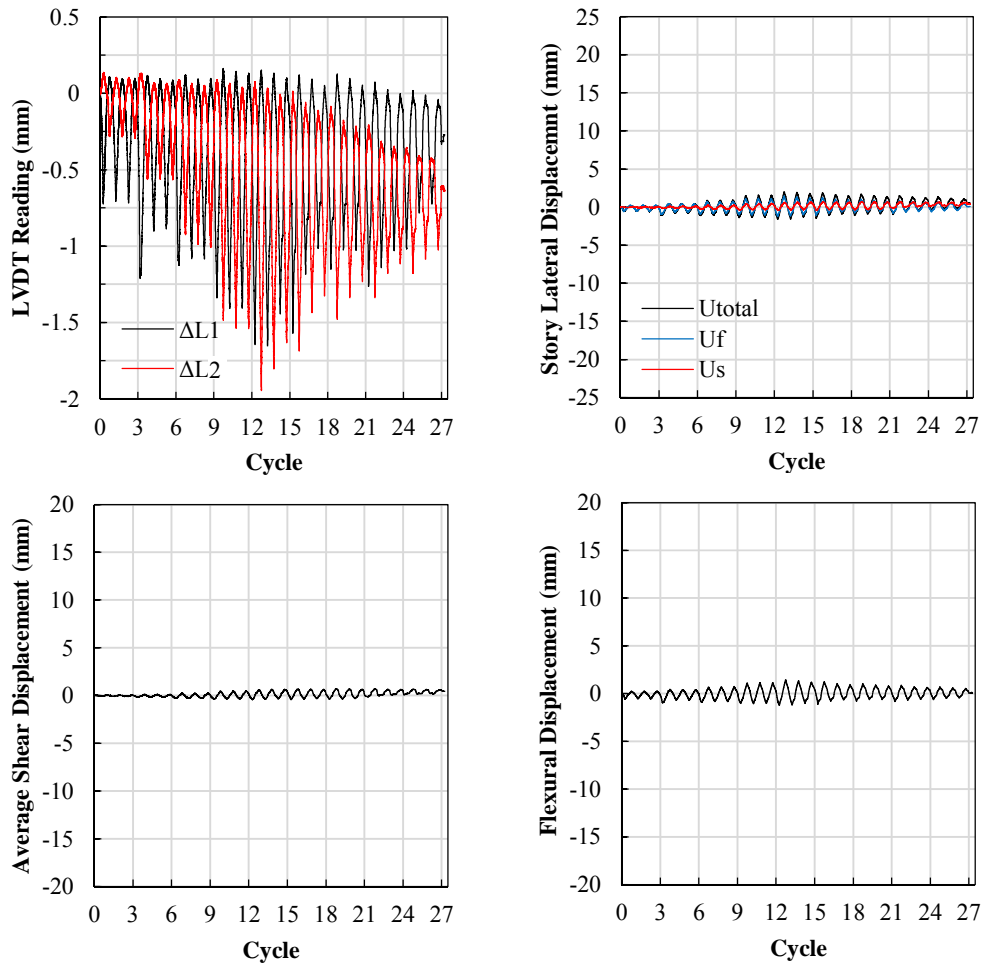
Figure B.19 Wall displacement components due to shear and flexural deformations at second story level
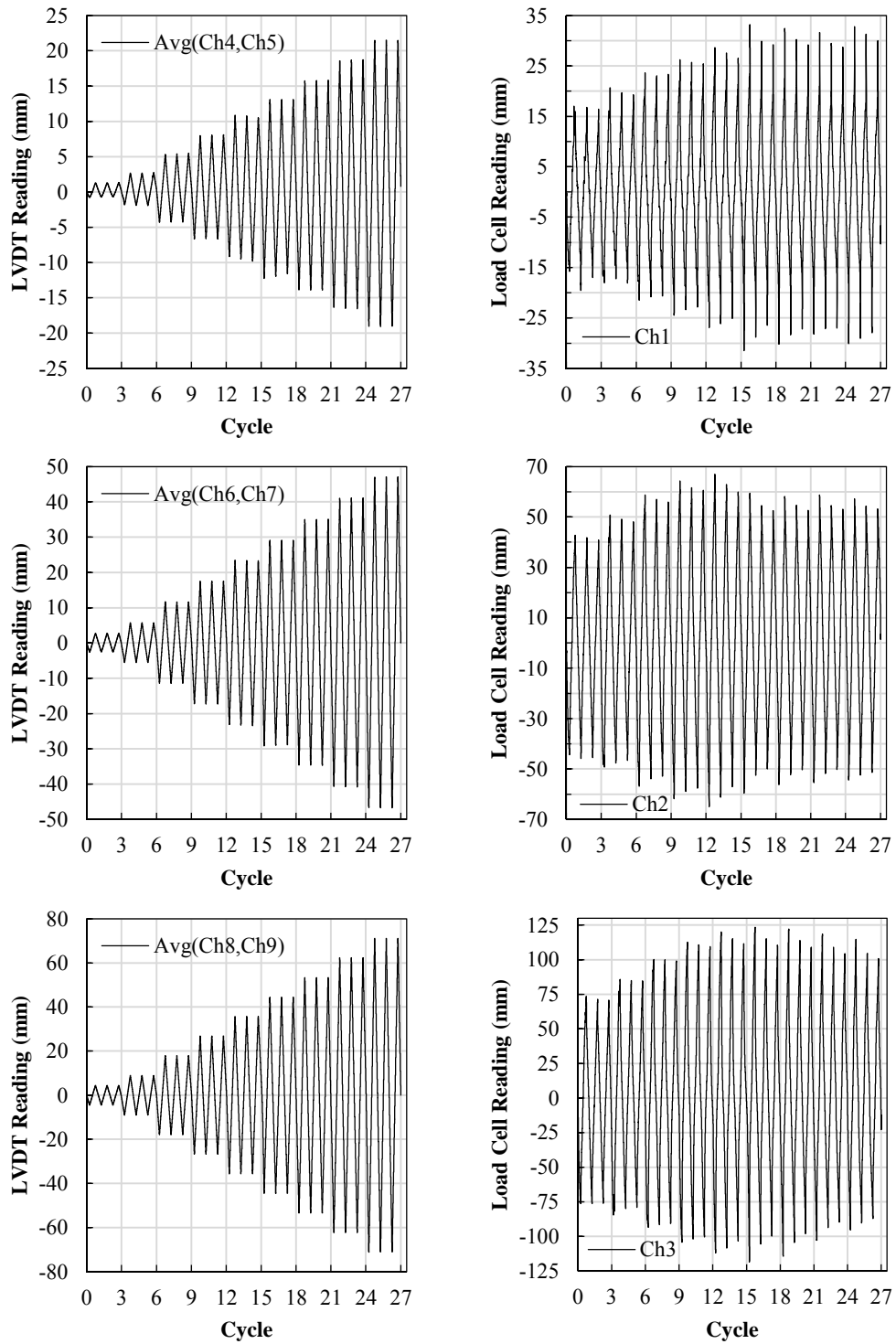
Figure B.20 RC-SW2 story displacements and forces

APPENDIX C

CHANG AND MANDER UNIAXIAL CONCRETE MODEL

The hysteresis concrete model proposed by Chang and Mander (1994) was used as the concrete constitutive model in pushover analysis conducted in SeismoStruct v7.0 software package. A brief introduction about this model and the values selected for the parameters of this model used in the software are provided in this appendix.

The uniaxial concrete model proposed by Chang and Mander (1994) is a continuous non-dimensional constitutive model. The material parameters used in this model can be calibrated according to experiments for confined and unconfined concrete. As it is clearly illustrated in Figure C.1, Chang and Mander (1994) model provides continues hysteresis behavior for concrete in both tension and compression. And owing to smooth transition parts, this model is numerically stable especially in cyclic behavior.

Figure C.2 shows the parameters used in the constitutive material formulations. In this figure, E_c is the initial tangent slope, ε_c and f_c are concrete strain and stress at maximum compressive strength point, respectively. ε_{cr} is the strain normalized with respect to ε_c. This point defines the starting point of the straight line until zero compressive stress and determines the shape of the descending branches of the curve. The shape of the model in tension is same as compression with similar parameters which is defined to model the concrete behavior in tension (Kolozvari et al., 2015).
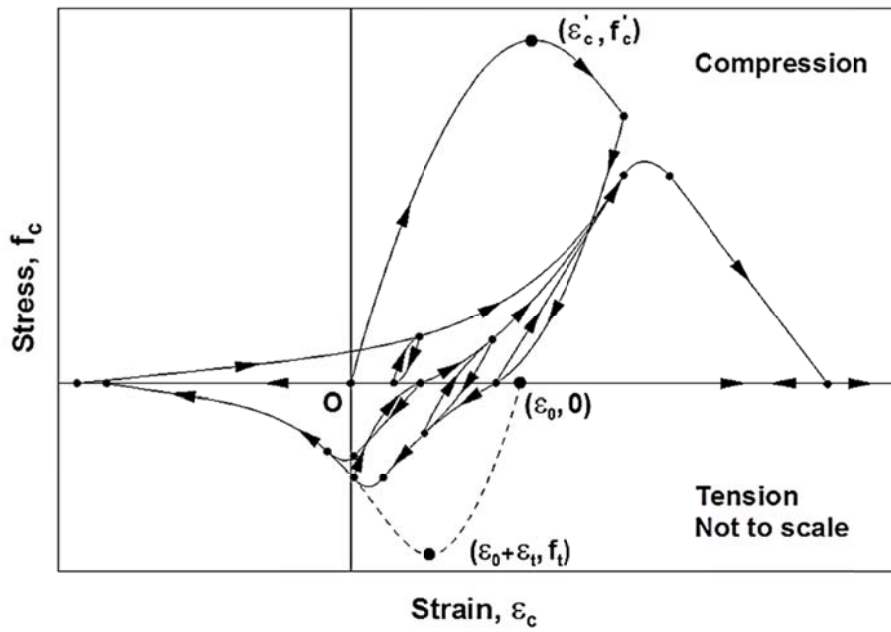
Figure C.1 Chang and Mander concrete hysteretic model (Kolozvari et al., 2015)
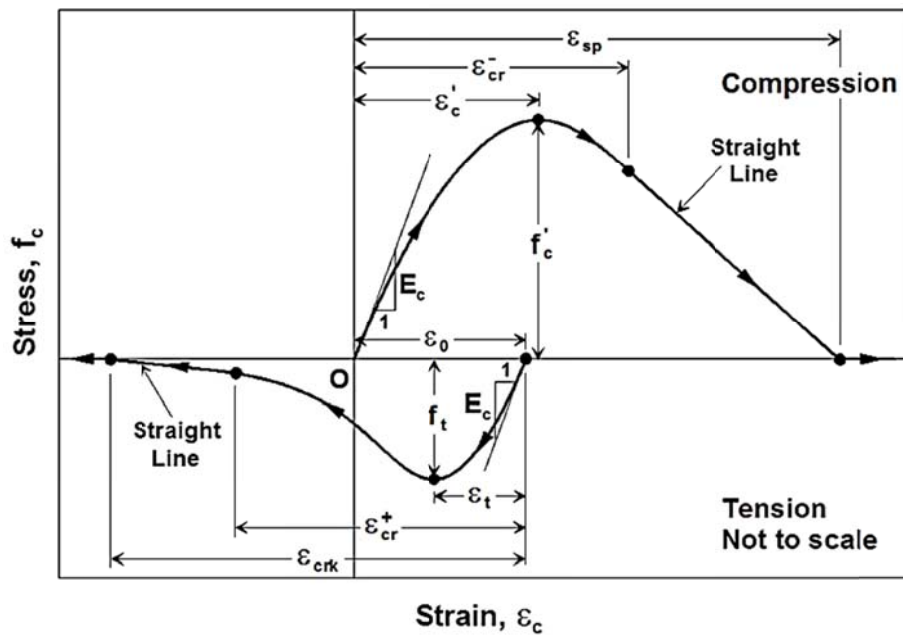
Figure C.2 Envelope of the constitutive model in tension and compression

(Kolozvari et al., 2015)

The concrete compressive strength, f_c', was obtained from standard cylinder tests. Strain at peak compressive stress was assumed equal to $\varepsilon_c' = \frac{f_c'^{1/4}}{1152.63}$ (in MPa) according to Mander (1988). The concrete tensile strength and cracking strain were calculated as $f_t = 0.34\sqrt{f_c}$ (in MPa) and $\varepsilon_t = \frac{f_t}{E_c}$, respectively. The concrete modulus of elasticity is $E_c = 4730\sqrt{f_c}$ (in MPa). Table C.1 and Table C.2 lists the other parameters used in SeismoStruct v7 software in order to define concrete behavior in tension and compression. These parameters of the constitutive model in compression and tension part were calibrated to obtain a backbone curve as close as possible to the envelope of the overall hysteresis experimental response.

Table C.1 Parameters used in order to define Chang and Mander (1994) model for specimen RC-SW1 in SeismoStruct v7

Parameters	
Mean Compressive strength (kPa)	29900
Mean tensile strength (kPa)	1900
Modulus of elasticity (kPa)	25864000
Strain at peak compressive stress (m/m)	0.002028
Strain at peak tensile stress (m/m)	0.000074
Non-dimensional critical compressive strain	1.05
Non-dimensional critical tensile strain	100000
Specific weight (kN/m^3)	22.6

Table C.2 Parameters used in order to define Chang and Mander (1994) model for specimen RC-SW2 in SeismoStruct v7

Parameters	
Mean Compressive strength (kPa)	36370
Mean tensile strength (kPa)	2100
Modulus of elasticity (kPa)	28525400
Strain at peak compressive stress (m/m)	0.002131
Strain at peak tensile stress (m/m)	0.000073
Non-dimensional critical compressive strain	1.10
Non-dimensional critical tensile strain	1.02
Specific weight (kN/m^3)	22.6

APPENDIX D

DODD AND RESTREPO-POSADA UNIAXIAL STEEL MODEL

The uniaxial steel model proposed by Dodd and Restrepo-Posada (1995) was used in order to define steel reinforcement stress-strain relationship in the analytical model constructed in SeismoStruct v7.0 software. A brief introduction about this model and the values selected for the parameters of this model used in the software are provided in this appendix.

This model considers Bauschinger effect, reduction in elastic modulus and isotropic strain hardening. The buckling of rebar is not considered in this model. In monotonic response, stress at yield plateau remains almost the same as yield value. The equation of yield plateau is $f_s = f_y e^{\varepsilon_s}$ which has a slope very close to zero. The equation for strain-hardening part is a power curve passing through three points which are the point at which hardening starts (ε_{sh}, f_{sh}), point of ultimate load (ε_{su}, f_{su}) and an intermediate point between these point which is used to define the shape of the curve ($\varepsilon_{su,1}$, $f_{su,1}$). Assuming zero slop for the skeleton curve of this model at ultimate point, the equation for hardening region is

$f_s = (f_{sh} - f_{su}) \left\{ \frac{\varepsilon_{su} - \varepsilon_s}{\varepsilon_{su} - \varepsilon_h} \right\}^P + f_{su}$ in which P is $P = ln \left[\frac{f_{su,1} - f_{su}}{f_{sh} - f_{su}} \right] / ln \left(\frac{\varepsilon_{su} - \varepsilon_{su,1}}{\varepsilon_{su} - \varepsilon_{sh}} \right)$.

Figure E.1 shows the parameters used in the constitutive material formulation.
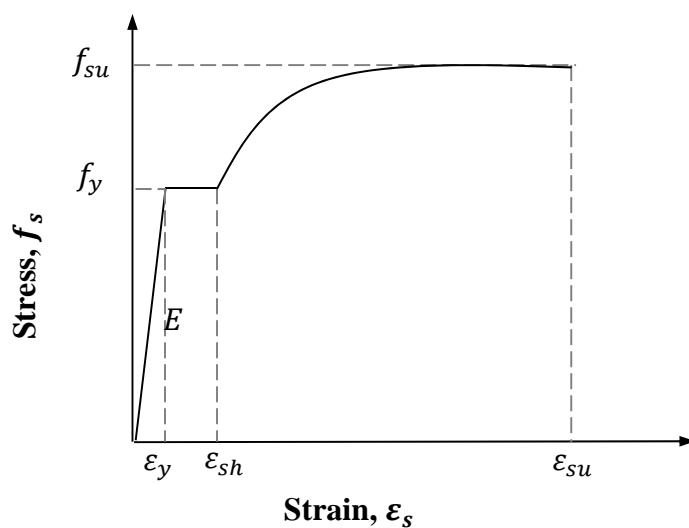
Figure D.1 Dodd and Restrepo-Posada (1995) steel model for monotonic response

Table D.1 Parameters used in order to define Dodd and Restrepo-Posada (1995)
model for 4-mm bars in SeismoStruct v7

Parameters	
Modulus of elasticity (kPa)	196090000
Yield Stress (kPa)	272457
Stress at peak load (kPa)	396898
Strain at initiation of strain hardening curve (-)	0.007
Strain at peak load (-)	0.138205
Strain of the intermediate point of the strain hardening curve (-)	0.04846
Stress of the intermediate point of the strain hardening curve (kPa)	344335
Specific weight (kN/m3)	78.5

Table D.2 Parameters used in order to define Dodd and Restrepo-Posada (1995) model for 8-mm bars in SeismoStruct v7

Parameters	
Modulus of elasticity (kPa)	199760000
Yield Stress (kPa)	434870
Stress at peak load (kPa)	571410
Strain at initiation of strain hardening curve (-)	0.02859408
Strain at peak load (-)	0.157586
Strain of the intermediate point of the strain hardening curve (-)	0.063031
Stress of the intermediate point of the strain hardening curve (kPa)	528286
Specific weight (kN/m3)	78.5

Table D.3 Parameters used in order to define Dodd and Restrepo-Posada (1995) model for 10-mm bars in SeismoStruct v7

Parameters	
Modulus of elasticity (kPa)	197410000
Yield Stress (kPa)	451383
Stress at peak load (kPa)	718635
Strain at initiation of strain hardening curve (-)	0.011895
Strain at peak load (-)	0.12
Strain of the intermediate point of the strain hardening curve (-)	0.049
Stress of the intermediate point of the strain hardening curve (kPa)	661524
Specific weight (kN/m3)	78.5

APPENDIX E

SHEAR AND FLEXURAL DEFORMATIONS

The average shear and flexural deformations of the first and second stories of the specimens RC-SW1 and RC-SW2 were computed using the method proposed by Massone and Wallace (2004). The total wall panel deformation consists of deformation due to pure bending and pure shear. Figure E.1a and Figure E.1b illustrates pure flexure and pure shear deformation, respectively.
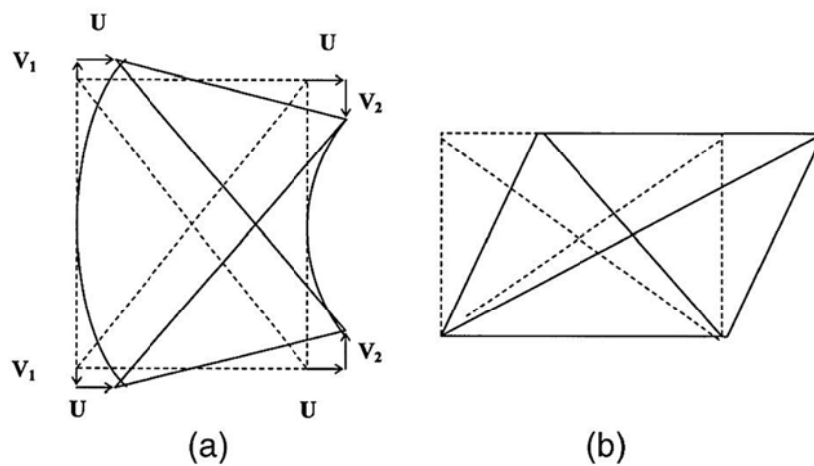
Figure E.1 Wall Panel deformations; a) pure Flexural b) pure shear (Massone and Wallace, 2004)

Figure E.2 shows a schematic view of deformed panel under combined shear and flexure. For slender walls vertical displacements at wall edges must be considered in shear distortion calculations (Massone and Wallace, 2004). These vertical deformations results in overestimation of the contribution of shear deformations to wall lateral displacement.
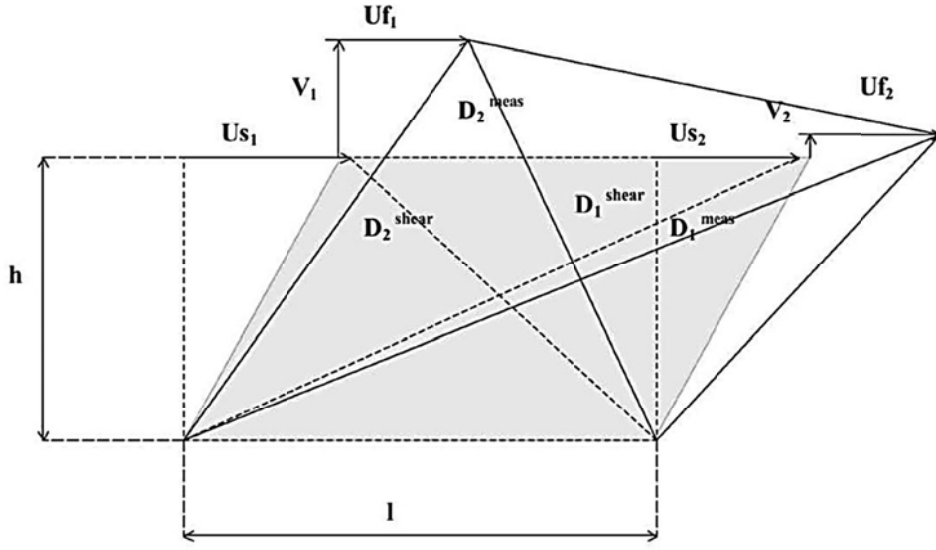
Figure E.2 Schematic view of deformed panel

Total average shear displacement, $\overline{U_s}$, can be estimated using Eq (E.1).

$$\overline{U_s} = \frac{\sqrt{D_1^{shear^2} - h^2} - \sqrt{D_2^{shear^2} - h^2}}{2} \qquad (E.1)$$

D_1^{shear} and D_2^{shear} are panel diagonal length due to pure shear. h is the story height. The Eq (E.1) can be written in terms of D_1^{meas} and D_2^{meas} ,which are diagonal length of deformed X confiquration of installed LVDTs, see Eq (E.2).

$$\overline{U_s} = \frac{\sqrt{D_1^{meas^2} - (h + V_2)^2} - U_{f2} - \left(\sqrt{D_2^{meas^2} - (h + V_1)^2} + U_{f1} \right)}{2} \qquad (E.2)$$

Assuming $U_{f1} = U_{f2} = U_f$ which is the lateral displacement corresponding to flexural deformations, Eq (E.2) can be simplified to Eq (E.3).

188

$$\overline{U_s} = \frac{\sqrt{D_1^{meas^2} - (h + V_2)^2} - \sqrt{D_2^{meas^2} - (h + V_1)^2}}{2} - U_f \qquad (\text{E.3})$$

In this equation, V_1 and V_2 are the vertical displacement at the top corners of the panel. The lateral displacement due to shear and flexure can be obtained by rearranging Eq (E.3).

$$U_{total} \equiv \overline{U_s} + U_f \qquad (\text{E.4})$$

$$U_{total} = \frac{\sqrt{D_1^{meas^2} - (h + V_2)^2} - \sqrt{D_2^{meas^2} - (h + V_1)^2}}{2} \qquad (\text{E.5})$$

Lateral displacement due to flexural deformation at the top of the panel can be calculated using the vertical LVDTs installed at the outer edges of the wall ,see Figure E.3. The rotation of the each wall segment is calculated by Eq (E.6).

$$\theta^k = \frac{V_2^k - V_1^k}{l} \qquad (\text{E.6})$$

In Eq (E.6), l is the horizontal distance between the vertical LVDTs installed at the outer edges of the wall panel. V_2^k and V_2^k are the vertical displacement measured by pair of LVDTs over the gage length x^k and k is the segment number. Assuming center of rotation at the middle height of each segment, lateral deformation at the top of the panel due to each segment rotation is obtained by Eq (E.7).

$$U_f = \sum_{k=1}^{N} \theta^k \left[\frac{x^k}{2} + \left(\sum_1^k x^{(k-1)} \right) \right], \quad x^0 = 0 \qquad (\text{E.7})$$

$$h = \sum_{k=1}^{N} x^k \qquad (\text{E.8})$$

CURRICULUM VITAE

PERSONAL INFORMATION

Surname, Name: Ezzatfar, Pourang

Nationality: Iran

Date and Place of Birth of Birth: 5 July 1981, Tabriz

Marital Status: Married

Email: ezzatfar@gmail.com

EDUCATION

Ph. D.	METU, Civil Engineering	2016
MS	University of Tehran, Civil Engineering	2008
BS	University of Tabriz, Civil Engineering	2005

EMPLOYMENT

2014-2016	TEDU, Civil Engineering Department	Teaching Assistant
2010-2013	METU, Structural Mechanics Lab	Project Assist
2007	Tadbir Sahel Pars Consultancy Company	Structural Engineer

FOREIGN LANGUAGES

Advanced English, Native Azari, Native Farsi, Fluent Turkish

PUBLICATIONS

INTERNATIONAL BOOKS OR BOOK CHAPTERS

1. Ezzatfar, P., Binici, B., Kurç, Ö., Canbay, E., Sucuoğlu, H. and Özcebe, G. (2013). Application of Mesh Reinforced Mortar for Performance Enhancement of Hollow Clay Tile Infill walls. In Seismic Evaluation and Rehabilitation of Structures (pp. 171-186). Springer International Publishing. DOI 10.1007/978-3-319-00458-7_10

INTERNATIONAL JOURNAL PAPERS

1. Sucuoğlu, H., Wei-Chin Lin, W., Binici, B., Ezzatfar, P. (2014). Pseudo Dynamic Testing, Performance Assessment and Modeling of Deficient Reinforced Concrete Frames. ACI Structural Journal, 111(5), 1203. DOI: 10.14359/51686922

2. Laura Redmond, Pourang Ezzatfar, Reginald DesRoches, Andreas Stavridis, Guney Ozcebe, and Ozgur Kurc (2016) Finite Element Modeling of a Reinforced Concrete Frame with Masonry Infill and Mesh Reinforced Mortar Subjected to Earthquake Loading. Earthquake Spectra: February 2016, Vol. 32, No. 1, pp. 393-414. DOI: 10.1193/081314EQS128M

3. Fenerci, A., Binici, B., Ezzatfar, P., Canbay, E., Ozcebe, G. (2016), The Effect of Infill Walls on the Seismic Behavior of Boundary Columns in RC Frames. Earthquakes and Structures. March 2016, Vol.10, No.3, pp.539-562. DOI: http://dx.doi.org/10.12989/eas.2016.10.3.539

INTERNATIONAL CONFERENCE PROCEEDINGS

1. M. Sadegh Azar, P. Ezzatfar (2008), "Evaluation of Behavior Factor of Vertical Pressure Vessels on Steel Skirt" (in Farsi), 1st International Conference on Seismic Retrofitting and 3rd National Conference on Retrofitting, Tabriz, Iran

2. Ezzatfar, P., Özcebe, G., Binici, B., Canbay, E. and Kurç, Ö. (2012), "Assessment of Seismic Behavior and Dynamic Characteristics of R/C Frames Enhanced with Mesh Reinforced Infill Walls under Consecutive Earthquake Loadings". 10th International Congress on Advances in Civil Engineering, 17-19 October 2012, Ankara, Turkey.

3. M. B. Mutlu, M.E. Ayatar, P. Ezzatfar, B. Binici, O. Kurç, E. Canbay, H. Sucuoglu, G. Ozcebe (2012), "Pseudo-Dynamic Testing and Numerical Simulations of Reinforced Concrete Frames". 10th International Congress on Advances in Civil Engineering,17-19 October 2012, Middle East Technical University, Ankara, Turkey.

4. Ezzatfar, P., Binici, B., Kurç, Ö., Canbay, E., Sucuoğlu, H. and Özcebe, G. (2013). "Seismic Behavior of Reinforced Concrete Frames with Hollow Clay Tile Brick Infill Walls". International Conference on Earthquake Engineering, 29-31 May 2013, Skopje, Macedonia.

5. Ezzatfar, P., Binici, B., Kurç, Ö., Canbay, E., Sucuoğlu, H. and Özcebe, G. (2013). "Performance Assessment of RC Frames With HCT Brick Infill Walls Rehabilitated With MRM by Using Pseudo Dynamic Test Protocols". 5th International Conference on Advances in Experimental Structural Engineering, 8-9 November 2013, Taipei, Taiwan.

PRESENTATIONS

1. P. Ezzatfar, M.E.Ayatar, B.Binici, O.Kurc, E.Canbay, H.Sucuoglu,.Ozcebe (2012), "Application of Mesh Reinforced Mortar for Performance Enhancement of Infill Walls". The 3rd International Workshop: "Role of research infrastructures in seismic rehabilitation", 8-9 February, 2012, Istanbul Technical University, Istanbul, Turkey

2. Ezzatfar. P. Özcebe, G. (2013). "Seismic Performance Evaluation of reinforced Concrete Frames With PSD Testing". İnşaat Mühendisliği Yüksek Lisans ve Doktora Günü. TMMOB İnşaat Mühendisleri Odası Ankara Şubesi, Ankara, Turkey.